The Role of Endoglin in Cell-Mediated Heart Repair

Rachael E. Redgrave
Institute of Human Genetics
Faculty of Medical Sciences

Thesis submitted for the degree of
Doctor of Philosophy

University of Newcastle
2012

DECLARATION

The work described in this thesis was undertaken in the laboratory of Dr Helen Arthur at the Institute of Genetic Medicine (Newcastle University) in fulfilment of the requirements for the degree of Doctor of Philosophy. This thesis is the result of my own work and I have correctly acknowledged the contributions of others where appropriate in the text. No material within this thesis has been submitted by me for a degree or diploma or other qualification in this or any other University. This thesis does not exceed the word limit prescribed by the Faculty of Medical Sciences.

Rachael Redgrave
May 2012

ABSTRACT

Despite substantial advances in pharmacological and interventional strategies for the treatment of ischaemic heart disease and acute myocardial infarction (MI) many patients go on to develop dilated heart failure with high morbidity and mortality rates. Increasing evidence suggests that stem cells can augment re-vascularisation of the infarcted myocardium leading to improved cardiac function. However, the precise mechanisms involved are not completely understood and further work is required to realise optimised cell based therapy.

The aim of this project was to investigate the role of endoglin, a pro-angiogenic TGFβ co-receptor, in bone marrow (BM)-derived endothelial progenitor cells (EPCs) and in cardiac-resident cardiosphere-derived cells (CDCs) using mouse models. I hypothesised that endoglin acts as a key marker and functional regulator of the pro-angiogenic repair properties of these stem cells and that manipulating TGFβ signalling by controlling endoglin levels could provide a better understanding of the properties of these cells, with the longer term goal of developing more effective revascularisation therapies.

My data show that inhibiting TGFβ/Alk5 signalling *in vitro* increases EPC yield from both endoglin heterozygous and wild-type BM cells. In addition, although endothelial specific knock-down of endoglin *in vivo* led to increased endoglin expression in cells from the BM, these cells did not incorporate into endoglin depleted heart or lung vasculature.

I also showed that endoglin deficiency results in a significant reduction in EPC yield from BM cells and inducible endoglin depletion in CDCs (using a conditional endoglin knock-out mouse model) impairs cellular proliferation and migration *in vitro* alongside up-regulated TGFβ/Alk5 signalling. Furthermore, injection of wild-type CDCs into the ischaemic border zone of the heart, following coronary artery occlusion in a mouse MI model, led to an increased angiogenic response at 4 weeks. This response was significantly reduced when endoglin depleted cells were transplanted. However both wild-type and endoglin depleted CDCs were able to rescue heart function, as measured using cardiac MRI.

In conclusion, the results of this thesis provide evidence of the important roles that endoglin and TGFβ signalling play in promoting angiogenesis in tissue repair. Further advances in this field could aid in the development of more effective cell therapies for MI patients.

ACKNOWLEDGEMENTS

I would like to extend my sincere gratitude to Dr Helen Arthur for giving me the opportunity to perform this research in her laboratory and for passing on her knowledge and guidance to me.

I would also like to convey a special thank-you to Dr Ben Davison for lending me his spectacular MR imaging skills as well as for the many invaluable discussions we shared – you certainly are a credit to research and I wish you every success for the future. My thanks also go out to the rest of my research group both past and present. The core support team of the IGM also deserve a lot of credit for the amazing work that they do. I would especially like to thank Neil Hamilton for the extended support he has given me in often very trying times as well as Lisa Hodgson for not only giving me great microscopy advice but also for her constant willingness to help everybody.

I would like to acknowledge and pass on my thanks to Professor Christine Mummery (Leiden University formerly Hubrecht Institute, Utrecht) for hosting me in her laboratory and to Dr Linda van Laake for teaching me her exquisite surgical skills and the murine MI model. I wish also to thank Dr Carolyn Carr and Dr Jun Jie Tan (Oxford University) for their invaluable advice regarding cardiosphere culture.

Extra special thanks go to Joff for loving me and always making me laugh (even when I've been intent on being glum). I appreciate the faith that you have in me and I could not have done this without you.

Above all I would like to thank my sister Emma for her never-ending support and supply of chocolate. I thank-you for staying with me when I've needed someone and for pretending to be interested in my rants, for always trying to build my confidence and generally for just looking after me.

I dedicate this thesis to my parents. For my mother and her selfless and enduring love and for my father and the pride that I know he would have felt if he were with us today.

Zip-a-Dee-Doo-Dah.

TABLE OF CONTENTS

LIST OF FIGURES

LIST OF TABLES

LIST OF ABBREVIATIONS

acLDL	acetylated low density lipoprotein
Acvr2	activin receptor type II
Alk	activin receptor-like kinase
AVM	arteriovenous malformation
β-gal	beta-galactosidase
bFGF	basic fibroblast growth factor
BM	bone marrow
BMP	bone morphogenetic protein
Bmpr2	BMP type II receptor
Bp	base pair
BRE	BMP responsive element
BSA	bovine serum albumin
CA	coronary artery
CAD	coronary artery disease
CDC	cardiosphere-derived cell
Cdh5	cadherin5
cDNA	complementary DNA
CFU	colony forming unit
CGM	cardiosphere growth media
CI	cardiac output index
CO	cardiac output
Co-Smad	common mediator Smad
CSC	cardiac stem cell
Csph	cardiosphere
DAB	3-3'-diaminobenzidine tetrahydrochloride
DEPC	diethyl pyrocarbonate
DMEM	dulbeccos modified Eagles medium
DNA	deoxyribonucleic acid
dNTPs	deoxyribonucleotide triphosphate
dpi	days post injection
E	embryonic day
ECs	endothelial cells
ECFCs	endothelial colony forming cells
ECM	extracellular matrix
EDC	explant derived cells
EDTA	ethylenediaminetetraacetic acid
EDV	end diastolic volume
EDVI	end diastolic volume index
EF	ejection fraction
EGF	epidermal growth factor
eGFP	enhanced green fluorescent protein
EMT	epithelial to mesenchymal transition
EndMT	endothelial to mesenchymal transition
Eng	endoglin
eNOS	endothelial nitric oxide synthase
EPC	endothelial progenitor cell
ESV	end systolic volume
ESVI	end systolic volume index

FACS	fluorescence activated cell sorting
FCS	fetal calf serum
FDG	fluorescein di-β-d-galactopyranoside
FGF	fibroblast growth factor
FITC	fluorescein isothyocyanate
fl	floxed
Flk-1	foetal liver kinase 1
G-CSF	granulocyte colony-stimulating factor
GM-CSF	granulocyte macrophage colony stimulating factor
GS domain	glycine- and serine- rich domain
HGF	hepatocyte growth factor
HHT	hereditary haemorrhagic telangiectasia
HRP	horseradish peroxidise
HSC	haematopoietic stem cell
HUVEC	human umbilical vein endothelial cell
iKO	inducible knockout
IL	interleukin
IP	intraperitoneal
I-Smad	inhibitory Smad
kb	kilobase
kDa	kilodalton
LAD	left anterior descending
LTC	long term culture
loxP	locus of X-over P1
LV	left ventricle
MEEC	mouse embryonic endothelial cell
mg	milligram
MI	myocardial infarction
MMP	matrix metalloproteinase
MNC	mononuclear cell
MRI	magnetic resonance imaging
mRNA	messenger RNA
MSC	mesenchymal stem cell
MTT	3-(4,5-dimethylthiazol-2-yl)-2,5-diphenyltetratetrazolium bromide
ng	nanogram
NO	nitric oxide
OEC	outgrowth endothelial cells
PAGE	polyacrylamide gel electrophoresis
PB	peripheral blood
PBS	phosphate buffered saline
PBST	PBS tween
PCR	polymerase chain reaction
PDGF-BB	platelet-derived growth factor beta
PFA	paraformaldehyde
Phospho-Smad	phosphorylated Smad
R26R	Rosa 26R
RNA	ribonucleic acid
rpm	revolutions per minute

R-Smad	receptor-regulated Smad
RT-PCR	reverse transcription PCR
SDS	sodium dodecyl sulphate
SD	standard deviation
SDF1	stromal derived factor 1
SEM	standard error of the mean
sEND	skin endothelial cell
Ser/Thr	serine/threonine
shRNA	small hairpin RNA
siRNA	small interference RNA
SMC	smooth muscle cell
STC	short term culture
SV	stroke volume
SVI	stroke volume index
TAE	tris-acetate EDTA
TBS	tris buffered saline
TBST	TBS tween
TGFβ	transforming growth factor beta
Tgfbr2	TGFβ type II receptor
Tie2	endothelium-specific receptor tyrosine kinase 2
UCB	umbilical cord blood
VE-Cadherin	vascular endothelial cadherin
VEGF	vascular endothelial growth factor
VEGFR2	vascular endothelial growth factor receptor 2
vWF	von willibrand factor
WT	wild-type
X-gal	5-bromo-4-chloro-3-indolyl-beta-D-galactopyranoside
ZP	zona pellucida

CHAPTER 1.

Introduction

1.1. Angiogenesis and Vasculogenesis

The vascular system is essential for growth, repair and survival and develops via two distinct processes: vasculogenesis and angiogenesis[1-2]. During embryonic development blood vessels are formed *de novo* by the patterned assembly and differentiation of angioblasts into endothelial cells (ECs) in a process termed vasculogenesis (figure 1.1). This results in the formation of a primary plexus of capillaries, which progressively expands during the angiogenic phase of vascular development either by sprouting angiogenesis, through end-to-end fusion of vessel sprouts or intussusceptive vascular growth[1-3] (figure 1.1). In sprouting angiogenesis ECs proliferate behind the tip cell of a growing branch in response to specific stimuli, such as vascular endothelial growth factor (VEGF), and lumens can form by vacuole fusion[4]. Alternatively intussusceptive angiogenesis describes the splitting and growing of vessels by the formation of translumen pillars, however the molecular mechanisms involved in this process are poorly understood[1, 3]. During vessel maturation, nascent endothelial vessels are stabilised via the recruitment of supporting mural cells and extracellular matrix (ECM) is deposited[1, 3, 5]. Mural cells include pericytes, which provide structural support and protect endothelial cells from apoptosis, and vascular smooth muscle cells that bestow vessels with vasomotor properties[5]. Angiogenesis remodels the primitive capillary plexus into a highly organized network of arteries, capillaries and veins as blood starts to circulate and both genetic mechanisms and local environmental cues dictate arterial or venous specification[3].

Angiogenesis is not restricted to development. In adult life angiogenesis is important for tissue repair (as well as in many pathologies, discussed in more detail below) and is a dynamic process consisting of both activation and resolution phases[1, 6]. During the activation phase, vascular permeability increases, extracellular matrix components are degraded and ECs proliferate and migrate to form new capillary sprouts. ECs cease to proliferate in the angiogenic resolution phase, the basement membrane reconstitutes and vessels become associated with stabilising mural cells as they mature and finally become quiescent. The transition between these two phases is referred to as the angiogenic switch and is tightly regulated by an intricate balance of growth inducers and inhibitors.

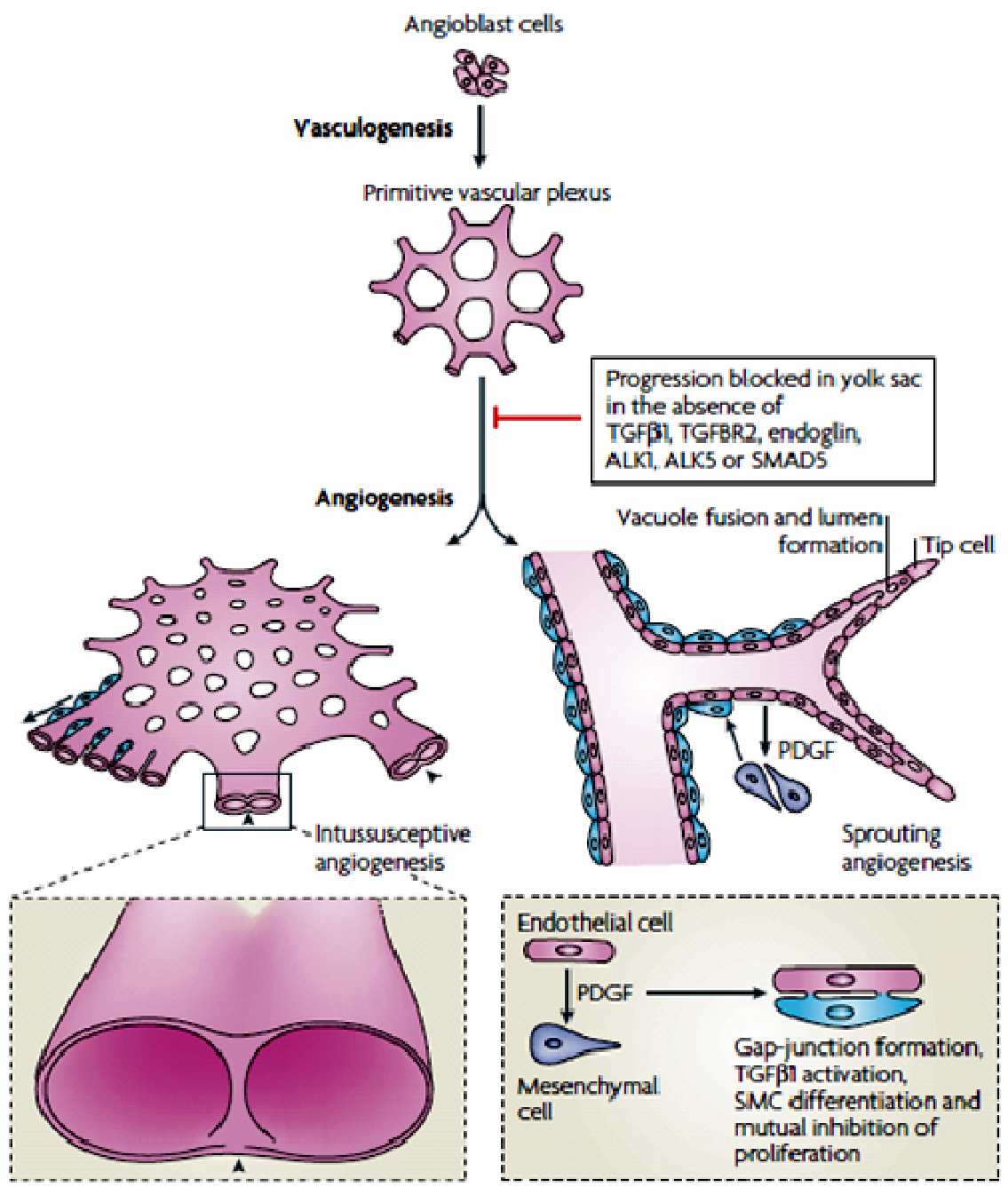

Figure 1.1. Development of the vascular system via vasculogenesis and angiogenesis. During embryonic development the process of vasculogenesis (the *in situ* differentiation and patterned assembly of mesoderm-derived angioblasts into a primary capillary plexus) first occurs in the extra-embryonic yolk sac as blood islands containing haemangioblasts differentiate from extra-embryonic mesodermal cells. Angiogenesis (the formation of new vessels from the pre-existing vessel plexus through sprouting or intussusceptive growth) expands and remodels this primary capillary network to generate mature vessels associated with stabilising mural cells. The primary blood plexus in the yolk sac connects with a primary blood plexus in the embryo proper and the circulatory system is established once the embryonic heart begins to beat. Primary embryonic vasculature is remodelled at later developmental stages and postnatally through both vasculogenesis and angiogenesis to meet the metabolic demands of the organism. Figure from[7].

Although *de novo* blood vessel formation (vasculogenesis) was once thought to be largely restricted to embryonic development recently it has been discovered that vasculogenesis can also take place in adult life via the incorporation of endothelial progenitor cells into neovessels, this will be discussed in greater detail in section 1.5.

1.2. Angiogenesis in Heart Repair

Physiological angiogenesis in the adult is largely restricted to the cycling ovary and uterus as most blood vessels remain relatively quiescent[2]. However angiogenesis is stimulated in response to injury and actively contributes to wound healing and repair by restoring blood flow to injured tissues[2, 8]. Additionally, in certain disease states the body may lose control of the tightly coordinated processes regulating angiogenesis resulting in either excessive or insufficient vessel growth. Excessive angiogenesis occurs in many diseases, such as macular degeneration and malignancy, and results from diseased cells producing abnormally high levels of angiogenic growth inducers, which overcome the suppressant effect of inhibitors[2]. In these conditions neovessels feed diseased tissues and in the event of malignant disease new vessels can allow tumour cells to metastasise. Anti-angiogenic therapies, aimed at preventing neovascularisation are currently being investigated and trialled to combat this dysregulation of angiogenesis. However, in other disease states such as ischaemic heart disease, heart failure and stroke, insufficient angiogenesis can occur whereby blood vessel growth is inadequate to meet the metabolic demands of the tissue and circulation is not properly restored, increasing the risk of tissue death[2].

Myocardial infarction (MI) occurs most commonly due to coronary artery occlusion following the rupture of an atherosclerotic plaque and causes irreversible damage to cardiac tissue secondary to prolonged ischaemia[9]. In contrast to adult zebrafish[10] and the neonatal mouse heart[11], the adult human heart has minimal regenerative capacity. Therefore following infarction a reparative process is triggered that ultimately results in the formation of a fibrotic scar which can be associated with adverse structural and functional cardiac changes. This complex endogenous repair process is described in detail in extensive reviews[9, 12-13] but will be briefly outlined here. Infarct healing involves three overlapping stages termed the inflammation, proliferation and maturation phases[9] (figure 1.2). Following prolonged ischaemia dying cells trigger the activation of

chemokine and cytokine cascades during the inflammatory phase of repair. This leads to a mass influx of leukocytes, which clear the ischaemic area of dead cells and matrix debris. In addition, recruited macrophages release an array of cytokines and growth factors that result in the formation of highly vascularised granulation tissue. Hereafter pro-inflammatory mediator expression becomes suppressed and fibroblast and EC numbers expand during the proliferation phase. At this stage activated myofibroblasts produce extracellular matrix proteins and an extensive microvascular network is formed. In the final stage granulation tissue associated cells apoptose and myofibroblasts deposit a network of collagen resulting in the formation of a mature, thin collagen-based scar[9]. Infarct healing is closely associated with ventricular remodelling, a process that can occur following MI involving major changes in ventricular architecture and geometry[12-13] (figure 1.2). Remodelling involves both infarcted and remote myocardium and occurs following MI due to an acute loss of viable tissue which results in an abrupt increase in loading conditions. During the early phase of remodelling the infarct zone expands whereas later stages involve the left ventricle globally and are associated with chamber dilatation and distortion of ventricle shape. This process can continue for weeks to months or until the forces of increased wall stress are counterbalanced by the tensile strength of the mature collagen scar. Failure to adequately normalise these forces can result in progressive ventricular dilatation, recruitment of border zone myocardium into the scar as well as deterioration in cardiac function[12-13]. Therefore ventricular remodelling is linked to the progression of heart failure and is associated with poor prognosis following MI.

Angiogenesis forms an important part of the healing process following MI[9, 14]. Hypoxic conditions and an array of secreted growth factors stimulate angiogenesis in the infarcted heart[9, 15]. Neovessels begin to appear soon after ischaemic assault and within 1 week the infarct zone and surrounding myocardium become rich in capillaries[14, 16]. These vessels allow increased blood flow, which greatly accelerates and promotes the healing response thus increasing the salvage of affected heart tissue. This new microvessel network is thought to develop to allow the formation of provisional granulation tissue and inflammatory cell infiltration[8, 14]. However, at a later stage of infarct healing whilst some newly formed capillaries mature into pericyte-coated vessels many others regress and degenerate through apoptosis as the collagen scar matures and remodelling resolves[9]. Following MI, in addition to angiogenesis, vascular perfusion of

the ischaemic area can also be enhanced by recruiting the pre-existing arterial circulation to bypass the site of major artery occlusion via arteriogenesis[1, 17]. This circumvention is achieved by the rapid growth of pre-existing collateral arteries and the maturation of capillaries into mature arterioles, which may then serve as an alternative route for blood flow. These collateral vessels are not used to enhance perfusion under normal conditions but can dramatically expand lumen diameter and increase blood flow to ischaemic regions at risk. Collateral vessel formation in MI patients has been associated with an improvement in myocardial viability as well as reduced infarct size leading to an overall reduction in mortality[18].

The enhancement of blood flow via adaptive angiogenesis and/or recruitment of pre-existing coronary collateral vessels is frequently insufficient following severe ischaemic damage, leading to inadequate tissue perfusion which may result in ongoing loss of viable tissue, infarct extension, and increased adverse ventricular remodelling. Therefore a major focus of cardiovascular research is therapeutic angiogenesis, which aims to promote the growth and proliferation of blood vessels to enhance blood flow to jeopardised ischaemic regions.

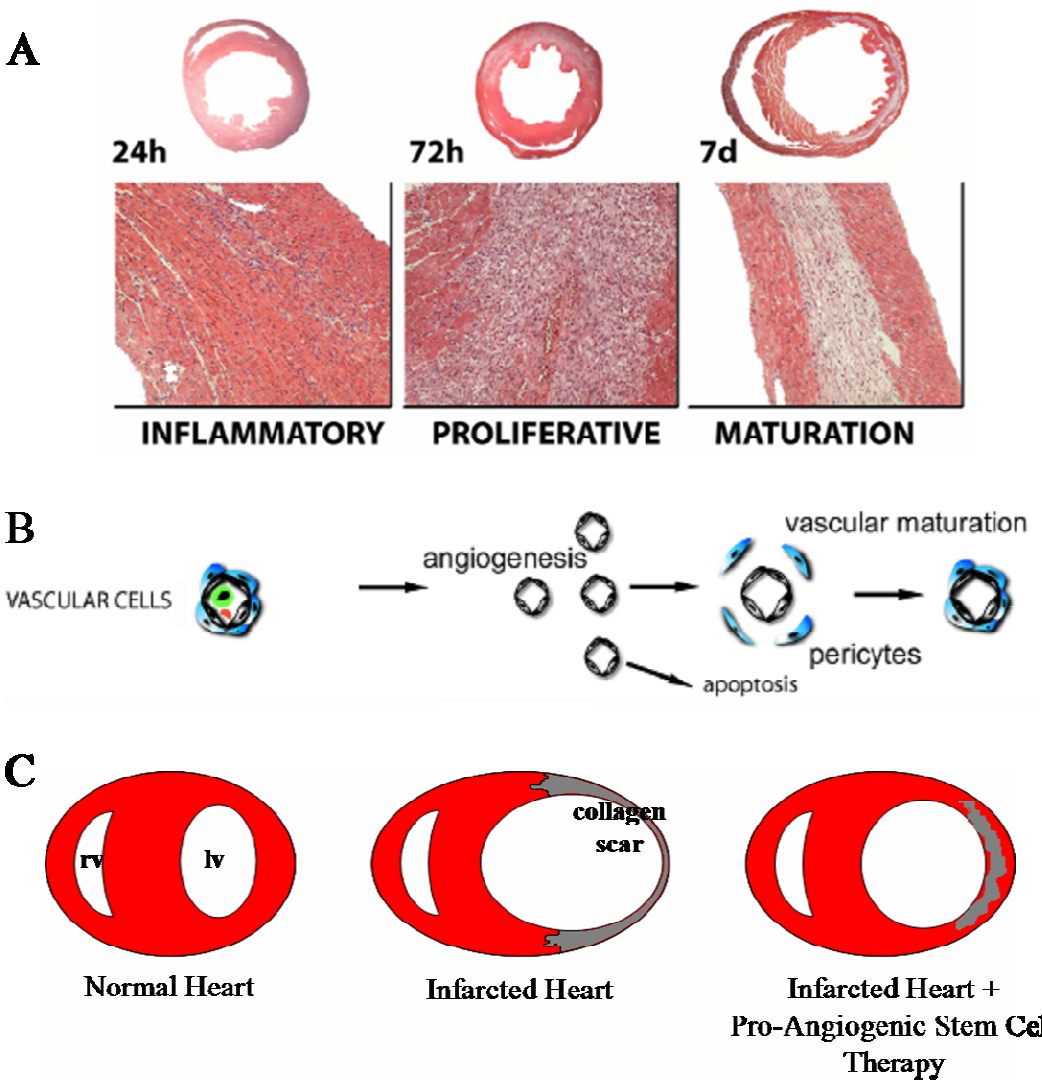

Figure 1.2. Infarct healing and ventricular remodelling; the angiogenic response. (A) The healing response following MI involves three distinct but overlapping phases; inflammatory, proliferative and maturation (discussed further in text) and is dependent on the sequential infiltration of the damaged myocardium with inflammatory, fibroblast and vascular cells. These processes are tightly associated with progressive remodelling which describes the structural and functional ventricular changes observed post MI, including LV wall thinning and dilatation and eventually damaged tissue is replaced with a collagen-based scar. (B) Following infarction an extensive microvascular network forms during the healing response to promote the formation of provisional granulation tissue and inflammatory cell infiltration as well as increasing blood flow to increase the salvage of injured myocardium. However, many neovessels regress at later stages as the collagen scar matures. As a result inadequate tissue perfusion can result in increased adverse ventricular remodelling. (C) Therapeutic angiogenesis aims to promote the growth and proliferation of vessels to enhance blood flow to jeopardised ischaemic regions. This can significantly attenuate the adverse effects of remodelling and rescue heart function. N.B. the time course presented here (applies to (A) and (B)) is representative of a mouse model of MI and reperfusion, larger animals and humans exhibit delayed healing in comparison (can extend from weeks to months). Figure adapted from[9].

1.3. Therapeutic Angiogenesis in Heart Repair

Early restoration of blood flow to the infarcted myocardium via catheter based coronary reperfusion (angioplasty) combined with pharmacological therapy is the preferred clinical course following acute MI. However, in recent years there has been tremendous enthusiasm for the utilisation of therapeutic angiogenesis as a strategy to augment conventional therapies as well as for treating patients who may be unsuitable for routine clinical therapy due to contra-indications (such as co-morbidities). The goal of therapeutic angiogenesis in ischaemic heart disease is to promote neovascularisation and restore cardiac function (figure 1.2). The augmentation of physiological vascularisation can be achieved via different means including; gene, protein and cell therapies.

Early strategies focused on the delivery of pro-angiogenic growth factors (such as VEGF and FGF) via protein or gene based approaches designed to stimulate vasculogenesis, angiogenesis and arteriogenesis (reviewed in[19]). However these studies resulted in limited success presumably due to the short half life of proteins; the strategies employed were found to promote rapid formation of neovessels following MI in pre-clinical models, but these vessels were leaky and regressed easily as they failed to mature and anastomose with the coronary circulation[20]. In addition, phase I and II clinical trials using angiogenic growth factors to improve revascularisation of hearts in coronary artery disease patients have generally delivered disappointing results[21]. Cell-based pro-angiogenic therapies may provide a more effective route to improve perfusion due to their ability to persist for prolonged periods following transfer, to differentiate into vascular cell types and also to secrete multiple pro-angiogenic factors that may work in synergy to create a more permissible environment for vessel formation.

1.4. Pro-Angiogenic Cell-Mediated Therapy for Myocardial Repair

In recent years the field of cell-based regenerative medicine has exploded and multiple cell-types have been used to treat cardiovascular disease in pre-clinical studies and early phase clinical trials. This new therapeutic strategy aims to improve heart function by delivering stem/progenitor cells with the capacity to stimulate myocardial regeneration and/or neovascularisation either directly or indirectly via cellular differentiation or paracrine mechanisms. In this thesis I will focus on pro-angiogenic mediated repair

although many of the proposed therapeutic cell types have also been implicated in direct myocardial regeneration. Cell therapy candidates include bone marrow (BM)-derived cells (including endothelial progenitor cells (EPCs), haematopoietic stem cells (HSCs) and mesenchymal stem cells (MSCs)), tissue derived cells (including resident cardiac progenitor cells) as well as embryonic stem cells (ESCs), inducible pluripotent stem cells (iPSCs) and skeletal myoblasts.

In this study I have investigated the use of BM-derived EPCs and cardiosphere derived cells (a heterogeneous population that includes cardiac resident stem cells) which are discussed in greater detail in sections 1.5 and 1.7, respectively. Advances using other cell types have been reviewed in several recent publications[22-23].

1.5. Endothelial Progenitor Cells

1.5.1. Isolation and Characterisation of Endothelial Progenitor Cells

In 1997 Asahara *et al*[24] first described the "isolation of putative progenitor endothelial cells". The authors identified a circulating $CD34^+$ mononuclear cell (MNC) population with the capacity to differentiate into ECs *in vitro* and incorporate into ischaemic tissues at sites of angiogenesis *in vivo*. Since this time evidence has accumulated that strongly supports the existence of BM-derived circulating vascular progenitor cells.

Although these cells are collectively referred to as endothelial progenitor cells (EPCs), it is highly likely that this term represents a heterogeneous population of cells at various stages of differentiation. Indeed, one of the most controversial issues surrounding EPC biology remains the definition of EPC phenotype and their characterisation[25-26]. Despite rigorous investigation over recent years the isolation of a definitive endothelial progenitor has been hampered by conflicting reports which are most likely attributed to the varying methods utilised by different studies including different cell sources, cell isolation methods, *in vitro* and/or *in vivo* assays, as well as data analysis and interpretation.

Flow cytometric immunophenotyping has been integral to the identification of putative EPCs residing in the BM-MNC, umbilical cord blood (UCB)-MNC or peripheral blood

(PB)-MNC fractions. Using this method EPCs have traditionally been characterised on the basis of a combination of mature endothelial and early HSC associated marker expression[24, 27-29]. The most common markers include CD34, a classic HSC marker that is also expressed at low levels on ECs[30-31], vascular endothelial growth factor receptor 2 (VEGFR2 also known as Flk-1 in mice or KDR in humans) a tyrosine kinase receptor vital to both endothelial and haematopoietic lineages[32-33] and CD133 (or AC133) an early haematopoietic marker of unknown function[34-35]. It has been proposed that co-expression of VEGFR2 and CD133 on CD34 positive cells phenotypically identifies a unique population of endothelial progenitors[27] and the differentiation of EPC to mature EC is suggested to be characterised by the loss of CD133, down-regulation of CD34 and the up-regulation of VEGFR2 expression[36] as well as expression of other endothelial markers including CD31 and von Willibrand factor (reviewed in[37]). However, although $CD34^+VEGFR2^+CD133^+$ cells are widely accepted as representing circulating EPCs in humans many studies have failed to test the ability of these cells to generate ECs *in vitro* or *in vivo*[25]. Furthermore, Case *et al*[38] report that $CD34^+VEGFR2^+CD133^+$ cells isolated from UCB and PB represent a population of $CD45^+$ haematopoietic progenitor cells that do not differentiate into ECs. Interestingly, it has also been shown that $CD34^+CD45^-$ BM and UCB-MNC cultures generate cells indistinguishable from ECs[39] and while these cells were positive for VEGFR2 they did not express CD133, suggesting that $CD34^+VEGFR2^+CD133^-CD45^-$ cells may be a more accurate phenotype of true endothelial progenitors. It is clear that further investigation including both *in vitro* and *in vivo* validation is necessary to definitively immunophenotype EPCs.

Many investigators have cultured unfractionated MNCs to isolate and enrich EPCs. MNCs are cultured on coated plastic plates in endothelial specific growth media to (i) promote endothelial differentiation[24, 27, 29, 35, 39-40], (ii) expand EPC populations *ex vivo*[41-43] and (iii) to assay endothelial progenitors for colony forming ability[44-47] or function (including angiogenesis[48-51], migration[50-52], adhesion[49-51] and proliferation[49-51] assays). Although many variations of the culture protocol have been devised three general methods are commonly described (summarised in figure 1.3). In the first method[45, 53] unfractionated MNCs are plated onto fibronectin-coated dishes for 24-48hours preceding a re-plating step in which non-adherent cells are removed and re-plated while the adherent cells (thought to include macrophages and mature ECs) are discarded. Discrete colonies appear after 5-9 days comprising of round central cells with spindle

shaped cells at the periphery. These colonies are widely referred to as CFU-Hill or CFU-EC and are thought to be derived from EPCs. This colony forming assay was used to identify an inverse correlation between EPC number and cardiovascular risk status[45] suggesting that EPCs can be used as biomarkers of cardiovascular disease. CFU-Hill concentration was found to be lower in patients at risk for vascular disease and higher during acute cardiovascular stress. However it has become apparent that CFU-Hill colonies contain an assortment of blood cells including monocytes, lymphocytes, and progenitor cells skewed towards the myeloid lineage[53-54]. Furthermore CFU-Hill were unable to form perfused vessels in an *in vivo* ischaemic experimental model[54].

In the second method[42, 55-58] (Figure 1.3) MNCs are cultured on fibronectin for 4 days before non-adherent cells are removed and discarded leaving a target adherent population that is cultured for up to 7 days. The resultant cells are spindle shaped in appearance with limited self renewal capacity, persisting in culture for only 2 weeks. These cells are often referred to as early EPCs, however controversy has arisen as evidence suggests that they may represent monocyte/macrophage cells rather than true endothelial progenitors (discussed in greater detail below). Interestingly, changes in circulating levels of early EPCs in patients with cardiovascular disease and associated risk are comparable to the trend observed for CFU-Hill levels. Vasa *et al*[57] observed an inverse correlation between the risk factors for coronary artery disease (CAD) and circulating early EPC number and Lambiase *et al*[58] corroborated this relationship by reporting a 70-75% reduction in circulating early EPC levels in patients with clinically diagnosed CAD.

In a third approach[39, 46, 59-61] (method 3, Figure 1.3) MNCs are cultured on fibronectin or collagen-I coated dishes and non-adherent cells are discarded after several days. Highly proliferative colonies arise from the adherent cell population after 2-3 weeks of culture and display a cobblestone-like phenotype typical of ECs. These cells are interchangeably referred to as late EPCs, outgrowth ECs (OECs), or endothelial colony forming cells (ECFCs) and can be maintained and expanded in culture for up to 12 weeks, are reportedly phenotypically indistinguishable from cultured mature ECs and have *de novo* vessel-forming ability[39, 46, 54, 59].

While late EPCs are believed to be derived from circulating adult angioblast-like cells and to develop exclusively from a $CD14^-$ sub-population, evidence suggests that the

majority of early EPCs may arise from a $CD14^+$ monocytic fraction of MNCs or that they simply represent mature ECs that have become sloughed from vessel walls[39, 54, 62-63]. Indeed, although early EPCs have been shown to display several EC-like features that are phenotypic (EC marker expression, LDL uptake, lectin binding), morphological (Weibel-Palade bodies), and functional (vascular network formation) it is now generally accepted that these cells represent a mixed population displaying endothelial-monocytic/haematopoietic phenotypes and may not differentiate into true ECs and are therefore not endothelial progenitors[39, 42, 56, 62-64]. Despite this mis-nomenclature, early EPCs have been shown to indirectly promote neovascularisation in pre-clinical models of acute MI and critical limb ischaemia[42, 62, 64-65]. Furthermore, Schmeisser *et al*[66] noted, that under angiogenic stimulation $CD14^+$ macrophages/monocytes developed an endothelial phenotype and formed tubular-like structures in a 3D Matrigel assay. Thus early EPCs have also become to be known as EC-like cells or circulating angiogenic cells[25-26]. The overlap of endothelial and haematopoietic phenotype and function has complicated analysis and made the discrimination between these two lineages difficult. It has now been proposed that uncultured monocytes do not possess pro-angiogenic properties and that culturing in angiogenic conditions is required to prime them[62]. Despite the confusion related to the different sub-types of proposed EPCs and the debate regarding appropriate nomenclature, both early and late EPCs are thought to potently promote tissue repair via neovascularisation although their modes of action are thought to differ *in vivo* (discussed further in section 1.5.2).

In summary there remains much controversy surrounding the identity and true phenotype of EPCs as well as their role in adult angiogenesis. The current definition includes a cell that: 1) resides within the BM and can be recruited to sites of vascular injury or tumour growth by environmental cues; 2) expresses both endothelial and haematopoietic cell surface markers; 3) can be distinguished from mature circulating ECs by these markers and the ability to form outgrowth colonies; 4) can integrate into sites of vessel repair or angiogenesis and promote tissue repair[67]. However due to multiple conflicting reports this definition remains continuously evolving.

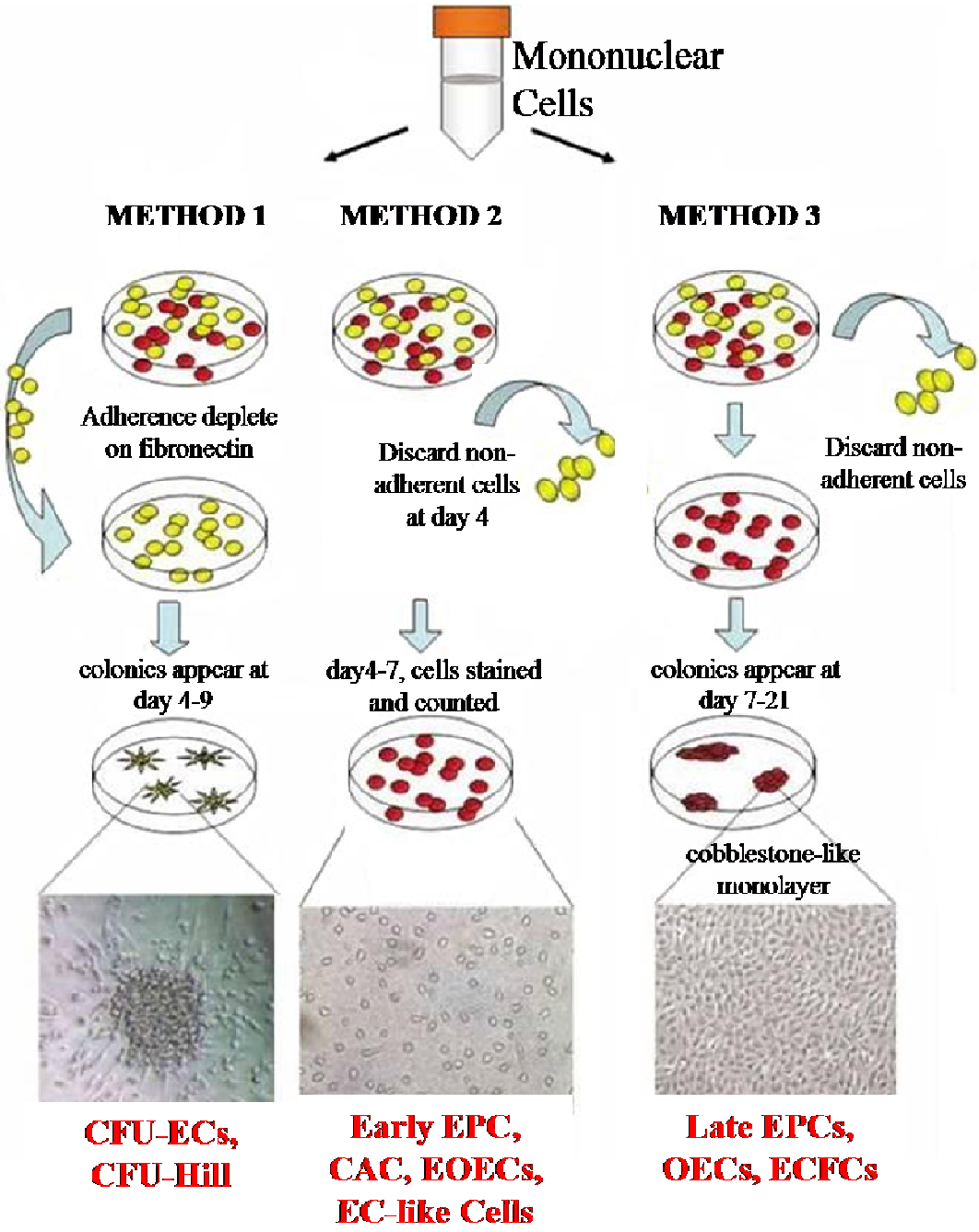

Figure 1.3. Schematic summarising common EPC culturing methods. Method 1, MNCs are cultured for several days prior to adherence depletion. Non adherent MNCs then give rise to EPC colonies (termed colony forming unit (CFU)-Hill or CFU-EC) within 4-9 days. Method 2, MNCs are cultured for 4 days, thereafter non-adherent cells are discarded whilst adherent cells form early EPCs (also known as circulating angiogenic cell (CAC), early outgrowth endothelial cell (EOECs) and EC-like cells). Method 3, Adherent MNCs are cultured for up to 12 weeks in endothelial conditions. Colonies appear between weeks 1 and 3 and give rise to a cobblestone-like cell monolayer. These cells are referred to as late EPCs, outgrowth endothelial cells (OECs) or EC-forming cells (ECFCs). Figure adapted from[26].

1.5.2. EPCs in Angiogenesis and Cardiac Repair; Pre-Clinical Models

Since the first publication detailing the discovery of an adult endothelial progenitor[24] many pre-clinical studies have supported a beneficial role for EPCs in vascular and cardiac repair. Early evidence indicated that circulating EPCs functioned as an endogenous repair mechanism to maintain the integrity of the endothelial monolayer by contributing to the re-endothelialisation of grafts and denuded arteries[68-70]. Many investigators also demonstrated that infusion of MNCs or *ex vivo* expanded EPCs (defined in a variety of ways) augments neovascularisation in both physiological and pathological pre-clinical settings including peripheral ischaemia[42, 62, 71-74], wound healing[75-77], atherosclerotic plaques[78-79] and tumour neovessels[28, 80]. Of particular interest, the injection of stem/progenitor cells in animal models of acute MI significantly increased neovascularisation and blood flow, reduced adverse left ventricular remodelling and improved cardiac function[65, 81-87]. Correspondingly, initial stage I and II clinical trials indicate that BM- and PB-derived progenitor cells are a useful tool for therapeutically improving the blood supply of ischaemic tissue (discussed in section 1.5.4).

Terminally differentiated mature ECs do not promote neovascularisation *in vivo* [42, 83, 88] suggesting that it is a property specific to EPCs that enhances vascular repair in pre-clinical models. However, different EPC sub-types have displayed functional differences with regard to their effects *in vivo*. Engraftment levels within experimental models vary widely and in some studies the incorporation rate of cells with an endothelial phenotype has been undetectable or relatively low[25, 89] therefore the direct contribution of BM-derived progenitors to the endothelium has been down-played in recent years. Indeed, Ziegelhoeffer *et al*[90] report that BM-derived cells do not incorporate into the adult growing vasculature but do provide structural support as primary leukocytes, fibroblasts or pericytes that accumulate around the growing vessels. Other studies corroborate these findings and report that the major contribution of the BM to angiogenic processes may come from progenitors for peri-endothelial mural cells, which contribute to vascular stability and remodelling[91-92] (discussed further below). Moreover the release of pro-angiogenic factors in a paracrine manner has been suggested as an alternative mechanism responsible for the augmentation of

neovascularisation. In this context, cultivated EPCs are known to secrete an array of pro-angiogenic growth factors and cytokines, including VEGF, HGF, G-CSF and GM-CSF[56, 93-96]. Thus, two phenotypes have emerged from data regarding the differentiation of the EPC; one which integrates into the endothelium and another that takes residence immediately around the vessel and provides paracrine signals to nearby ECs[56, 91, 95, 97]. In the second of these situations, early EPCs act similarly to monocytes/macrophages, which can increase arteriogenesis by providing cytokines and growth factors[98-99], further fuelling the hypothesis that early EPCs represent a subset of 'angiogenic monocytes'. However Urbich *et al*[62] demonstrated that an infusion of macrophages did not incorporate into vessel-like structures and induced only a slight increase in neovascularisation after ischaemia, indicating that the capacity of EPCs to physically contribute to vessel-like structures may contribute to their capacity to improve neovascularisation. In contrast to early EPCs, late EPCs are thought to enhance neovasculogenesis by providing a sufficient number of ECs to allow for structural integration into new vessels[88]. Interestingly, evidence suggests that co-transplantation of both early and late EPCs results in enhanced neovascularisation *in vivo* compared to that achieved using single-cell-type transplantation as these cells can act in synergy during vascular repair[100].

Indeed, vessel formation involves multiple additional cell types other than ECs. Arguably the most important of these are the mural cells (or pericytes) which commonly originate from mesenchymal cells, surround the surface of the blood vessel and are associated with vessel stabilisation, haemodynamic processes as well as having a direct role in vessel formation via a complex communication with ECs (reviewed in[101]). The importance of cell–cell interactions in the development of mature vasculature is further demonstrated by several studies in which the transplantation of endothelial lineage cells alone was not sufficient to produce a stable vascular network. The newly formed vessels tended to show minimal perfusion and rapidly regressed[102-103]. Furthermore, although the potential of EPCs to form functional vascular networks *in vivo* has previously been reported many times, more recent reports show that to obtain stable and durable vessels co-implantation with perivascular-like cells is required[104-105] and MSCs are currently championed as the most appropriate clinical source of these cells[106-107].

1.5.3. Molecular Mechanisms Controlling the Mobilisation and Homing of EPCs

In the BM the majority of EPCs remain quiescent within the 'stem cell niche'[108]. This microenvironment governs the maintenance and mobilisation of stem cells, which are bound to stromal cells by integrins. Although the exact mechanisms of cellular mobilisation are not completely understood many contributing factors have been identified and the process is thought to be regulated by complex crosstalk between a myriad of cytokines/chemokines, growth factors, proteinases and cell adhesion molecules. Mechanistically, mobilising cytokines/chemokines or growth factors interfere with interactions between stem and stromal cells permitting the stem cells to leave the BM via transendothelial migration[94]. This process is mediated by the activation of proteinases such as elastase, cathespin G and matrix metalloproteinases (MMPs), which cleave cellular adhesive bonds[94] between stem and stromal cells. MMP9 has been shown to cleave the membrane-bound Kit ligand (mKitL) and induce the release of soluble KitL (sKitL or stem cell factor (SCF)), which is known to promote the proliferation and motility of stem cells within the BM[109].

Physiologically, vascular trauma and ischaemia are believed to be the predominant events inducing EPC mobilisation[94, 110-111] and have been associated with the upregulation of SDF1 (CXCL12)[112-113] and VEGF[76], which enter the circulation and induce mobilisation and homing of EPCs from the BM via a MMP9-dependent mechanism. The SDF1/CXCR4 axis has an important role in stem cell retention within the BM niche as well as mobilisation and migration to sites of injury (reviewed in[114]). The crosstalk between EPCs expressing CXCR4 (the predominant receptor for SDF1) and BM stromal cells expressing SDF1 is thought to be involved in stem cell retention, whereas the release of SDF1 by damaged or ischaemic tissues induces EPC mobilisation and homing. Therefore it appears that both cleavage of SDF1 within the BM, to disrupt the adhesive bonds between EPCs and stromal cells, and increased circulating levels of SDF1 are required for EPC mobilisation. Such that SDF1 over-expression by adenoviral vector delivery augmented circulating EPC levels in murine models[115], whereas fucoidan (a drug which displaces SDF1 bound to BM endothelium and extracellular matrix (ECM)) resulted in mass egress of $CD34^+$ EPCs from the BM[116]. VEGF acts in a similar chemotactic manner to SDF1; it is also produced by damaged/ischaemic tissues

and is thought to direct EPCs to sites of injury. In experimental models increasing VEGF levels enhances circulating levels of EPCs[76, 117], while in patients with peripheral vascular disease EPC expansion and motility were promoted following VEGF gene transfer[73, 118]. Interestingly it appears that VEGF and SDF1 are interdependent with VEGF up-regulating the SDF1/CXCR4 axis and SDF1 is more potent when infused with VEGF-A implying that these cytokines act synergistically[119]. Additional factors shown to enhance levels of circulating EPCs in both human and animal studies include erythropoietin[120], GM-CSF[71], angiopoietin-1[115, 117], IL8[121-122] and physical exercise[123].

Pharmacologically, HMG-CoA reductase inhibitors (statins) have been shown to elevate the levels and functional activity of EPCs *in vitro* and *in vivo*[124-125]. This was confirmed by the demonstration that statins augmented the incorporation of BM mobilised EPCs into foci of corneal neovascularisation[124]. Similarly, the anti-diabetic and anti-inflammatory peroxisome proliferator-activated receptor-γ (PPAR-γ) agonists promote differentiation and mobilisation of BM-derived angiogenic progenitor cells and improve re-endothelialisation after vascular injury[52]. Angiotensin converting enzyme inhibitors and angiotenisin II receptor antagonists have also been shown to be beneficial in the mobilisation of EPCs[126-127].

Several studies indicate that the activation of the PI3K/Akt pathway plays a role in the statin-induced augmentation of EPC levels[125, 128]. Additionally SDF1, VEGF, EPO and exercise are also known to augment the PI3K/Akt pathway[129-132]. Akt1 inhibits cellular apoptosis and stimulates endothelial nitric oxide (NO) synthesis by endothelial nitric oxide synthase (eNOS), which has been shown to be essential in maintaining adequate progenitor cell mobilisation in response to distinct stimuli including VEGF, statins and exercise[130-131, 133]. Therefore the activation of Akt appears to promote phosphorylation of eNOS, increasing endothelial NO production and hence EPC growth and migration[94]. Thus it seems apparent that although the mechanisms governing EPC mobilisation are complex, several of the contributory factors may share signalling pathways.

1.5.4. Therapeutic use of EPCs: Clinical Trials using Adult Autologous Cell Therapy to Treat Ischaemic Heart Disease

Following encouraging pre-clinical studies suggesting that stem cell treatment can dramatically improve cardiac function following ischaemic injury (see section 1.5.2), autologous BM cell transplantation has rapidly been introduced into the clinical setting. Initial phase 1 trials showed that this technique was safe, feasible and overall demonstrated a beneficial effect on ventricular function[134-136]. Subsequently, a number of small randomised and controlled trials have been performed. In most studies unselected BM- or PB-MNCs have been injected either into the circulation supplying the ischaemic region or directly into the damaged tissue, however conflicting results have been reported.

Schächinger *et al*[137] published the results of the 4 month REPAIR-AMI trial (multicenter, double-blind and fully controlled) and revealed that following BM cell infusion, the absolute improvement in ventricular function was greater amongst cell-recipient MI patients than those given placebo. Subgroup analysis also suggested that the benefit was greatest in those patients with the largest infarcts. Furthermore, a reduction in death, recurrence of MI and re-hospitalisation was observed at 12 months[137-138]. These findings provide evidence of the beneficial effects of BM cell transplantation after acute MI, however enthusiasm was somewhat restrained due to the modest size of the effect (approximate 5.5% increase in left ventricular ejection fraction (LVEF) in cell-recipient group). Furthermore, the longer term results of the BOOST trial showed that the relative improvement in ventricular function after infusion of BM-MNCs observed at 6 months was no longer significant at 18 months suggesting that the controls eventually "caught up" with the treated group and that the predominant effect of the cells was an acceleration of recovery[139-140]. The smaller ASTAMI trial did not detect a significant improvement in ventricular function in the BM cell group at 6 months as compared with the control group[141]. Technical differences in the characteristics or handling of the infused cells might explain the different outcomes between trials, for example the ASTAMI trial injected $7x10^7$ ficoll separated BM-MNCs into patients compared to $2.4x10^8$ of the same cell type used in the REPAIR-AMI trial. However, Janssens *et al*[142] also failed to report an improvement in global ventricular function in patients who received infusions of BM-MNCs as compared with

the control group at 4 months, although infarct size was reduced and regional wall motion was improved in the BM cell treated group.

The heterogeneous cell populations used during BM cell infusion may help explain why apparently similar protocols can yield contrasting results. Identifying which of the cellular constituents is necessary for beneficial effects, and whether these effects are mediated directly by the transplanted cells or indirectly through involvement of other cells, would enable targeted delivery of essential components and is a likely critical step in the optimisation of this therapy. Furthermore, it may be that unselected BM-MNCs do not represent the ideal cell population to treat cardiovascular disease and that greater efficacy could be realised by the delivery of a more defined cell type. However to date $CD34^{+143-144}$ and $CD133^{+145-148}$ selected MNCs have not resulted in greater benefit than unselected cells in the few clinical trials that have adopted this approach and importantly one study has linked $CD133^{+}$ cell infusion with an increase in adverse coronary events following acute MI[149]. It remains unknown whether marker-based selection of cardiac repair cells will increase their efficacy and further investigation is required. Also of interest, the TOPCARE-AMI trial compared the efficacy of cultured circulating progenitor cells and freshly isolated BM mononuclear cells. Both cell types led to a similar small but significant increase in LVEF (approximately 10%), improved regional wall motion in the infarct zone and reduced end-systolic left ventricular volumes at 4 months[150]. In addition Assmus *et al*[151] evaluated the effects of BM and PB progenitor cells in patients with chronic ventricular dysfunction in the TOPCARE-CHD crossover trial. The absolute change in ventricular function was significantly greater among patients receiving BM cells than among those receiving circulating progenitor cells. The groups received the other type of cell in the next phase of the trial, but the result was independent of the order in which the cells were given, suggesting that the superior effect of BM-derived cells is specific.

Despite conflicting reports, recent systemic reviews and meta-analyses of randomised studies summarising data from over 1000 patients have revealed a significant, albeit moderate, improvement in LVEF, infarct size and end systolic volumes (ESV) post MI following cell treatment (in addition to conventional treatment)[134-136]. Overall, these analyses concluded that stem cell treatment for acute MI still holds promise and the data suggests that improvement over conventional therapy can be achieved. Furthermore,

subgroup analysis revealed that there was a significant difference in LVEF in favour of BM cells when they were infused within 7 days following acute MI and when the cell dose administered was higher than 10^8 cells, thus highlighting the numerous factors that need to be considered to optimise this therapeutic approach[135] (figure 1.4).

Critically, several possible concerns have arisen regarding the role and risks of cell based therapies. Whereas the regeneration of the endothelium by EPCs protects against lesion formation, BM-derived progenitor cells may also contribute to plaque angiogenesis thereby promoting plaque instability[152]. Additionally, EPCs have been implicated in tumour neovascularisation and thus are being considered as novel targets for anti-angiogenic therapies (reviewed in[153]). Furthermore, several 'unknowns' have been identified during the clinical translation of cell-based therapy for cardiovascular disease, these include; the source and subtype of cells, preparatory methodology, the time at which cells are administered, the route by which they are given, the number of cells transplanted, the volume given and outcome measurement (figure 1.4). The task force of the European Society of Cardiology propose that the clinical need, feasibility, and safety of the treatment as well as the need to resolve discrepant results mandate larger, adequately powered trials using optimal dosing, longer term outcome assessments, and more patient-centred outcomes[154]. The field will also be further advanced by simultaneously attempting to elucidate the mechanisms underlying physiological improvements observed with cell transplantation through basic research. This can help guide clinical investigation by encouraging future work and also introduce more pragmatic approaches to demonstrating clinical efficacy[154].

In summary, despite the positive preliminary clinical evidence for patient benefit from EPC therapy, the rapid transfer from 'bench to bedside' has meant patients are being given a therapy about which very little is known. It is important to rectify this knowledge gap and to elucidate the true identity of EPCs as well as the mechanisms responsible for modulating EPC function, which may lead to improved therapeutic strategies. Also, additional larger multicenter and controlled trials are needed to evaluate the clinical effect of this therapy in the longer term, to deduce optimal dosing regimes and to address other identified uncertainties including route and timing of delivery[154] (see figure 1.4).

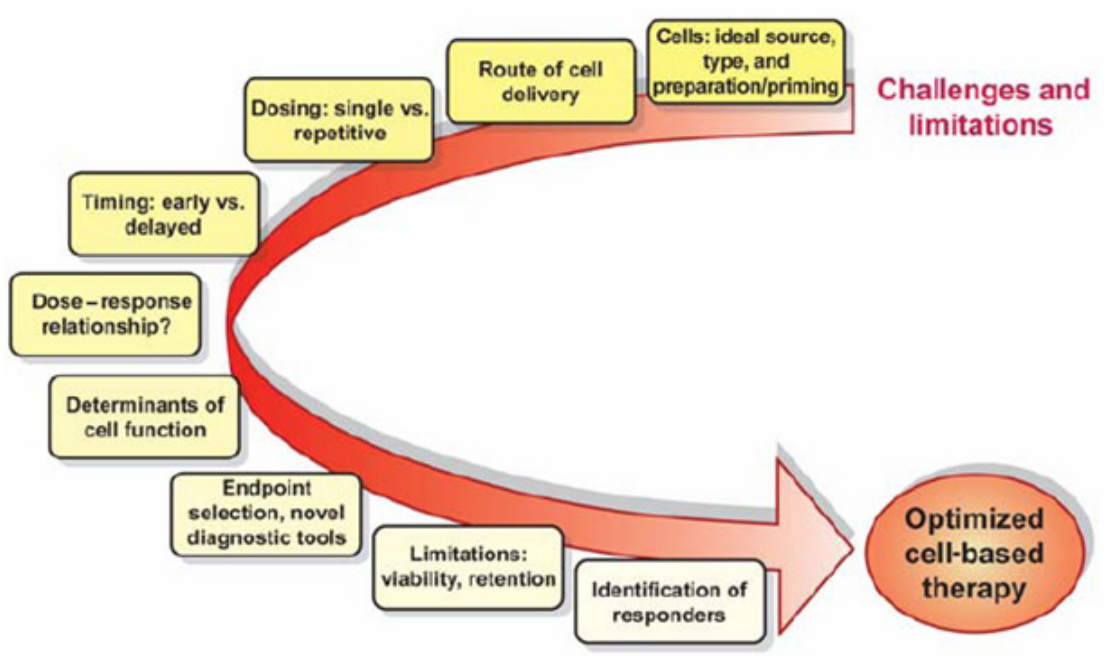

Figure 1.4. A summary of the outstanding challenges, limitations and open questions that remain to be addressed for the optimisation and clinical translation of stem cells for therapeutic angiogenesis following MI. Figure from [155].

1.6. Cardiac-derived Stem Cells for Therapeutic Repair

Until recently the adult heart was considered a terminally differentiated organ without the ability to regenerate. However the discovery of antigenically distinct cardiac-resident stem/progenitor cell populations (CSCs) has challenged this prevailing dogma. CSCs have been shown to retain the capacity to differentiate into and repopulate the three major cardiovascular cell lineages: cardiomyocytes, endothelial and smooth muscle cells both *in vitro* and *in vivo*[156]. CSCs are presumed to function physiologically to offset a low rate of cardiac cell loss over time. However, the number of CSCs in the adult heart is thought to be relatively low and quantitative data from mouse, rat, dog, and human studies have estimated that there is 1 CSC per approximately 30,000 to 40,000 myocardial cells[156]. Such a low presence may offer an explanation as to why endogenous repair mechanisms are insufficient to reverse major injury, such as after acute MI. Furthermore, it has been observed that within one day of MI up to 40% of resident CSCs are depleted[157] and it may be speculated that ischaemic injury may limit the proliferation and self-renewal of remaining CSCs, thereby precluding restoration of the stem/progenitor cell pool and preventing myocardial repair. Therefore, there has been a great effort to try to identify and expand CSC populations *ex vivo* with a view to define and harness their therapeutic potential. CSCs have been identified in many

species including humans, although they were initially identified in rodents by their expression of stem cell-related markers, including c-Kit (CD117, the receptor for stem cell factor), and Sca-1 (stem cell antigen-1), as wells as displaying other phenotypic properties such as those attributed to progenitor side populations (ability to efflux Hoechst dye and expression of Abcg2) and expression of the embryonic-related cardiac progenitor islet-1 (reviewed in[156]). Several studies have isolated and expanded CSCs exclusively based upon the expression of stem cell related antigens (e.g. $cKit^+$ or Sca-1) and have further demonstrated the ability of these sub-populations to attenuate heart damage in rodent models (reviewed in[156]) although it is undetermined whether these different CSC sub-types have clearly distinct phenotypes. In addition to CSC isolation and expansion based on antigen expression, CSCs have also been identified by their ability to form spheres following *ex vivo* 3D culture of myocardial tissue. This method of CSC isolation and expansion was employed in this thesis and will now be discussed in more detail.

1.7. Cardiospheres and Cardiosphere-derived Cells

1.7.1. Isolation and Characterisation of Cardiosphere-derived Cells

In 2004 Messina and colleagues[158] observed that cardiac surgical biopsy specimens yielded an outgrowth of cells when cultured as explants *ex vivo.* Once subjected to a second phase of suspension culture, these explant derived cells (EDCs) spontaneously formed spherical cell clusters that were shown to be progenitor rich aggregates containing sub-populations of cKit and Sca-1 positive cells. These spherical structures were termed 'cardiospheres' (Csphs) in analogy to the observation that neural stem cells can be expanded from primary tissue as self-assembling spherical aggregates dubbed 'neurospheres'. Following this discovery, Eduardo Marban's laboratory proceeded to slightly modify the original protocol by introducing a post-cardiosphere expansion stage to advance this cell type towards clinical translation[159]. Cardiospheres were plated and expanded as a monolayer of cardiosphere-derived cells (CDCs) to achieve therapeutically relevant cell numbers in a timely manner from relatively small amounts of starting tissue (percutaneous right ventricular endomyocardial biopsy specimens, approximately 10-40mg)[159]. Cardiospheres generated in their study consistently expressed cKit, endoglin (a TGFβ family regulatory receptor discussed further in

section 1.9.3) and the gap junctional protein connexin 43 as well as staining positive for Ki67 within the core of the sphere indicating proliferating cells. Following *in vitro* CDC expansion, the majority of cells at passage 2 were endoglin positive (>95%), with significant sub-populations also expressing cKit (~20%), CD90 (~40%), CD34 (~5%) or CD31 (~10%), whilst being largely negative for CD45 and blood lineage markers. Thus as well as stem cells, CDCs also appear to contain sub-populations that resemble mesenchymal cells or fibroblasts ($CD90^+$, $endoglin^+$) and endothelial cells ($endoglin^+$, $CD31^+$, and $CD34^+$).

Since this first study describing and characterising the derivation of CDCs from cardiac tissue the Marban group have further characterised CSph and CDC properties[160-162] and many independent laboratories have reproduced and verified the Csph and CDC phenotype[163-167]. Furthermore the Csph/CDC method of CSC isolation has been reported in many animal species including mouse[158, 166], rat[161-163], dog[164, 168] and pig[169-171] and has also been successful with biopsies from chronic heart failure patients[159] as well as those with congenital heart defects[172].

However, other studies have challenged the cardiac explant and Csph culture method for isolating and enriching cardiac resident stem cells, claiming that resultant cell populations do not represent progenitor/stem cells but rather are blood-borne derived cells, without multi-lineage differentiation potential or clonogenic capacity[173-174]. Detailed rebuttals of these critical works refuted these claims and attributed their findings to significant technical and methodological deviations in cell culture techniques[175-176]. The Marban group went on to confirm that EDCs, Csphs and CDCs represent a complex heterogeneous population of cells with clonogenic and multilineage potential (cardiomyocyte, smooth muscle and endothelial). Furthermore, they demonstrated consistently that both EDCs and cardiospheres contain cKit positive sub-populations, whilst uniformly staining negative for markers of haematological lineages, CD45 and the mast cell marker AA4. In contrast, Anderson *et al*[174] postulate that cardiospheres consist predominantly of fibroblasts as well as blood-borne cells. It is generally accepted that a significant sub-population of CDCs do express the mesenchymal marker CD90, which is also found on fibroblasts. However, Carr *et al*[163] found that less than 10% of CDCs expressed the fibroblast-specific marker DDR2. In addition, both of the papers critiquing cardiospheres as a source of stem cells[173-174]

failed to identify a cKit positive population in their cell populations. This important difference suggests that Anderson *et al*[174] were indeed characterising a cell population distinct to that described by Marban and others, rendering comparisons difficult. However comparing these studies does imply that even slight technical deviations in culture methods can have significant consequences on the marker profile of CDCs. This is an important consideration in preparing these cells for future heart repair studies.

Another matter that is currently debated is the true origin of cardiac resident stem cells. It has been suggested cKit$^+$ progenitor cells within the heart are actually derived from extra-cardiac tissue and as such have been described as BM cells 'out of place'[177]. This follows a study by Massberg *et al*[178] showing that cKit positive cells leave the BM in small numbers to scavenge pathogenic molecules in peripheral tissues, including the heart, as part of a local innate immune response. Furthermore in human heart transplant patients, recipient derived cardiomyocytes and ECs have been observed within the donor heart suggesting that circulating stem cells may migrate into the myocardium[179], although it has also been suggested that host stem cells may simply have migrated from residual atrial tissue into the donor heart[156]. Still, a study of patients receiving allogeneic BM transplantation revealed that at least 2-5% of cardiomyocytes were chimeric indicating that circulating cardiac committed cells are able to reach the myocardium[180]. Conversely, using retrospective clonal analysis in mouse, Eberhard *et al*[181] show the intracardiac origin of adult myocytes and do not support the notion of an influx of stem cells with cardiogenic capacity into the adult heart, at least under physiological conditions. Their study, however, does not discount the presence of circulating stem cells in the heart, just their ability to develop into cardiomyocytes and the authors do concede that the effect of pathological insult, such as acute MI or heart transplantation, may trigger a mass influx of BM-derived stem cells with multi-lineage potential. In relation to the preparation of cardiosphere cultures, White *et al*[182] have recently shown that endogenous CDCs have no detectable extra-cardiac contribution using short-tandem nucleotide repeat testing, fluorescence in situ hybridization and Q-PCR in cells cultured from heart transplant patients. However sample sizes in this study were small (n=2 to 10) and none of the hearts were known to be affected by ischaemia which may be required for extra-cardiac derived stem cell re-population of the heart. Consequently, Barile *et al*[156] have shown that in an ischaemic setting BM-derived cKit positive stem cells do migrate into the heart. In this study GFP-expressing donor BM cells were

transplanted into WT irradiated recipient mice and following haematological reconstitution and experimental MI, cardiospheres were cultured from recipient mouse cardiac tissue. The majority of these spheres contained GFP positive cells thus suggesting that under pathological conditions circulating cKit positive cells are able to populate the heart. In conclusion the true origin of stem cell sub-populations residing in the heart is still being debated and extensive *in vivo* lineage tracing will be required to resolve this issue. Whilst there is strong evidence suggesting that the heart may become enriched for BM-derived stem cells following injury, this does not exclude the possibility that adult stem cells of intrinsic cardiac origin do exist. Regardless of their specific cellular origins, it is the ability of these cells to contribute to endogenous cardiac repair that should remain the focus of ongoing studies. Indeed, it may be that the migration and residence of BM-derived stem cells in the heart following injury primes them to promote superior cardiac repair over that achieved by transplanting stem cells isolated directly from the BM.

When prepared correctly CDCs are a heterogeneous mix of cells which express multiple markers of stem/progenitor (cKit, Sca-1, CD34 and endoglin), endothelial (CD31, vWF and endoglin), cardiac (troponin1, α-sarcomeric actin, connexin-43) and mesenchymal (CD90, endoglin, DDR2) cells (refer to table 1.1 for references). In addition, CDCs are clonogenic and exhibit multilineage differentiation potential (cardiomyocyte, endothelial and smooth muscle cells)[158, 175] thus fulfilling key criteria for cardiac stem cells. Furthermore, cardiospheres and CDCs derived from adult tissue have been shown to express cardiac transcription factors (Nkx2-5, GATA-4 and islet-1)[159, 163, 172, 183], which are crucial markers of cardiac progenitor cell state in foetal hearts, as well as pluripotency markers (Oct3/4, sox-2 and nanog)[160, 163].

Three-dimensional (3D) culture is known to maintain embryonic stem cells in an undifferentiated state[160]. Although this technique has not been well studied in adult stem cells the rationale for including a 3D cardiosphere stage in the generation of a CSC population *ex vivo* is the postulation that sphere culture encloses a mixed population of cells which, as in the stem cell niche, could promote the viability and proliferation of stem cell sub-populations[184]. Similarly it is the hypothesis of Marban *et al*[159] that a mesenchymal cell sub-population within CDC expansion culture may serve to provide physical or secretory support to cKit positive progenitor cells.

Li *et al*[160] tested the hypothesis that growing human cardiac EDCs as 3D cardiospheres recapitulates a stem cell niche-like microenvironment favouring cell survival by comparing cardiospheres with EDCs cultured under traditional monolayer conditions. As previously demonstrated, EDCs self-assembled into spherical stem cell niche-like structures *in vitro* and immunostaining revealed that these cardiospheres consisted of centrally localised cKit positive cells surrounded by cells expressing collagen IV and endoglin[160]. Thus architecturally, cardiospheres resembled *in vivo* stem cell niches, where central stem cells are bound together by supporting cells and linked by interactive ECM molecules[185]. Li *et al*[160] also showed that cKit$^+$ cells were significantly increased in cardiosphere cultures relative to baseline EDC levels (16.9%±2.1% vs. 9.1%±0.7%, $p<0.01$), whereas when EDCs were expanded directly as a monolayer the proportion of cKit positive cells markedly declined (5.2%±1.0%, $p<0.01$ vs. baseline). Furthermore, Q-PCR and immunostaining revealed the increased expression of many stem cell-related factors in cardiosphere cultures as compared with monolayer expanded EDCs. These factors included (i) transcription factors (Nanog and Sox2), (ii) proteins associated with stem cell growth and maintenance of a stem-like undifferentiated state (including IGF-1, HDAC2 and Tert) and (iii) ECM and adhesion molecules (such as collagen IV and MMPs). Additionally, in response to oxidative stress, apoptosis was blunted in cardiospheres in comparison to monolayer cultured cells[160]. Therefore this study concluded that compared with traditional monolayer culture, the formation of cardiospheres augments the "stemness" profile of cells and enhances the expression of many ECM and adhesion molecules. The authors suggest this may be attributed to a recreation of a stem cell niche-like microenvironment and HDAC2-mediated epigenetic modification. However, it should be noted that although it is suggested that 3D cardiosphere culture acts to enrich a CSC population the formation of spheres in culture is not a feature specific to stem cells as other terminally differentiated cells (such as fibroblasts) have also been found to form spherical structures under cardiosphere culture conditions[167, 174].

Despite evidence from the Marban laboratory pointing to the high stem cell content and efficacy of cardiospheres in heart repair[160], another study from the same group advocated the use of EDCs for myocardial repair directly thus avoiding the time taken for cardiosphere formation or CDC expansion[162]. Here the authors characterised EDCs and identified markers of cardiac progenitor cells (Abcg2, cKit and SSEA-1) in cells

derived from rat atrial and ventricular tissue using RT-PCR. Two distinct cKit sub-populations were identified defined by the co-expression of either Abcg2 (a side population marker) or SSEA-1 (a marker of embryonic origin). It is standard practice in many studies to repeatedly harvest EDCs from cardiac tissue explants. Interestingly this study showed a peak of cKit expression at the third harvest (~12%). A small population of SSEA-1 expressing cells peaked at harvest 1 at 1.0±0.1% and was undetectable by the final harvest. In contrast, the proportion of cells expressing Abcg2 increased during culture (harvest 5: 7±1%). EDCs also showed constant expression of the mesenchymal marker CD90 (~30%) as well as small sub-populations expressing endothelial markers that declined with progressive time in culture (harvest 1: $CD31^+$ 3.2±1.2%, $CD34^+$ 3.1±2.9%; harvest 5: $CD31^+$ 2.2±0.5%, $CD34^+$: 2.4±0.3%). Minimal co-segregation was evident between stem cell markers and those of mesenchymal and endothelial lineages. EDCs were negative for the markers Sca-1 and Isl-1 as well as markers of haematological origin (including CD3, CD11b, CD45) and mast cell lineage ($AA4^+$).

The *in vivo* repair capacity of EDCs, cardiospheres and CDCs will be discussed below.

1.7.2. Cardiosphere and CDC-Mediated Cardiac Repair; Pre-Clinical Models

In their original study Messina *et al*[158] showed that cardiosphere transplantation in a mouse model of experimental MI successfully contributed to attenuated adverse LV remodelling as evidenced by increased anterior LV wall thickness and fractional shortening. Since this time, many studies have shown that EDCs[162, 166], cardiospheres[158, 160, 186] and CDCs[159, 161, 163, 169, 172, 187] are able to improve heart function in pre-clinical mouse[158-160, 166, 187], rat[161-163, 172, 186] and pig models[169, 171] of heart injury (selected studies are summarised in table 1.1). Taken together these studies predominantly demonstrate that cell transplantation results in increased LVEF and improved haemodynamic function. Of particular interest is the efficacy of the distinct cell populations identified at each of the 3 stages that make up the cardiosphere culture method: EDCs, cardiospheres and CDCs. As discussed above the 3D cardiosphere structure is thought to recreate a stem cell niche-like environment, favouring stem cell survival as well as improving functional benefit *in vivo*. Several studies have borne this proposal out in direct comparisons between cardiospheres and CDCs. Using the mouse

MI model Li *et al*[160] have shown that implantation of human cardiospheres into infarcted mouse hearts disproportionately enhances cardiac function relative to dissociated cardiospheres cultured as monolayers of CDCs (LVEF; 15% versus 10% increase over vehicle only recipient controls). Furthermore, in a mini-pig model of cardiomyopathy either cardiospheres or CDCs were delivered to animals via intramyocardial injection 4 weeks following MI. While both cell treated groups showed an equivalent increase in LVEF relative to placebo controls 8 weeks after treatment, those animals receiving cardiospheres showed superior haemodynamic function and a greater attenuation of adverse remodelling than CDC recipients[169]. Despite these observations the benefit of CDC monolayer culture over cardiospheres lies in the significantly faster proliferative rate of these cells (3-fold versus 1.2 fold increase after 7 days)[160], leading to therapeutically relevant cell numbers being produced in a timely manner. Additionally, cell transfer in the clinic tends to be via the less invasive percutaneous catheter based intracoronary route which is simple and safe, but due to the relatively large size of cardiospheres (50 to 200μm in diameter) intracoronary infusion runs the risk of embolising blood vessels therefore direct intramyocardial injection would be necessary[169]. However, Johnston *et al*[170] report that the larger size of human CDCs relative to BM-MNCs (20.6±3.9μm versus 8.6±1.8μm) also poses a risk to microvascular occlusion given that the average capillary luminal diameter is 7-10μm. More importantly, the authors associated this risk with the observation of microinfarction in dogs receiving MSCs (similar size to CDCs at 21.0±3.3μm) via intracoronary delivery (myocardial ischaemia observed in 2/6 animals)[188]. Therefore precautions were taken to limit risk in their porcine study[170]. They found that 100U/ml heparin in the cell suspension sufficed to eliminate cell-related thrombus formation. In animals receiving catheter-based intracoronary CDC delivery 4-weeks post MI, in the optimised infusion solution, troponin levels were measured after 24 hours. Interestingly troponin I remained within normal limits (<0.5ng/ml) following transplantation of $<2.5x10^7$ CDCs indicating safe infusion without thromboembolic complication. However greater cell doses raised troponin levels in a dose-dependent manner, likely due to micro-infarction. This study defined a safe dosage range for future clinical trials (discussed in section 1.7.4).

CDCs and EDCs were shown to be equivalent in their capacity to improve cardiac function following MI in a rat model[162]. Clinical use of EDCs directly (i.e. without

subsequent cardiosphere stage) is an attractive option as it would improve production efficiency as well as limit the possibility of culture-associated phenotypic drift or cancerous transformation. However, a conflicting report failed to demonstrate any beneficial effect of EDCs *in vivo*[189]. Additionally cKit-positive lineage-negative EDCs have been shown to increase LVEF by only 8% over controls when delivered into infarcted mouse hearts[166] whereas several Csph/CDC studies show increases in LVEF (over controls) in the region of 15%[159-161, 187]. These studies are summarised in table 1.1 and possible reasons for variable outcomes are discussed further below.

Similar to studies addressing BM-derived cell transplantation in heart injury models and their subsequent inferences regarding primary functional mode of repair, it has been noted that the number of engrafted cells following Csph/CDC delivery into ischaemic hearts is too low to account for the observed improvements in cardiac improvement[160, 163, 187] – see also table1.1. Therefore there has been a shift towards the 'paracrine hypothesis' to explain the beneficial effect of Csph/CDC delivery, whereby transplanted cells produce soluble factors that are beneficial to the injured heart. Indeed, Chimenti *et al*[187] have shown that human CDC-conditioned media exerts both anti-apoptotic and pro-angiogenic effects *in vitro* and CDCs secrete VEGF and HGF when transplanted into infarcted mouse hearts. In fact, this study claims that paracrine mechanisms account for up to 80% of the observed functional benefit (approximately 15% increase in LVEF relative to fibroblast control group) as opposed to only 20-50% assigned to direct myocardial and/or vascular regeneration (as judged by the number of engrafted human-specific cells). In support of their conclusion the authors also report that injection of CDCs in the peri-infarct zone increases the expression of Akt as well as decreasing the apoptotic rate (judged by activated caspase 3 levels in the heart) indicative of an overall cardio-protective role. In light of these findings it is important to highlight that while significant progressive decline in cardiac function is observed in untreated infarcted hearts, CDC/Csph recipient mice show reduced detrimental progression and therefore exhibit an increased functional capacity in comparison to these control groups; cell transplantation does not improve function over baseline measurements (typically taken 1-3 days following surgery). For example, Smith *et al*[159] describe an ~15% increase in LVEF relative to controls 3 weeks following CDC transplantation ($p<0.05$) however there was no significant change from baseline measurements (2 day since surgery) in these mice. This suggests that the role of the transplanted cells is to promote higher

tissue resilience and attenuate adverse remodelling by limiting fibrosis and increasing capillary density rather than by regenerating the myocardium. This is in agreement with the findings of Chimenti and colleagues[187]. Also of interest is the demonstration by this study that cardiospheres express higher levels of both VEGF and HGF than CDCs in culture and they additionally secrete IGF1[187]. These findings imply that any paracrine contribution of these factors is maximal at the cardiosphere stage, however this was not tested *in vivo*. Delivery of HGF and IGF-1 into a porcine MI model has been reported to activate endogenous cKit positive cardiac stem cells and improve cardiomyocyte survival as well as reducing fibrosis and cardiomyocyte hypertrophy[190], indicating the potential functional importance of the above findings.

Multiple pre-clinical studies have demonstrated the positive effect of CDC/Csph transplantation on *in vivo* cardiac function (see table 1.1). Improved parameters include increased LVEF and haemodynamic function, reduced infarct size, as well as increased fractional shortening, increased viable myocardium within the infarct zone and increased LV wall thickness (table 1.1). However, conflicting reports regarding the efficacy of these cells for heart repair have also arisen. Intracoronary delivery of $3x10^6$ porcine CDCs into pig hearts 8 weeks following balloon occlusion and reperfusion was shown to reduce infarct size and improve haemodynamic function however no difference in LVEF was detected[170]. Furthermore, in another study, Li *et al*[189] showed that injection of *in vitro* expanded EDCs into infarcted mouse hearts did not result in any change in cardiac function, haemodynamics or infarct size. Additionally, wide variation exists between studies reporting functional benefit following cell transplantation. While Chimenti *et al*[187] report a 16% increase in LVEF (measured by echocardiography) at 3 weeks following the injection of 10^5 CDCs into infarcted mouse hearts, Davis and colleagues[162] describe only a 6% increase (measured using cardiac MRI) at 3 weeks following administration of 10^6 CDCs into a rat model of MI. Conflicting reports and variation may be attributable to differences in culture techniques, model species, cell number, delivery route or analysis methods. Interestingly human cardiospheres were shown to increase LVEF and attenuate LV remodelling to a greater extent than spheres derived from rat tissue when both were transplanted into a rat MI model[186]. Additionally, the degree of engraftment and survival of delivered cells may dictate the differences in functional outcome reported by these studies. Indeed, using *in*

vivo bioluminescent imaging Li *et al*[189] showed very poor transplanted cell survival 8 weeks following transplantation.

Expanding this point, it has been demonstrated that irrespective of which cell type or pre-clinical model is used for cardiac repair, the level of functional improvement attained is limited to the level of cell retention. Following delivery into the heart, reported cell seeding efficiencies vary, whilst acute cell retention in many studies is reported to be less than 10%[191]. This represents a major obstacle to the cardiac stem cell therapy field. Survival of transplanted cells is largely dependent upon the status of the host tissue. Therefore, paradoxically, transplantation of donor repair cells into the ischaemic heart may result in large losses due to an inhospitable environment. Furthermore, in addition to cell death, both venous drainage and the mechanical force of the beating heart are proposed to account for a significant loss of donor cells[192]. Poor cell retention would arguably be detrimental to the ability of infused cells to contribute to repair either by direct or paracrine means. Mechanisms that improve functional outcome in pre-clinical models of heart injury with CDC/Csph treatment include co-administration of donor cells with basic fibroblast growth factor (bFGF)[171], preconditioning cells in physiological (5% O_2)[193] or hypoxic (0.1% O_2 for 6 hours)[166] conditions as well as magnetic targeting of cells to the infarct zone[161] and application of a fibrin glue seal over the intramyocardial injection site[194]. These measures were all found to significantly improve cell survival and retention and positively correlated with an improvement in cardiac function. The significance of these studies lies in the demonstration that additional interventions/mechanisms may be employed to improve the efficacy and outcome of cardiac stem cell therapy.

In summary both Csphs and CDCs are able to improve cardiac function following transplantation into pre-clinical models of heart injury, including clinically relevant large animal models of myocardial infarction. Despite this generally consistent finding, several conflicting reports do exist which call into question the degree of efficacy of these repair cells and highlight the importance of recognising variations between studies, especially methodological differences with respect to CSC isolation. Furthermore the beneficial effect of cell therapy may be improved via a number of modifications that target donor cell survival and retention *in vivo*. In addition, several studies suggest that cardiospheres confer an improved functional benefit over

monolayer expanded cells. The mechanisms underlying the superiority of cardiospheres over CDCs have been postulated as (i) an increase in cKit expressing cells in 3D culture with a concurrent up-regulation of stem cell related genes, (ii) higher levels of growth factor secretion and (iii) an enhanced resistance to oxidative stress over monolayer cultured cells. In addition, increased retention and engraftment *in vivo* has been proposed to be due to the increased expression of ECM proteins by cardiospheres[160]. It is clear that further work is required to determine if the cardiosphere culture stage is required or indeed if it offers any advantage over expanded CDC monolayers. Nevertheless, significant proof of principle has been demonstrated and CSC therapy has now moved towards clinical translation, this will be discussed in greater detail in section 1.7.4.

Cell Type & Source	Markers	Study Details	Cell Engraftment	Cardiac Function	Angiogenic Response	Ref
EXPLANT-DERIVED CELLS (EDCs)						
Rat EDCs (versus CDCs)	SSEA1, cKit, abcg2, CD90, CD31	Rat: acute MI Peri-infarct I/M injection (~10^6 cells/mouse) 6 weeks; cardiac MRI; n=6-8 (fibroblast control)	EDC engraftment (not quantified)	↑ LVEF: (EDCs & CDCs: (+) ~6-8% vs fibroblast) ↓LVEDP:(EDCs & CDCs:(-)~2mmHg vs fibroblast) ↑ Contractility	*In vitro*: EDCs & CDCs formed tubules on Matrigel	162
Mouse ckit+lin- EDCs	Not Determined	Mouse: acute MI Tail vein infusion (10^6 cells/mouse) 28 days post injection; Echocardiography	EDC engraftment (not quantified)	↑ LVEF: ((+) ~8% vs vehicle controls) ↑Fractional shortening: ((+)~5% vs vehicle controls) ↓ Infarct size: ((-) ~15% vs vehicle controls)	↑ peri-infarct capillary density ((+) ~36% vs controls) vWF+ engrafted donor cells	166
CARDIOSPHERES (Csphs)						
Human Cshps	CD34, cKit, CD31, Sca1	Mouse: acute MI Peri-infarct I/M injection (~10 spheres/mouse) 18 days; echocardiography; n=3-6	Csph engraftment (not quantified)	↑ Infarcted anterior wall thickness ↑Fractional shortening: ((+) ~ 2-fold vs vehicle controls)	*In vivo*: neovessels containing aSMA+ and CD31+ engrafted donor cells (not quantified)	158
Human and Rat CSphs (sheet form)	cKit, αβMHH, cardiac Troponin, vimentin, SMA, vWF	Rat: acute MI 3 weeks: LV pressure-volume loops	<10% engraftment at day 21	↑ LVEF: (Rat: (+) ~19%; Human (+) 28% vs controls) ↓ ESV and EDV	↑ capillary density ((+) ~100% vs controls) vWF+ engrafted donor cells	186
Human Cshps (versus CDCs)	cKit, endoglin, collagenIV	Mouse: acute MI Peri-infarct I/M injection, ~10^5 cells/mouse 21days; echocardiography; n=7-11	Csph: 1.69%±0.70% CDC: 0.41%±0.25% (% area)	↑ LVEF: (Csphs: (+) ~15% vs vehicle controls; CDCs: (+) ~10% vs vehicle controls) ↓ LV adverse remodelling (Csphs>CDC)	vWF+ engrafted donor cells identified, not quantified	160
CARDIOSPHERE-DERIVED CELLS (CDCs)						
Human CDCs	cKit, Endoglin, CD90, CD31, cardiac Troponin, Connexin 43	Mouse: acute MI Peri-infarct I/M injection, ~10^5 cells/mouse 21days; echocardiography; n=7-11 (fibroblast control)	CDC engraftment (not quantified)	↑ LVEF: ((+) ~15% vs controls) ↑ Viable tissue: ((+) ~1.4-1.8-fold vs controls)	vWF+ engrafted donor cells identified, not quantified	159
Human CDCs	Not Determined	Mouse: acute MI Peri-infarct I/M injection (10^5 cells/mouse) 21 days; echocardiography; n=>3 (fibroblast control)	CDC engraftment (not quantified)	↑ LVEF: ((+) ~16% vs controls) ↑ Viable tissue: ((+) ~1..2 fold vs controls)	↑ neo-angiogeneis: ((+) ~50% infarct border capillary density; ~20% of neo-vessels contain human cells)	187
Rat CDCs	cKit, CD90, CD31	Rat: acute MI Peri-infarct I/M injection (10^6 cells/mouse) 21 days; echocardiography; n=9-12	24hour: 20% retention 21days: 2% retention	↑ LVEF: ((+) ~15% vs vehicle controls; (+)~20% with magnetic targetting)	vWF+ engrafted donor cells identified, not quantified	161
Pig CDC	Not Determined	Pig: Cardiomyopathy (4 weeks post MI) Intracoronary infusion (300,000 cells/kg) 8 weeks; Cardiac MRI; n=7	Low, not quantified	(-) LVEF ↓ infarct size ↑ Haemodynamic function	Engrafted cells identified lining arteriole	170
Pig CDCs (vs Csphs)	Not Determined	Pig: Cardiomyopathy (4 weeks post MI) Peri-infarct I/M injection (x10^7 cells/pig) 8 weeks; Ventriculography, echocardiography; n=5-9	CDC engraftment (not quantified)	↑ LVEF: (CDCs & Csphs: (+) ~8% vs vehicle controls) ↑ Haemodynamic function: (Csphs>CDCs)	Not Determined	169
Human CDCs (neonate–2 years)	cKit, CD90, Endoglin, Connexion43, NKX2-5, α-Sarcomeric actin,	Rat: acute MI Peri-infarct I/M injection (10^6 cells/mouse) 28 days: echocardiography; n=4-6 (fibroblast control)	CDC engraftment (not quantified)	↑ LVEF: ((+) ~11% vs fibroblast controls) ↑Fractional shortening: ((+)~3% vsfibroblast group) ↑ viable tissue: ((+) ~1.4 fold vs fibroblast controls)	*In vivo:* vWF+ engrafted donor cells identified, not quantified *In vitro*: EC differentiation (CD31)	172
Neonatal Rat CDCs	cKit, CD90, Endoglin, vWF DDR2, α-Sarcomeric actin	Rat: acute MI/reperfusion Peri-infarct I/M injection (2x10^6 cells/rat); 48 hours later tail vein infusion (4x10^6 cells/rat) 16 weeks; Cardiac MRI; n=3-7	Cell retention observed at 16 weeks (not quantified)	↑ LVEF: ((+) ~10% vs vehicle controls) ↓ ESV and Infarct Size ↓ Collagen Density	↑ peri-infarct capillary density ((+) 44% over control hearts; ~12±3% vWF+, ~8±2% SMA+) *In vitro*: EC differentiation (vWF)	163

Table 1.1. A summary of pre-clinical studies addressing the potential of cardiac tissue derived EDCs, cardiospheres and CDCs to contribute to repair and improve heart function following MI.

1.7.3. The Role of CDCs in Neovascularisation following Heart Injury

The majority of studies investigating the repair efficacy of Csphs and CDCs have heavily focused on the potential of these putative CSCs to contribute to myocardial regeneration via direct differentiation into cardiomyocytes rather than their effect on angiogenesis. However several publications have addressed this important mode of repair[162-163, 166, 171-172, 186-187]. Table 1.2 summarises the major findings of several of these studies in terms of their pro-angiogenic effect following cell transplantation into preclinical disease models (predominantly acute MI). Although a number of the listed publications do not perform an in depth analysis of the effect of cell transplantation on neo-angiogenesis, they do demonstrate that these cells are able to differentiate into both endothelial and smooth muscle cells *in vitro* and *in vivo*. In addition both EDCs and CDCs have been shown to spontaneously form tubules in a 2D Matrigel angiogenesis assay *in vitro* potentially indicating that these cells retain intrinsic pro-angiogenic capacity[162]. However this should be interpreted with caution as tubule formation on matrigel is not unique to ECs. More robust evidence for a pro-angiogenic role of these cells has come from *in vivo* studies, demonstrating that cKit-positive, haematopoietic lineage-negative EDCs, Csphs and CDCs significantly increase capillary density following delivery into ischaemic hearts. Tang *et al*[166] found a 36% increase in peri-infarct capillary density 4 weeks following intravenous injection of murine $cKit^+$ EDCs as compared to control mice. Moreover hypoxic preconditioning of these cells (0.1% O_2 for 6 hours) enhanced neovessel formation by approximately 50%, likely due to the increased secretion of vascular growth factors (e.g. VEGF, osteopontin, basic FGF, erythropoietin and stem cell factor) observed following hypoxic culture[166]. Human cardiosphere transplantation into rats led to a 2 fold increase in capillary density in ischaemic myocardium 3 weeks post infusion[186]. Similarly, Chimenti *et al*[187] noted a 50% increase in ischaemic border zone vessel density in human CDC treated mice as compared to untreated controls at 3 weeks. Approximately 20% of the neo-vessels contained human derived cells, indicating that significant paracrine contribution

accounts for the majority of neovascularisation[187]. Finally, capillary density, measured using immuno-staining for CD31, was increased by 44% in the peri-infarct region of CDC-treated rats at 16 weeks compared with untreated infarcted hearts[163]. Although CDC differentiation along the endothelial lineage was observed *in vivo,* the authors suggested that paracrine factors most likely accounted for the majority of neovascularisation however this was not directly quantified.

Taken together these results strongly suggest that neo-angiogenesis plays an important role in CDC mediated heart repair. Importantly, whilst Csphs and CDCs have been shown to differentiate into ECs *in vitro* and *in vivo* this tends to occur at relatively low frequency. Indeed Mishra *et al* reported a <1% endothelial differentiation efficiency *in vitro* (as indicated by CD31 staining)[172] and Carr *et al* note an increased frequency of cardiomyocyte rather than EC differentiation[163]. Given that during development coronary ECs are derived from the sinus venosus and/or epicardium[195-196], while the haemangioblast (common ancestor to both haematopoietic and ECs) is resident within the BM it is tempting to speculate that BM-derived cells in the adult are more likely than CSCs to contribute directly to vascular regeneration. However, it is also likely that enhanced angiogenesis following CSC delivery into ischaemic myocardium is largely due to paracrine mechanisms rather than the ability to differentiate into ECs. This theory is supported by the studies of both Tang *et al*[166] and Chimenti *et al*[187], which both demonstrated CDC secretion of vascular related growth factors.

1.7.4. Therapeutic Potential of CDCs following Myocardial Infarction

With regard to clinical translation the Marban group have recently announced the preliminary results of the first phase I/II clinical study of CDCs (CADUCEUS; Cardiosphere-Derived Autologous Stem Cells to Reverse Ventricular Dysfunction)[197-198]. In this trial 17 male human subjects with a recent MI (~10 weeks previous) and left-ventricular dysfunction (LVEF ranging from 25–45%) received 12.5–25x10^6 autologous CDCs (harvested from endomyocardial biopsies) via intracoronary infusion. An additional 8 patients served as controls and received conventional treatment only. The preliminary 6 and 12 month follow-up data included MRI-assessment of infarct scar mass, viable mass, LV volumes and function. Interestingly there was no change in

LVEF between cell recipient subjects and controls although trends did indicate attenuated adverse LV remodelling in the former group (reduced end diastolic and end systolic volumes). CDC treatment also appeared to improve regional function in treated segments as indicated by a reduction in peak systolic strain as well as a significant increase in systolic wall thickness relative to controls. Marban and colleagues have also revealed that CDC recipient patients had a reduced scar mass with a corresponding increase in viable myocardial mass as judged by reduced delayed gadolinium enhancement on MRI. They conclude that these results provide the first evidence of stem cell mediated myocardial regeneration in human subjects. However, although a shrinking scar with concomitant increase in viable mass would be expected in true regeneration further evidence is required to definitely prove that this is occurring. An alternative interpretation of these results may be that CDC treatment results in "reduced vascular permeability with evidence for enhanced muscle mass associated with improved muscle regional function"[199]. Importantly this trial did demonstrate that autologous CDCs could be safely infused into patients via intracoronary infusion[197]. Of note vascular function and tissue perfusion was not assessed in this study however it cannot be discounted that the observed benefit associated with CDC treatment may be partly due to an increase in neovascularisation.

In addition the initial results of another phase I trial of heart derived stem cells (SCIPIO; Stem Cell Infusion in Patients with Ischaemic CardiOmyopathy) were recently published[200]. Rather than treating patients before they developed heart failure, as was the study design in the CADUCEUS trial, here the aim was to directly treat severe heart failure resulting from ischaemic heart disease (defined as a LVEF of less than 40%). A total of 0.5-1x10^6 cKit purified heart derived cells (atrial outgrowth) were infused into coronary artery bypass patients via the intracoronary route 4 months after tissue harvesting. A total of 16 patients were assigned to the treatment group and 7 to the control group (conventional therapy only). No adverse cell-infusion related problems were reported at 12 months. Using echocardiography and MRI analysis cardiac function in treated patients was found to be markedly improved within 1 year relative to controls. Baseline measurements of LVEF in the treatment group averaged at 30.3%, however 4 months after receiving CSCs this increased to 38.5% and in 8 patients who were followed for 12 months LVEF increased to an average of 42.5%. Additionally in 7 of the treated patients in whom cardiac MRI could be performed infarct size was also

found to be reduced by up to 30% at 12 months. Interestingly the control group showed no change in LVEF (30.1% at baseline and 30.2% at eight months post CABG), although the natural tendency is for cardiac function to slowly and progressively improve following coronary artery bypass grafting (CABG) therefore this lack of change in LVEF is surprising. Neither the CADUCUES trial nor the SCIPIO study were blinded therefore they were not controlled for the placebo effect. In addition the small sample sizes involved make it difficult to generalise findings to a larger population of heart disease patients. However these initial trials do suggest that CSC infusion via the coronary route is safe and provides encouraging results regarding efficacy, however it is clear that larger phase II trials are required.

To summarise CDCs are safe to use in MI patients; and although they do not show significant cell retention following delivery they do have pro-angiogenic properties that may be fundamental to their ability to reduce adverse ventricular remodelling following acute MI. As the majority of CDCs express endoglin, I was interested to discover whether this was a functional marker that affected CDC properties during heart repair. Endoglin is a co-receptor for certain members of the transforming growth factor β (TGFβ) family and affects cell responses to this important family of ligands.

1.8. Transforming Growth Factor-β Superfamily Signalling

1.8.1. TGFβ Superfamily of Ligands

TGFβ isoforms (TGFβ1-3) are the prototypic members of the TGFβ superfamily of cytokines, a group of over 30 evolutionary conserved and structurally related secreted growth factors that additionally include bone morphogenetic proteins (BMPs), activins and growth differentiation factors (GDFs)[201]. TGFβ superfamily members are multifunctional and play pivotal roles in embryonic development, adult tissue homeostasis as well as the pathogenesis of many disease states[201]. BMPs are known to have important roles in embryonic patterning and morphogenesis whereas the TGFβ ligands regulate many processes including wound healing, cellular proliferation, adhesion, and immunity[202]. Extensive studies have also revealed pivotal roles for both TGFβ and BMP signalling in angiogenesis and vascular homeostasis (discussed in section 1.9).

Many TGFβ family proteins are generated as inactive prepropeptide dimers with each polypeptide consisting of a small C-terminal mature domain and a larger N-terminal pro-region[7]. Specific sites between these two domains are cleaved to generate active C-terminal dimers. However, even after proteolytic cleavage the active domains of many TGFβ ligands remain non-covalently associated with the propeptide which blocks binding to receptors thus rendering the ligands latent[7]. Extracellular dissociation of these latent complexes to release active ligands is achieved via a variety of mechanisms including proteolytic processing[7]. This post-transcriptional regulation determines the bioavailability of TGFβ ligands for their receptors, while other family members (such as BMPs) are secreted in active form and are regulated by reversible interactions with extracellular antagonists[203]. The active ligands mediate their pleiotropic effects from cell membrane to nucleus by signalling through heteromeric complexes of type I and type II serine/threonine-kinase receptors and activating downstream nuclear effectors, the Smad proteins.

1.8.2. TGFβ Receptors and the TGFβ Smad Signalling Pathway

The structures of type I and II receptors are very similar with both consisting of small cysteine rich extracellular domains, single transmembrane regions and intracellular parts that contain serine/threonine kinase domains[204]. However the type I receptors also have a characteristic glycine/serine sequence upstream from the kinase domains, which is phosphorylated by the type II receptor[204]. At the cell surface these receptors exist as homodimers but in the presence of active ligand they form heteromeric signalling complexes that are thought to minimally consist of a heterotetramer with two type I and two type II receptors[204]. While some ligands are able to bind directly to their type II receptors, others bind preferentially to a type I receptor or a type I-type II complex.

Upon ligand binding and formation of a signalling complex the constitutively active type II receptor phosphorylates and activates the type I receptor which determines signalling specificity[205]. Thereafter subsequent phosphorylation of Smad proteins takes place allowing propagation of signal to the nucleus[206-207]. There are three distinct types of Smads: receptor regulated (R-Smad1, 2, 3, 5 and 8), common mediator (Co-Smad4) and inhibitory Smads (I-Smad6 and 7). R-Smads are phosphorylated by the type I receptor and interact with Co-Smad4. This complex translocates to the nucleus where it

participates in transcriptional regulation of target genes[208-209]. R-Smads and Co-Smad-4 share two conserved domains, termed MAD homology (MH)1 and MH2, which can both interact with sequence-specific transcription factors[204]. I-Smads prevent the activation of R-Smads by antagonistically competing for receptor interaction[210-211], recruiting ubiquitin ligases to activated receptors[212-213] or by recruiting phosphatases to dephosphorylate activated type I receptors[214].

Seven type I (also termed activin receptor-like kinases (Alk1-7)) and five type II (Tgfbr2, Bmpr2, Acvr2a, Acvr2b and Amhr2) serine/threonine-kinase receptors have been identified. In addition two accessory receptors (or type III receptors), endoglin and betaglycan, are known to regulate ligand–receptor interactions and have a more indirect role in TGFβ signal transduction[204]. Versatility in receptor combinations allows for differential ligand binding or differential signalling in response to the same ligand. Additionally, a receptor combination may bind different ligands, and patterns of ligand and receptor expression often dictate which receptors are activated. This infers a high level of cross-talk between the different TGFβ signalling pathways, allows for context dependent responses and partially explains the complex and divergent range of cellular functions regulated by the TGFβ superfamily.

1.9. The Role of Endoglin and TGFβ Signalling in Angiogenesis

1.9.1. TGFβ Signalling is Pivotal to the Regulation of Angiogenesis and Vascular Homeostasis

Genetic studies in mice have revealed that TGFβ signalling pathways play essential roles in vascular development including the maintenance of the vessel wall integrity, smooth muscle cell recruitment, deposition of extracellular matrix and differentiation of arteries and veins[215]. Furthermore, perturbed TGFβ signalling has been implicated in several human diseases[7]. TGFβ acts as both an inhibitor and stimulator of angiogenesis *in vitro* and *in vivo* depending on experimental conditions[6, 215] and BMPs have also been shown to play an important role in angiogenesis and vascular homeostasis via an interplay between two groups of pro- and anti-angiogenic ligands[216]. During embryogenesis TGFβ1 is expressed in many tissues including endothelial and haematopoietic progenitor cells[215] and targeted disruption of this ligand in C57Bl/6 mice results in mid-gestation lethality due primarily to defects in the yolk sac

vasculature[217]. Although initial differentiation of mesodermal precursors into ECs occurs, subsequent differentiation and remodelling into capillary-like tubules is defective resulting in fragile vessels with decreased wall integrity. Tgfbr2-deficient mice demonstrate a similar mutant phenotype[218] and gene knockout mouse models of additional TGFβ receptors and downstream signalling proteins also cause vascular defects (see table 1.2), providing further evidence of the central role of TGFβ signalling in vascular development.

1.9.2. TGFβ Type I Receptors Balance the Activation State of the Endothelium and Regulate the Angiogenic Switch

Within the endothelium TGFβ is known to bind Alk5 as well as Alk1 type I receptors in conjunction with Tgfbr2 leading to both TGFβ/Alk5 dependent phosphorylation of Smad2/3 and TGFβ/Alk1 induced Smad1/5 activation[219] (figure 1.5). Thus in ECs TGFβ can activate two distinct type I receptor/Smad signalling cascades. Functional studies have revealed that these divergent pathways have opposite roles in endothelial biology and it is proposed that a fine balance between TGFβ/Alk5 and TGFβ/Alk1 signalling regulates angiogenesis[6, 219]. Hence, whilst TGFβ signalling via the Alk5/Smad2 pathway leads to a quiescent endothelial phenotype by inhibiting EC proliferation and migration, in contrast TGFβ dependent Alk1/Smad1/5 signalling activates the endothelium and stimulates cellular migration and proliferation[219]. In support of this model, microarray analyses have revealed marked differences in target gene expression profiles for these two signalling pathways[220]. For example, the Alk5 pathway stimulates expression of fibronectin (an ECM protein involved in endothelial cell adhesion) and plasminogen activator inhibitor type I (*Pai1*)[220] (an inhibitor of fibrinolysis and a negative regulator of EC migration *in vitro* and angiogenesis in *vivo*). Target genes of the Alk1-Smad1/5 pathway include inhibitor of DNA binding 1 (*Id1*), which is involved in cell cycle progression, proliferation and inhibition of differentiation, as well as interleukin 1 receptor-like 1 (*Il1rl1*), which is suggested to participate in cell growth[220].

In addition to mediating opposite responses in ECs, Alk5 and Alk1 receptors also cross talk with each other. Alk5 is necessary for both Alk1 recruitment into a TGFβ receptor complex and efficient Alk1 activation[221]. Also, Alk1 has been shown to directly

antagonize Alk5/Smad2/3 signalling at the Smad level[221]. Thus, the requirement for Alk5 in Alk1 signalling and the opposing actions of Alk1 and Alk5 provide ECs with an intricate mechanism for precisely regulating TGFβ-induced biological responses during angiogenesis.

Gene	Knock-Out Phenotype	Lethality	Ref
TGFβ1	Defect in embryonic mesoderm and haematopoiesis. Inadequate tube formation.	E10.5	[217]
Tgfbr2	Defect in yolk sac vasculogenesis and haematopoeisis	E10.5	[218]
Bmpr2	Abnormal mesoderm formation. Heterozygotes; thickened arteries, increased pulmonary vascular resistance. Transgenic BMPR2-mutant allele; vascular defects	Embryonic lethal (pre-angiogenesis)	[222-224]
Alk5	Defects in angiogenesis. Impaired EC migration, proliferation and fibronectin production	E10.5	[225]
Alk1	Defects in angiogenesis. Impaired differentiation and recruitment of SMCs	E11.5	[226-227]
Smad5	Lack or normal development of the yolk sac vasculature. Irregular distribution of blood cells and large blood cells	E9.5-E11.5	[228-229]
Smad1	Failure in establishing chorion-allantoic circulation. Lack of VCAM-1 expression	E9.5	[230-231]
Endoglin	Defects in angiogenesis. Impaired differentiation and recruitment of SMCs. Cardiac malformations due to defects in mesenchymal transformation and cushion tissue formation	E10-E11.5	[232-234]
Betaglycan	Cardiac defects	E13.5	[235]

Table 1.2. TGFβ signalling: Gene ablation studies in mice. Defects in components of the TGFβ signalling pathway lead to cardiovascular abnormalities and embryonic lethality.

The precise roles of the Alk1 and Alk5 pathways during angiogenesis have been difficult to determine. Over-expression studies have demonstrated that signalling through Alk1 may inhibit EC proliferation and migration suggesting a role in the resolution phase of angiogenesis[226, 236]. Importantly, these observations concur with the phenotype of *Alk1* knock-out mice, which have fragile blood vessels and display up-regulated expression of pro-angiogenic genes[226-227]. The discrepancies between these findings and data from other studies implying a pro-angiogenic role for Alk1[219, 237] may be explained by different cell types/experimental models being used, adaptive processes occurring in response to Alk1 loss or it may be that Alk1 signalling cascades are involved in both angiogenic activation and resolution phases. Interestingly, BMP9 and BMP10 were recently identified as novel ligands of Alk1[238-239]. BMP9 has been shown to induce both Smad1/5 and Smad2 phosphorylation through Bmpr2/Alk1 and the activin type II receptors in ECs[240]. It was observed that both Bmpr2 and activin type II receptors were required for Smad1 activation whereas Smad2 phosphorylation was

mediated mainly through activin type II receptors[240]. Interestingly, BMP9 was found to reduce angiogenesis using a number of different assays: BMP9 inhibited (i) EC proliferation and migration *in vitro*[238-239], (ii) VEGF-induced angiogenic sprout formation in a mouse metatarsal assay *ex vivo*[239], (iii) bFGF-induced angiogenesis in a murine sponge assay and (iv) blocked angiogenesis in the chick chorioallantoic membrane (CAM) assay *in vivo*[241]. Shao *et al*[242] have proposed BMP9 to be a vascular quiescence factor following observations that high doses of BMP9 could attenuate the pro-angiogenic effects of TGFβ in ECs. Although these findings suggest that BMP9 and BMP10 may have predominantly anti-angiogenic effects, other studies have reported that BMP10 induces angiogenesis in the CAM assay[243] while BMP9 was found to stimulate EC proliferation both *in vitro* and *in vivo*[244]. Additionally in combination with TGFβ, BMP9 has been shown to potentiate VEGF-induced EC proliferation *in vitro* and VEGF/bFGF-induced angiogenesis *in vivo*[245]. Therefore it may be that BMP9 signalling in ECs exhibits both pro- and anti-angiogenic effects in a context dependent manner. Pardali *et al*[201] propose a working model whereby TGFβ/Alk1 signalling leads to the activation of angiogenesis whereas BMP9 signalling through Alk1 can stimulate endothelial quiescence or activation in a context dependent manner (see figure 1.6.). Further studies are required to elucidate the true role of Alk1 signalling in angiogenesis.

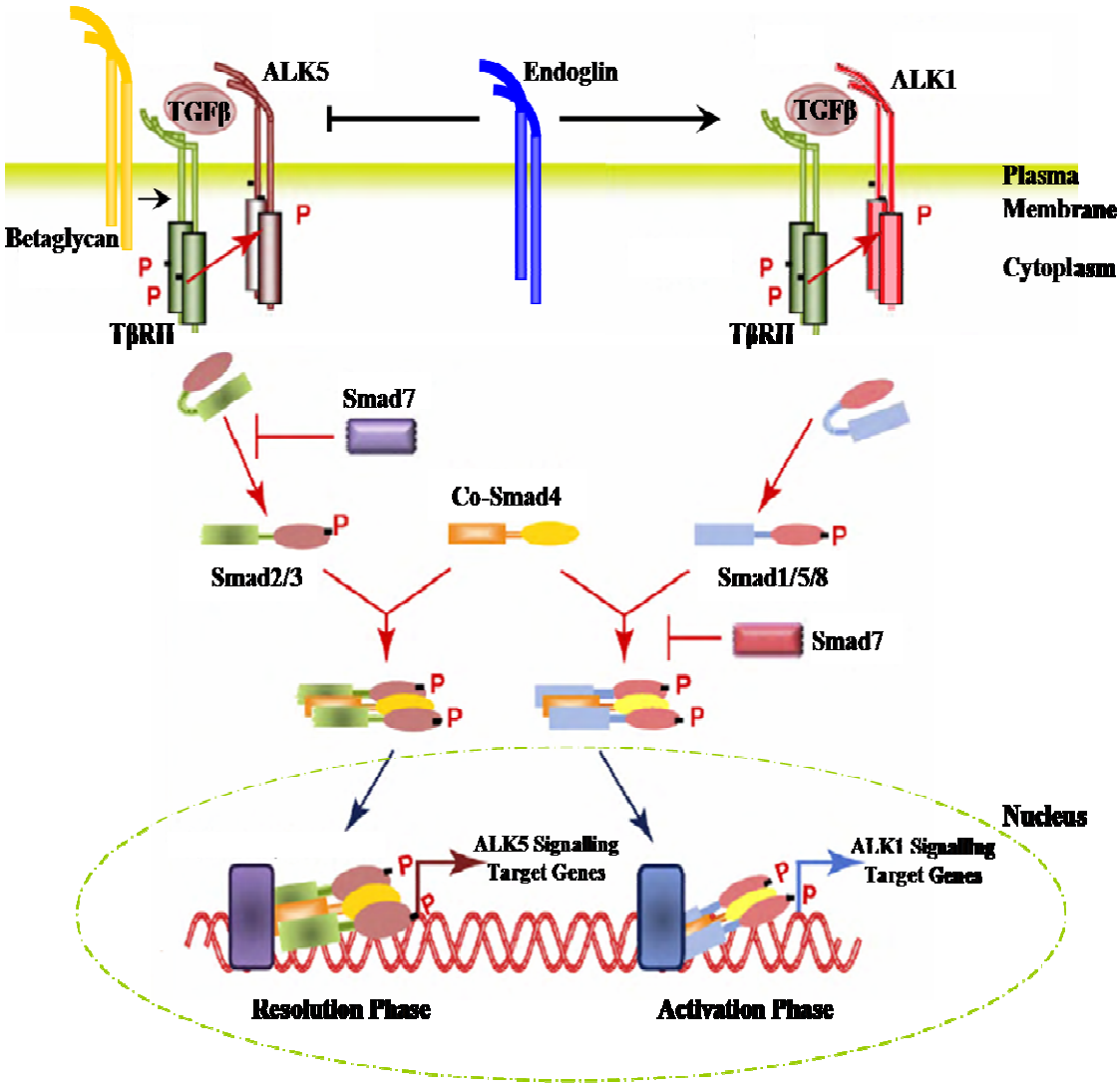

Figure 1.5. TGFβ Signal transduction through the Smad signalling pathway. TGFβ superfamily ligands bind to specific serine/threonine kinase type I and II receptors and induce heteromeric complex formation. The type II receptors activate type I receptors via phosphorylation and subsequently, the type I receptor propagates the signal to the nucleus by phosphorylating intracellular effector proteins; R-Smads, which form heteromeric complexes with Smad4 (Co-Smad). These Smad complexes translocate to the nucleus and interact with transcription factors to regulate gene expression. TGFβ activates two distinct signalling pathways with opposite effects in endothelial cells. Signalling through the TGFβ/Alk5 pathway and subsequent Smad2/3 phosphorylation leads to inhibition of cell proliferation and migration to maintain endothelial quiescence and hence is associated with the resolution phase of angiogenesis. In contrast, signalling through the TGFβ/Alk1 pathway (via phosphorylation of Smad1/5) induces both cell proliferation and migration and promotes the activation state of angiogenesis. The accessory receptors betaglycan and endoglin can modulate signalling via the type II and type I receptors. Betaglycan has been shown to enhance TGFβ2 binding to TGFβ receptors, whereas endoglin is required for efficient Alk1 signalling and has been implicated in the inhibition of the TGFβ/Alk5 pathway. Figure adapted from [201].

1.9.3. The Role of Endoglin in TGFβ Signalling and Angiogenesis

Endoglin (also known as CD105) is a disulphide-linked homodimeric transmembrane glycoprotein and as previously mentioned it is a TGFβ accessory receptor[246]. Endoglin belongs to the zona pellucida (ZP) family of proteins and consists of a large extracellular domain that harbours a ZP region and a short cytoplasmic domain containing serine/threonine residues which can be targeted by serine/threonine kinases including type I and II TGFβ receptors[246]. The N terminus region of the ZP domain plays a role in protein-protein interactions and is involved in ligand dependent and independent associations with TGFβ family receptors[246]. With the exception of BMP9 endoglin cannot directly bind exogenous ligands in the absence of type I and II signalling receptors although it can bind to heteromeric TGFβ receptor complexes independently of bound ligand[247-248]. It has been shown that endoglin interacts with TGFβ1, TGFβ3, activin-A, BMP2 and BMP7 ligands when associated with type I and type II TGFβ receptors[247-248] but can bind BMP9 directly through its extracellular domain[239, 249]. Endoglin is thought to modulate cellular responses by regulating the activation of receptor complexes in response to TGFβ family ligands and subsequent signalling via downstream Smads.

Endoglin is predominantly expressed by proliferating ECs during angiogenesis, wound healing and inflammation, all of which are associated with vascular structural alterations and TGFβ signalling (reviewed in[250]). In addition to activated ECs, endoglin is expressed by monocytes and upregulated during monocyte-macrophage transition[251]. Endoglin is also upregulated by injured vascular smooth muscle cells in patients with athersosclerosis[252] and is expressed by cardiac fibroblasts[253]. Furthermore endoglin is expressed by circulating MSCs[254], a subset of neural crest stem cells[255], in syncytiotrophoblasts of term placenta[256], in adult BM-HSCs[257] and is a functional marker that defines long-term repopulating HSCs[258].

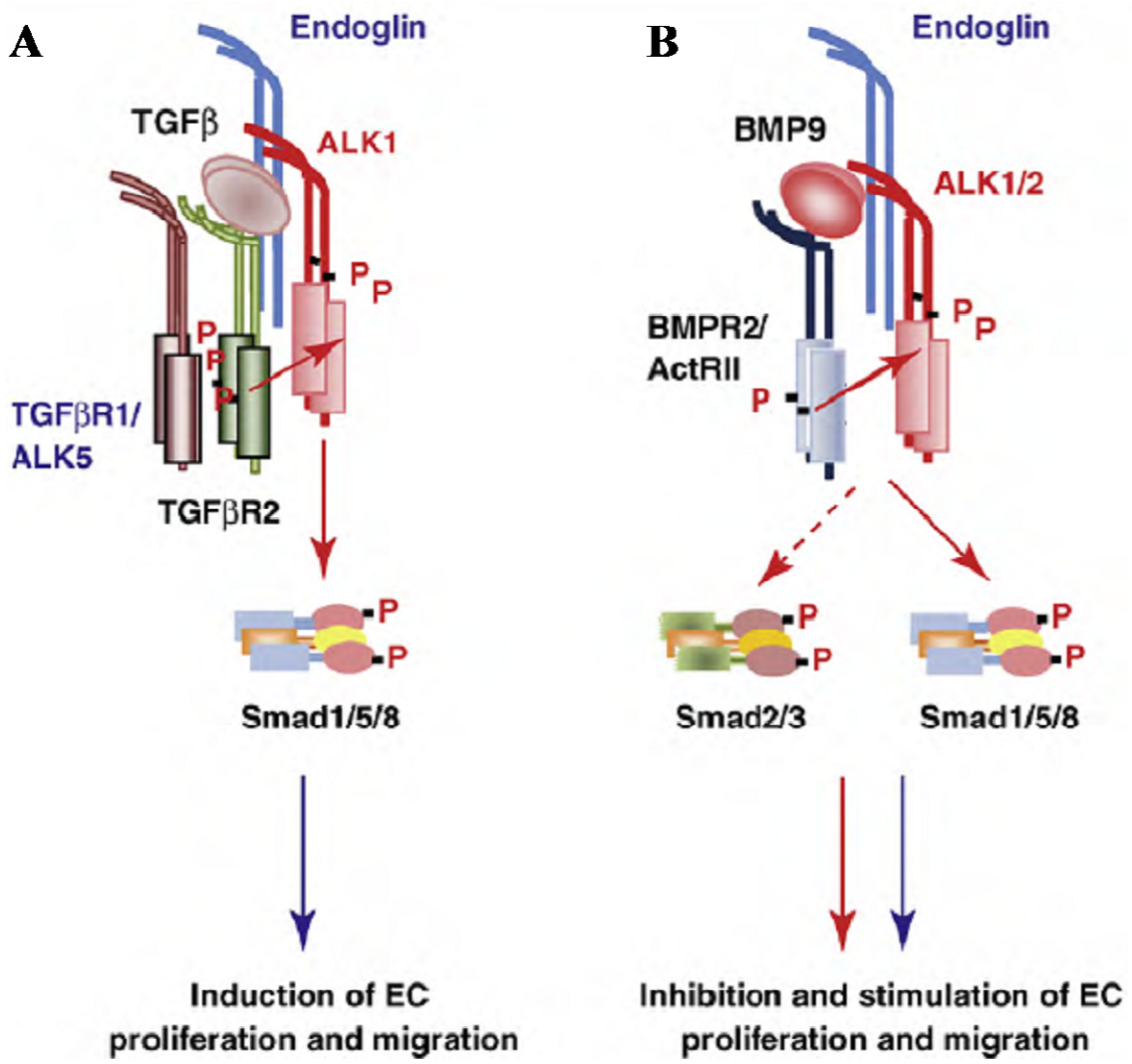

Figure 1.6. A working model for TGFβ/Alk1 and BMP9/Alk1 signalling in endothelial cells. (A) TGFβ binds to Tgfbr2, which subsequently recruits and phosphorylates Alk5 and Alk1 in a common complex. Activated Alk1 induces Smad1/5 phosphorylation resulting in the activation of Alk1-specific target genes, which induce endothelial activation. (B) BMP9 can induce both Smad1/5 and Smad2 phosphorylation in ECs through the Bmpr2/Acvr2/Alk1/2 pathways leading to both pro- and anti-angiogenic effects in a context dependent manner. Endoglin is required for efficient TGFβ/Alk1 and BMP9/Alk1 signalling. Figure adapted from [201].

Mouse embryos homozygous for mutations in the *endoglin* gene die at E10.5 due to a failure to form mature blood vessels with evidence of endothelial dysfunction secondary to impaired smooth muscle cell differentiation and recruitment[232-234]. Although vessels can form in the yolk sac of mutant animals they are dilated, fragile and readily susceptible to damage and haemorrhage. The *in situ* differentiation of ECs does take place but there is a subsequent failure to remodel the primitive vasculature into a more mature network suggesting a role for endoglin in angiogenesis rather than in vasculogenesis. This phenotype is similar to that of TGFβ1, Tgfbr2, Alk1 and Alk5

deficient mice indicating a functional link between endoglin and TGFβ signalling during embryonic vascular development (see table 1.2). There is a further link between these gene families in that patients with mutations in *endoglin* or *Alk1* have been associated with variant forms of an autosomal dominant multi-system vascular dysplasia termed hereditary haemorrhagic telangiectasia (HHT). HHT1 and HHT2 are associated with mutations in *endoglin* and *Alk1* respectively[259-261], and the similar clinical phenotype of HHT1 and HHT2 patients suggests that *endoglin* and *Alk1* share a common signalling pathway. HHT is characterised by small dilated blood vessels (telangiectases) in the nasal, oral, and gastrointestinal mucosa as well as larger arteriovenous malformations (AVMs) in the vasculature of the lung, liver and brain. Telangiectases are prone to bleed, and can lead to patient anaemia, whilst the clinical consequences of AVMs include an increased disposition to stroke, cyanosis or high output cardiac failure.

Mice heterozygous for mutations in *endoglin* have been used to model HHT1 however the manifestation of clinical symptoms appears to be strain dependent. While endoglin heterozygous mice of the 129/Ola strain display fragile blood vessels, telangiectases and nosebleeds[233, 262], mice from other genetic backgrounds failed to show such a phenotype indicating the existence of modifier genes[233, 263]. Haploinsufficeincy is the proposed mechanism underlying HHT1 with reduced endoglin levels leading to dysfunctional TGFβ/BMP9 signal transduction.

The defective vascular phenotype resulting from endoglin deficiency reveals an important role in angiogenesis and several studies provide evidence that endoglin modulates the angiogenic switch by balancing TGFβ/Alk1 and TGFβ/Alk5 signalling pathways. Indeed, endoglin has been shown to potentiate TGFβ/Alk1 signalling, while attenuating the TGFβ/Alk5 pathway in ECs as well as in other cell types (see figure 1.5). Lebrin *et al*[237] identified endoglin as a requirement for efficient Alk1 signalling in mouse embryonic ECs (MEECs) with endoglin deficient cells displaying abrogated Alk1 signalling (loss of TGFβ dependent Smad1 activation and impaired cell proliferation) and upregulated Alk5 signalling. Supporting these findings it was shown that endoglin counteracts the inhibitory effect of TGFβ/Alk5 on cellular proliferation, migration and tubule formation in human umbilical vein endothelial cells (HUVECs)[264]. Furthermore, ectopic expression of endoglin prevented TGFβ-induced growth inhibition

in monocytes and myoblasts[248, 265] and ECM synthesis in myoblasts[266]. Thus endoglin is regarded as a negative regulator of the Alk5 pathway. Corroborating this theory, neutralizing antibody for endoglin was found to potentiate the inhibitory effect of TGFβ on EC migration and growth[267] and ectopic expression of endoglin inhibited Smad3 transcriptional activity in rat myoblasts[268]. However the hypothesis that endoglin promotes EC proliferation and migration has been contradicted by several reports. Pece-Barbara *et al*[269] reported that endoglin null MEECs proliferated faster than control cells in response to TGFβ1 treatment, while in another study although endoglin deficiency resulted in reduced numbers of neovessels in an *in vivo* subcutaneous Matrigel implant assay, endoglin-deficient retinas from the same inducible endoglin knock out mouse model exhibited increased endothelial proliferation[270]. In addition to promoting the TGFβ/Alk1 pathway, endoglin has also been shown to mediate BMP9/Alk1 signalling responses which are associated with both angiogenic activation and resolution (see figure 1.6). Despite these conflicting reports and the suggestion that the role of endoglin may be context dependent the balance of evidence strongly supports the prevailing hypothesis that endoglin plays an important and functional role in angiogenesis. Additionally this role is likely to be pro-angiogenic therefore indicating that this receptor may also be important in cell-mediated therapeutic angiogenesis.

1.10. The Role of TGFβ Family Signalling and Endoglin in Cell-Mediated Cardiac Repair

Although a role for TGFβ in cardiac fibrosis and remodelling following MI is well recognised this is not the focus of this thesis and has been reviewed elsewhere[9].

At the advent of this study there was little data on how TGFβ might affect stem cell proliferation, mobilisation or pro-angiogenic repair potential. However, although not much research has been conducted specifically using CDCs, preliminary data does suggest that TGFβ signalling may be important in the regulation of EPC migration and differentiation. Human EPCs and MNCs have been shown to express TGFβ receptors (*Tgfbr2, Alk1, Alk5* and *endoglin*) and exhibit downstream Smad phosphorylation/activation following exposure to TGFβ ligand[61, 271], strongly indicating that EPCs have an active TGFβ pathway. In addition preliminary published data supports the idea that TGFβ plays a pivotal role in controlling proliferation and

differentiation responses of EPCs *in vitro*. Henrich *et al*[272] propose TGFβ1 plays a pivotal role in EPC differentiation induced by serum of polytrauma patients. The authors cultured MNCs with serum derived from multiple trauma victims and observed a significant increase in EPC numbers, which displayed enhanced capacity to form vascular structures in matrigel, while neutralisation of TGFβ1 in the serum using specific antibodies resulted in a significant decrease in EPC differentiation[272]. Data from Zhu *et al*[273] also indicate TGFβ1 is critical for regulating EPC differentiation. The vascular wall is mainly composed of ECs and SMCs and the cross talk between these two cell types is critical in the vascular maturation process. The authors report TGFβ1 expressed in SMCs increases EPC differentiation (as judged by positive staining for endothelial markers vWF and VE-cadherin) as well as adhesion (as judged by the adhesion force between EPCs and SMCs)[273]. They propose TGFβ1 can also induce EPC migration and differentiation by increasing the amount of VEGF and VEGFR1. Furthermore Sales *et al*[274] have shown that TGFβ1 enhances ECM production and modulates the proliferation and apoptosis of EPCs in tissue engineering scaffolds.

In addition the importance of endoglin in stem-cell mediated heart repair has been established. Endoglin is expressed by MNCs and in endothelial culture conditions expression levels increased from 15% of the total MNC population to 80% after only 4 days[271]. Furthermore, when grown over a longer period, the resultant endothelial-like cells derived from MNCs with endoglin mutations (from HHT1 patients) have disorganized and depolymerised actin fibers and demonstrated impaired tubule formation in an *in vitro* angiogenesis assay[61]. In 2006 Linda van Laake *et al*[275] provided the first evidence indicating the essential role of endoglin in endogenous heart repair. Decreased levels of endoglin in endoglin heterozygote mice resulted in reduced angiogenesis one week following MI and a 50% reduction in LV function at 4 weeks post MI compared with WT controls. This study also showed that normal levels of endoglin are critical for human MNCs to promote heart repair in a mouse model of MI. Essentially although the number of EPCs (defined by FACS analysis for standard EPC markers; CD34 and VEGFR2) was the same in the peripheral MNC fractions of control and endoglin-deficient (HHT1) patients, the biological activity of the latter group was impaired. EPCs were injected into infarcted mice intravenously via the tail vein and cells from HHT1 patients were found to reach the infarcted region of the heart at reduced efficiency and were less able to promote repair than control cells. In

collaboration with the authors of this seminal study Post *et al*[276] went on to demonstrate that these endoglin deficient MNCs displayed a defective CXCR4/SDF1 axis suggesting perturbed homing of the MNCs to the site of injury. However the effect of transplanting endoglin deficient cells directly into the coronary circulation or myocardium was not assessed. In addition, Gaebel and colleagues[277] recently reported that endoglin enriched MSCs from human UCB showed increased survival and led to reduced fibrosis following transplantation into infarcted hearts when compared to transplanted total MSCs. These studies all serve to highlight the potential importance of endoglin in cell mediated heart repair.

1.11. Aims of Thesis

Endogenous pro-angiogenic stem cells form part of the bodies defence against vascular assault and the threat of ischaemic injury. However as the number of cells that can be isolated from any one patient are limited, *ex vivo* expansion of repair cells will be an important part of future therapies. This is especially true for patients with cardiovascular disease and associated risk factors, such as those with hypertension or diabetes, who tend to have reduced numbers of both EPCs and cardiac resident stem cells and attempts to increase the endogenous mobilisation of EPCs using stimulatory growth factors have proved incompatible with the severity of their clinical condition. Therefore, to improve the efficacy of autologous cell-mediated therapies it would be beneficial to expand harvested populations and identify factors that both distinguish repair cells as well as control their proliferation while maintaining or even enhancing their pro-angiogenic properties. This will help to maximise patient benefit and optimisation of this process will be critical for the success of future therapies.

Drawing parallels with recent findings relating to the functional significance of the balance of endothelial TGFβ/Alk1 and TGFβ/Alk5 signalling on angiogenesis as well as the regulatory role of endoglin in this process, it is likely that these pathways act as critical mediators of the balance between cell differentiation and proliferation responses *in vivo*. Furthermore as endoglin is expressed in mesenchymal stem cells such as CDCs and a subset of the EPC populations prepared from BM it is probable that the activity of endoglin will be important in these cell types for their contribution to vascular repair.

The overall goal of this project was to investigate the regulation of EPCs and CDCs via TGFβ signalling, focussing on the role of endoglin. I tested the hypothesis that manipulating TGFβ/Alk5 signalling can direct EPC proliferation and differentiation responses; and that endoglin performs an important role in CDC-mediated heart repair.

The specific aims of this project were to;

1) Determine the effect of inhibiting Alk5 kinase activity and reducing endoglin expression on EPC yield from mouse BM *in vitro*
2) Investigate the effect of endoglin depletion on CDC function and TGFβ signalling responses *in vitro*
3) To establish a mouse model of myocardial infarction and test the effect of endoglin depletion on the ability of CDCs to contribute to neovascularisation and reduce adverse ventricular remodelling *in vivo*.

CHAPTER 2.

Materials and Methods

2.1. Suppliers

Chemicals and reagents were purchased from Becton Dickinson (BD), BD Pharmingen, VWR International, eBiscience, Sigma-Aldrich, Vector Laboratories, Fisher Scientific, Polysciences Inc., Severn Biotech Ltd., GE Healthcare, Pierce Biotechnology, Qiagen, Roche or Invitrogen.

All plasticware and apparatus for tissue culture, western blotting and general laboratory use was purchased from BioRad Laboratories, Iwaki, Greiner, RA Lamb, or Scientific Laboratory Supplies.

Medium and supplements for cell culture were purchased from Promocell, Gibco Invitrogen, Lonza and Peprotech.

Oligonucleotides were purchased from the Molecular Biology Facility (Newcastle University, Newcastle upon Tyne, U.K.) or TAGN (Centre for Life, Newcastle upon Tyne, U.K.).

Surgical equipment and instruments were purchased from Harvard Apparatus and Fine Science Tools (FST).

2.2. Mouse Strains and Genotyping

All animal procedures were permitted under UK Home Office licence and were preformed in accordance with national guidelines for the care and use of laboratory animals.

Mice were maintained in a ventilated, germ free facility in a 12 hour light-dark cycle and fed a standard diet with water *ad libitum*.

2.2.1. Mouse Strains

Endoglin heterozygote (*Eng*$^{+/-}$) Line

Eng$^{+/-}$ mice were developed in my host laboratory[232]. In the targeted allele a premature stop codon was introduced into exon 8 (via homologous recombination in ES cells)

resulting in the expression of a truncated, non-functional protein. *Eng*$^{+/-}$ mice were generated and maintained in a pure NIH background (backcrossed for 16 generations).

Endoglin floxed/floxed (*Eng*$^{fl/fl}$) Line

Eng$^{fl/fl}$ mice were developed in my host laboratory[278]. *LoxP* sites flank exons 5 and 6 which are subsequently deleted when exposed to transgenic Cre-recombinase. This results in a frameshift mutation and the introduction of a premature stop codon in exon 7 of the endoglin gene, giving rise to a truncated, non-functional protein. *Eng*$^{fl/fl}$ mice were maintained in a C57Bl/6 background (backcrossed for 5 generations).

Inducible *Cdh5(PAC)-CreER*^{T2} Line

Cdh5(PAC)-CreER^{T2} mice were obtained from Dr Ralf Adams (CRUK, London). They express tamoxifen-inducible Cre recombinase (*CreER*^{T2}) under the regulation of the vascular endothelial cadherin (VE-Cadherin or Cdh5) promoter. *Cdh5(PAC)-CreER*^{T2} mice were backcrossed for 5 generations with C57BL/6 to generate an approximately syngeneic line and were mated with *Eng*$^{fl/fl}$ mice to generate *Eng*$^{fl/fl}$*;Cdh5(PAC)CreER*^{T2} mice.

Inducible *Rosa-CreER*^{T2} Line

Inducible *Rosa-CreER*^{T2} mice were generated in Dr. A. Joyner's Lab (New York, USA) and obtained from Dr. Caiying Guo (University of Connecticut, USA). This mouse expresses tamoxifen-inducible Cre recombinase (*CreER*^{T2}) under the regulation of the ubiquitously expressed Rosa26 promoter and is on a C57Bl/6 background. *Rosa-CreER*^{T2} mice were mated with *Eng*$^{fl/fl}$ mice to generate a *Eng*$^{fl/fl}$*; Rosa-CreER*^{T2} line.

Rosa26R Line

Rosa26R mice[279] (in a mixed genetic background) were obtained from Professor Deborah Henderson (Newcastle University). These mice contain a transcriptional stop sequence flanked by *loxP* sites upstream of the *LacZ* gene. The expression of *LacZ* is driven by the ubiquitous Rosa26 promoter and is conditional on the removal of the preceding stop codon by Cre-mediated excision. Subsequent expression of the *LacZ* gene product (β-galactosidase) can be detected by X-gal staining and used to map expression of Cre-recombinase in murine tissue or primary cell types. *Rosa26R* mice were crossed with inducible *Cdh5(PAC)-CreER*^{T2} and inducible *Rosa-CreER*^{T2} mice.

CAG-farnesylated-eGFP (*CAG-farnesyl-eGFP*) Line

CAG-farnesyl-eGFP mice were obtained from Prof A. Medvinski (Edinburgh University) and maintained in a pure C57Bl/6 background. In this line *eGFP* expression is under control of the CAG promoter (a combination of the chicken beta actin promoter and the CMV promoter) whilst the farnesyl group anchors the eGFP to the cell membrane. CAG-farnesylated-eGFP mice were intercrossed with $Eng^{fl/fl}$; $Rosa\text{-}CreER^{T2}$ mice over sufficient generations to generate a homozygous triple transgenic $Eng^{fl/fl}$; $Rosa\text{-}CreER^{T2}$; *CAG-farnesyl-eGFP* line.

Tamoxifen-mediated Cre-Recombinase Activation *in vivo*. To activate $CreER^{T2}$ and induce the conditional knockout of endoglin via Cre-recombinase mediated excision *in vivo,* adult mice (≥8 weeks) were injected (via intraperitoneal route) with 2mg tamoxifen (Sigma) injections for 5 consecutive days followed by a 2 further injections on days 7 and 9.

Please refer to figures 4.1, 4.2 and 4.4 for an explanation of the Cre-LoxP recombination strategy and schematics detailing the inactivation of the endoglin allele and the activation of the Rosa26 reporter.

2.2.2. DNA Extraction

Lysis buffer 1 (25mM NaOH and 0.2 mM EDTA)
2.5ml of 0.5M NaOH + 0.02ml of 0.5M EDTA in 50ml of milli-Q H2O, adjust to pH12 with NaOH.

Lysis buffer 2 (40mM Tris-HCl)
4ml of 0.5M Tris-HCl in 50ml milli-Q H2O, adjust to pH5 with HCl.

Tissue. Ear clips of adult mice and tail tips of young pups were used for DNA extraction and subsequent genotyping of the animal. Each biopsy was incubated for 1 hour in 100µl of lysis buffer 1 in a thermomixer set at 95°C and 350rpm. The tubes were then vortexed and 100µl of lysis buffer 2 was added to neutralize the pH. Again, tubes were briefly vortexed and then centrifuged at 13,000rpm for 5 minutes to pellet any undigested tissue or impurities. The extracted DNA contained within the supernatant was stored at -20°C until required.

Cells. 10^6 cells were pelleted and used for preparing DNA for genotying. The protocol used was as described above.

2.2.3. Genotyping

All genotyping was performed using the polymerase chain reaction (PCR).

Standard PCR Amplification: PCR reactions were made up to a total volume of 25µl in 0.2ml thin walled PCR tubes. Individual reaction mixtures consisted of 2.5µl 25mM $MgCl_2$, 2.5µl 10x Reaction Buffer IV, 0.2µl Red Hot *Taq* DNA Polymerase (all purchased from ABgene, Thermo Scientific), 0.25µl of each forward and reverse primer (20µM), 0.5µl 10mM dNTPs (New England Biolabs), 2µl template DNA and dH_2O made up to a final volume of 25µl.

Primer details are listed below in table 2.1

All genotyping PCR included both negative (sterile ddH_2O) and positive controls and reactions were carried out using the conditions detailed in table 2.2 with an annealing temperature of 58^{o}C and a programme of 35 cycles. A C1000 thermal cycler (Biorad) was used.

Agarose Gel Electrophoresis:
1X TAE Buffer
40mM tris base-acetate and 1mM EDTA

DNA Loading Dye
0.25% bromophenol blue, 0.25% xylene cyanol FF and 40% sucrose in dH_2O

All PCR products were resolved on 2% agarose gels, which were made by dissolving 2g of DNA agar (Seakem® LE Agarose for gel electrophoresis) in 100ml of 1xTAE buffer by boiling in a microwave until the agarose was fully dissolved. The gel was allowed to partially cool before it was cast in a horizontal gel tray with well combs and left to set for at least 45 minutes. Once set, the well comb was carefully removed and the gel was placed in an electrophoresis tank and fully immersed in 1xTAE buffer. Following PCR, samples were prepared by adding DNA loading dye to ensure accurate loading into the gel and to allow visual tracking of DNA migration during electrophoresis. A 1kb DNA ladder (Invitrogen) was also loaded alongside the samples to allow assessment of PCR

product size. The loaded gel was left to run at approximately 80volts for 60 minutes. The DNA bands were visualised by immersing the agarose gel in Ethidium Bromide solution (1µg/ml in dH_2O) for 30 minutes followed by exposure to UV light and image capture using a GeneGnome System and GeneSnap Software (Syngene Bio Imaging).

Line	Primer	Sequence (5'-3')	Product Size (bp)
NIH Eng+/-	meng9a-F	ACCATCTTGTCCTGAGTAGCG	330^{Eng+}
	meng9b-R	TGAGCCTGACGGGAAACTG	
	Neo F	ACGTACTCGGATGGAAGCC	266^{Eng-}
	Neo R	CAAGCTCTTCAGCAATATCACG	
Eng^{2fl} VECad-Cre^{ERT2} Eng^{2fl} Rosa-Cre^{ERT2}	Eng F4	GGTCAGCCAGTCTAGCCAAG	602 null allele
	Eng R7	CCACGCCTTTGTCCTTGC	
	Eng F6	GACGCCATTCTCATCCTGC	420 wt allele
	Eng R7	CCACGCCTTTGTCCTTGC	500 floxed allele
	CreS F	TGCCACCAGCCAGCTATCAACT	191
	CreS R	AGCCACCAGCTTGCATGATCTC	
CAG-f-eGFP	eGFP F	TCGTCCTTGAAGAAGATGGTG	244
	eGFP R	ACGTAAACGGCCACAAGTTC	
Rosa26R	WT-R26	GCGAAGAGTTTGTCCTCAACC	600 wt allele
	R26	GGAGCGGGAGAAATGGATATG	
	R26Gtrgeo	AAAGTCGCTCTGAGTTGTTAT	310 R26 allele

Table 2.1. Details of primers used to genotype different mouse lines.

Reaction Steps	Reaction Conditions
1	95°C – 1 minute
2	95°C – 15 seconds
3	58°C – 30 seconds
4	74 °C – 1 minute
5	74 °C – 7 minutes
6	4 °C infinite
Cycles (steps 2-4)	35

Table 2.2. PCR programme used to genotype mouse lines.

2.3. Cell Culture

2.3.1. Primary Cell Culture

2.3.1.1. Endothelial Progenitor Cells

2.3.1.1.1. Long and Short Term Culture of Mouse BM Cells

Endothelial Cell Growth Medium 2 - EGM-2 (Lonza)
Endothelial basal media supplemented with 20% fetal calf serum, 100Units/ml penicillin, 100µg/ml streptomycin, hEGF, hydrocortisone, gentamicin, amphotericin B, VEGF, hFGF-B, IGF-1, ascorbic acid and heparin

Commercial fibronectin and collagen I pre-coated plates (BD)

All procedures were carried out under sterile conditions in a tissue culture hood.

Isolation and Culture of Mononuclear Cells from Murine Bone Marrow. Adult mice (≥ 8 weeks old) were culled via CO_2 inhalation and femurs/tibias were dissected from the animal using sterile instruments. Murine bone marrow (BM) was extracted by flushing the femurs and tibias with PBS (approx 10ml into a 15ml greiner falcon tube) using a 25G needle and syringe. BM was washed once by spinning cells in excess PBS at 1500rpm for 10mins at room temperature. The supernatant was carefully removed and discarded while the cell pellet was re-suspended in 3ml of PBS. The mononuclear cell (MNC) fraction was then isolated by density gradient centrifugation in Histopaque-1083 (Sigma). Briefly, 3ml total BM suspension was carefully layered on top of 3ml Histopaque-1083, pre-equilibrated to room temperature, and further centrifuged for 30mins at 1700rpm without brake. MNCs were aspirated from the 'buffy coat' using an 18G needle (approx. 2ml) and transferred to a 15ml falcon tube. PBS was added to a total volume of 10ml and the cell suspension was centrifuged at 1500rpm for 10min at room temperature. The supernatant was discarded and the cell pellet re-suspended in 3ml PBS. A sample (20µl) was used to calculate cell number using a modified neubaur counting chamber slide. The cell suspension was centrifuged a final time at 1500prm for 10minutes and the cells re-suspended in an appropriate amount of EGM-2 media to give $3x10^6$ MNCs per ml of media.

Short Term Culture. $3x10^6$ cells were plated in one well of a 24 well plate coated with fibronectin (BD). A minimum of 3 wells were plated per experiment. Cells were incubated at 37 ^oC in 5% CO_2. Media was changed on the fourth day of culture and on the seventh day early EPCs were quantified.

Long Term Culture. $3x10^6$ cells were plated in one well of a 24 well plate coated with collagen I (BD). A minimum of 3 wells were plated per experiment. Cells were incubated at 37^oC in 5% CO_2. Media was changed on the fourth day of culture and 3 times weekly thereafter for 4-6 weeks.

2.3.1.1.2. Isolation of Mouse CD31$^+$ BM Cells using Magnetic Dynabeads

<u>0.1% BSA/PBS</u>

0.05g BSA (≥ 98%, Sigma-Aldrich) disolved in 50ml sterile PBS and filter sterilised using a 0.22µm filter. The solution was stored at 4^oC and used within 48 hours of preparation.

All procedures were carried out under sterile conditions in a dedicated tissue culture hood.

Preparation of anti-CD31 Dynabeads. 75µl sheep anti-rat Dynabeads (approx. $4x10^8$ beads/ml, Invitrogen) were re-suspended in 5ml of filter sterilised 0.1% BSA/PBS in a 15ml falcon tube and then placed on a magnetic separator (DynaMag-15, Invitrogen) for 1min. The supernatant was removed and this washing step was repeated 3 times. Beads were then re-suspended in 1ml 0.1% BSA/PBS in a cryovial and incubated with 15µl of rat anti-mouse CD31 antibody (0.5mg/ml, BD Pharmingen) overnight at 4^oC with constant agitation. Excess antibody was removed by washing beads with 0.1% BSA/PBS four times using the magnetic separator as previously described. Finally, beads were re-suspended in 1ml 0.1% BSA/PBS, stored at 4°C and used within 48 hours.

Magnetic Cell Sorting. Within a sterile laminar flow hood a cell suspension of short or long term cultured MNCs was filtered through a 70µm cell strainer (Falcon) into a 50ml tube containing 20ml of EGM-2 medium and centrifuged for 5 minutes at 1500rpm. The supernatant was carefully removed and the cell pellet was re-suspended in 1ml EGM-2 medium. This cell suspension was incubated with anti-CD31 pre-coated Dynabeads for 40 minutes at 4^oC (to reduce phagocytic activity and other metabolic processes) with constant rotation. The cell/bead suspension was then transferred to a 15ml falcon tube and 0.1% BSA/PBS was added up to 5ml. The tube was mounted onto a magnetic separator and left for 1 minute. Thereafter the supernatant was removed following rigourous trituration (to reduce the incidence of contaminating non-endothelial mesenchymal cells and increase purity of yield) and discarded. This washing step was repeated three additional times, until the supernatant became clear. Finally, the cells were re-suspended in EGM-2 growth medium and plated into collagen-coated 6-well tissue culture plates. The following day the cells were washed three times with growth medium to remove any loosely adherent cells and surplus beads. Cultures were maintained by replacing medium every 3 days. When sub-confluent, cells were washed with PBS and detached with a 0.25% Trypsin, 0.03% EDTA (Life Technologies) solution at 37°C for 15-20 minutes. Cells were spun at 1000rpm for 5 minutes and re-seeded at a 1:2 dilution.

2.3.1.2. Cardiosphere-Derived Cells

Complete Explant Medium (CEM)
IMDM supplemented with 20% fetal calf serum, 1% L-glutamine, 100Units/ml penicillin, 100µg/ml streptomycin and 0.1mM 2-mercaptoethanol

Cardiosphere Growth Medium (CGM)
35% CEM/65% DMEM-Ham's F-12 mix supplemented with 2% B27, 0.1 mmol/L 2-mercaptoethanol, 20ng/ml EGF, 80ng/ml bFGF, 40nmol/L Cardiotrophin-1 and 40nmol/L thrombin.

Preparation of fibronectin-coated plates: (i) explant culture: add 100µl aliquot of stock fibronectin (1mg/ml, BD) to 12 ml PBS. Use 1ml of working solution to coat a 35mm petri dish. Incubate at 37^{o}C for 30 minutes, then remove the solution and wash once with PBS prior to use. (ii) CDC culture: add 25µl aliquot of stock to 6 ml PBS. Use 3ml of working solution to coat a T75 flask. Incubate at 37^{o}C for 30 minutes, then remove the solution and wash once with PBS prior to use.
Preparation of Poly-D-Lysine-coated plates: add 100µl aliquot of stock poly-D-lysine (2mg/ml low molecular weight, BD) to 12 ml PBS. Use 0.5ml of working solution to coat each well of a 24 well plate. Incubate at 37^{o}C for 30 minutes, then remove the solution and wash once with PBS prior to use.

All procedures were carried out under sterile conditions in a dedicated tissue culture hood.

Tissue Dissection. 3-6 day old mouse pups were culled via cervical dislocation and whole hearts were dissected using sterile instruments. Tissue was stored in ice cold serum-free CEM and processed for explant culture within 20minutes.

Explant Culture. Following three washes in PBS isolated myocardial tissue was digested in 0.05% Trypsin/EDTA for 5minutes whilst being cut into 1-2mm^3 pieces using sterile instruments. Enzyme activity was inhibited by the addition of CEM. The tissue fragments were individually seeded onto fibronectin coated (~8.4µg/ml) 35mm Petri dishes and cultured as explants in 2ml CEM at 37°C and 5% CO_2. Every third day of culture 0.5ml of CEM was added to each dish to prevent adherent explant fragments from drying out. After a period ranging from 10 to 14 days a confluent layer of outgrowth fibroblast-like cells appears, over which loosely adherent small phase bright cells migrate. These cells were collected by pooling; one PBS wash, one 1-2 min incubation with Versene (0.53 mmol/L EDTA) and one 2-3 min incubation with 0.05% Trypsin/EDTA (Invitrogen) at room temperature followed by gentle trituration.

Cardiosphere Culture. The collected explant derived cells (EDCs) were seeded at $1x10^5$ cells per well onto poly-D-lysine-coated (~2.4µg/ml) 24 well plates with 400µl cardiosphere-growing medium (CGM) per well. After four days of culture an additional 200µl of CGM was added to each well. By culture day six loosely adherent cardiospheres had formed and these were counted before being harvested using gentle trituration. Cardiospheres were collected in a 50ml falcon tube and allowed to settle at the bottom of the tube. The supernatant was discarded to remove any contaminating stromal-like cells. This sedimentation step was repeated before the cardiospheres were spun down at 1000rpm for 8 minutes. The pelleted cells were gently triturated to promote partial dissociation of the cardiospheres.

Cardiosphere-derived Cell Culture. Cardiospheres were seeded onto fibronectin coated (4.2µg/ml) T75 flasks in 15ml of CEM (generally the yield from one 24 well plate was plated into one T75 flask) and cultured at 37^{o}C in humidified air with 5% CO_2. Cells were maintained by replacing medium every three days and cultures were passaged once they reached sub-confluency (generally performed every 3-5 days). Cells were dissociated by washing with 5ml of PBS before being incubated with 5ml of Accutase cell detachment reagent (eBioscience) for 10min at room temperature and the flask was knocked harshly to release cells into suspension. Cells were spun at 1000rpm for 8 minutes and re-seeded at a 1:2 dilution.

2.3.2. Immortalised Cell Lines

The mouse skin endothelial (sEND-1) cell line was originally derived from skin microvasculature of transgenic mice expressing polyoma middle T oncogene and was obtained from Dr. Roy Bicknell (University of Oxford). The NIH-3T3 fibroblast cell line was originally derived from mouse embryos and was obtained from Caroline Dalgliesh (Newcastle University).

All procedures were carried out under sterile conditions in a dedicated tissue culture hood.

Cell Culture. Both immortalised cell lines were grown as monolayers at 37^{o}C in humidified air with 5% CO_2 and were cultured in Dulbecco's modified Eagle's medium

(DMEM) supplemented with 10% heat inactivated fetal calf serum. The medium was replaced every 3 days. When sub-confluent, cells were washed with PBS and detached with a 0.05% Trypsin/EDTA solution at 37 °C for 5 minutes. Cells were centrifuged at 1000rpm for 5 minutes and re-seeded at a 1:4 to 1:12 dilution.

Cryopreservation and Cell Recovery. Sub-confluent cells were detached with Trypsin/EDTA as described above and pelleted in cold medium. Cells were then re-suspended in ice-cold recovery cell culture freezing medium (Invitrogen) on ice (~1ml per T75 flask) and 0.5ml of cell suspension was transferred into one pre-labelled cryovial. Cells were slowly cooled to -80^{o}C using a cell freezing container containing isopropanol and after 1–3 days the cryovials were transferred to liquid nitrogen for long-term storage. To recover frozen cells, cryovials were removed from liquid nitrogen storage and transferred to a cell culture fume hood on dry ice. The cells were then rapidly rolled between hands and once they started to thaw 1ml of pre-warmed growth media containing 10% FCS was added to the cryovial. This cell suspension was transferred to a falcon tube containing a total volume of 10ml media and cells were centrifuged at 1000rpm for 5 minutes. Cells from each cryovial were seeded into one T25 flask and cultured as standard.

2.4. Cell Staining

2.4.1. Acetylated-LDL and Isolectin-B_4 Dual Staining

Short term cultured (STC)-EPCs were identified via positive staining for DiI-labelled acetylated-LDL (Invitrogen) uptake and FITC-labelled-GSL-I-B_4 (Griffonia simplicifolia I B4 Isolectin 4, Vector Laboratories) binding. Day 7 BM-MNC cultures (in 24 well tissue culture plates) were washed once with fresh media prior to being incubated with 0.5ml DiI-acetylated-LDL (5μg/ml EGM-2 media) per well, for 1 hour at 37 ^{o}C. The cells were then washed twice with media and incubated with 0.5ml FITC-GSL-I-B_4 (10μg/ml media) again for 1 hour at 37^{o}C. Cells were washed twice and then imaged under a Zeiss Axiovert microscope with phase contrast and fluorescence conditions using a digital camera.

2.4.2. Immunofluorescent Cell Staining

Cells were seeded onto 8-well glass chamber slides (Lab-Tek, Nunc) and allowed to adhere and grow for 24 hours. Additional cell treatments were performed as indicated in the following results chapters for the stated times. Cells were then washed twice with PBS and fixed with acetone for 5 minutes at room temperature. The fixative was removed by washing cells 3 times with excess PBS. To diminish background fluorescent signal, the cells were incubated with blocking solution (5% goat serum, 1% BSA) for 20 minutes at room temperature. The blocking solution was removed and primary antibody (diluted in blocking solution) was applied and cells were incubated at $4^{o}C$ overnight (see table 2.3 for antibody details and dilutions). The slides were then washed three times in excess PBS and (if a non-conjugated primary antibody was used) a fluorochrome-conjugated secondary antibody (see table 2.3) was applied for 1 hour at room temperature (1/200 dilution in blocking solution). Cells were again washed three times in excess PBS and finally slides were mounted with anti-fade hard set mountant with DAPI (Vector Laboratories) under a glass coverslip prior to examination using fluorescent microscopy.

Primary Antibody	Stock Concentration	Dilution	Incubation	Source
CD31 (MEC13.3 Clone)	0.5mg/ml	1/25	Overnight at $4^{o}C$	BD Pharmingen
Endoglin (MJ7/18)	0.5mg/ml	1/100	Overnight at $4^{o}C$	eBioscience
GFP-alexa 488	2mg/mL	1/100	1 hour at room temperature	Invitrogen
Secondary Antibody	**Stock Concentration**	**Dilution**		**Source**
Goat anti-Rat IgG Alexa-488 or 594	2mg/ml	1/200	1 hour at room temperature	Invitrogen

Table 2.3. Antibodies and conditions used for immunofluorescent cell staining.

2.4.3. X-Gal Cell Staining

X-Gal Staining Solution
6ml of 0.5M K3 Ferricyanide, 6ml of 0.5M K4 Ferrocyanide, 120ml of 0.5M Phosphate Buffer (pH7.2), 1.2ml of 1M $MgCl_2$, 6ml of 1%NaDeoxycholate, 1.2ml of 10% NP40, make up to 600ml with dH_2O. This staining solution should be stored in the dark at 4°C.

X-Gal
0.25g of X-gal dissolved in 10ml of dimethylformamide and stored at a stock concentration of 25mg/ml in the dark at -20°C. Added to pre-warmed staining solution at a final concentration of 1mg/ml immediately prior to use.

Glutaraldehyde
Stock glutaraldehyde is at 25% and stored at $-20^{O}C$.

Cells were seeded onto 8-well glass chamber slides (Lab-Tek, Nunc) and allowed to adhere and grow for 24 hours. Tamoxifen-mediated Cre-Recombinase activation *in vitro* was achieved by treatment with 1μM-5μM 4-hydroxy Tamoxifen to cell cultures and incubation for 24-96 hours, as indicated in the following results chapters. Cells were then washed twice with PBS and fixed with 0.5% gluteraldehyde/PBS for 10 minutes at room temperature. The fixative was removed by washing cells 3 times with excess PBS containing 1mM $MgCl_2$. X-Gal staining solution was added to the cells prior to incubating chamber slides at 37^{o}C until the desired staining was achieved (2-16hours). The cells were washed three times with PBS and lightly counterstained with eosin (slides stained with 1/30 eosin dilution for 1 minute and briefly washed in tap water). Slides were mounted with histomount (National Diagnostic) under a glass coverslip prior to examination under the microscope.

2.5. *In vitro* Cell Proliferation and Migration Assays

2.5.1. Proliferation/Cell Count Assay

Cells were seeded at a density of $2x10^4$ cells per well in 24 well cell culture plates (standard culture media), they became adherent after 6-12hours and were transferred to a live cell imaging facility (Nikon Biostation). Cells were maintained at 37^{o}C/5% CO_2 and after a period of 2hours (to allow for acclimatisation and to minimise condensation) the Biostation was programmed to take phase contrast images at regular 2 hour intervals using a 10X objective. A minimum of 4 fields of view were programmed per well and each experiment was performed in triplicate. Images were downloaded and cells were counted at each timepoint using Image J software.

2.5.2. MTT Assay

The 3-(4,5-dimethyl-2-thizolyl)-2,5-diphenyl-2H-tetrazolium bromide (MTT) colorimetric assay is used to measure cell viability. Yellow MTT tetrazolium salt is enzymatically reduced to form quantifiable purple formazan crystals in metabolically active cells[280]. Cells were seeded at $5x10^3$ cells per well in 96-well flat bottomed plates and cultured for 24hours with or without additional treatments. Thereafter 10μl of MTT (5mg/ml in dH_2O) was added to each well and plates were incubated for a further 5 hours at 37^{o}C. Cell media was removed and 100μl DMSO was added to each well to solubilise formazan. The plate was shaken to ensure all crystals were dissolved and

metabolic activity was recorded using a spectophotometric plate reader (MultiScan Ascent, Thermo Labsystems) set to measure absorbance at 570nm. Each experiment was performed in triplicate.

2.5.3. Wound Healing/Scratch Assay

The scratch assay was used to study cell migration *in vitro*. Cells were seeded at a density of $5x10^4$ cells per well in 12 well plates and cultured in standard growth medium until the monolayer became confluent (~90%). A sterile trimmed cell scraper (~1.5-2mm) was used to scrape the cell monolayer in a straight line to create a 'scratch' wound. Each well was rinsed twice with PBS to remove debris. Growth medium was replaced and plates were transferred to the live imaging facility (Nikon Biostation). Cells were maintained at $37^oC/5\%$ CO_2 and after a period of 2hours (to allow for acclimatisation and to minimise condensation) the Biostaion was programmed to take phase contrast images of the closing 'scratch' at regular 2 hour intervals using a 4X objective until the cells on the edge of the 'scratch' migrated to fully close the gap. A minimum of 3 fields of view were programmed per well and each experiment was performed in triplicate. Images were downloaded and the area between the two migrating fronts was calculated by drawing around them and employing the measure tool using Axioviosion Rel. 4.8 software (Zeiss). These measurements were used to calculate the percentage of area healed (gap closed) at each time-point.

2.6. Flow Cytometry

2.6.1. Murine BM-MNCs

2.6.1.1. Immunophenotyping BM-MNCs

Bone marrow (BM) was harvested by flushing freshly dissected femurs and tibiae with PBS using a 25G needle and syringe as described above. Cells were washed once by centrifuging at 1500rpm for 10minutes and red blood cells were lysed by incubating with Pharmlyse solution (BD biosciences, ammonium chloride at proprietary concentration; 1:10 dilution) for 10minutes at room temperature. Cells were then filtered through a 40µM cell strainer (BD biosciences) and quantified using a modified nebauer counting chamber slide. Cells were re-suspended in PBS at $5x10^6$ cells/ml and 100µl of cell suspension was transferred to 12x75mm round bottom FACS tubes. Primary antibody or IgG isotype control was added to $5x10^5$ cells at a dilution listed in

table 2.4 in a 100µl final staining volume. Cells were protected from light and incubated for 20minutes at 4°C before washing three times using a cell lyse/wash assistant (BD Biosciences). If unconjugated primary antibody was used, cells were then stained with secondary antibody (goat anti-rat alexa fluor 647 conjugated IgG (dilution 1:40, Invitrogen)) for 20minutes at 4°C and again washed three times. To allow exclusion of dead cells, DAPI was added at a final concentration of 1µg/ml and cells were incubated for a further 5-10minutes at room temperature. FACS analysis was performed immediately using a FACSCalibur instrument with CellQuest software or a LSRII flow cytometer and FACSDIVA software (all BD biosciences).

Each analysis included a minimum of 30,000 events. Only viable, single cells were included and they were identified on the basis of a forward scatter and side scatter plot. Data was displayed on dot plots and histograms with gates to delineate the boundary for negative cells. Gates were positioned using negative IgG isotype and no primary antibody controls. A minimum of three replicates were included per sample.

Primary Antibody	Stock Concentration	Dilution	Source
CD34-FITC	0.5mg/ml	1/100	BD Pharmingen
FLK1-PE	0.1mg/ml	1/100	BD Pharmingen
Endoglin (MJ7/18)	0.5mg/ml	1/100	eBioscience
CD45-FITC	0.5mg/ml	1/100	eBioscience
Secondary Antibody	**Stock Concentration**	**Dilution**	**Source**
Goat anti-Rat Alexa-647	2mg/ml	1/40	Invitrogen

Table 2.4. Antibodies used to immunophenotype BM cells.

2.6.1.2. FDG Staining to Detect LacZ Expressing Cells

Fluorescein di-β-D-Galactopyranoside (FDG, Marker Gene Technologies Inc.) is a β-galactoside analogue, which is cleaved by-galactosidase yielding fluoroscein in LacZ expressing cells.

BM cells were harvested as previously described and washed twice by centrifuging for 5minutes at 1200rpm in excess PBS/5%FCS. Cells were then filtered through a 40µM cell strainer (BD biosciences) and quantified using a modified nebauer counting chamber slide. Cells were re-suspended in ice-cold PBS/5%FCS at a concentration of $5x10^7$/ml. Cytoplasmic loading of cells with FDG was achieved by adding 20µl of 2mM of FDG (diluted in dH_2O) to 20µl of cell suspension (10^6 cells) for 75 seconds at 37°C. N.B. total volume is critical as it aids uptake by osmotic shock. Cell-uptake was stopped

with the addition of 500µl ice cold PBS/5% FCS and then cells were incubated on ice for 3 hours in the dark to allow enzymatic cleavage of the FDG substrate. Cells were washed three times using a cell lyse/wash assistant (BD Biosciences) and DAPI was added at a final concentration of 1µg/ml to allow exclusion of dead cells. FACS analysis was performed using a LSRII flow cytometer (BD biosciences). Fluorescein isothiocyanate (FITC) and DAPI were detected on the 488/530 and 407/450 channels, respectively, and data were analysed using FACSDIVA software (BD biosciences). Each analysis included a minimum of 50,000 events per sample (performed in triplicate) and only viable, single cells were included. Data was displayed on dot plots and histograms with gates to delineate the boundary for negative cells. Gates were positioned using positive and negative controls: isolated BM cells from a *Rosa-CreER^{T2}* mouse with ubiquitous lacZ expression were used as a positive control for lacZ staining, and NIH-wild type BM cells were used as a negative control.

2.6.2. Immunophenotyping Murine Cardiosphere-derived Cells

Sub-confluent passage 2 CDCs were harvested from culture flasks by incubating with accutase dissociation reagent for 10 minutes at room temperature. The cell suspension was transferred to a 50ml falcon tube and excess PBS was added prior to centrifuging cells at 1000rpm for 8minutes at room temperature. The resultant cell pellet was re-suspended in 20ml PBS and centrifuged again. Cells were re-suspended in 5ml PBS and a small sample (600µl) was used to quantify cell number using a ViCell automated cell counter (BD Biosciences). Cells were once more centrifuged at 1000rpm for 8minutes prior to being re-suspended in PBS at $5x10^6$cells/ml and 100µl of cell suspension was transferred to 12x75mm round bottom FACS tubes. Primary antibody was added to $5x10^5$ cells at a dilution listed in table 2.5 in a 100µl final staining volume. Separate IgG isotype controls were also included and protein concentration was matched to that of the appropriate antibody. Cells were protected from light and incubated for 20minutes at 4^oC before washing three times using a cell lyse/wash assistant (BD Biosciences). If unconjugated primary antibody was used, cells were then stained with secondary antibody (goat anti-rat alexa fluor 647 conjugated IgG (dilution 1:40, Invitrogen)) for 20minutes at 4^oC and again washed three times. For triple stained samples unconjugated anti-endoglin or anti-CD31 antibodies were applied first followed by alexa-647 conjugated IgG secondary antibody, after the designated washing steps. Thereafter cells

were washed again and cKit-PE-Cy5.5 and CD90-PE antibodies were added together. To allow exclusion of dead cells DAPI was added at a final concentration of 1µg/ml and cells were incubated for a further 5-10minutes at room temperature. FACS analysis was performed immediately using a LSRII flow cytometer (BD biosciences). Alexa-647 was detected on the 638/660 channel, whereas phycoerythrin (PE), PE-Cy5.5 and DAPI were detected on the 488/585, 488/710 and 407/450 channels respectively and both FITC and GFP were detected using the 488/520 channel. Data were analysed using FACSDIVA software (BD biosciences).

Each analysis included a minimum of 30,000 events and only viable, single cells were included. Data was displayed on dot plots and histograms with gates to delineate the boundary for negative cells. Gates were positioned using negative isotype and no primary antibody controls, as previously. A minimum of three replicates of each sample were analysed.

Primary Antibody	Stock Concentration	Final Dilution	Source
Endoglin	0.5mg/ml	1µl stock /100µl staining volume	eBioscience
cKit-PE-Cy5.5	0.2mg/ml	1µl (1/2 stock)/100µl staining vol.	eBioscience
CD90-PE	0.5mg/ml	1µl stock /100µl staining volume	BD Pharmingen
CD31	0.5mg/ml	1µl stock /100µl staining volume	BD Pharmingen
CD45-FITC	0.5mg/ml	1µl stock /100µl staining volume	eBioscience
GFP-alexa-488	0.5mg/ml	1µl stock /100µl staining volume	Invitrogen
Secondary Antibody	**Stock Concentration**	**Dilution**	**Source**
Goat anti-Rat alexa-647	2mg/ml	1µl (1/40 stock)/100µl staining vol.	Invitrogen

Table 2.5. Antibodies used to immunophenotype cardiosphere-derived cells.

2.7. RT-PCR

2.7.1. Primer Design

Previously published primer pairs used in this study are highlighted and referenced in table 2.6. All other primers were designed using Primer3 software[281]. The genomic DNA (gDNA) and complementary DNA (cDNA) sequences of the genes of interest were obtained from the UCSC Genome Browser and to confirm primer specificity BLAST searches for primer sequence similarity were performed.

RT-PCR primers were designed to span an intronic sequence between two exons to allow easy distinction between products derived from target cDNA template and products arising from the presence contaminating gDNA.

Gene	Sequence [5'-3']	Exon	cDNA bp	gDNA bp	Tm °C	Ref
Tgfbr2	F: GGAAGTCTGCGTGGCCGTGTGG R: CTATGGCAATCCCCAGCGGAGG	2-4	299	21349	61	[282]
Bmpr2	F: CTCAGAATCAAGAACGGCTGTG R: TGAATGAGGTGGACTGAGTGGT	2-4	359	27854	61	-
Endoglin	F: CAATGCCAGCATTGTCACCTCC R: AGAGGCTGTCCATGTCGATGCA	7-11	428	5139	58	[283]
Alk1	F: GACCTTGGGGAGCTTCAGA R: TGCAGAAGGATCTATAGCAGCA	3-4	281	835	58	-
Alk5	F: GCACCATCTTCAAAAACAGGGG R: GCCAAACTTCTCCAAACCGACC	2-4	415	12532	61	[284]
Pai1	F: GCTGTAGACGAGCTGACACG R: ACGTCATACTCGAGCCCATC	4-5	203	903	60	-
Id1	F: TCCTGCAGCATGTAATCGAC R: GAGAGGGTGAGGCTCTGTTG	1-2	356	582	60	-
β-Actin	F: TGAACCCTAAGGCCAACCGTG R: GCTCATAGCTCTTCTCCAGGG	3-4	396	850	61	[282]

Table 2.6. Details of primers used for RT-PCR. (Tm is annealing temperature)

2.7.2. RNA Extraction from Mammalian Cells and Reverse Transcription

RNA. Total RNA from cell lysates (approximately 10^6 cells per sample) was isolated using the RNeasy Mini Kit (Qiagen) followed by the RNeasy Micro Kit (Qiagen) to purify and concentrate the final yield. Protocols were followed according to manufacturers' recommendations including the on column DNase digestion step. RNA is vulnerable to degradation therefore prior to doing any practical work the laboratory bench was cleaned with RNase Zap wipes (Invitrogen), gloves were worn and barrier filter tips were used. RNA concentration (in ng/ul) was measured using the Nanodrop ND-1000 spectrophotometer (Thermo Scientific) at an absorbance of 260nm (A260). Purity of obtained RNA was also assessed; RNA was considered pure when the A260/A280 ratio was above 1.9 and the A260/A230 was between 1.8-2.2 (if either ratio is appreciably lower than these values this suggests the presence of contaminating protein or co-purified contaminants respectively). RNA was stored at -80^{o}C in RNase free water until required.

Complementary DNA. cDNA was prepared from extracted RNA using a High Capacity cDNA Reverse Transcription kit (Applied Biosystems). Briefly, 1µg RNA in 10µl DEPC- treated dH_2O was added to a reaction mix consisting of 2µl 10X reverse transcription buffer, 0.8µl 25X dNTP mix, 2µl 10X random primers, 2µl Multiscribe

Reverse Transcriptase and made up to a final volume of 20µl with 4.2µl with DEPC-treated dH_2O. The mixture was incubated at 25°C for 10minutes (to allow primer extension), 37°C for 120 minutes, 85°C for 5 minutes and cooled down swiftly to 4°C degrees and stored at -20°C until required.

2.7.3. RT-PCR of Cell-derived Material and Densitometric Analysis

RT-PCR. Reaction mixtures were made up to a total volume of 50µl in 0.2 ml thin walled PCR tubes and consisted of 5µl $MgCl_2$ (25mM), 5µl 10X Buffer IV, 0.4µl *Taq* red hot polymerase (Applied Biosystems), 1µl 20mM dNTPs (New England Biolabs), 1µl forward primer (20µM), 1µl reverse primer (20µM), 33.6µl dH_2O, and 2µl sample cDNA. Reactions were carried out using a C1000 thermal cycler (Biorad).

Primer details and the expected sizes of the amplified cDNA sequences are shown in table 2.6 and the RT-PCR cycling conditions used are shown in table 2.7.

Reaction Step	Primer Pairs				
	Tgrbr2 and Bmpr2	Endoglin	Alk5 and β-Actin	Alk1	Id-1 and Pai-1
1	94°C-5mins	95°C-5mins	95°C-5mins	95°C-5mins	94°C-2mins
2	94°C-15secs	95°C-75secs	95°C-30secs	95°C-30 secs	94°C-15secs
3	61°C-30secs	58°C-75secs	61°C-45secs	58°C-45secs	60°C-30secs
4	72°C-45secs	72°C-2mins	68°C-60secs	68°C-60secs	68°C-5secs
5	72°C-5mins	72°C-7mins	68°C-7mins	68°C-7mins	68°C-5mins
Cycles (Steps 2-4)	33	33	33	33	33

Table 2.7. Details of PCR conditions used for gene-specific RT-PCR.

Agarose Gel Electrophoresis. Successful and specific amplification of RT-PCR products were confirmed by ethidium-bromide stained gel electrophoresis as described in section 2.2.4.

Densitometry Analysis. Band intensity was measured by scanning ethidium bromide-stained agarose gels using an Typhoon Trio scanner (GE Healthcare) and performing densitometry analysis using ImageQuant TL image analysis software (GE Healthcare) which allows fully automatic lane and band detection and quantitation. Results were expressed as the densitometry ratio of target gene bands to the β-actin bands.

2.8. Protein Analysis

2.8.1. Protein Extraction and SDS-PAGE

Lysis Buffer
10mM Tris-HCl pH 7.4, 1% Triton X-100, 1/100 dilution of protease inhibitors (Sigma), 1/10 dilution pf 10X phosphatase inhibitor (PhosSTOP tablets, Roche)

2X SDS Loading Buffer
12.5ml 0.5M Tris-base pH 6.8, 10ml glycerol, 20ml 10% Sodium Dodecyl Sulphate (SDS), 7ml dH_2O, 0.5ml β-mercaptoethanol, 20mg Bromphenol Blue

1X SDS Running Buffer
14.4g Glycine, 3g Tris-base and 10ml of 10X SDS dissolved in 1 litre of dH_2O

Protein Extraction. Approximately 2.5 x 10^5 cells were washed in PBS, pelleted and stored at -80^{o}C until required. To extract proteins a defined volume of lysis buffer (typically 50-100µl) was added to each sample followed by repeated trituration. Prior to separation via SDS-PAGE a volume of 2X SDS loading buffer was added to each sample at a 1:1 2X SDS loading buffer: lysis buffer volume ratio to denature proteins, aid loading into wells and allow tracking of the sample during gel electrophoresis. The protein samples were denatured at 95°C for 10 minutes in a thermomixer, briefly sonicated and centrifuged for 3minutes at 1300rpm.

SDS-PAGE. Approximately 30µl of whole cell lysate was loaded per well of a pre-cast 10% Tris-HCl polyacrylamide mini-gel (Bio-Rad). The gels were run in 1X SDS running buffer for 1hour at 100 volts. Molecular weights of the proteins were determined using a pre-stained protein marker (New England Biolabs). Equal loading of protein was assessed by using α-tubulin as a loading control (discussed below).

2.8.2. Western Blotting

Transfer Buffer
14.4 g Glycine, 3g Tris-base dissolved in 1 litre dH_2O

TBST
150mM NaCl, 50mM Tris-HCl, 0.1% Tween-20

Stripping Buffer
0.1M Glycine dissolved in dH_2O, adjust pH to 2.2 with HCl

Protein Transfer to Membrane. Following protein separation by SDS-PAGE, the separated proteins were transferred in a wet transfer apparatus (BioRad) to polyvinylidene fluoride (PVDF) membrane (GE healthcare) at 4^{o}C in cold transfer buffer for 1hour at 100 volts. Prior to transfer the PVDF membrane was activated in methanol for 30seconds, dH_2O for 5minutes and equilibrated in cold transfer buffer for 20minutes. Successful transfer and equivalence of protein loading was confirmed using Ponceau S stain (Sigma). Briefly, membranes were incubated with Ponceau S solution for 5 minutes at room temperature then rinsed in dH_2O to remove background staining and allow clear visualisation of the transferred protein bands. To de-stain membranes were washed 2 x 10 minutes in TBST wash buffer.

Immunoblotting, Membranes were incubated in blocking buffer (5% Marvel dry milk/TBST) for 1 hour at room temperature to avoid non-specific antibody binding. This was followed by incubating membranes overnight at 4^{o}C with primary antibodies diluted to a specific concentration (see table 2.8 for antibody details) in primary antibody diluent (0.5% marvel/TBST). Membranes were then quickly rinsed in TBST before being washed 4 x 10 minutes in 5% Marvel/TBST. The membranes were then incubated with a secondary antibody conjugated to horse-radish peroxidase (HRP) directed against the primary antibody's species of origin (see table 2.8). The HRP conjugated secondary antibodies were diluted to a 1/2,000 concentration in 5% Marvel/TBST and left to incubate for 1 hour at room temperature. Membranes were again briefly rinsed in TBST before being washed 2 x 10 minutes in 5% Marvel TBST, followed by 4 x 10minutes in TBST.

Successful antibody binding was visualised by enhanced chemiluminescence (ECL) using the SuperSignal West Pico or Dura ECL Chemiluminescent Substrate kits (Pierce Biotechnology), which bind HRP antibodies and produce a light reaction that can be detected by exposure to X-ray film. Therefore band signals were detected after exposure of Western blot membranes to X-ray film (GE Healthcare) and processing in a Xograph Compact X4 automatic X-ray film developer (Xograph Imaging Systems Ltd.).

Membrane Stripping and Re-blotting. To strip the membrane of bound antibodies, it was incubated with stripping buffer for 30 minutes at room temperature followed by 3 x 10 minute washes in TBST. The membrane was then subjected to chemiluminescence

treatment and X-ray film developing to ensure successful stripping of bound antibody. Following 3 x 10 minute washes in TBST the membrane was ready to be re-blotted (beginning at the membrane block step).

Primary Antibody	Blocking Solution	Working Dilution	Secondary Antibody	Working Dilution	ECL Kit	Size (kDa)
phospho-Smad 1/5/8 (Cell Signalling)	5% Marvel/TBST	1:500 in 0.5% Marvel/TBST	α-rabbit HRP	1:2000 in blocking solution	Dura	60
Smad 1 (Cell Signalling)	5% Marvel/ TBST	1:500 in 0.5% Marvel/TBST	α-rabbit HRP	1:2000 in blocking solution	Dura	58-60
phospho-Smad 2 (Cell Signalling)	5% Marvel/ TBST	1:500 in 0.5% Marvel/TBST	α-rabbit HRP	1:2000 in blocking solution	Dura	60
Smad2 (Cell Signalling)	5% Marvel/ TBST	1:2000 in 0.5% Marvel/TBST	α-mouse HRP	1:2000 in blocking solution	Pico	60
Tubulin (Sigma)	5% Marvel/ TBST	1:1000 in 0.5% Marvel/TBST	α-mouse HRP	1:2000 in blocking solution	Pico	50
Endoglin (eBioscience)	5% Marvel/ TBST	1:150 in 0.5% Marvel/TBST	α-rat HRP	1:1000 in blocking solution	Dura	90

Table 2.8. Antibodies and conditions of use for western blotting.

2.9. Histological Procedures

2.9.1. General Solutions

10 x Phosphate Buffered Saline (PBS)
80g NaCl, 2g KCl, 14.4g Na_2HPO_4 and 2.4g KH_2PO_4 dissolved in 800ml of ddH_2O. Adjust pH to 7.4 with HCl then add ddH_2O to make volume up to 1 litre.

4% Para-formaldehyde (PFA)/PBS Solution
Add 4g of para-formaldehyde powder to 100ml of PBS and dissolve at 60°C. Divide into aliquots and store at -20°C until required.

4% Formaldehyde/PBS Solution
10.5ml of 38% formaldehyde solution (BDH, AnalaR, VWR International) and make up to 100ml with 1xPBS. Divide into aliquots and store at -20°C until required.

0.2% Para-formaldehyde (PFA)/PBS Solution
Add 0.2g of para-formaldehyde powder to 100ml of 1xPBS and dissolve at 60°C. Divide into aliquots and store at -20°C until required.

2.9.2. Paraffin Embedded Tissue

2.9.2.1. Tissue Processing and Sectioning

Tissue Dissection, Fixation and Paraffin wax embedding. Dissected tissue was washed twice in ice-cold PBS (5 minute each) and then fixed in 4% paraformaldehyde

or 4% formaldehyde (required for Masson trichrome staining; see 2.7.2.2) overnight at room temperature. The fixative was removed following three 1 hour washes in excess PBS with gentle agitation. The tissue was then incubated in 50% ethanol/dH_2O for a minimum of 2 hours at room temperature with gentle agitation of the tubes. The tissue blocks were then left at room temperature overnight in 70% ethanol/dH_2O. The tissue was then further dehydrated through 3 x 2 hour changes of 100% ethanol at room temperature before being left in a glass container containing Histoclear overnight in a fume cupboard. The following day, the tissue blocks were equilibrated in a minimum of 3 x 2 hour changes of molten paraffin wax at 60°C, followed by an overnight incubation in molten paraffin wax at 60°C before embedding the tissue in paraffin wax and allowing it to set in plastic moulds (RA Lamb). Tissue blocks were stored at 4°C.

Sectioning. Tissue blocks were sectioned using a Leica RM2235 rotary microtome with disposable microtome blades at a thickness of 8µm. Transverse or saggital serial sections were cut into small ribbons and transferred onto HistoBond adhesive glass slides (RA Lamb) bathed in water on a hot plate pre-heated to 37^{o}C to aid in flattening sections and remove creases. Slides were left to air dry on the hot plate for a minimum of 2 hours and any excess water was carefully removed using the edge of a tissue while taking care not to touch the tissue sections. The slides were incubated at 40^{o}C overnight to ensure that the sections adhered well to the HistoBond slides.

2.9.2.2. Masson Trichrome Histological Staining

Working Weigert's Iron Hematoxylin Solution (Sigma)
Equal volumes of solution A (1% Hematoxylin in 95% EtOH) and solution B (1.2% Ferric Chloride and 1% Acetic Acid in distilled water). The working solution is stable for approximately 10 days.

Phosphomolybdic/Phosphotungstic Acid Solution
1 volume of Phosphotungstic Acid Solution, 1 volume of Phosphomolybdic Acid Solution and 2 volumes of distilled water.

Sections were dewaxed and hydrated using the method described in table 2.9. Slides were then ‘mordanted’ in Bouin's Solution at room temperature overnight in fume hood to intensify the final colouration of the tissue. The slides were then washed in running tap water to remove yellow colour from sections and then rinsed briefly in distilled water. The sections were stained in working Weigert's Iron Hematoxylin solution

for 5 minutes followed by a 5 minute wash in running tap water and a rinse in distilled water. Sections were then stained in Biebrich Scarlet-Acid Fuchsin for 5 minutes and then briefly rinsed in distilled water. Slides were placed in freshly prepared working Phosphomolybdic/Phosphotungstic Acid solution for 5-10 minutes (allows for uptake of the aniline blue stain). Sections were finally stained in Aniline Blue solution for 5 minutes before a brief rinse in distilled water and differentiation in 1% acetic acid for 3-5 minutes to render the shades of colour more delicate and transparent. Sections were rapidly dehydrated through a graded ethanol series and cleared in Histoclear as listed in table 2.9 Finally, the stained sections were then mounted under cover slips using Histomount mounting medium and left to dry in a fume cupboard overnight. In Masson Trichrome stained sections, haematoxylin stains nuclei blue-black, Beibrich scarlet-acid fuchsin stains cytoplasm and muscle red while Aniline blue stains collagen blue.

Dewaxing and Rehydration		Dehydration and Clearing	
Treatment	**Incubation Time**	**Treatment**	**Incubation Time**
Slides at 60°C	1 hour	50% Ethanol	5 seconds
Histoclear	2 x 10 minutes	70% Ethanol	5 seconds
100% Ethanol	2 minutes	100% Ethanol	5 seconds
70% Ethanol	2 minutes	100% Ethanol	5 minutes
50% Ethanol	2 minutes	Histoclear	2 x 10 minutes
30% Ethanol	2 minutes		
Tap water	2 minutes		

Table 2.9. Method for (i) dewaxing and rehydrating paraffin sections prior to staining (white) and (ii) dehydrating and clearing sections prior to mounting (grey).

2.9.2.3. X-Gal Staining (Lung Wholemounts)

0.2% Gluteraldehyde Fixative Solution
Add 0.2% Gluteraldehyde, 0.02% NP40, 0.005M EGTA, 0.002M $MgCl_2$, and 0.1M Phosphate buffer at pH 7.6; make up to a total volume of 20ml with ddH_20

X-Gal Staining Solution
6ml of 0.5M K3 Ferricyanide, 6ml of 0.5M K4 Ferrocyanide, 120ml of 0.5M Phosphate Buffer (pH7.2), 1.2ml of 1M $MgCl_2$, 6ml of 1%NaDeoxycholate, 1.2ml of 10% NP40, make up to 600ml with dH_2O. This staining solution should be stored in the dark at 4°C.

X-gal
0.25g of X-gal dissolved in 10ml of dimethylformamide and stored at a stock concentration of 25mg/ml in the dark at -20°C. Added to pre-warmed staining solution at a final concentration of 1mg/ml immediately prior to use.

Wash Buffer
0.02% NP40 in PBS

Lung lobes were dissected and washed in ice-cold PBS prior to incubation in pre-cooled 0.2% gluteraldehyde fixative solution for 30 minutes at 4^0C. Post fixation the tissue was rinsed in PBS to remove excess fixative, washed thoroughly with wash buffer (3 x 30minutes) and then stained with pre-warmed 1mg/ml X-Gal staining solution overnight at 30^oC with gentle agitation. Following X-Gal staining the lung lobes were then washed in PBS (3 x 30minutes) to remove staining solution and fixed in 4% formaldehyde/PBS for 3 hours at room temperature. Tissue was washed in excess PBS (3 x 60minutes) before being imaged as wholemounts using a Stereomicroscope (Leica) and then processed through alcohol dehydration, embedded in paraffin wax and sectioned (see section 2.7.2.1).

2.9.3. Frozen Tissue

2.9.3.1. Tissue Processing and Sectioning

Lung and heart tissue was dissected quickly and carefully from adult mice (≥8 weeks) immediately after humane killing. Tissue was washed twice in ice-cold PBS and fixed in 0.2%PFA/PBS overnight at 4°C with gentle agitation followed by an overnight incubation in PBS + 2mM $MgCl_2$ + 30% sucrose solution at 4°C with gentle agitation. The dissected tissue was then attached to cork discs using OCT tissue freezing medium (Lamb) before being frozen (either snap frozen in liquid nitrogen-cooled isopentane or slow frozen using dry ice) and sectioned.

Further modifications of the method were employed as required. To clear the lungs of blood, lung tissue was perfused with PBS prior to dissection by inserting an insulin syringe into the pulmonary artery through the right ventricle and an incision was made in the left atrium to allow outflow of perfusate. For improved section quality, a 1:1 OCT:PBS mixture was injected through the trachea prior to dissection to inflate the lungs and help maintain their morphology. In this case it was important that the tissue was immediately snap frozen in liquid nitrogen-cooled isopentane. Heart tissue was fixed directly following washes in ice-cold PBS and prior to slow freezing a 1:1 OCT: PBS mixture was injected into the ventricular cavities. To freeze, heart tissue was orientated in small dispomoulds (Lamb), embedded in OCT compound and slowly frozen by incubating on dry ice for (approximately 15 minutes). Frozen samples were stored at -80^oC until required.

Cryo-sectioning frozen tissue blocks: Tissue blocks were sectioned using a Microm HM 560 CryoStar cryostat (Thermo Scientific). Following an equilibration period of approximately 30mins at -20^{o}C, 10µm serial sections were cut and mounted on polylysine glass slides (VWR International). The slides were left to air dry for a minimum of 60 minutes before being transferred to labelled slide mailers and stored at -80°C until required.

2.9.3.2. Immunohistochemistry using the Vectastain ABC System

Blocking Solution
5% rabbit serum diluted in PBS.

Heart and lung cryo-sections were removed from -80°C storage and allowed to reach room temperature for 30 minutes inside slide mailers to minimise condensation. Subsequently slides were transferred to a slide rack and left at room temperature for a further 30minutes. Sections were circled using a hydrophobic barrier pen whilst drying followed by a brief 5minute wash in PBS. Sections were then fixed in cold AnalaR acetone for 10 minutes and allowed to air dry for 30minutes prior to commencing the immunostaining protocol. All the incubation steps were performed in a humidified chamber at room temperature unless stated otherwise.

Following fixation, cryosections were washed in PBS for 1 x 5mins prior to a 1 hour incubation with blocking solution. Sections were then subjected to treatment with an Avidin/Biotin blocking kit according to manufacturer's instructions (Vector Laboratories) to block non-specific binding of Biotin/Avidin System reagents and endogenous biotin activity. Briefly the sections were incubated with Avidin D solution for 15 minutes and rinsed in PBS prior to a second 15 minute incubation with the Biotin solution and finally 2 x 5 minute washes in PBS. Sections were subsequently incubated with primary antibody at a specified dilution overnight at 4^{o}C followed by 3 x 5 minute PBS washes (see table 2.10 for antibody details; antibodies diluted in blocking solution). The sections were then incubated with a biotinylated rabbit anti-rat secondary antibody, diluted to a 1/200 working concentration in blocking solution, for 30 minutes. The Vectastain® ABC reagent (Vector Laboratories) was made up according to the manufacturer's instructions and allowed to stand for 30 minutes at room temperature before use. Sections were washed for 3 x 5 minutes in PBS, incubated in Vectastain®

ABC reagent for 30 minutes and then washed again in three changes of PBS (5 minutes each). Antibody binding was visualized using the liquid DAB substrate kit (BioGenex), which was prepared according to the manufacturer's instructions. Sections were rinsed under running tap water then counterstained with Mayer's Haematoxylin (RA Lamb) for 2-3 minutes followed by a final wash under running tap water before being dehydrated and cleared, according to the steps listed in table 2.9. Finally, slides were mounted under cover slips using Histomount mounting medium and allowed to dry overnight.

Negative or 'no primary' control sections were prepared as described above (primary antibodies replaced with blocking solution) to assess specificity of staining.

Primary Antibody	Working Dilution	Incubation	Additional Treatment	Blocking Solution	Secondary Antibody
Endoglin (MJ7/18) (eBiosciences)	1/400 (diluted in blocking solution)	Overnight at 4°C	Avidin/Biotin Blocking	5% rabbit serum/PBS	Rabbit anti-rat IgG (Vector Laboratories)
CD31 (MEC13.3 clone) (BD Pharmingen)	1/25 (diluted in blocking solution)	Overnight at 4°C	Avidin/Biotin Blocking	5% rabbit serum/PBS	Rabbit anti-rat IgG (Vector Laboratories)

Table 2.10. Antibodies and conditions of use for immunohistochemistry (Vectastain ABC System) on paraffin embedded tissue sections.

2.9.3.3. Immunofluorescence

Blocking Solution
5% goat serum, 1% BSA, 0.5% Tween-20 diluted in PBS

PBST
0.25% triton diluted in PBS

0.2% PFA fixed heart cryosections were removed from the -80°C freezer and allowed to thaw for 30minutes at room temperature inside their slide mailers, followed by drying for a further 30minutes in a slide rack. Sections were circled using a hydrophobic barrier pen (Vector Laboratories) whilst drying. All incubation steps were performed in a humidified chamber at room temperature unless stated otherwise. Antibody details, conditions and additional treatments are listed in table 2.11.

Sections were blocked by incubating in blocking solution for 2 hours at room temperature. The sections were then incubated with primary antibody at the appropriate

dilution and temperature (see table 2.11). Following 3x5miute washes in excess PBS and 1x5 minute wash in PBST sections were then incubated with the appropriate secondary antibody (diluted 1/200 in blocking solution, see table 2.11) for 1 hour at room temperature. Following 3x5 minute washes in excess PBS and 1x5 minute wash in PBST, sections were mounted under glass slides using Vectashield with DAPI hard set mounting media (Vector Laboratories) and left to dry at 4^{o}C in the dark.

Sections to be stained with biotinylated or CD11b antibodies were also pre-treated with a Streptavidin/Biotin blocking kit (Vector Laboratories) as per manufacturer's instructions. Briefly, following incubation in standard blocking solution, sections were incubated with Streptavidin solution for 15 minutes, rinsed in PBS and then incubated with Biotin solution for 15 minutes (all at room temperature).

For α-actinin staining, the Streptavidin/Biotin blocking step was used in place of blocking solution and was followed by treatment with the mouse on mouse (M.O.M.) immunodetection kit which enables the specific localisation of mouse primary antibodies on mouse tissues. Tissue sections were incubated with M.O.M. mouse Ig blocking reagent for 1 hour, washed in PBS (2x2minutes) and incubated in M.O.M dilute for 5minutes. Excess M.O.M. diluent was tipped off prior to α-actinin (1/400 in M.O.M diluent) being added and sections were incubated for a further 30mins. Following 2 x 2minute washes in excess PBS, sections were incubated with M.O.M. biotinylated anti-mouse IgG reagent for 10minutes and then washed again in PBS (2x2minutes). The tissue sections were then incubated with a 1/200 dilution of streptavidin alexa 594 conjugate in M.O.M. diluent for 30min (see table 2.11) and washed in excess PBS (3x5minutes), prior to mounting as above. All steps were performed at room temperature.

Double Immunofluorescent Staining. Antibodies directly conjugated to a fluorochrome were added to sections together (eg SMA-Cy3.3 and anti-GFP-alexa 488). For unconjugated antibodies (endoglin, CD31, cKit and CD11b), GFP staining was achieved by incubating sections with both the appropriate secondary antibody and anti-GFP-alexa 488 together, prior to final washes and mounting. For α-actinin staining sections were incubated with anti-GFP-alexa 488 following incubation with streptavidin alexa 594 and associated washes.

Negative or 'no primary' control sections were prepared as described above (primary antibodies replaced with blocking solution) to assess specificity of staining.

Primary Antibody	Working Dilution	Incubation	Additional Treatment	Secondary Antibody
Endoglin (eBiosciences)	1/100	Overnight at 4°C	-	anti-rat alexa 594 (Invitrogen)
CD31 (BD Pharmingen)	1/50	Overnight at 4°C	-	anti-rat alexa 594 (Invitrogen)
α-Actinin (Sigma)	1/400	30minutes at room temp.	Streptavidin/ Biotin Blocking Kit MOM Immunodetection Kit	streptavidin-alexa 594 (Invitrogen)
SMA-Cy3 (Sigma)	1/200	1 hour at room temp.	-	n/a
cKit (eBioscience)	1/100	1 hour at room temp.	-	anti-rat alexa 594 (Invitrogen)
CD11b (BD Pharmingen)	1/100	1 hour at room temp.	Streptavidin/ Biotin Blocking Kit	streptavidin-alexa 594 (Invitrogen)
GFP-alexa 488 (Invitrogen)	1/25	1 hour at room temp.	-	n/a

Table 2.11. Antibodies and conditions of use for immunofluorescence staining on frozen heart sections. All secondary antibodies were diluted 1/200 in blocking solution (streptavidin-alexa 594 diluted in M.O.M. diluent for α-actinin staining) and washed in PBST.

2.10. Microscopy & Image Analysis

For light microscopy, cells grown in tissue culture dishes or flasks were viewed using a Zeiss Axiovert 200 inverted microscope. Stained tissue sections and wholemounts were viewed using a Ziess Axioplan microscope and a Zeiss Stemi microscope respectively. For fluorescence microscopy, a Zeiss Axio Imager II was used (with optional apotome feature for the generation of higher resolution images) to view both cell and tissue slides. The Nikon biostation was used for live cell imaging and a Leica MZ 125 was used for mouse surgery and tissue dissection.

Images were recorded with a digital camera and analysed using Axiovision Release v4.8 or ImageJ (NIH) software packages,

2.11. Statistical Analysis

Statistical analyses were performed using SPSS software (version 19, SPSS Inc.). The Shapiro-Wilk normality test was used to assess if data was normally distributed. If data was normally distributed parametric analyses were performed; for multiple group data sets one-way ANOVA was used while comparisons between two independent groups

were made using the students unpaired *t*-test. The Mann Whitney statistical test (non-parametric) was used to analyse non-normally distributed data. Pearson's correlation coefficient was also used to assess correlation between two variables. A p value of <0.05 was accepted as being statistically significant.

2.12. Mouse Model of Myocardial Infarction and Intramyocardial Cell Injection

Pre-surgery Preparation. Prior to beginning any surgery the entire work area was thoroughly cleaned with 70% ethanol and equipment was checked for function. Surgical tools, drapes and accessories (sterilised by autoclaving) were assembled and tools were re-sterilised where appropriate during batch surgeries by using a hot bead steriliser (Harvard Apparatus)). The intubation cannula was checked to ensure that it was patent and free from obstruction. Sterile surgical gowns, face mask and gloves were worn and special care was taken to ensure aseptic technique was maintained throughout the procedure. A detailed record of each mouse was made prior to surgery including identification (denoted by cage number and earclipping), genotype and strain, date of birth and pre-operative weight. In addition details of administered drugs and the anaesthesia/ventilation regime were included and subsequent notes relating to the surgery were added during the recovery period.

Inducing anaesthesia, Intubation and Mechanical Ventilation. The mouse was injected (via IP route) with 0.2ml/kg Hypnorm, (a neuroleptanalgesic mixture of fentanyl/Fluanisone, Janssen) as a pre-sedative to aid in anaesthesia induction and maintenance, and was then placed in an anaesthetic induction chamber (97% O_2/3% (vol/vol) isoflurane, flow rate ~3 liters min^{-1}) for 1-2minutes prior to shaving the left side of the chest and the throat area. The animal was then transferred to an anaesthetic nose cone on a surgery panel (directly onto a sterile drape covering a heat blanket maintained at 37^{o}C (Harvard apparatus)) beneath a Leica MZ 125 microscope. Isoflurane was reduced to 97.5% O_2/2.5% (vol/vol) at a flow rate of ~2 liters min^{-1} and an 'activated charcoal filter gas scavenger' (Cardiff Aldasorber, Shirley Aldred & Co Ltd) was switched on to collect waste anaesthetic gases. The mouse was placed in a supine position in preparation for surgery with both forelimbs taped down either side of the body with care taken not to overstretch the limbs. A cotton bud was used to clean

the shaved regions with hydrex chlorhexidine solution (Ecolab). The microscope was focused over the throat region and a midline ventral skin incision of about 1cm in length was made slightly below the position of the cricoid cartilage using blunt scissors and rounded forceps. Skin was separated from connective tissue using blunt dissection and once the salivary glands were visualised they were split on their natural midline division by simultaneously pulling each part sideward with forceps. With this same manoeuvre the paratracheal muscles on the midline fascia were spilt to expose the trachea in the larynx area (care was taken to avoid pinching the trachea or the adjoining vessels and nerves). Anaesthetic flow was then opened to the ventilator to pre-flush the system with isoflurane. To intubate the mouse it was removed from the nose cone and, working quickly (to avoid the animal regaining consciousness during this part of the procedure), moved to a horizontal position and fixed at its front teeth using suture material. The trachea was exposed with forceps in the left hand while sliding the intubation cannula carefully into the mouth, then the trachea with the right hand (cannula tip should be visible through the displayed larynx and trachea). The cannula was immediately connected to the ventilator (Minivent, Harvard Apparatus) which was set at ~200µl min^{-1} / ~150 strokes min^{-1} and tubing supplying anaesthetic gases to the mouse was secured with tape. Anaesthetic flow to the nose cone was closed and outflow rate was reduced to 0.75 liter min^{-1}, while isoflurane concentration was reduced to 1.5-1.8%. The tracheal incision was covered with a sterile PBS soaked sponge to protect it and prevent the tissue from drying out.

Thoracotomy. The mouse was then positioned for thoracotomy; both forelimbs were fixed sidewards, the right hindlimb parallel to the tail and the left hind leg was turned to the right side. With blunt scissors and rounded forceps, a 1-1.5cm long skin incision was made over the left thoracic region starting from 1cm medial of the left axilla at a 45^{o} angle cranial-ward to the sternum. The skin was loosened from the connective tissue / muscle layers by blunt dissection and the left pectoralis major muscles were loosened, moved towards the right shoulder and fixed with a muscle retractor, while the left rectus thoracis and serratus anterior muscles were retracted towards the left side of the mouse. Fine scissors were used to carefully cut the sheets of connective tissue that prevent retraction, taking care not to damage the muscles or major blood vessels in the vicinity. Several intercostal spaces were visible and the following criteria were used to ensure the right space was chosen to ensure optimum exposure of the heart (usually between the

third and forth ribs); (i) curvature (after first rib that is less curved than the rib above), (ii) vessel landmark (a large vessel runs from outside to inside the thoracic cavity; take the intercostal space just cranially of this vessel), (iii) lungs (the lower edge of the left lung should be one intercostal space distal, or left of the surgeon's viewpoint, to the thoracotomy). The chosen intercostal muscle layer was perforated approximately 3mm from the sterno-costal junction to avoid injury to the left internal mammary artery, by pinching with small, rounded forceps. Once a hole was made, the closed tips of the forceps were inserted into the thoracic cavity from medial to lateral orientation with the tips parallel to the muscle thereby avoiding contact with the lungs. The tips of the forceps were then pushed up through the lateral side of the intercostal muscles and opened slightly while the overlying muscle was cut with fine scissors to produce thoracotomy. A small piece of sterile PBS soaked sponge was inserted into the thoracic cavity to protect the lungs and heart from instruments and a chest retractor (Mini Goldstein Retractor, Fine Science Tools) was used to expose the heart.

LAD ligation. The pericardium was opened and removed using two pairs of small, round forceps and the upper- and mid- left ventricle with its partly overlapping auricle and blood vessels were made visible. The left anterior descending coronary artery (LAD) was then identified as a bright red to orange/pink, pulsatile vessel running from below the left auricle to the apex. It has several side branches, which may also be visible, but the occlusion was made proximal to these branches to obtain maximal reproducibility of infarct size. Once identified, the LAD was enclosed in approximately four times its diameter of surrounding myocardium just distal to the left auricle with 7-0 Prolene suture material (Johnson & Johnson Medical Ltd) while taking care to avoid perforating the ventricle cavity. The suture was closed using a double surgeon's knot, fixed with two extra half-stitches and the suture ends were cut just long enough to prevent slipping of the knot. A successful infarction was characterized by (i) immediate change colour of the LAD after occlusion from bright red/orange to dark violet (ii) discoloration (pallor) of the LV free wall, (iii) a clear border between ischaemic and non-affected area and (iv) reduced or absent motility of the infarct area.

Intramyocardial Cell Injection. Cells were washed and prepared as a single cell suspension in PBS (without Ca^{++}) at a concentration of 10^6 cells per 5µl of PBS. Cells were stored on ice prior to being delivered via intramyocardial injection (within 15

minutes of preparation) using a 25µl Hamilton Microliter™ syringe and 33 gauge needle. Cells were injected into two sites bordering the ischaemic zone of the LV free wall (approx 2.5µl per site, see figure 6.1). The injection was superficial to prevent perforation of the LV wall and the injection sites were distal to the septum and RV to minimise contact with the conduction system. Successful injection was evident by the absence of cell backwash and the appearance of a white area in the myocardium.

Wound Closure. The retractor was removed and the thoracic cavity closed by enclosing the two separated ribs with two stitches of 5-0 vicryl suture material (round bodied needle, Johnson & Johnson Medical Ltd), keeping some distance from the ribs to prevent damage to the intercostal vessels and nerves. The internal sponge was removed prior to tying the sutures with one double surgeons knot secured with two half-stitches. The lungs were re-inflated by closing the ventilator expiratory tube three times very swiftly to generate a positive end expiratory pressure (PEEP), which helps the small airways to fill with air again. The pectoral muscles were moisturised with sterile PBS and gently pulled back into their original positions. The skin incision was closed with a continuous mattress suture using 5-0 vicryl suture material (cutting needle, Johnson & Johnson Medical Ltd) and the incision over the tracheal region was closed with one or two simple interrupted stitches.

Recovery. At this point the isoflurane flow was switched off and flow rate of oxygen increased to 2 liters min^{-1}, while a heating lamp was directed towards the mouse and all tapes were removed. Effective analgesia was achieved by injecting buprenorphine (Reckitt Benckiser Healthcare Ltd) subcutaneously into the scruff at a dose of 0.3mg/kg. Once the mouse started to breathe without mechanical aid the intubation cannula was removed from ventilator tubing and if the mouse continued to breathe independently the cannula was gently and carefully removed, if not artificial ventilation was resumed. The mouse was placed on the nose cone on its right side to receive oxygen. Within minutes the mouse recovered and became mobile, at this time it was transferred to a pre-warmed recovery cage in an incubator maintained at 33°C. The mouse was placed on a soaked diet to support recovery and if necessary the mouse received a second dose of analgesia 24-48 hours following surgery.

CHAPTER 3.

Effect of Altered TGFβ Signalling on EPC Yield from Mouse Bone Marrow

3.1. Introduction

EPCs have therapeutic potential for treating ischaemic heart disease, however in order to maximise the positive effects of EPC therapy a greater understanding of the fundamental regulatory mechanisms underlying cell-mediated heart repair are required. Autologous therapy is favoured to avoid immunological rejection. As the number of cells available for autologous therapy is limited it would be advantageous to enrich and deliver an optimised cell type. This study investigated how TGFβ signalling regulates the proliferation and differentiation properties of EPCs and whether this could be used to manipulate cells *ex vivo* to increase numbers to optimally high levels.

TGFβ controls the balance of proliferation and differentiation responses in many cell types. Evidence from endothelial studies strongly supports the prevailing hypothesis that TGFβ signalling through Alk1 versus Alk5 type I receptors represents a major angiogenic switch with TGFβ/Alk1 signalling promoting EC proliferation and angiogenesis while the TGFβ/Alk5 pathway opposes pro-angiogenic processes (reviewed in[6]). Both endoglin-dependent inhibition and promotion of TGFβ signalling has been observed, mediated by Alk5 and Alk1 related Smad signalling, although the exact mechanisms involved remain incompletely understood[237, 247, 265, 268, 285].

Given the inherent importance of the TGFβ superfamily to both vasculogenesis during embryonic development and angiogenesis in adult life, it is likely that components of this family play central roles in fundamental mechanisms underlying EPC-mediated vascular repair and biology.

In this study I tested the following two inter-related hypotheses:

(i) *EPC differentiation and proliferation responses are mediated by the TGFβ/Alk1 versus TGFβ/Alk5 angiogenic switch.* Consequently, inhibition of the TGFβ/Alk5 signalling pathway *in vitro* will enhance EPC proliferation and differentiation towards the endothelial lineage, leading to an increased yield of cells from mouse BM. To test this, EPCs cultured from mouse BM-MNCs were treated with SB431542, a synthetic molecule that potently inhibits the kinase activity of Alk5[286].

ii) *Endoglin acts as a critical regulator of the balance between TGFβ/Alk1 versus TGFβ/Alk5 responses and the resulting TGFβ–dependent differentiation and proliferation of EPCs.* Consequently, endoglin deficiency will reduce endoglin dependent attenuation of TGFβ signalling resulting in impaired proliferation and endothelial differentiation *in vitro,* leading to a decreased yield from mouse BM. To test this part of the hypothesis, EPC number was assessed in EPC cultures derived from $Eng^{+/-}$ mice.

3.2. Results

3.2.1. Characterisation of EPCs in Culture

Early and late EPCs residing in the MNC fraction of murine BM were isolated using commonly accepted methods involving short (7 days)[42, 55-56, 60] and long term (several weeks)[46, 59-61] cell culture (figure 3.1). Ficoll density gradients were used to separate BM-MNCs from red blood cells as described in chapter 2.3.1.1.1. After 4 days in culture non-adherent cells were removed and discarded while adherent cells were cultured further to generate early EPCs by day 7 and these cells were assessed for features of endothelial lineage. Additional cell cultures were maintained over several weeks to derive late EPCs. These formed endothelial colonies after 2 to 3 weeks and were further expanded to form a confluent cell monolayer with cobblestone morphology at 3 to 6 weeks. I assessed these cells for the expression of endoglin and the pan endothelial marker CD31.

Early EPCs were assessed for endothelial features through dual binding of the endothelial marker GSLI–isolectin-B_4[287] and uptake of acetylated low-density lipoprotein (acLDL)[288] (figure 3.2). Although this dual staining assay is not considered to be specific to endothelial cells, as it can also stain other cell types including monocytes/macrophages, it is widely used as a positive indicator of endothelial lineage[66, 89, 289]. Adherent cells dual-positive for acLDL up-take and isolectin B_4 binding were counted as early EPCs (figure 3.2) and for simplicity these cells will be referred to as short term cultured-EPCs (STC-EPCs) throughout the remainder of this thesis. Freshly isolated BM cells subjected to ficoll gradient separation are referred to as BM-MNCs and cells cultured for 7 days without further characterisation are referred to as STC cells.

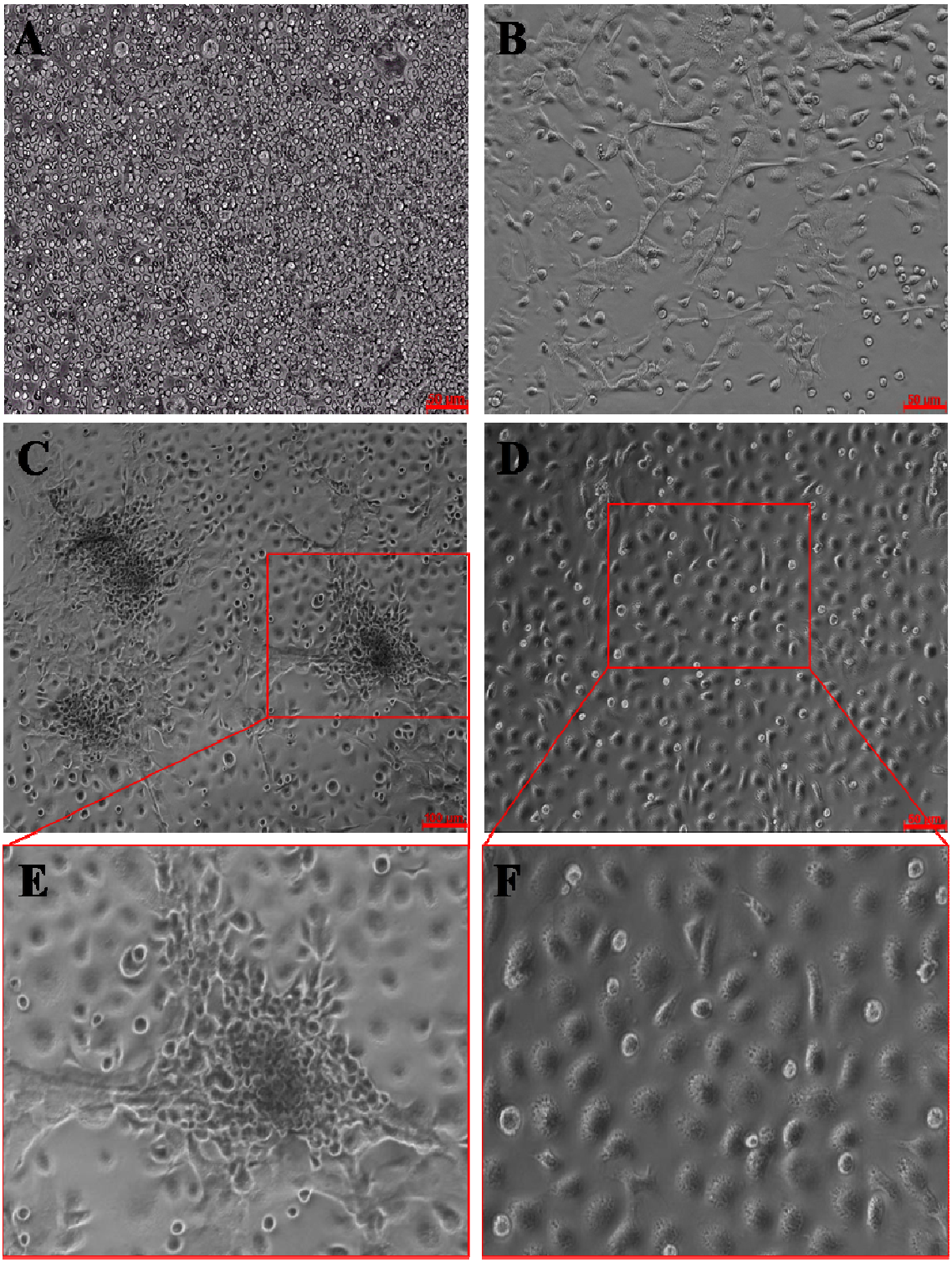

Figure 3.1. Short- and long-term culture of murine BM-MNCs. (A) Murine BM-MNCs immediately after seeding onto fibronectin coated dishes in endothelial culture conditions. (B) Adherent spindle-shaped cells 7 days after seeding. These cells represent STC cells. (C) Emergence of LTC outgrowth colonies 14 days after plating. Colonies were defined as a cluster of >30 central cells with spindle shaped cells radiating outwards. (D) Formation of cobblestone-like monolayer after 3 weeks in culture. Scale bars = 50µM (C) and 100µM (A, B and D). E and F=digital zoom of images C and D.

The original staining protocol involved the incubation of cells with 10µg/ml of both DiI-acLDL and FITC-GSLI-isolectin-B_4 for 1 hour consecutively. However I often observed cell death following staining, which complicated quantification of dual positive cells (figure 3.3). I hypothesised that the cells were 'over'-endocytosing acLDL substrate leading to cell membrane damage and lysis. To test this possibility, acLDL concentration and incubation time were titrated and the lower concentration of 5µg/ml (1 hour incubation) showed a notable decrease in cell damage without compromising staining intensity (figure 3.4). Therefore in all subsequent experiments cells were stained using an optimised protocol with 5µg/ml DiI-acLDL followed by 10µg/ml FITC-GSLI-isolectin-B_4 (one hour incubation each) (figure 3.2).

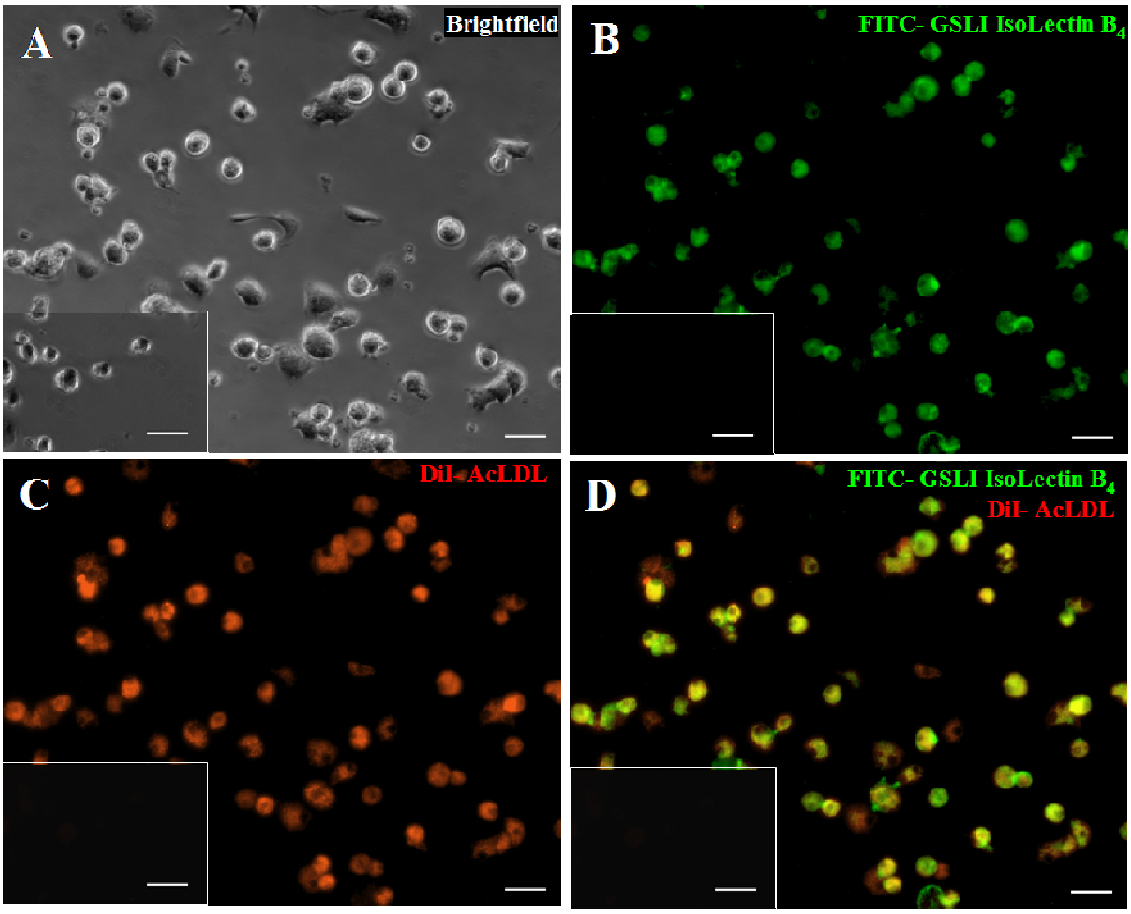

Figure 3.2. Staining STC-EPCs with DiI-acLDL and FITC-GSLI-isolectin B_4 using optimised staining conditions. Representative images of short term cultured (day 7) cells (A, phase contrast) stained with FITC-GSLI Isolectin-B_4 (B, green) and DiI-Ac-LDL (C, red). In merged images dual positive cells (STC-EPCs) appear yellow (D). Inset images represent unstained cells as negative controls. Scale bar = 20µm.

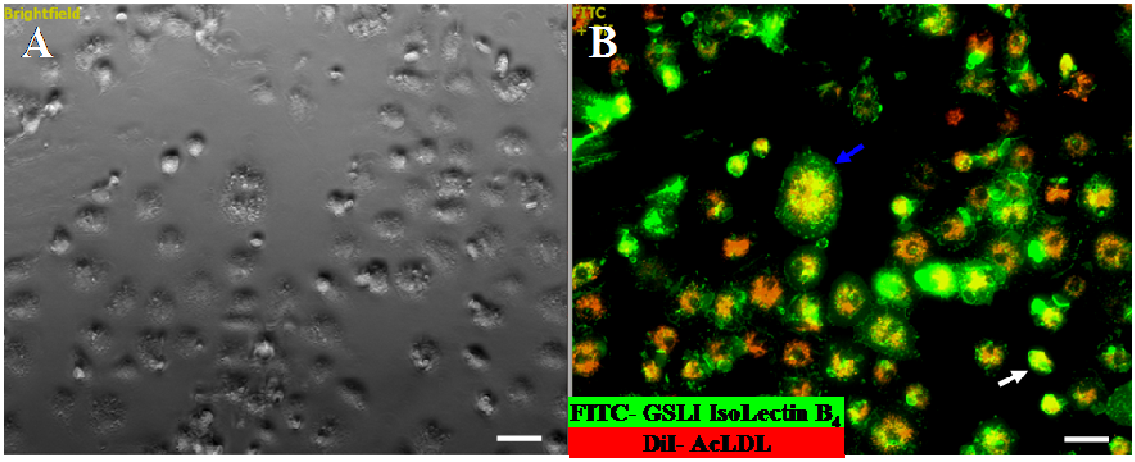

Figure 3.3. Staining STC-EPCs with DiI-acLDL and FITC-GSLI-isolectin B_4 using the original (non-optimised) staining conditions. Representative phase contrast (A) and dual stained (B) images using the pre-optimised staining protocol. The blue arrow highlights a damaged cell with abnormal membrane morphology whereas the white arrow indicates a typical normal cell. Scale bar = 20µm.

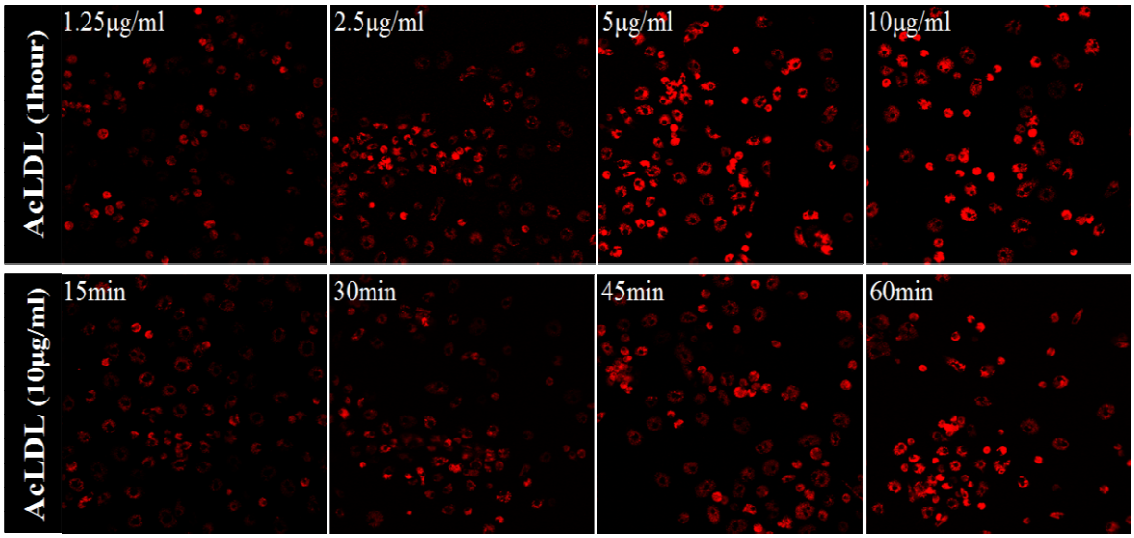

Figure 3.4. Titration of DiI-labelled acLDL to optimise cell labelling. Top panel, representative images of STC cells incubated for 1hour with DiI-acLDL concentration ranging from 1.25µg/ml to 10µg/ml. Bottom panel, cells incubated with 10µg/ml DiI-acLDL for 15min to 60min. Optimum staining of cells (defined as strongest signal with minimum cell membrane damage) determined as incubation at 5µg/ml for 1 hour. Images taken at X20 magnification.

Additionally, I noted a gradient of weak to strong fluorescence signal following DiI-acLDL and FITC-GSLI-isolectin-B_4 staining which led to a level of uncertainty in counting dual positive cells. To confirm the reproducibility of quantifying STC-EPCs using this optimised staining protocol multiple randomly selected microscopic fields were analysed and counted by myself and three independent observers (figure 3.5). Cell counts (total and dual positive cells) were compared between observers and revealed

only minor non-significant variations (analysed by ANOVA; total cell number p=0.804, STC-EPC p=0.996) suggesting that this is a robust quantitative method.

		Obs 1	Obs 2	Obs 3	Obs 4
field	Total	75	66	71	72
1	EPC	22	26	22	22
field	Total	94	98	98	101
2	EPC	42	46	49	47
field	Total	45	46	49	46
3	EPC	33	25	30	32
field	Total	85	85	89	82
4	EPC	45	42	42	46

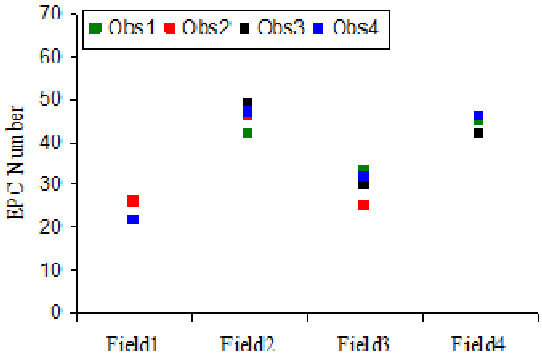

Figure 3.5. Confirmation of cell counting reliability and assessment of inter-observer variability. 3 independent observers (obs 2-4) and I (obs 1) counted i) total cell number and ii) total dual positive cell number (FITC-isolectin B_4/DiI-acLDL) in the same 4 random fields of view. Results were compared and analysed using ANOVA which revealed no significant difference between observers (total cell number p=0.804, STC-EPC p=0.996) indicating that the cell staining/enumerating method is reliable with minimum inter-observer variability. This test verified my counting method.

BM-MNCs cultured over longer periods (up to 6 weeks) were monitored for their ability to form colonies. These colonies were termed long term culture EPCs (LTC-EPCs) and consisted of clusters of round central cells with spindle-shaped cells radiating from this core. To assess the feasibility of using enumeration of outgrowth colonies to quantify LTC-EPC number *in vitro* I titrated cell seeding density ($5x10^6$, $4x10^6$, $3x10^6$, $2x10^6$ and $1x10^6$ cells per well of a 24 well plate) with the expectation of observing a proportional increase in colony number with increasing seeding density. Colonies were counted in a minimum of three wells per group and experiments were repeated three times to confirm results. A cell seeding density of below $3x10^6$ MNCs per well resulted in limited and highly variable LTC-EPC colony forming capacity, which reached an average of 7.7±3.9 colonies per well at day 12 (figure 3.6). Plating densities of $\geq 3x10^6$ MNCs per well, produced substantially elevated numbers of highly proliferative LTC-EPC colonies, which were comparable between groups (in replicate experiments the average outgrowth colony number ranged from 44.7±4.8 to 49.3±3.5 colonies per well). However, there was no proportional increase in LTC-EPC colony number as plating density increased from $3x10^6$ to $5x10^6$ MNCs per well indicating that this assay was not truly quantitative (figure 3.6). Based upon these observations I would argue that the colony assay is an unreliable method for assessing LTC-EPC number *in vitro*. However,

this experiment showed that a minimum of $3x10^6$ MNCs per well of a 24well plate are required for optimal yield of LTC-EPCs and this seeding density was used in all subsequent cell culture experiments.

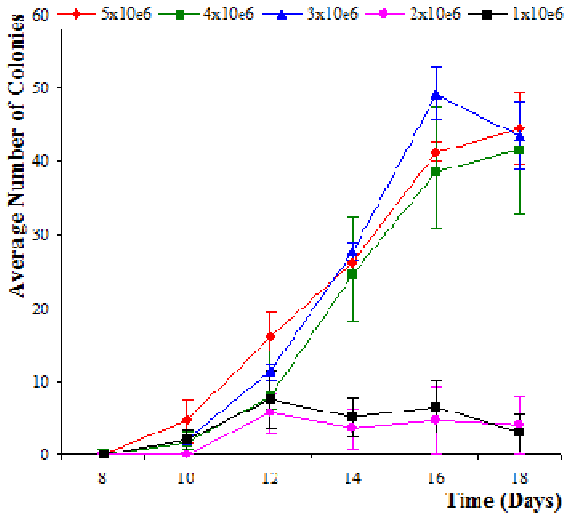

<u>Figure 3.6.</u> BM-MNC seeding density titration and formation of LTC-EPC colonies. There is a dramatic increase in mean LTC-EPC colony number as BM-MNC plating density increases from $1x10^6$ to $3x10^6$ per well. However, final LTC-EPC colony number is not proportional to plating density. Note that in cultures with $3x10^6$ cells/well initial plating density, the peak mean LTC-EPC colony number at day 16 and subsequent drop at day 18 is due to colonies reaching confluence and merging together. Error bars represent SEM.

LTC-EPCs which emerge from BM-MNC long term cultures were further cultured as a monolayer of outgrowth cells for up to an additional 2-4 weeks (figure 3.1D and F) and characterised by immunostaining with specific antibodies against the pan-endothelial marker CD31 as well as endoglin, a marker of endothelial and mesenchymal cells. Contrary to several studies employing similar methodologies[46, 59-61], I found that the cells emerging from LTC-EPC colonies were heterogeneous populations with marked variation in the expression levels of both CD31 and endoglin (figure 3.7) and were therefore not mature EC populations. Moderate to high endoglin expression was observed (65±12%), whilst CD31 expression was seen at much lower levels (35±6%). Furthermore, I noted limited proliferation potential in these populations, with cultures dying out after only 2-4 passages (approximately equivalent to 30 days in culture). This is in stark contrast to published data[59, 88, 290] citing a high proliferation rate and potential for self renewal, indeed this feature has alone been declared as strong evidence of the 'stemness' profile of LTC-EPCs. I attempted to enrich LTC-EPC number by introducing a $CD31^+$ cell purification step following initial colony formation (approximately 18 days after plating BM-MNCs) using magnetic beads (see 2.3.1.1.2), in a similar manner to Melero-Martin *et al*[104], however little difference was observed in proliferation potential.

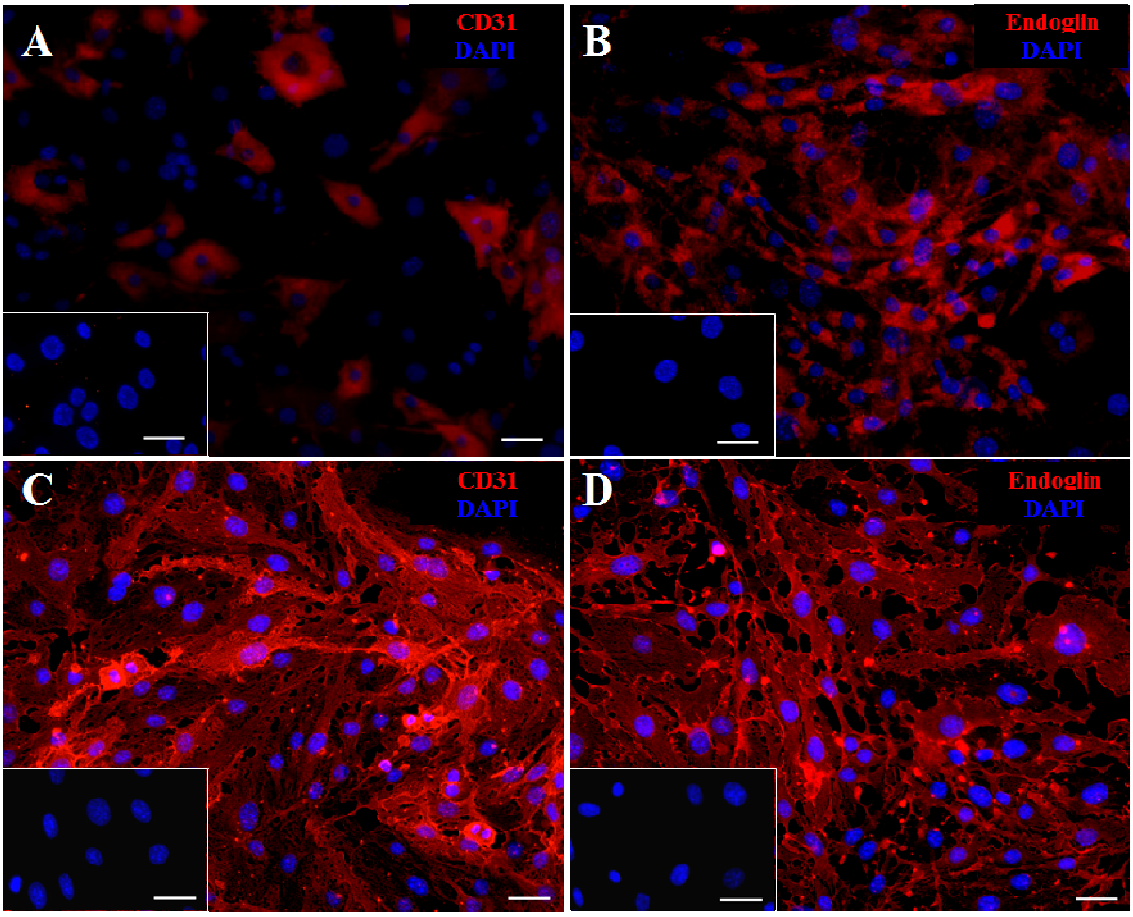

Figure 3.7. Immunofluorescent staining of LTC-EPC derived monolayer outgrowth with CD31 (A) and endoglin (B) at approximately 24 days from plating (passage 2). An anti-rat secondary antibody conjugated to alexa fluor 594 (red) was used and nuclei stained with DAPI (blue). Approximately 35±6% of LTC-EPC outgrowth stained positively for CD31, while endoglin expression was 65±6% (n=6 fields of view). Inset images in A &B represent no primary antibody controls. (C) and (D) show the positive control sEND-1 cell line immunostained for CD31 and endoglin respectively. Inset images in C & D show the NIH-3T3 fibroblast cell line is negative for CD31 and endoglin expression and acts as a negative staining control. Scale bars = 20μm.

3.2.2. Characterisation of Freshly Isolated BM-MNCs by FACS Analysis

EPCs occur at low abundance in fresh BM. These EPCs are defined as mononuclear cells with the potential to differentiate into functional ECs both *in vitro* and *in vivo* and express a combination of stem and endothelial markers. Common surface markers used to define EPCs in mouse BM are CD34 and Flk1 (also known as Vegfr2). I therefore used flow cytometry to identify EPCs residing in freshly isolated murine BM using these markers. In order to optimise a FACS protocol I first titrated both CD34 and Flk1 antibodies to minimise non-specific staining and maximise the separation between

positive and negative cells (figure 3.8). Additional optimisation steps, which were aimed at reducing non-specific staining, included lysing red blood cells, increasing cell wash number and pre-treating cells with an fc receptor block (CD16/32, BD Pharmingen). All steps were associated with a reduction in non-specific staining as assessed through comparison with matched isotype control stained samples (in which positive cells represent non-specific staining), however a significant amount of non-specific staining persisted (figure 3.8). This prohibited clear identification of the low numbers of Flk1 positive cells present and I was unable to develop a reproducible protocol allowing robust evaluation of EPC populations by FACS analysis. This also meant I was unable to use FACS to purify a defined population of EPCs in fresh BM. This work was further hampered by problems in removing the cells from fibronectin coated dishes for FACS analysis. For these reasons, short-term cultured BM-MNCs (either total cell populations (STC) or cells defined by acLDL and lectin staining (STC-EPCs)) were used for the remaining work described in this chapter.

3.2.3. Expression of Endoglin in Myeloid Cells

A major theme of this thesis is to investigate whether endoglin positive progenitor cells are capable of vascular repair. I therefore used flow cytometry to determine the expression of endoglin in total BM compared with the BM-MNC fraction of wild type (WT) mice (figure 3.9). I found that 2.4%±0.13 of WT total BM cells express endoglin and this positive population is enriched in the BM-MNC sub-population with a 3 fold increase in endoglin expression (7.3%±0.5). In order to investigate the role of endoglin in EPCs *in vitro* I used an $Eng^{+/-}$ mouse line to derive endoglin deficient BM-MNC cultures. Endoglin levels are reduced in $Eng^{+/-}$ total-BM and BM-MNC populations (1.4%±0.12 and 3.6%±0.32 respectively) compared with the equivalent cells derived from WT mice; however the enrichment of endoglin expression by BM-MNCs is maintained (2.5 fold increase in endoglin positive cell number in BM-MNCs compared with fresh BM). Experiments were repeated 3 times to confirm findings and figure 3.9 illustrates the results of one representative experiment.

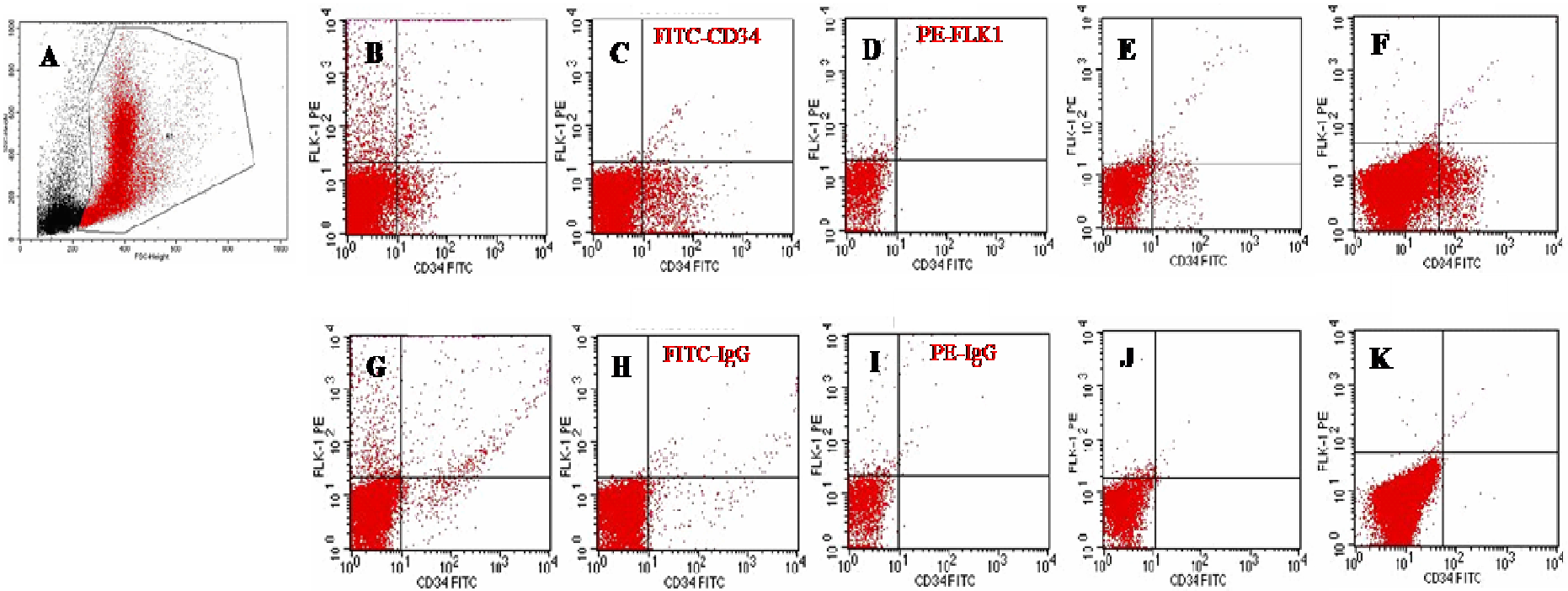

Figure 3.8. Representative images of the optimisation stages of murine (NIH) BM-MNC FACS analysis of CD34 and FLK1 vascular progenitor markers. Plot A shows side scatter (x axis, signal intensity is proportional to the amount of cytosolic structure in the cell) and forward scatter (y axis, signal intensity is proportional to cell size) properties of the cell population. A gate (shown in red) is placed around cells to be analysed further (cells not within this region represent cell debris and are not included). Plots B-F represent cell samples stained with FITC-CD34 (x-axis) and PE-FLK1 (y-axis), whereas plots G-K represent cell samples stained with FITC- and PE-isotype matched controls. Cells (or 'events') placed in the lower left quadrant of the dot plot are negative for both markers. Plots B and G show results of analysis with no optimisation. Note the extensive non-specific staining in the isotype control (G). Plots C (and H) and D (and I) represent optimal titration of CD34 and FLK1 antibodies respectively. Plots E (and J) show that lysing contaminating red blood cells in the sample and increasing cell washes post staining substantially reduced non-specific staining. As did pre-incubation with a mouse IgG block (plots F and K). However despite these interventions I could not reliably identify a dual positive cell population (upper right quadrants of dot plots in E and F) due to the low number of Flk1 positive cells.

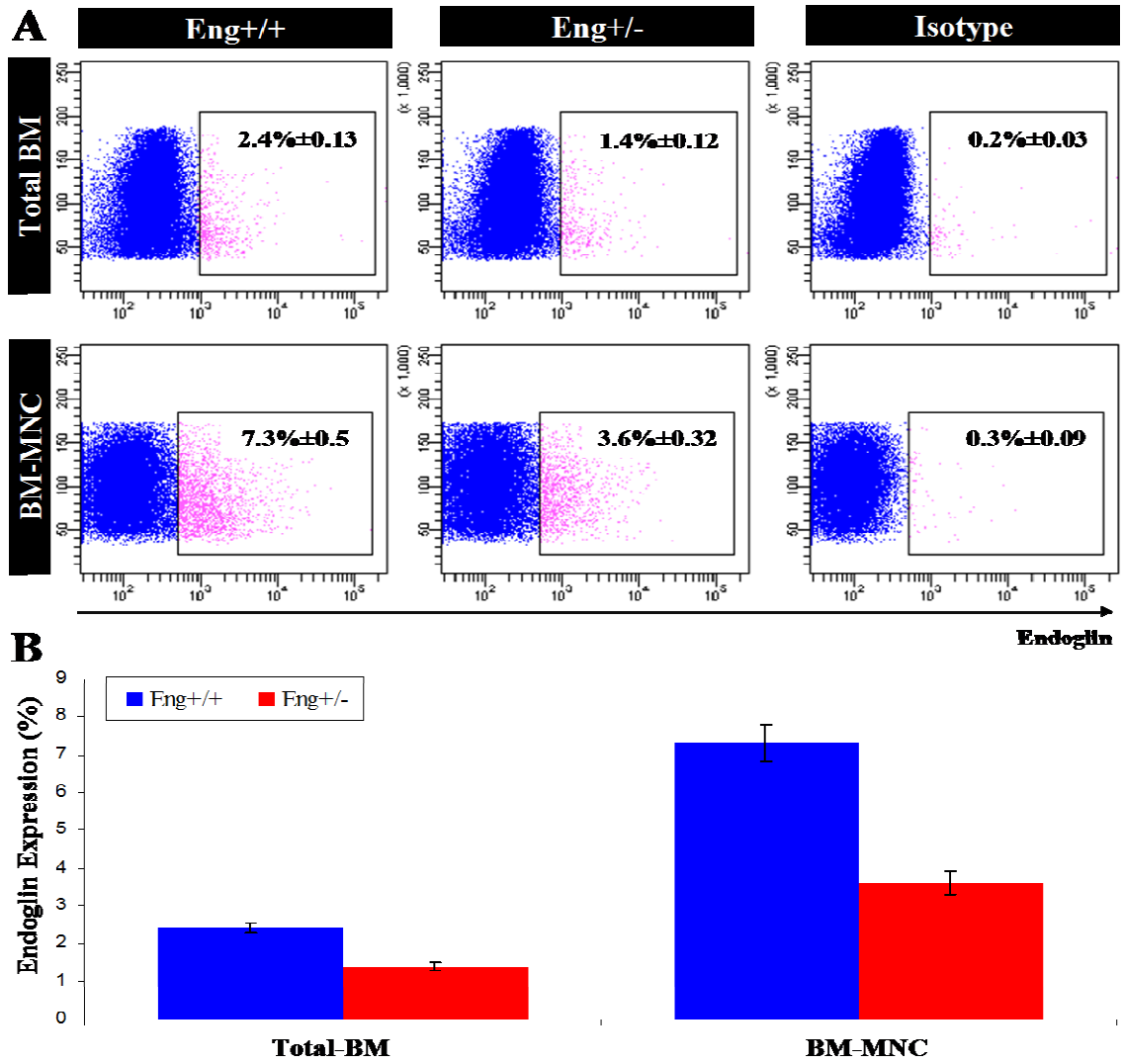

Figure 3.9. Endoglin expression in WT versus *Eng*$^{+/-}$ total BM and fractionated BM-MNCs. (A) representative dot plots (negative cells = blue, endoglin positive cells = pink) and (B) histogram showing that endoglin expression is enriched in BM-MNCs and reduced in cells derived from *Eng*+/- mice.

3.2.4. Modulating TGFβ Receptor Expression in EPCs

As endoglin was expressed in approximately 7% of fresh BM-MNCs (figure 3.9) and this increased to over 65% after long term culture (figure 3.7), I proceeded to examine endoglin expression in STC cells using semi-quantitative RT-PCR. Also, because endoglin is a co-receptor for TGFβ signalling I investigated whether BM-MNCs and STC cells expressed type I (Alk1 and Alk5) and type II (Tgfbr2 and Bmpr2) TGFβ receptors. In addition I tested whether reduced endoglin levels in *Eng*$^{+/-}$ cells or Alk5 kinase inhibition would affect the relative expression of these receptors.

Semi quantitative RT-PCR compares reaction products removed during cycles within the exponential amplification range of the PCR and allows semi-quantification and comparison of transcripts from different samples by relative densitometric analysis. RNA was prepared from freshly isolated MNCs and STC cells derived from WT and *Eng*$^{+/-}$ mice. Densitometric analysis was performed following RT-PCR and data from individual genes were plotted as ratios to the *β-actin* signal. Experiments were repeated three times and the statistical significance of differences between groups were determined using one-way ANOVA and unpaired *t*-tests.

All receptors analysed were expressed by WT BM-MNCs and STC cells (figure 3.10). Interestingly, *endoglin*, *Alk1* and *Alk5* showed differential expression profiles following short term culture, whereas the type II receptors, *Tgfbr2* and *Bmpr2*, showed comparable expression to freshly isolated BM-MNCs. In WT samples, *endoglin* and *Alk5* expression were significantly up-regulated following culture whereas levels of *Alk1* transcripts were markedly decreased (figure 3.10).

3.2.4.1. Effect of Reduced Endoglin Levels

As expected the levels of *endoglin* expression were significantly reduced in *Eng*$^{+/-}$ BM-MNCs compared to WT cells (figure 3.10B and 3.10C). Furthermore up-regulation of *endoglin* expression post-culture was of a lower magnitude in endoglin deficient samples than in WT counterparts. Interestingly, there was little difference observed in *Alk1* and *Alk5* gene expression in *Eng*$^{+/-}$ samples (figure 3.10B and 3.10D-E).

3.2.4.2. Effect of Alk5 Inhibition

Western blotting was used to examine the effect of the Alk5 inhibitor on TGFβ signalling (see figure 1.5). TGFβ1 treated (5ng/ml for 1hour) STC cells show phosphorylation of Smad2 confirming the ability of these cells to activate the TGFβ/Alk5 pathway in response to stimulation (figure 3.10A). As expected the phospho-Smad2 response was almost completely abolished in STC cells following a 24 hour pre-treatment with the Alk5 inhibitor (SB431542, 5μM) (figure 3.10A).

RNA samples were derived from WT-STC cells cultured either alone or with the Alk5 inhibitor (SB431542, 5μM) to determine whether the expression profile of TGFβ

receptors was altered. Densitometric analysis revealed no difference in expression of *Alk5* following kinase activity inhibition, nor was any significant difference detected in *endoglin, Alk1, Tgfbr2* or *Bmpr2* expression (figure 3.10B-E).

This work shows that WT STC cells express TGFβ receptors with increased expression of *endoglin* and *Alk5* following culture whereas *Alk1* levels are reduced compared to uncultured BM-MNCs. Neither endoglin deficiency nor Alk5 kinase inhibition appeared to have any effect on *Alk1* or *Alk5* expression.

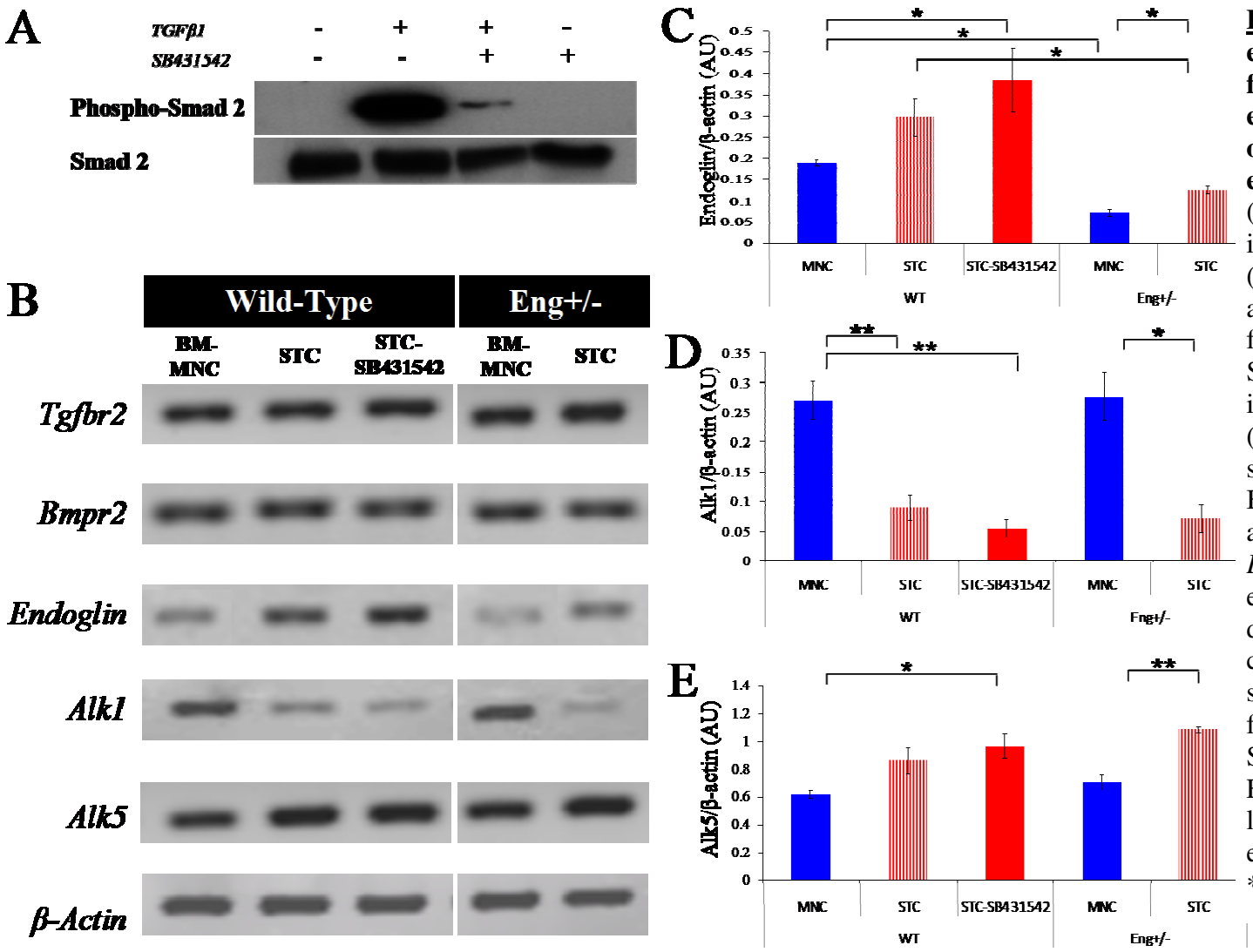

Figure 3.10. TGFβ receptor expression in BM-MNCs following short term endothelial culture; effects of Alk5 inhibition and endoglin deficiency.
(A) phosphorylation of Smad2 in the presence of TGFβ1 (5ng/ml, 30minutes) is abolished in STC BM-MNCs following treatment with 5μm SB431542. (B) Representative images of receptor expression. (C) *Endoglin* expression is significantly upregulated in BM-MNCs following STC and is reduced in cultured *Eng*+/- cells. (D) *Alk1* expression is significantly down-regulated following culture. (E) *Alk5* expression is significantly up-regulated following culture with SB431542 treatment. C, D and E show receptor expression levels relative to *β-actin* expression. * denotes $p < 0.05$, ** denotes $p < 0.01$.

3.2.5. Manipulating Yield of STC-EPCs *in vitro*

3.2.5.1. Effect of Reduced Endoglin Levels on STC-EPC Yield

As endoglin can counter the growth inhibitory effects of TGFβ[264], and can affect the balance of proliferation versus differentiation responses[237], I compared the number of STC-EPCs derived from WT and $Eng^{+/-}$ mice. BM-MNCs were seeded into multiwell plates (6 wells per genotype) and STC-EPCs were identified via DiI-acLDL and FITC-GSLI-isolectin-B_4 staining and counted after 7 days using 4 randomly selected fields of view per well (n=24 images per group). Experiments were performed three times independently to confirm results. Cell counts were normally distributed and statistical significance was determined using the unpaired *t*-test. To standardise results the STC-EPC number was also expressed as a ratio of total cell count and subjected to statistical testing.

Levels of STC-EPCs were significantly reduced in endoglin deficient cultures as compared to WT cells in three independent experiments with mean levels ranging from 27.8%-37% fewer EPCs (figure 3.11A-B, table 3.1). No significant difference in total cell count was found between the two groups (figure 3.11A). Additionally there was no significant difference found between ac-LDL and GSLI-isolectin-B_4 positively stained cells when analysed separately indicating that levels of both markers were equally affected in $Eng^{+/-}$ STC-EPCs (fig 3.11C). These results suggest that endoglin levels are important for EPC differentiation and/or proliferation in short term culture.

To determine the effect of reduced endoglin levels on STC-EPC viability and proliferation the colorimetric MTT assay was used. This assay examines the mitochondrial metabolic capacity of viable cells. The reduction of tetrazolium salts by mitochondrial dehydrogenase into a water insoluble formazan product results in purple crystal deposits in the cell medium which are re-suspended in DMSO and the optical density (OD) of this solution can be measured. Increased mitochondrial activity of cells reflects increased ATP production to fuel cell replication, whereas lower levels of reduction are observed in senescent or apoptosing cells. The MTT assay revealed no significant difference between WT (OD 0.195±0.005) and $Eng^{+/-}$ (OD 0.178±0.006) STC-EPCs as confirmed by the unpaired *t*-test ($p>0.05$) (figure 3.11D). This data suggests that endoglin deficient STC-EPCs do not display reduced proliferation or

viability and differences observed in cell count may be due to a reduced capacity to differentiate towards the endothelial lineage.

Genotype	Total Cell Count mean±SEM	STC-EPC Count mean±SEM	% STC-EPC mean±SEM	Unpaired t-test *p* Value	% Change
WT	63.29±1.85	34.08±2.57	54±4	0.008	(-) 27.8%
***Eng*+/-**	63.00±1.61	24.54±2.47	39±4		
WT	65.46±2.21	44.54±1.90	68±2	<0.001	(-) 27.8%
***Eng*+/-**	65.67±1.72	32.46±1.39	49±2		
WT	62.50±3.24	34.00±3.05	54±3	<0.001	(-) 37%
***Eng*+/-**	65.00±2.01	21.46±1.86	34±3		

Table 3.1. Reduced endoglin levels leads to a significantly reduced yield of STC-EPCs. Table illustrating the results and statistical analyses of 3 independent experiments analysing the effect of endoglin deficiency on STC-EPC yield. The statistical significance of differences between groups was determined using unpaired *t*-tests. *p* values <0.05 considered significant.

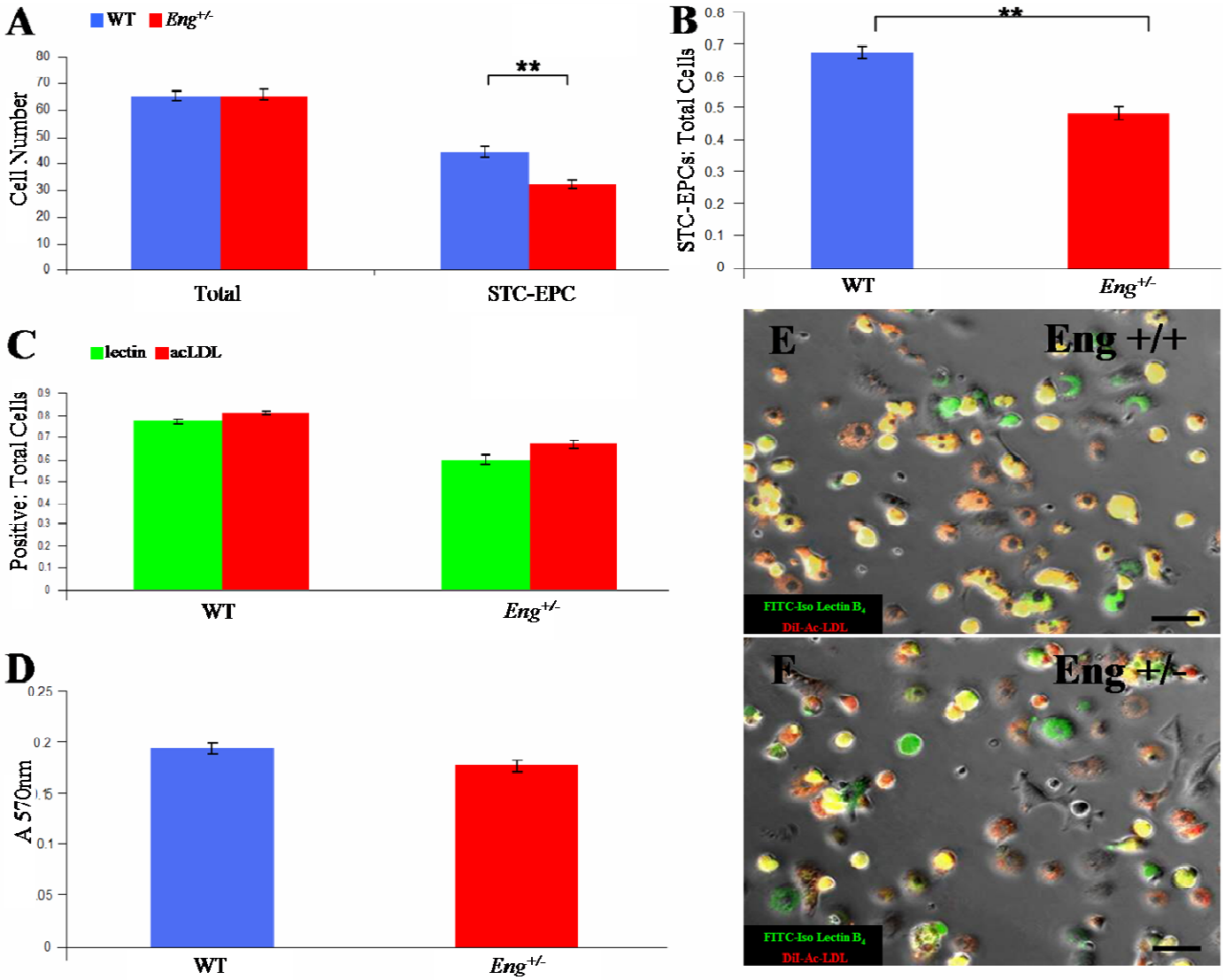

<u>Figure 3.11.</u> Effect of endoglin deficiency on STC-EPC number *in vitro*. Histograms showing absolute counts of total cell and STC-EPCs (A), EPC counts proportional to total cell number (B). Analysis of isolectin+ and acLDL+ cell number (C). Effect of endoglin deficiency on STC-EPC viability using MTT assay (D). Representative images of WT (E) and endoglin heterozygous (F) short term cultured BM-MNCs stained with DiI labelled acLDL (red) and FITC labelled GSLI-Isolection-B_4 (green) merged with phase contrast images to allow visualisation of all cells. Scale bar = 20µm.

3.2.5.2. Effect of Alk5 Inhibition on STC-EPC Yield

Endothelial TGFβ signalling through the type I receptor Alk5 is associated with cellular growth inhibition and the resolution phase of angiogenesis[6]. I tested the hypothesis that inhibiting this signalling pathway would increase EPC proliferation during short term culture by quantifying STC-EPCs following treatment with SB4315452 (5μm versus 10μm). Data was normally distributed and differences in STC-EPC number between groups were initially assessed using one-way ANOVA. Where this analysis suggested significant differences existed ($p<0.05$) unpaired *t*-tests were then used to calculate precise differences between pairs of groups. Experiments were repeated a minimum of three times to confirm findings.

Inhibitor treated cultures contained significantly higher levels of dual positive cells than untreated cultures (figure 3.12). The increase in STC-EPC number ranged from 20% to 35.8% in 5μM SB431542 treated cultures and from 24.1% to 39.3% in those cultures treated with 10μM SB431542 (table 3.2). Total cell number was also shown to be significantly higher in inhibitor treated cultures (figure 3.12A) suggesting either increased proliferation of non-endothelial cell types or increased adhesion to the fibronectin matrix, which may also be attributable to the inhibition of TGFβ/Alk5 signalling. This increase in total cell number exemplifies the need to quote STC-EPC yield as a ratio to avoid misrepresenting levels of EPC in different treatment groups.

MTT assays revealed significantly increased viability and/or proliferation in STC-EPC cultures treated with SB431542 (both 5μM and 10μM) as compared to untreated cells (figure 3.12D). However, cell viability was similarly affected in 10μM compared with 5μM treated cultures. Overall this part of the study confirmed the hypothesis that STC-EPC yield could be increased by inhibiting Alk5 signalling and that this may have occurred by increasing the viability and/or proliferation of these cells.

3.2.5.3. Alk5 Inhibition Rescues the Low Yield of STC-EPCs Associated with Endoglin Deficiency

As Alk5 inhibition increased the yield of STC-EPCs I also tested whether SB431542 treatment would rescue the low yield of STC-EPCs generated from $Eng^{+/-}$ cultures. BM-MNCs were derived from adult WT and $Eng^{+/-}$ littermate mice and treated with or

without 10μM SB431542 for 7 days. STC-EPC number was compared between untreated and inhibitor treated groups. Again, the experiment was repeated 3 times to confirm results and statistical analysis was performed as previously described (see section 3.2.5.1.). Results (shown in figure 3.13) revealed that Alk5 inhibition partially rescued the defect in STC-EPC yield from endoglin deficient cultures. STC-EPC number was significantly increased in SB431542 treated cultures from both WT and *Eng*$^{+/-}$ BM (34% to 51.5% and 29.2% to 60.7% increase respectively, table 3.3) with levels in *Eng*$^{+/-}$ inhibitor treated cultures being comparable to WT untreated levels (table 3.3).

However, total cell counts were not significantly different between SB431542 treated and untreated cells in these cultures (Fig 3.13A) in contrast to earlier experiments (Fig 3.12A). This may be due to the intrinsic variability of the culture method.

Analysis of proliferation and viability using the MTT assay revealed a positive effect of Alk5 inhibition in endoglin deficient cultures (Fig 3.13C), in a similar manner to that observed previously in inhibitor treated WT cultures (Fig 3.12D).

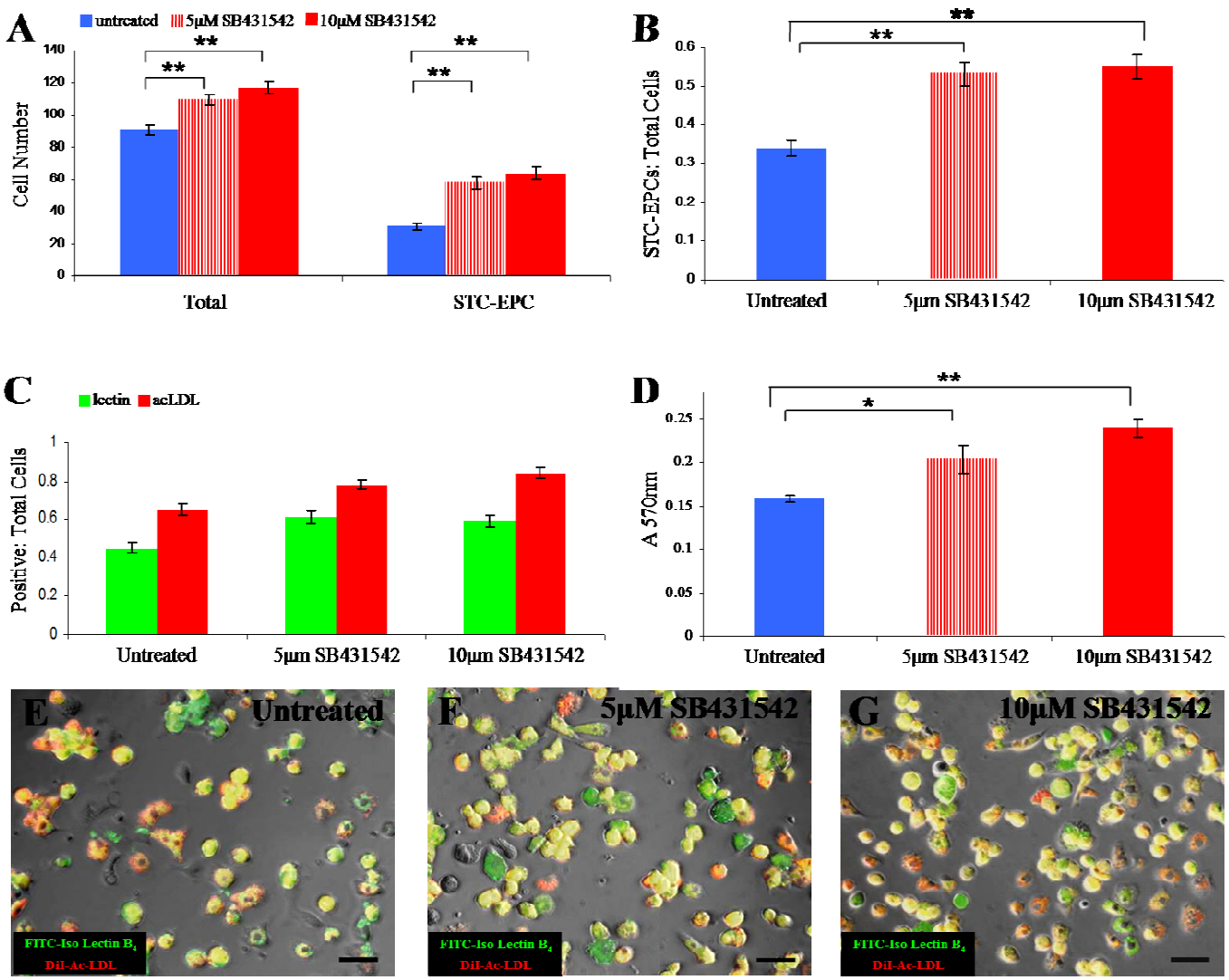

Figure 3.12. Effect of Alk5 inhibition on STC-EPC number *in vitro*. Histograms showing absolute counts of total cells and STC-EPCs (A), STC-EPC counts (expressed as a ratio of total cell number) (B) reveal a significant increase in cells of endothelial lineage following Alk5 kinase activity inhibition. Analysis of cell number using single stains (isolectin$^+$ or acLDL$^+$) reveal a similar increase in cells of endothelial lineage following Alk5 inhibition (C). Analysing the effect of Alk5 inhibitor treatment on STC-EPCs using MTT assay (D) reveals a significant increase in cell viability/proliferation.
Representative images of untreated WT (E) and SB431542 treated (5μm (F) vs 10μm (G)) WT STC-EPCs stained with DiI labelled acLDL (red) and FITC labelled GSLI-Isolection-B_4 (green) merged with phase contrast images to allow visualisation of all cells. Scale bar = 20μm.

	Total Cells at day 7 mean±SEM	Anova Total cell number *p*-value	STC-EPC Count mean±SEM	% STC-EPC mean±SEM	ANOVA % STC-EPC *p* value	% STC-EPC Unpaired *t*-Tests, *p* Value			% Change
						Unt vs 5µM	Unt vs 10µM	5µM vs 10µM	
Untreated	68.13±1.71		29.71±1.06	44±2					
SB-5uM	83.21±2.93	<0.001	46.08±2.61	55±2	<0.001	<0.001	<0.001	n/s	(+) 20%
SB-10uM	86.46±2.65		49.50±1.62	58±1					(+) 24.1%
Untreated	90.75±3.06		30.79±2.41	34±2					
SB-5uM	109.42±3.08	<0.001	57.75±3.55	53±3	<0.001	<0.001	<0.001	n/s	(+) 35.8%
SB-10uM	117.04±3.83		63.92±3.74	55±3					(+) 38.2%
Untreated	73.83±2.68		25.08±1.92	34±3					
SB-5uM	87.33±3.88	0.012	41.25±3.02	48±4	<0.001	0.006	<0.001	n/s	(+) 29.2%
SB-10uM	93.17±6.01		51.42±3.54	56±3					(+) 39.3%

Table 3.2. Inhibition of Alk5 kinase activity leads to a significantly increased yield of STC-EPCs. Table illustrating the results and statistical analyses of 3 independent experiments analysing the effect of Alk5 inhibitor (SB43152 (SB)) treatment on STC-EPC yield. The statistical significance of differences between groups was determined using one-way ANOVA ($p<0.001$) and unpaired *t*-tests (*p* values <0.05 were considered significant; n/s = not significant).

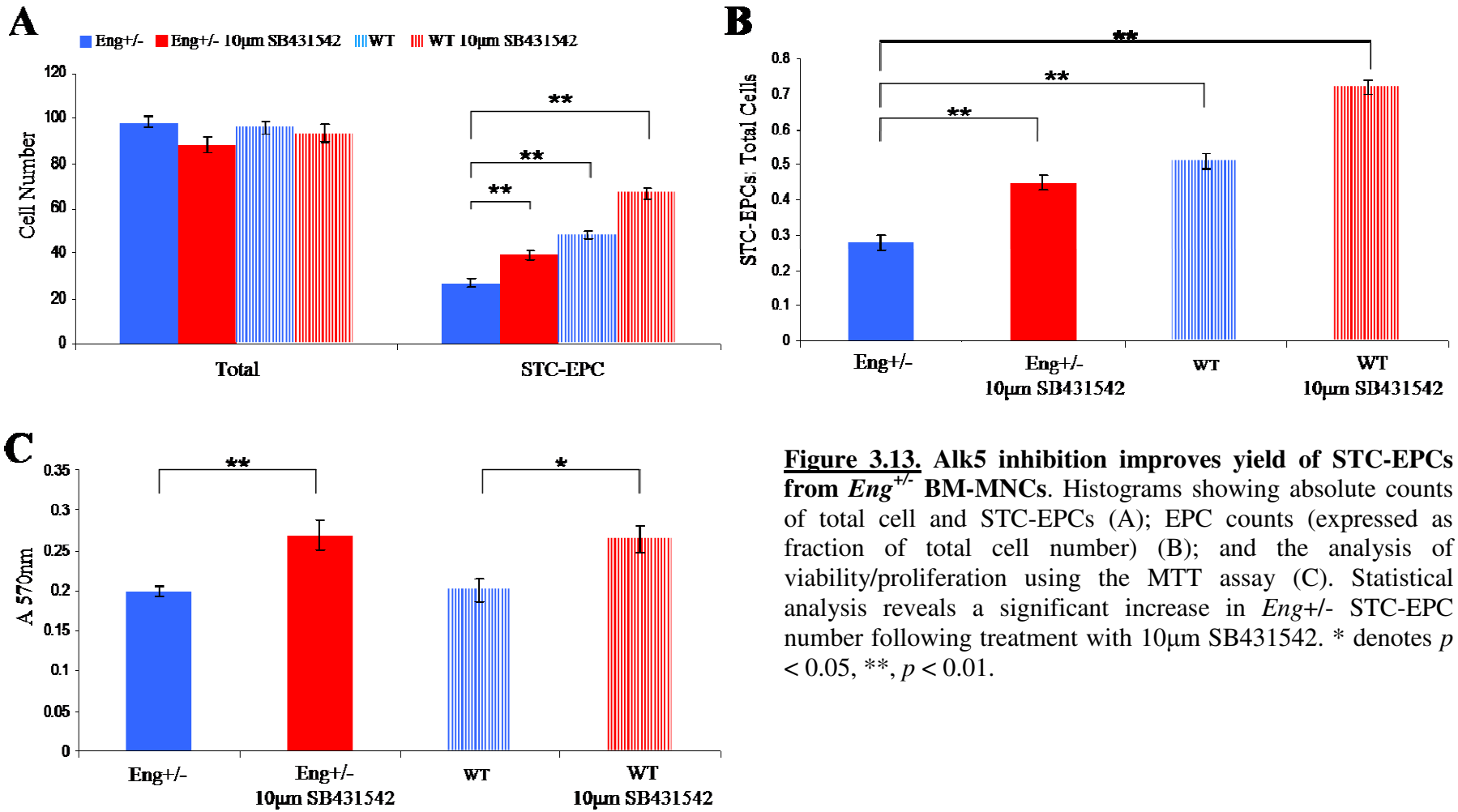

Figure 3.13. Alk5 inhibition improves yield of STC-EPCs from *Eng*$^{+/-}$ BM-MNCs. Histograms showing absolute counts of total cell and STC-EPCs (A); EPC counts (expressed as fraction of total cell number) (B); and the analysis of viability/proliferation using the MTT assay (C). Statistical analysis reveals a significant increase in *Eng*+/- STC-EPC number following treatment with 10µm SB431542. * denotes $p < 0.05$, **, $p < 0.01$.

	Total Cells at Day7 mean±SEM	Number of STC-EPC mean±SEM	% STC-EPC/Total mean±SEM	Unpaired *t*-Test comparing %STC-EPC/Total, *p* Value and % Change		
				***Eng*+/- SB-10µM vs *Eng*+/-**	***Eng*+/- vs WT**	**WT SB-10µM vs WT**
***Eng*+/- Untreated**	98.29±2.32	26.96±1.82	28±2			
***Eng*+/- A5i-10µM**	88.25±3.58	39.38±2.30	45±2	<0.001	<0.001	<0.001
WT Untreated	96.20±2.83	48.25±1.80	51±2			
WT SB-10µM	93.46±3.84	66.71±2.30	72±2	(+) 60.7%	(-) 82.1%	(+) 41.2%
***Eng*+/- Untreated**	107.21±3.37	33.92±1.70	32±1			
***Eng*+/- SB-10µM**	100.46±1.87	48.21±1.50	48±1	<0.001	<0.001	<0.001
WT Untreated	92.38±2.17	48.08±1.24	50±1			
WT SB-10µM	93.46±2.94	62.75±2.20	67±1	(+) 50%	(-) 56.3%	(+) 34%
***Eng*+/- Untreated**	133.67±7.16	31.29±2.28	24±2			
***Eng*+/- SB-10µM**	134.46±6.74	41.04±3.05	31±2	0.01	<0.001	<0.001
WT Untreated	119.21±4.53	38.79±1.48	33±1			
WT SB-10µM	117.46±3.81	57.5±2.16	50±2	(+) 29.2%	(-) 37.5%	(+) 51.5%

Table 3.3. Inhibition of Alk5 kinase activity rescues the low STC-EPC phenotype associated with *Eng*$^{+/-}$ genotype. Table illustrating the results and statistical analyses of 3 independent experiments analysing the effect of the Alk5 inhibitor SB43152 (SB) on the yield of STC-EPCs from WT and *Eng*+/- BM-MNCs. The statistical significance of differences between groups was determined using one-way ANOVA and unpaired *t*-tests (*p* values <0.05 were considered significant).

3.2.6. Effect of Alk5 Inhibition on TGFβ Signalling Responses

TGFβ signalling is reported to regulate the activation of ECs via a fine balance between the Alk5 and Alk1 pathways[6]. To give a greater insight into the effect of Alk5 inhibition in STC-EPCs at the signalling level semi-quantitative RT-PCR was used to elucidate Alk1 and Alk5 signalling responses. Alk1 specifically induces the expression of *Id1*, which promotes EC proliferation and migration[219-220] and Alk5 specifically stimulates expression of *Pai1*, which is a negative regulator of EC migration *in vitro* and angiogenesis *in vivo*[219-220]. Expression levels of *Id1* and *Pai1* in WT BM-MNC and STC cells with or without Alk5 inhibitor treatment (7 days 10μM) were assessed as a readout of the endogenous level of TGFβ signalling activity in STC cells and results were subjected to statistical analyses as previously described in section 3.2.4.

No change in *Id1* expression was observed in STC cells compared with total BM-MNCs although levels were slightly decreased in Alk5 inhibitor treated cultures (figure 3.14A). *Pai1* expression was markedly increased in STC cells and a significant decrease in expression was observed following inhibitor treatment (figure 3.14B). These results suggest that both TGFβ/Alk1 and TGFβ/Alk5 signalling is depressed in SB431542-treated cultures.

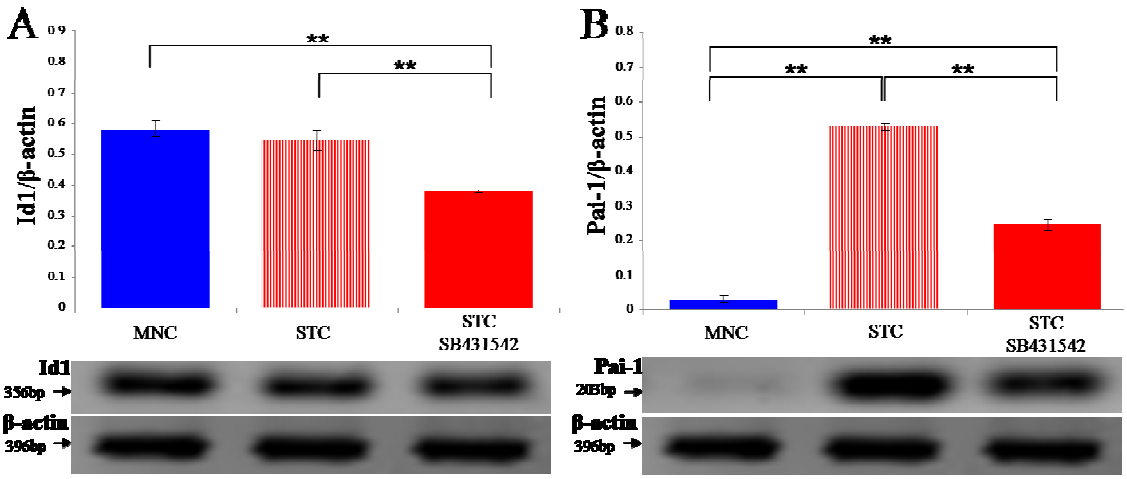

Figure 3.14 The effect of Alk5 inhibtion on downstream TGFβ signalling responses. Expression levels of *Id1* (A) and *Pai1* (B) mRNA were determined by semi-quantitative rtPCR and used as readouts of Alk1/TGFβ and Alk5/TGFβ signalling respectively in BM-MNCs, STC cells and STC cells treated with 10μM SB431542. Densitometric analysis of PCR band intensity was determined using ImageQuant TL software. *Id1* expression levels were signicantly reduced in SB431542 treated STC-EPCs. *Pai1* levels were almost undetectable in fresh BM-MNCs, dramatically increased in STC-EPCs and significantly reduced following Alk5 kinase actvity inhibition.

3.3. Discussion

3.3.1. Challenges of Isolating and Quantifying Murine BM-derived EPCs

Despite extensive investigation over the past decade the phenotype and function of EPCs are topics that remain complex and under heavy debate. The controversy surrounding EPC definition is confounded by a myriad of studies reporting a variety of isolation methods and phenotypes with interchangeable and confusing terminology. At the time that the present study was conceived the methods described in this thesis were widely regarded to isolate populations of EPCs; however it is now generally accepted that cells of diverse lineages and functions are being investigated and ambiguously placed under the single term EPC[25-26]. A major limitation of this study was the inability to isolate a more defined population of putative EPCs.

In this study mouse STC-EPCs were defined as BM-MNCs that attached to fibronectin-coated culture dishes within 1-4 days of culture and displayed the ability to take-up acLDL and bind GSLI-isolectin-B4 on day 7. Defining STC-EPCs using these criteria has been adopted extensively by many studies characterising EPCs[24, 56, 291-293]. However it has been shown that neither acLDL uptake nor lectin binding are specific to cells of endothelial lineage. During endothelial culture conditions monocytes have been shown to express many endothelial-associated proteins and are likely to express scavenger receptors that bind acLDL[89]. Similarly GSLI-isolectin-B4 binds many epithelial and haematopoietic cell types in addition to ECs[89]. Additionally, in human blood cultures, fibronectin is known to isolate and enrich monocytes for differentiation into macrophages[294]. Thus in recent years Yoder *et al*[89] among others have called for scrutiny to be applied to papers in which EPCs are being defined on the basis of lectin/acLDL binding to adherent MNCs as the sole criteria. However despite the relatively recent acceptance that 'early EPCs' actually represent pro-angiogenic monocytic cells which exhibit several endothelial features but do not differentiate into mature ECs, the presence of these cells in the circulation are associated with cardiovascular health and they are thought to have therapeutic benefit. Thus, TGFβ signalling in early EPCs is still likely to be of importance. Nevertheless, there is a need to identify which cell types contribute to neovascularisation, what roles they play and

how to optimally manipulate them in order to allow us to develop effective cell-mediated therapies.

Colony forming assays have also been used to identify and isolate EPCs. First described by Asahara *et al*[24] the original assay was later adapted by Hill and colleagues[45] to identify EPC colonies that emerged from non-adherent cultured human PB-MNCs. However in recent years the true lineage and fate of these colony forming cells has been called into question (discussed in section 1.5.1). Adherent cultured human PB-MNCs also form a different type of colony that have been called OECs[59], late EPCs[88] or ECFCs[46]. The characteristics of these cells are described in more extensive detail in section 1.5.1 but briefly hallmarks include a high proliferation potential, expression of endothelial markers and the ability to form vessels in *vivo* which can anastomose with host vasculature following transplantation into pre-clinical animal models. Despite several enthusiastic attempts at culturing OECs from mouse BM-MNCs I struggled to maintain self-renewal capacity and consistently observed low CD31 expression and high endoglin expression (which is also expressed by mesenchymal cells as well as monocytes and macrophages) therefore I did not progress to testing the angiogenic ability of these cells. It has since been suggested that mouse-derived OECs have limited proliferative and angiogenic capacity (personal communication, Dr Joyce Bischoff) and in general do not display the same functional characteristics as human derived OECs, however exceptions have been cited[290]. Interestingly OECs can be successfully derived from mouse lung EC preparations[295]. We too have cultured ECs from mouse lungs but due to a limited proliferative capacity and the tendency of cells to reach senescence at early passage number we found it necessary to introduce an immortomouse allele (H-2KbtsA58), which permits cells to bypass the G1 cell cycle check-point under certain conditions and hence allows for the derivation of longer lasting primary endothelial cell lines[296].

3.3.2. The Effect of Manipulating TGFβ Signalling on STC-EPC Yield *in vitro*

3.3.2.1. Effect of Alk5 Kinase Inhibition

The development of EPC-mediated therapeutic angiogenesis is impeded due to the low frequency of these cells, their tendency to readily differentiate in culture and their

limited proliferation potential. *Ex vivo* expansion of EPCs provides an alternative means to expand the number of pro-angiogenic cells for direct application or intravenous infusion. The TGFβ superfamily is known to control the balance of proliferation and differentiation responses in many cell types and EPCs are likely to be amongst these. Synthetic kinase inhibitors are useful tools for investigating the roles of growth factor signalling within cells *in vitro.* SB431542 is a synthetic compound that inhibits Alk5 kinase activity[286] and was added to the culture media in this study to assess the inhibition of Alk5 signalling on EPC biology.

Inhibition of the type I TGFβ receptor Alk5 using SB431542 led to a significant increase in STC-EPC number. Increased proliferation/ viability (as indicated by MTT assay data (figure 3.12)) may at least partially explain this observation. This is in agreement with the role of TGFβ/Alk5 signalling in the canonical TGFβ signalling pathway in which it opposes EC migration and proliferation (see figure 1.5). Furthermore, an increase in EPC proliferation is supported by several studies which have shown that Alk5 inhibition in mouse ES derived ECs lead to increased cell growth and integrity[297-299]. SB431542 treatment also significantly enhanced VEGF-induced formation of EC sheets from foetal mouse metatarsals in culture[300]. Therefore it appears rational to assume that inhibition of Alk5 kinase activity does indeed increase the proliferative potential of adherent MNCs that display endothelial properties to generate STC-EPCs. However the MTT assay only measures metabolic activity of total cells in the well over a limited time (24 hours) and this only indirectly relates to proliferation therefore a more direct method of assessing cell proliferation in culture (such as Ki67 staining) would be necessary to definitively prove that Alk5 inhibition increases STC-EPC proliferation.

Another possible explanation of my findings is that TGFβ ligand contained within culture media serum could have affected BM-MNC differentiation. While Alk5 inhibition may have allowed STC-EPCs to maintain an endothelial-like phenotype, TGFβ1 ligand stimulation could have induced differentiation into a more mesenchymal-like phenotype as this ligand is known to promote epithelial or endothelial to mesenchymal transition (EMT or EndMT)[301-302]. EPCs have been shown to differentiate into mesenchymal cells that express smooth muscle actin[303-304]. Diez *et al*[299] investigated whether TGFβ signalling may contribute to EPC acquisition of a

mesenchymal phenotype. The authors reported that EPCs (commercially sourced human $CD133^+$ progenitor cells) differentiate into SMC-like cells through an EndMT-like process and that TGFβ1 plays an important role in this process and in EPC fate generally. Alk5 inhibition (SB431542 treatment) increased numbers of BM-derived ECs but the authors found no direct effect on EPC proliferation or apoptosis (assessed using FACS based cell cycle analysis). Instead, Alk5 inhibition led to a partial block in the acquirement of mesenchymal markers thus facilitating the retention of an endothelial phenotype. James *et al*[298] have also described an increase in human ESC-derived ECs following inhibition of the TGFβ/Alk5 pathway. Initially, although a small number of ECs could be isolated from human ESC cultures, these could not be expanded without the majority of cells adopting a non-endothelial phenotype. SB431542 treatment of human ESC cultures resulted in increased cellular proliferation (indicated by a higher percentage of phospho-histoneH3+ mitotic ECs) and a preservation of vascular phenotype. The authors have shown that *Id1* expression is sustained in these cells and suggest that this maintenance of high expression levels preserves an immature proliferative phenotype. *Id1* expression has been shown to inhibit growth arrest and differentiation in multiple cell types[305]. However, in my study STC-EPCs showed a significant decrease in endogenous *Id1* expression in the presence of the Alk5 kinase inhibitor (Fig 3.14). The different outcomes may be due to differences between the role of Id1 in human embryonic cells in the James *et al*[298] study versus murine adult cell types in this study. Moreover, James and colleagues were using a highly homogenous cell population and serum free culture conditions to enhance vascular differentiation and they also FACS sorted $Id1^{high}$ and $Id1^{low}$ $CD31^+$ cells, correlating increased expansion with high levels of Id1 whereas the readout of *Id1* expression in my own cultured MNCs was derived from a heterogeneous cell population, cultured in high serum conditions which was likely to affect TGFβ signalling as well as crosstalk with other pathways. Furthermore Alk5 has been shown to be important for Alk1 recruitment into the TGFβ receptor complex and Alk5 kinase activity is essential for efficient Alk1 activation and mediation of *Id1* expression[219, 221] which could at least partially explain the reduced *Id1* levels observed in SB431542 treated STC-EPC cultures described in this chapter.

Bringing together my own observations and those of related studies it is likely that the inhibition of Alk5 kinase activity can be used to expand EPCs *ex vivo* whilst

maintaining their endothelial-like phenotypes. However, further work would be required to establish the effect of Alk5 inhibition on STC-EPC proliferation (for example by FACS-based cell cycle analysis or Ki67 staining) and its effect on transition to a mesenchymal cell phenotype (by assessing changes in EndMT associated gene expression such as *twist* and *snail* as well as mesenchymal markers including αSMA or calponin). Additionally, it would be necessary to test the functional relevance of these findings *in vivo* to evaluate if the use of an Alk5 inhibitor is safe and whether it has therapeutic potential.

3.3.2.2. Effect of Endoglin Deficiency

As discussed in chapter 1.9.3 the precise role of endoglin in TGFβ/BMP signalling cascades remains unclear. *In vitro* studies suggest that endoglin functions within the endothelium to potentiate TGFβ/Alk1 signalling and antagonise the TGFβ/Alk5 pathway[237, 264] and as such acts as a positive facilitator of endothelial proliferation and migration. However, contradictory *in vitro* findings have found that $Eng^{-/-}$ ECs display increased proliferation[269 270]. Furthermore, it has been shown that in response to both BMP9 and BMP10 ligands endoglin (and Alk1) promote endothelial cytostasis[238-239, 241]. In a number of different cell types, including ECs and monocytes, endoglin has been shown to oppose a variety of TGFβ1-dependent responses, including the inhibition of cell proliferation and migration, as well as modulating cellular apoptosis, adhesion and the expression of ECM components[306]. In this chapter I have shown that endoglin deficiency results in a significant decrease in the number of STC-EPCs cultured from BM-MNCs. Cell counting revealed no difference between the total numbers of WT and $Eng^{+/-}$ cells, nor were differences in viability/proliferation detected between these two groups using the MTT assay. These results suggest that the decrease in STC-EPC number is not directly, or entirely, due to the inhibition of cellular proliferation as was proposed in the original study hypothesis. However, despite observing a general increase in endoglin expression following culture of BM-MNCs to STC-EPCs it is unknown which cell types within the heterogeneous STC-EPC population express endoglin and to what extent each distinct cell type is affected by reduced protein levels. Cells of endothelial nature (STC-EPC) account for just 50% (approximately) of the STC population (see table 3.3) therefore it is possible that cells that either do not express

endoglin or are unaffected by a reduction in endoglin expression could be masking an inhibitory effect on proliferative capacity.

Linda van Laake *et al*[275] published seminal research identifying endoglin as a crucial component in circulating cell-mediated vascular repair. Human circulating MNCs deficient in endoglin expression (derived from HHT1 patients) were less able to promote cardiac repair than WT control cells due to a proposed deficiency in the SDF1/CXCR4 homing gradient[276]. The authors did not detect any effect of endoglin deficiency on MNC attachment, apoptosis, proliferation or TGFβ signalling *in vitro*, however they did not exclude the possibility that these processes may be defective and contribute to the underlying pathological mechanism *in vivo*. Interestingly following short term culture of human MNCs (using a similar approach to that described in this thesis), no difference in STC-EPC number (defined using lectin and acLDL co-staining) was found between WT and endoglin deficient (HHT1 patient) cells[275]. This stark difference to my own results may be explained by the source of MNCs used for culture. In my study mouse BM-MNCs were used, which may contain more primitive endothelial precursors than human peripheral blood. Endoglin is expressed by a number of BM mononuclear cell types including EPCs, MSCs and HSCs. It is possible that these cells in the BM are potentially more sensitive to a change in endoglin levels and more likely to reveal functional differences following *in vitro* culture. Therefore, my study may represent the effect of endoglin deficiency on several distinct types of endothelial progenitor cell at varying early stages of differentiation, whereas the van Laake study is restricted to analysing circulating MNC cell-types at a more advanced stage of differentiation. Additionally peripheral blood is more likely to be contaminated with ECs sloughed from mature vessel walls that enter the circulation and could skew results.

Alternative explanations of my findings include an EPC specific increase in apoptosis or a reduced capacity to differentiate towards an endothelial phenotype. Endoglin null mice die at mid-gestation due to cardiovascular abnormalities and impaired angiogenesis[232-234], however endothelial differentiation and vasculogenesis appear normal in these embryos up to embryonic age E9.5, suggesting that endoglin is not essential for endothelial differentiation during early development. In addition to ECs, both HSCs[257-258, 307-308] and mature haematopoietic cells are known to strongly express

endoglin[265, 309], which is thought to be required for haemangioblast specification and early haematopoietic commitment[308, 310]. *Eng*$^{-/-}$ mouse ESCs show impaired myelopoiesis and definitive erythropoiesis[308], whilst *Eng*$^{-/-}$ blast colony forming cells (BL-CFCs, regarded as the *in vitro* haemangioblast equivalent) also show impaired haematopoiesis, but endothelial differentiation is not affected[310]. My results do not support the view that endothelial differentiation is unrelated to endoglin function, but it is possible that distinct TGFβ family signalling pathways that differentially utilise endoglin lead to alternative outcomes in adult progenitor cells compared to their developmental counterparts. In the adult mouse it has been reported that HSCs can give rise to true endothelial progeny[311-313] and that early EPCs or EC-like cells are derived from heterogeneous haematopoietic cells[53-54, 56, 62-63]. By using acLDL and iso-lectin to label STC-EPCs I was unable to differentiate between true endothelial and EC-like cells and attempts to further characterise a more specific population of EPCs by FACS were thwarted by technical problems (discussed above in 3.2.2). In BL-CFCs, whilst endoglin loss does not impair endothelial differentiation, there is a defect in haematopoietic cell formation[310]. Therefore it is feasible that there are reduced numbers of haematopoietic stem/progenitor cells available to differentiate into EC-like cells in *Eng*$^{+/-}$ mice compared with WT. This would be difficult to assess because the composition of the BM-MNC population is heterogeneous and it is likely that multiple cell types, identified by overlapping surface marker expression are subsequently regarded as EPCs but actually represent distinct lineages. This heterogeneity may also explain the variability in results observed in replicate experiments described in this chapter.

I observed no difference in the expression of either *Alk5* or *Alk1* transcripts in STC cells derived from WT or *Eng*$^{+/-}$ mice. This is of interest because levels of Alk5 have been shown to be reduced in ECs derived from endoglin heterozygote mouse embryos[237]. Additionally, Xu *et al*[314] have reported vascular defects associated with a reduction of Alk5 expression in VEGF-induced microvessels of endoglin heterozygous mice. Lebrin *et al* proposed the following model: in ECs with reduced endoglin levels, Alk5 signalling is increased. In order to compensate for this "over activity of Alk5 signalling" leading to inhibition of EC growth, ECs adapt by down-regulating Alk5 expression[204]. That no such down-regulation was observed in my cultures suggests that this compensatory adaptation is not present. This could also account for the decreased STC-

EPC number in my endoglin deficient cultures due to the inhibitory effects of Alk5 (expressed at WT levels). This proposal is further supported by my observation that Alk5 kinase inhibition leads to increased STC-EPC yield in $Eng^{+/-}$ cultures. In addition van Laake *et al*[275] did not detect a decrease in *Alk5* expression in endoglin deficient MNCs using real time-PCR therefore it is possible that this compensatory mechanism proposed for terminally differentiated ECs has not been acquired by more primitive cells of endothelial lineage. Another important consideration is the heterogeneous nature of STC cell cultures, approximately 50% of cells showed endothelial characteristics (see table 3.3) in comparison to the homogenous endothelial populations used in endothelial cell studies and this may have masked possible EPC-specific differences in *Alk5* expression. To give a greater insight into the role of the canonical endothelial TGFβ pathway in endothelial progenitors it would be of immense benefit to sort these progenitors based on surface cell markers, perform lineage tracing and to examine EPCs at various differentiation stages.

SB431542 treatment in multiple cell types, including cultured BM-MNCs, has resulted in enhanced cellular growth due to increased proliferation and/or increased differentiation towards the endothelial lineage. Hence, the observation that Alk5 inhibition using SB431542 rescued the low yield of STC-EPCs in endoglin deficient cultures suggests that endoglin too is important in modulating vascular progenitor cell fate. I therefore looked in more detail at the effect of reduced endoglin in endogenous vascular repair. This is discussed in the next chapter.

CHAPTER 4.

Endothelial Progenitor Cells and Endogenous Endothelial Repair

4.1. Introduction

Given the role of endoglin in enhancing the yield of EPCs *in vitro* shown in the previous chapter I set out to investigate whether endoglin depletion had an effect on vascular repair *in vivo.*

Gene ablation of endoglin in the germ line results in early embryonic lethality[232-234], precluding analysis at later developmental and postnatal stages. Recent advances in mouse genetics has led to the development of conditional knock-out mice permitting spatio-temporal control over gene activation at any time during prenatal or postnatal development. The Cre/*loxP* site-specific recombination system is commonly used to generate conditional gene deletion[315]. In this system Cre-recombinase excises a region of genomic DNA essential for the production of a functional gene product. *LoxP* (locus of X-over P1) sites are 34 base-pair (bp) sequences absent from the mammalian genome, which act as recognition sites for Cre-recombinase[316]. Two *loxP* sites are introduced to flank the target DNA sequence and binding with Cre-recombinase leads to inversion or excision of the intervening 'floxed' DNA sequence depending upon *loxP* site orientation (figure 4.1). Temporal control over gene deletion is achieved through the use of inducible Cre-recombinases. Fusion of Cre-recombinase with mutated hormone-binding domains of nuclear receptors permits inducible activation of the enzyme in the presence of synthetic exogenous ligands. The $CreER^{T2}$ fusion protein is obtained by fusing Cre-recombinase to a mutated ligand binding domain of the human oestrogen receptor ERα, which is activated by the synthetic oestrogen-like agonist tamoxifen but not by endogenous oestrogen[317-318]. Consequently expression of the $CreER^{T2}$ fusion protein allows efficient tamoxifen dependent Cre-mediated recombination at loci flanked by *loxP* sites. Gene ablation can be directed within target cells by using transgenic mice expressing Cre-recombinase under the control of a tissue or cell specific promoter. Vascular endothelial cadherin (VE-Cadherin or Cdh5) is an endothelial specific adhesion molecule that is essential for endothelial cell-cell interaction[319]. In this chapter I have used a tamoxifen inducible *Cdh5(PAC)-CreER^{T2}* transgenic mouse model[270, 320] (courtesy of Ralf H. Adams, CRUK London) to achieve inducible gene knockdown specifically in vascular endothelial cells.

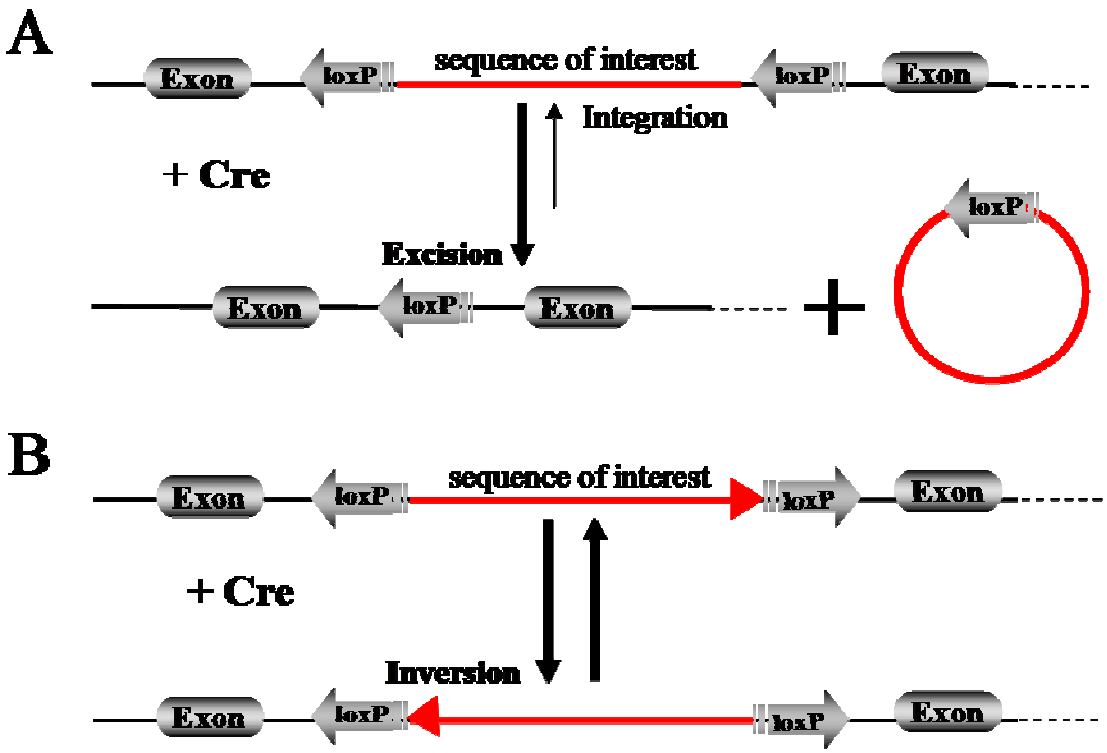

Figure 4.1. Cre-mediated *loxP* recombination reactions. Cre recombinase catalyzes intra-molecular excision or inversion. Cre-recombinase binds the *loxP* sequences flanking the target sequence and facilitates cleavage of DNA. If two *loxP* sites are in homologous orientation (A) recombination will preferentially produce excision and circularisation of the target sequence. Cre can also catalyze the re-integration of the target DNA into a single *loxP* site but this is kinetically unfavourable and occurs rarely. Recombination between inverted *loxP* sites (B) leads to a 50:50 probability of segment inversion. (Figure adapted from[321]).

A bifloxed endoglin allele ($Eng^{fl/fl}$) has been generated in my host laboratory[278] (figure 4.2). Exons 5 and 6 are flanked by *loxP* sites and Cre-mediated recombination results in deletion of these exons, as well as a frame shift in exon 7 which introduces a premature stop codon into the sequence. Consequently, if translated, the knockout allele generates a non-functional peptide consisting of the extracellular domain encoded by exons 1-4 and two additional amino acids encoded by exon 7. To confirm that $Eng^{\Delta ex5-6}$ is a null allele Allinson *et al*[278] have shown that offspring derived from $Eng^{fl/\Delta ex5-6}/Eng^{fl/\Delta ex5-6}$ breeding show a similar phenotype to conventional endoglin knock-out mice displaying embryonic lethality at mid-gestation[278].

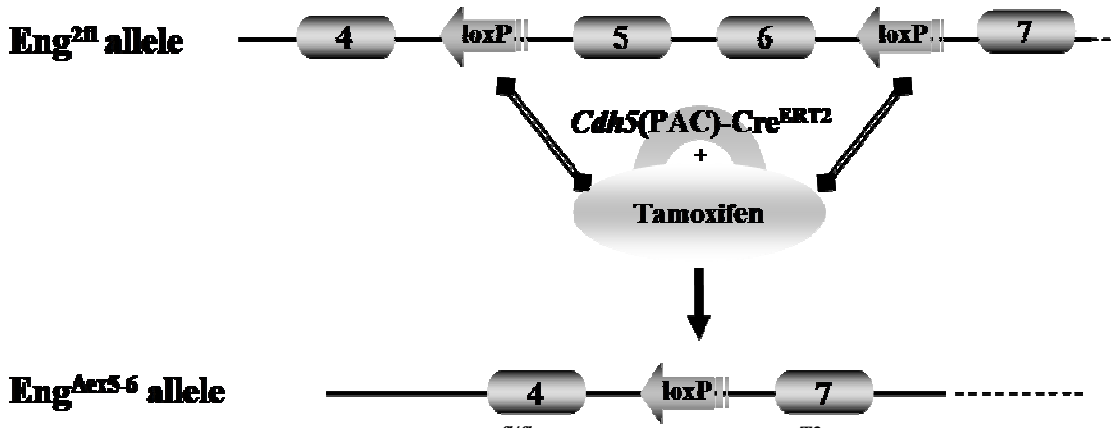

Figure 4.2. Schematic of the *Eng$^{fl/fl}$;Cdh5(PAC)-CreER^{T2}* inducible knock-out mouse model. Tamoxifen treatment activates *Cdh5*(PAC)-CreER^{T2} recombinase leading to endothelial specific recombination between *loxP* sites and deletion of endoglin exons 5 and 6, resulting in a frame shift mutation, giving rise to a null allele encoding a truncated, non functional protein.

Early characterisation of the *Eng$^{fl/fl}$;Cdh5(PAC)-CreER^{T2}* conditional knock-out mouse model reported an initial high level of endoglin depletion in the pulmonary vasculature three weeks following tamoxifen administration however in two out of three mutants an apparent re-establishment of expression was observed (figure 4.3) (personal communication, Dr Marwa Mahmoud). This rescue suggests a role for circulating EPCs in vascular repair and maintenance. Additionally, an *in vivo* angiogenesis assay using subcutaneously implanted Matrigel matrix plugs revealed evidence of a potential invasion of endoglin positive cells into the Matrigel of mutant mice (figure 4.3) (courtesy of Zhen Zhai, unpublished data). Although it is possible that these results reflect an incomplete knockdown of endoglin in the ECs, it is also possible that systemic endothelial specific endoglin depletion is sufficient to stimulate large scale proliferation and migration of BM-derived circulating EPCs that are unaffected by the *Cdh5(PAC)-CreER^{T2}* line and can contribute to endogenous endothelial replacement. Endothelial turnover is normally a very slow process, in the order of 3 years[322]. An *in vivo* model in which this process is enhanced would provide an important new tool for investigating vascular repair. For example, injection of labelled EPC sub-populations and pre-treated cells into mutant mice would permit *in vivo* visual tracking of these cells and would establish to what extent they are capable of differentiating into mature ECs, incorporating into the vasculature and contributing to repair. Such a large scale or 'hyper' repair model could be used to screen proposed therapeutic strategies and may be extremely beneficial in elucidating the optimal repair cell type and associated mechanisms of repair.

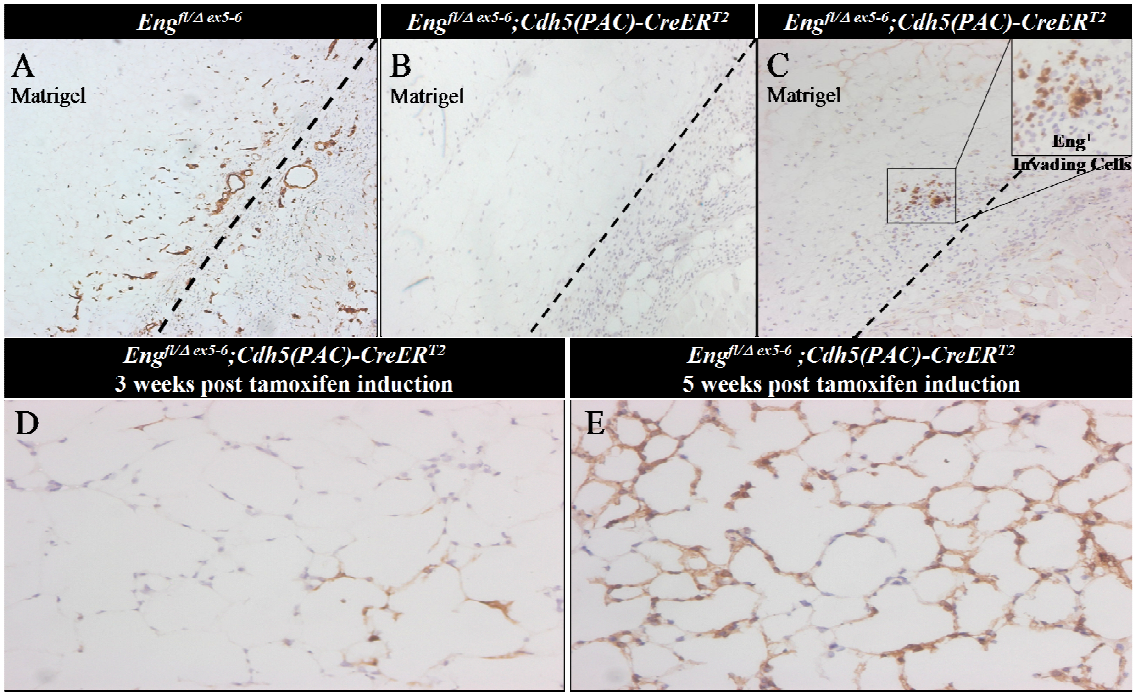

Figure 4.3. Preliminary evidence for endothelial replacement following endoglin depletion. (A-C) Immunohistochemical staining for endoglin (brown stain) on skin sections confirm efficient loss of endoglin protein following tamoxifen treatment (B) as compared to matched controls (A) however several mutants (n=3/5) show a possible invasion of endoglin expressing cells into growth factor enriched Matrigel pellet (C). The Matrigel-skin boundary is indicated by dashed lines. (Images courtesy of Dr Zhenhua Zhai). (D-F) Efficient knockdown of endoglin (brown stain) in the pulmonary vasculature was seen in mutant lungs harvested 3 weeks after tamoxifen treatment (D) however other mutant lungs (n=2/3) harvested at 5 weeks showed clear endoglin expression (E) that was comparable to the level of endoglin expression seen in matched control lungs. (Images courtesy of Dr Marwa Mahmoud).

To test this novel repair/replacement model endoglin protein expression was analysed in heart, lung and BM tissues following endoglin depletion (by tamoxifen injection) in *Eng*$^{fl/fl}$*;Cdh5(PAC)-CreER*^{T2} mice. Animals were humanely killed and tissues analysed at weekly intervals over a 6 week period.

As an additional way of determining the specificity and efficiency of Cre-recombinase expression and activation *in vivo,* mice also carried a *Rosa26* Cre-reporter (*Rosa26R*) allele[279]. The *Rosa26R lacZ* reporter line carries a bi-floxed STOP cassette in front of the bacterial gene *lacZ*, driven by the ubiquitously expressed *Rosa26* promoter (*Rosa26* is now known to be *Thump domain-containing protein 3* gene). The *lacZ* gene expresses β-galactosidase upon Cre-mediated excision of the STOP cassette, therefore detection of β-galactosidase provides a readout of Cre-recombinase activity (figure 4.4). With the

standard chromogenic substrate X-Gal, β-galactosidase is visualized in tissue as an intense blue precipitate.

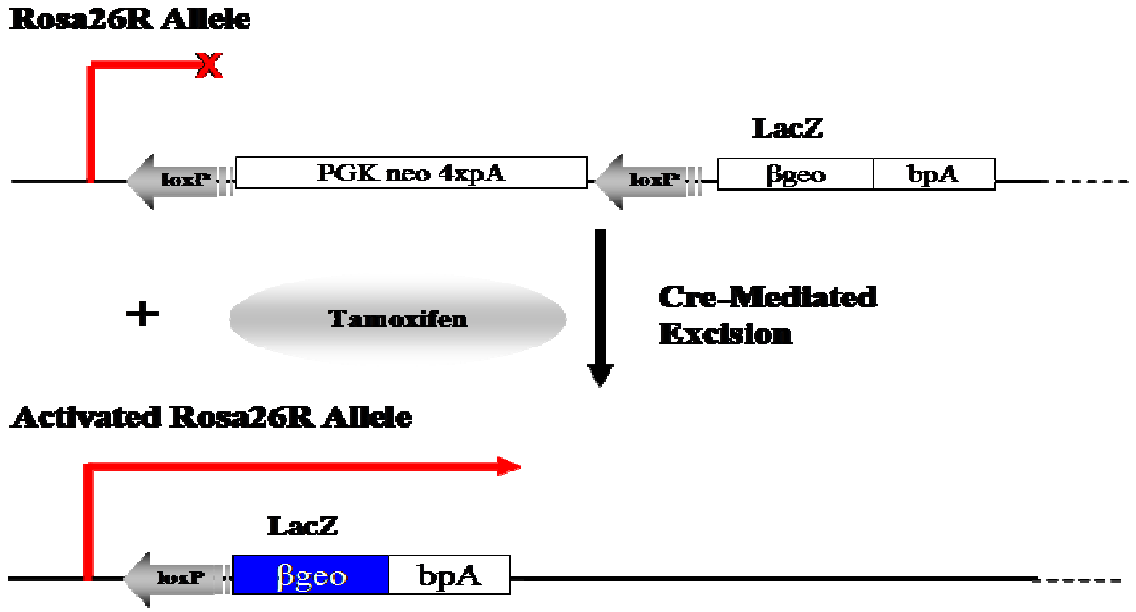

Figure 4.4. Cre-mediated recombination of the *Rosa26R* allele. The expression of *LacZ* is driven by the ubiquitously expressed *Rosa26* promoter and is conditional on the removal of the preceding *loxP* flanked neo expression cassette stop codon by Cre-mediated excision. Subsequent expression of the *LacZ* gene product, β-galactosidase, can be detected by X-gal staining and used to map expression of Cre-recombinase in murine tissue or primary cell types.

Two tamoxifen treated $Eng^{fl/\Delta ex5\text{-}6}$;*Cdh5(PAC)-CreER*^{T2};*R26R*$^{T/+}$ adult mice (referred to as endoglin–inducible knockout (Eng-iKO) mutants) were culled and their tissues harvested for analysis at each time point. Additionally each time point included a tamoxifen treated $Eng^{fl/\Delta ex5\text{-}6}$ matched control lacking *Cdh5(PAC)-CreER*^{T2} and a $Eng^{fl/fl}$ mouse as a further control. An additional group of control mice did not receive tamoxifen treatment and were analysed to exclude the possibility of secondary or toxic effects of tamoxifen. The average age of mice involved in this study was 22.5 weeks (±1.0 week) with a range of 16.7 to 31.3 weeks.

The purpose of this study was to test whether tamoxifen administration reproducibly leads to endoglin depletion and whether this is followed by active endothelial replacement that would increase over time. This represented a pilot study with 2 experimental animals used for each of 6 time points over 44 days.

4.2. Results

4.2.1. Conditional Endoglin Knock-Out Mouse Model

4.2.1.1. Efficiency of *Cdh5(PAC)-CreER^{T2}* Expression and Activation in Lung Tissue

Recombination was induced in a group of 12 adult *Eng$^{fl/\Delta ex5\text{-}6}$;Cdh5(PAC)-CreER^{T2} ;Rosa26R$^{T/+}$* mice by administering 7 intraperitoneal (IP) injections of 2mg tamoxifen over 9 days (total of 14mg delivered). The mice were humanely killed at different time points and the middle lobe of the right lung of each mouse was removed and stained with X-Gal to determine the efficiency and reproducibility of Cre-mediated recombination. Efficiency of *Cdh5(PAC)-CreER^{T2}* activation was graded according to X-Gal staining intensity (see figure 4.5 for grading criteria). All mutant mice showed high levels of positive X-Gal staining throughout the lobe (graded +++ or ++++) across all 6 time points with the exception of a single mouse from group 4 (identified as AN3) which was given a grading of ++ due to patches of unstained tissue (figure 4.5A). Positive staining was observed throughout the pulmonary vasculature and is indicative of strong *Cdh5(PAC)-CreER^{T2}* expression (figure 4.5C). Correlation with endoglin depletion will be discussed below (section 4.2.3). As expected, lobes from both tamoxifen treated and untreated control mice showed no evidence of X-Gal staining (figure 4.5B).

4.2.1.2. Expression of *Cdh5(PAC)-CreER^{T2}* in Bone Marrow

Cdh5 (VE-Cadherin) is expressed in mature ECs but in only a small fraction of BM-MNCs. To confirm *Cdh5(PAC)-CreER^{T2}* expression in BM cells of *Eng$^{fl/\Delta ex5\text{-}6}$;Cdh5(PAC)-CreER^{T2};Rosa26R* mice I adopted a FACS-based method to detect β-galactosidase expression. Fluorescein di-β-D-galactopyranoside (FDG) is a fluorogenic substrate of β-galactosidase, which releases a fluorescent product (FITC) when cleaved and is quantified using flow cytometry[323-324].

FDG staining and subsequent FACS analysis revealed very low levels of *lacZ* expression (0.43%±0.12) in BM cells from tamoxifen treated *Cdh5(PAC)-CreER^{T2}; Rosa26R$^{T/+}$* mice, which was similar to that displayed by BM from tamoxifen treated controls (0.53%±0.07) (figure 4.6A and B). The widely expressed *Rosa26-CreER^{T2}* line with an incorporated *Rosa26R lacZ* allele was used as a positive control and showed

approximately 50% recombination in BM (figure 4.6D), while conversely the NIH WT negative control showed no expression. These results show that the inducible *Cdh5(PAC)-CreER*^{T2} enzyme is not active in the vast majority of BM cells following tamoxifen induction, implying that BM cells would retain the functional *Eng*^{fl} allele and would not undergo recombination to *Eng*$^{\Delta ex5\text{-}6}$ null allele in the Eng-iKO animals. These findings do concur with results from similar Cdh5-Cre deleter lines (see section 4.3.2.) indicating that the low Cre expression in BM cells in *Cdh5(PAC)-CreER*^{T2} mice, as observed here, is a true finding.

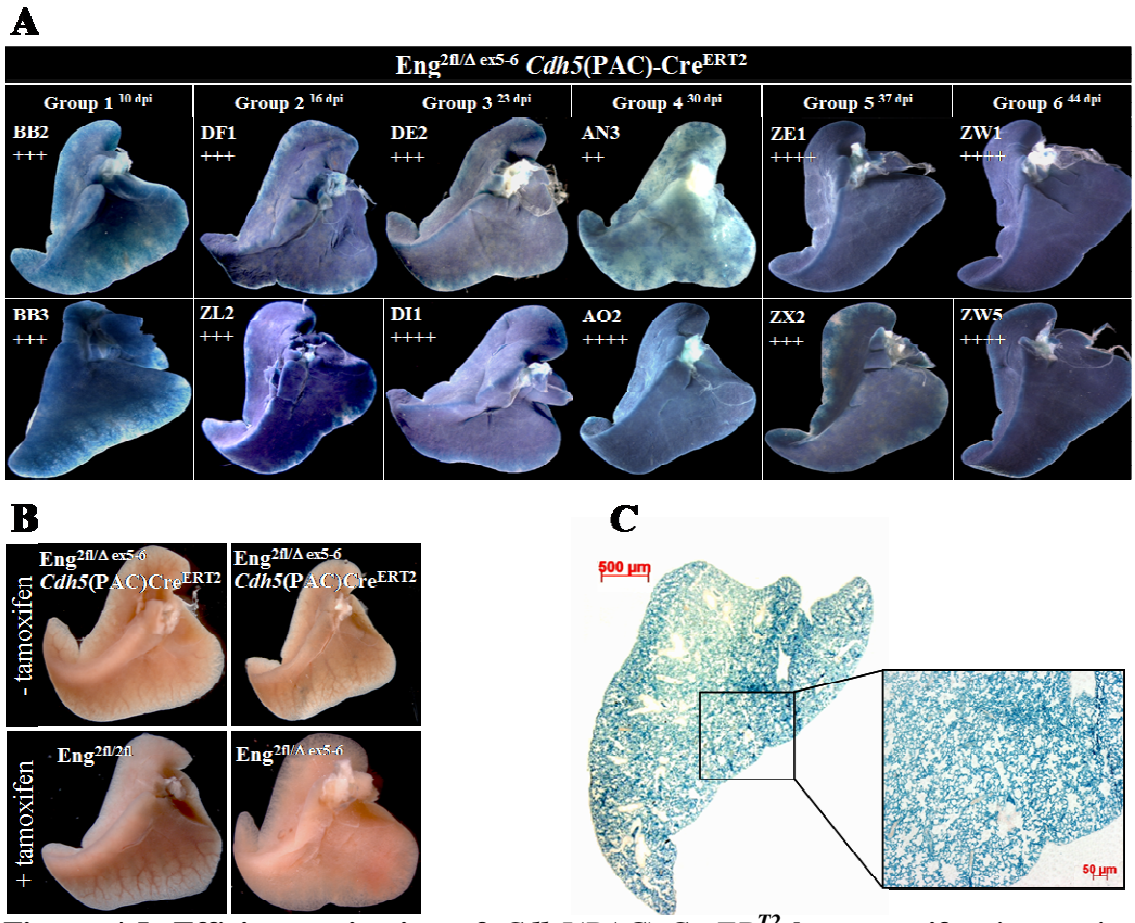

Figure 4.5. Efficient activation of *Cdh5(PAC)-CreER*^{T2} by tamoxifen in murine pulmonary vasculature. Application of tamoxifen (7 intraperitoneal injections of 2mg tamoxifen over 9 days) to *Eng*$^{fl/\Delta ex5\text{-}6}$*;Cdh5(PAC)-CreER*^{T2}*;Rosa26R*$^{T/+}$ mice leads to efficient Cre activation in vascular endothelium as indicated by blue X-Gal staining of lung lobes (A). Groups (1 to 6) are categorised according to time period from first tamoxifen injection to time of tissue harvest. Grading of stain intensity is assigned beneath mouse identity (+ = negligible staining, ++ = low level or patchy *lacZ* expression, +++ = majority of vessels exhibiting intense staining, ++++ = maximum). X-Gal stained tamoxifen treated and untreated negative controls (B). Section of wholemount X-Gal stained lung lobe showing *lacZ* expression throughout the vascular network (C). Abbreviations: dpi = days post first injection.

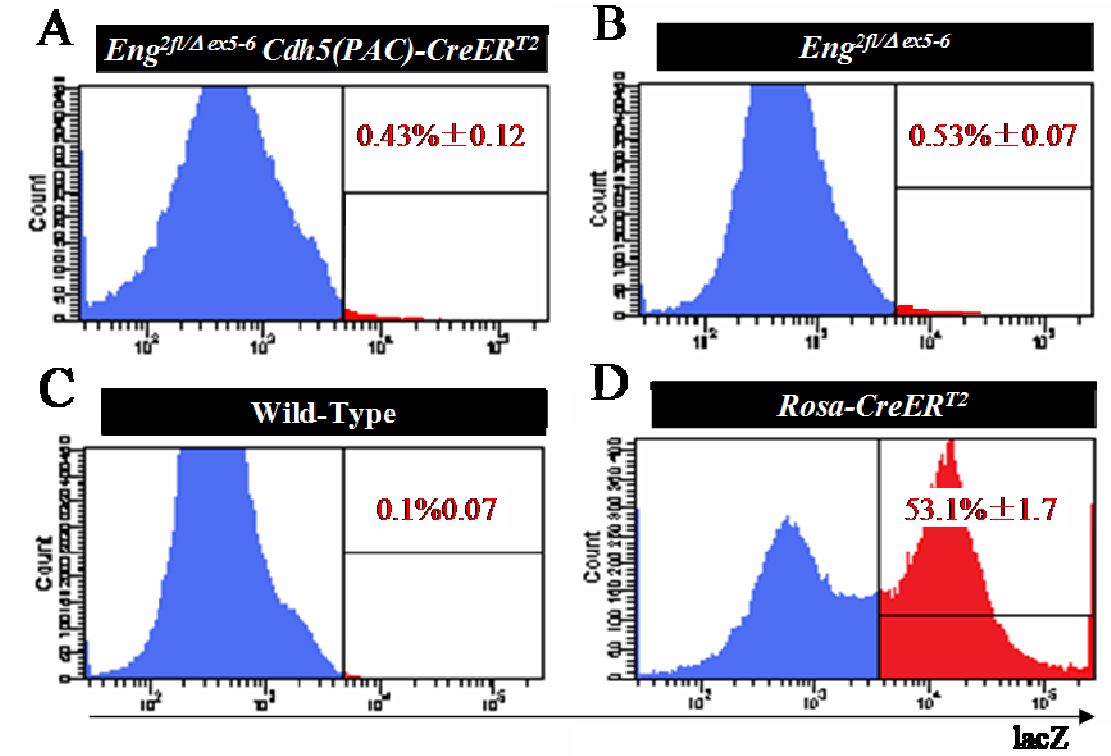

Figure 4.6. LacZ expression in Murine BM Cells from *Cdh5(PAC)-CreER^{T2}* mice. Flow cytometry histograms showing lacZ expression as a percentage of total fresh bone marrow cells (A-D). Low activity of *Cdh5*(PAC)-CreER^{T2} (as determined by staining with the ß-galactosidase substrate FDG) was detected in BM cells of mutant mice (A), which is comparable to that observed in *Eng*$^{fl/\Delta ex5\text{-}6}$ controls (B). High expression of *Cdh5(PAC)-CreER^{T2}* detected in the BM of the ubiquitously expressed *Rosa-CreER^{T2}* line (C) and wild type mice (D). All mice received 7 x (2mg) tamoxifen injections (via intraperitoneal route) over 9 days prior to FACS analysis.

4.2.2. Endoglin Depletion Results in an Increase of Endoglin Expression in Bone Marrow Cells

To identify alterations in endoglin expression in the BM of mutant mice following tamoxifen treatment it was important to establish the normal expression profile of endoglin in control mice. To do this flow cytometry was used to analyse freshly harvested BM cells from *Eng*$^{fl/\Delta ex5\text{-}6}$ (n=7) and *Eng*$^{fl/fl}$ (n=7) mice lacking *Cdh5(PAC)-CreER^{T2}*. Mean values of endoglin expression (represented as percentage of total BM ± SEM) were calculated.

Unlike the endoglin expression profile of NIH strain mice (see figure 3.9), the normal expression profile of BM cells from mice used in this study (mixed genetic background) revealed both bright and dim endoglin positive populations. The dim population occurs when the antigen expression for a subset of cells is poorly resolved and can appear as a

continuous population from those cells not expressing the antigen. Eng^{bright} subsets were 0.53±0.04% and 1.44±0.12% in the BM from *Eng*$^{fl/\Delta ex5\text{-}6}$ and *Eng*$^{fl/fl}$ mice respectively, while Eng^{dim} sub-populations were 7±0.6% and 12.4±0.8% (see figure 4.7 for representative dot plots). As expected, the number of endoglin positive BM cells (either Eng^{dim} or Eng^{bright}) was reduced by approximately 50% in the *Eng*$^{fl/\Delta ex5\text{-}6}$ mice compared with *Eng*$^{fl/fl}$ controls (figure 4.7).

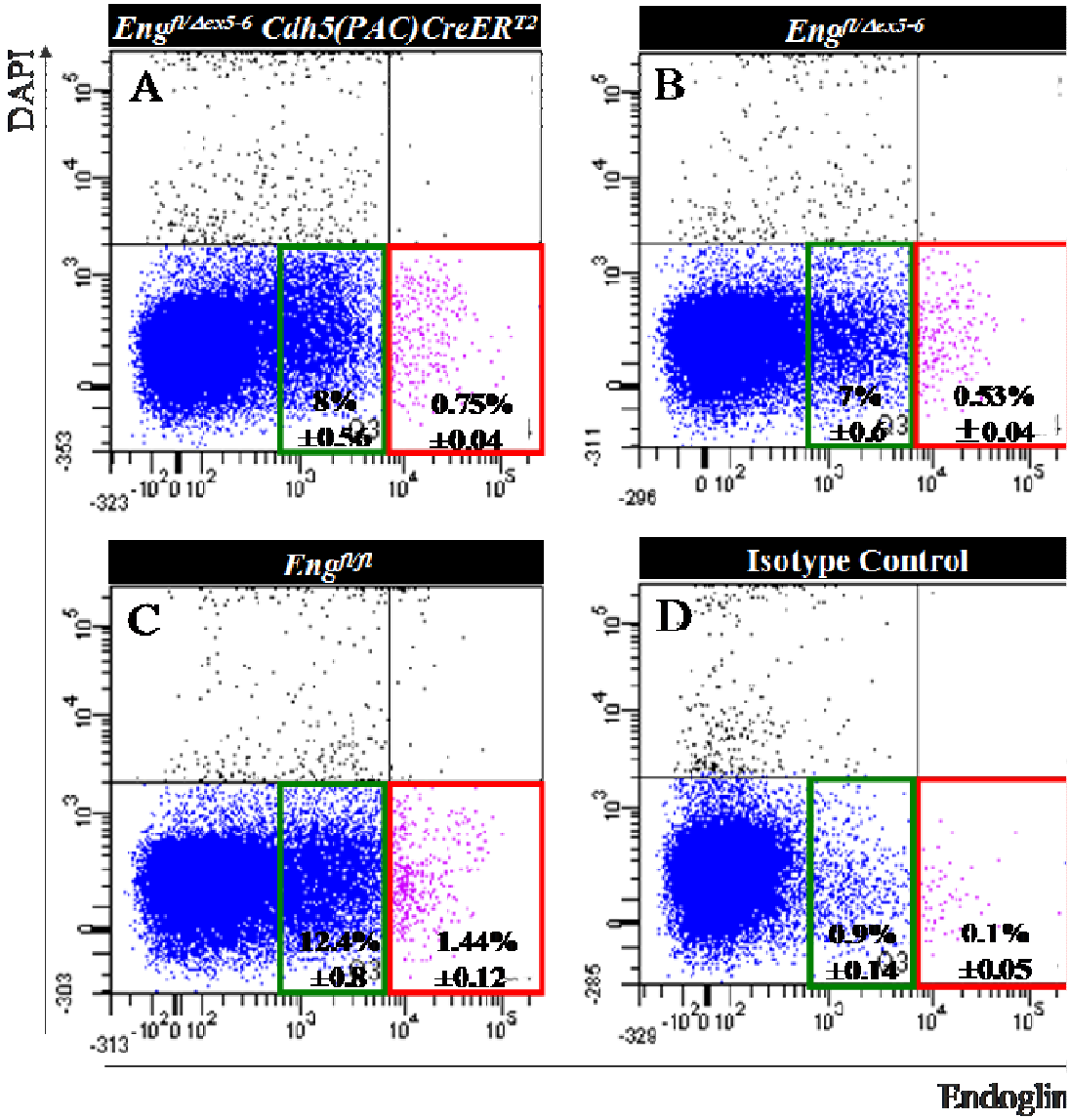

Figure 4.7. Endoglin expression in BM is up-regulated in tamoxifen treated Eng-iKO mutants. Representative dot plots A-D show mean values of endoglin expression as a percentage of total bone marrow cells (red box correlates to Eng^{bright} sub-population, green box correlates to Eng^{dim} sub-population). Tamoxifen treated endoglin mutant mice show up-regulated levels of endoglin (n=12) (A) as compared to *Eng*$^{fl/\Delta ex5\text{-}6}$ tamoxifen treated controls (n=7) (B). Dot plot C represents endoglin expression in BM of *Eng*$^{fl/fl}$ mice (=7) and (D), an isotype matched control.

Due to the low level of *Cdh5(PAC)-CreER^{T2}* induction observed in BM cells (refer to section 4.2.1.2) I did not expect to see endoglin knock down in mutant mice. Surprisingly, analysis revealed an up-regulation of endoglin expression in several Eng-iKO mutant mice compared with *Eng$^{fl/\Delta\ ex5\text{-}6}$* controls (figure 4.7). Expression of the Eng^{bright} sub-population ranged from 0.58% to 0.93% in mutant mice (figure 4.8) and from 5% to 10.8% for the Eng^{dim} sub-population (figure 4.9). Cell counts were not normally distributed and Mann Whitney statistical tests were used to assess the significance of differences between mutant mice and *Eng$^{fl/\Delta\ ex5\text{-}6}$* matched controls (table 4.1 summarises statistical analyses). Three technical replicate FACS analyses were performed for each BM cell population. Six out of twelve mutant mice had a higher percentage of Eng^{bright} cells than controls, while three out of twelve reached statistical significance in the Eng^{dim} sub-set. These mutants were distributed throughout the 6 week period and too few mice were analysed to see a difference related to time from commencement of endoglin depletion. Additionally, an insufficient number of mutant mice were analysed at each time point to determine a reliable pattern of expression. However the data indicate both the number of endoglin positive cells and the level of endoglin expression increased in the BM of Eng-iKO mice.

These results appear independent of any secondary effects of tamoxifen administration as both tamoxifen treated and untreated control mice presented with similar levels of expression (table 4.1). However only 1 *Eng$^{fl/fl}$* and 1 *Eng$^{fl/\Delta ex5\text{-}6}$* untreated animal was included in this analysis (versus 6 tamoxifen-treated controls of each genotype) therefore further investigation using a wider cohort of control mice (without tamoxifen administration) would be required to absolutely discount this possibility.

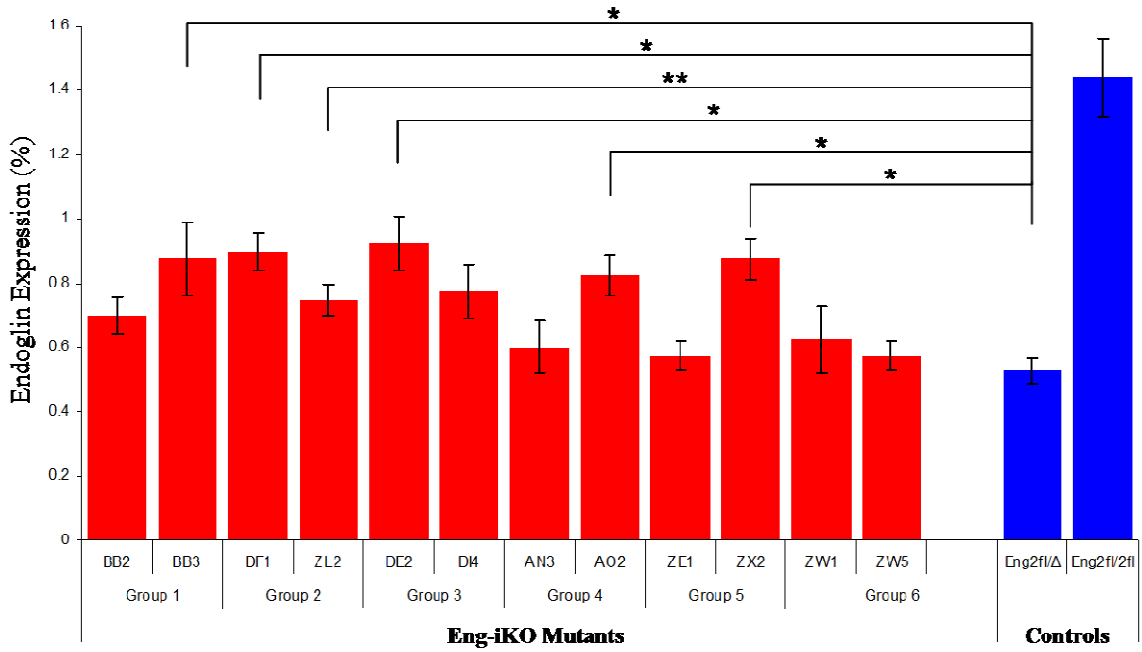

Figure 4.8. FACS analysis of the Eng^{bright} sub-population in BM cells of Eng-iKO mice. Red bars correspond to tamoxifen treated Eng-iKO mice categorised according to time interval from tamoxifen treatment to tissue harvest. Blue bars correspond to endoglin positive cells in BM from tamoxifen-treated *Eng*$^{fl/\Delta ex5\text{-}6}$ (n=7) and *Eng*$^{fl/fl}$ (n=7) mice. Horizontal bars identify significant results of Mann Whitney tests between individual mutant mice and *Eng*$^{fl/\Delta ex5\text{-}6}$ levels. *= p<0.05, **= p<0.01. Error bars represent ±SEM. Abbreviations; dpi = days post first injection.

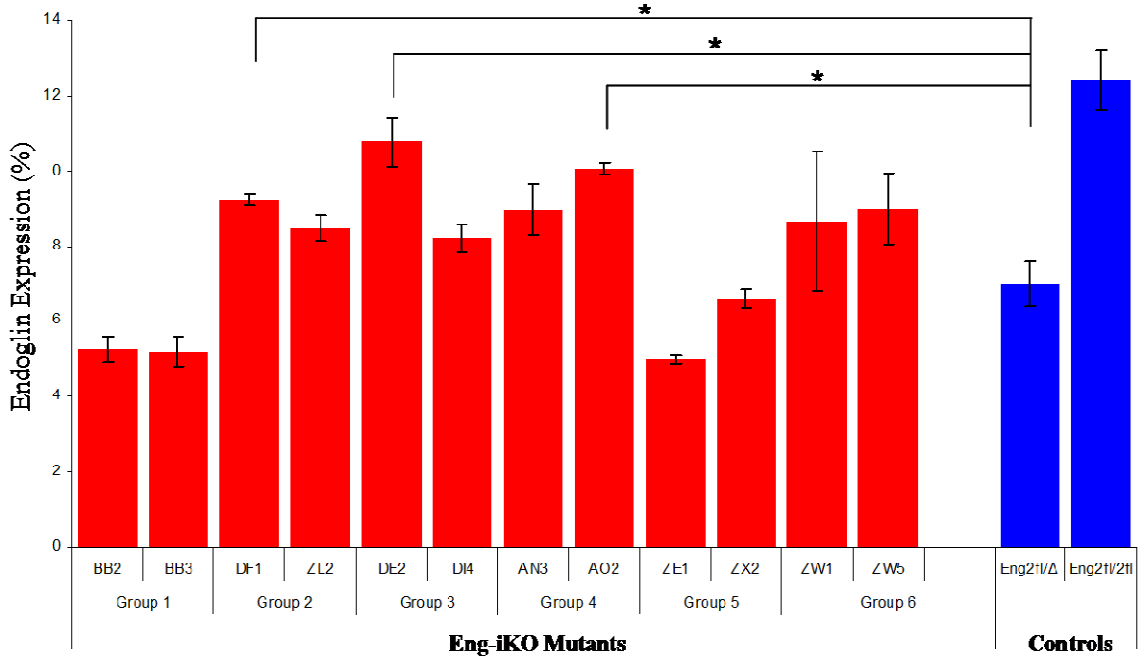

Figure 4.9. Expression of the Eng^{dim} sub-population in BM cells of Eng-iKO mice. Red bars correspond to tamoxifen treated Endoglin mutants with groups categorised according to time interval from tamoxifen treatment to tissue harvest. Blue bars correspond to tamoxifen-treated *Eng*$^{fl/\Delta ex5\text{-}6}$ and *Eng*$^{fl/fl}$ controls. Horizontal bars identify significant results of Mann Whitney tests between individual mutant mice and *Eng*$^{fl/\Delta ex5\text{-}6}$ levels. * = p<0.05. Error bars represent ±SEM. Abbreviations; dpi = days post first injection.

Eng-iKO	Mutant	Eng^{bright} (%)	Mann Whitney *p* Value	% Change	Eng^{dim} (%)	Mann Whitney *p* Value	% Change
Group1^{10pi}	BB2	0.7	N.S.	(+) 32.1	5.275	N.S.	(-) 24.6
	BB3	0.875	0.029	(+) 65.1	5.2	N.S.	(-) 25.7
Group2^{16dpi}	DF1	0.9	0.007	(+) 69.8	9.225	0.047	(+) 31.8
	ZL2	0.75	0.028	(+) 41.5	8.475	N.S.	(+) 21.1
Group3^{23dpi}	DE2	0.925	0.01	(+) 74.5	10.775	0.018	(+) 53.9
	DI4	0.775	N.S.	(+) 46.2	8.225	N.S.	(+) 17.5
Group4^{30dpi}	AN3	0.6	N.S.	(+) 13.2	8.975	N.S.	(+) 28.2
	AO2	0.825	0.019	(+) 55.7	10.075	0.04	(+) 43.9
Group5^{37dpi}	ZE1	0.575	N.S.	(+) 8.5	5	N.S.	(-) 28.6
	ZX2	0.875	0.011	(+) 65.10	6.6	N.S.	(-) 5.7
Group6^{44dpi}	ZW1	0.625	N.S.	(+) 17.9	8.675	N.S.	(+) 23.9
	ZW5	0.575	N.S.	(+) 8.5	9	N.S.	(+) 28.6
Eng$^{fl/\Delta ex5-6}$		0.53	n/a	n/a	7	n/a	n/a
Eng$^{fl/fl}$		1.44	n/a	n/a	12.4	n/a	n/a
Eng$^{fl/\Delta ex5-6}$,	no tamoxifen	0.58	n/a	n/a	5.4	n/a	n/a
Eng$^{fl/fl}$,	no tamoxifen	1.25	n/a	n/a	9.7	n/a	n/a

Table 4.1. Statistical analyses of Eng^{bright} and Eng^{dim} populations (displayed as percentage of total BM cells) in Eng-iKO mutant mice. The results of Mann Whitney tests between individual mutants and tamoxifen-treated *Eng*$^{fl/\Delta ex5-6}$ control populations for both Eng^{bright} and Eng^{dim} populations are shown, as well as percentage changes in expression. Both tamoxifen-treated and untreated *Eng*$^{fl/\Delta ex5-6}$ and *Eng*$^{fl/fl}$ control populations are listed for comparison (red). $p<0.05$ is considered significant; N.S. denotes not significant ($p>0.05$), and n/a is not applicable.

4.2.3. EPCs Do Not Contribute to Endothelial Repair in Endoglin Knock-Out Mice

Immunohistochemistry using an anti-endoglin antibody was performed on heart and lung cryosections from all mutant mice and controls to determine the efficiency of endoglin depletion following tamoxifen treatment and to assess the contribution of BM-derived progenitor cells to endothelial replacement. To accurately confirm efficient endoglin knockdown in mutants following tamoxifen induction I first established the normal expression profile of endoglin in heart and lung tissues. Figure 4.10 shows representative images of staining for endoglin in heart and lung tissue from *Eng*$^{fl/\Delta ex5-6}$ and *Eng*$^{fl/fl}$ control mice.

Analysis of Lung Tissue in Endoglin Knock-Out Mutants

Lung tissue from mutant mice was examined at each time-point and endoglin expression was graded according to staining intensity (for grading criteria see figure 4.11). If endothelial repair/replacement had occurred then I would have expected to see low

expression of endoglin protein at early time-points in the study, followed by increasing levels as BM derived EPCs replaced the endoglin-negative resident ECs. However, no clear temporal pattern was observed. In particular, group 6 animals (analysed at day 44) did not show a clear increase in endoglin expression compared with other groups analysed at earlier time points. Overall, negligible positive staining (grading +) was observed in 6 out of 12 mutants indicative of extensive endoglin knock-down. In 5 out of 12 mutants there was a reduction in expression compared to $Eng^{fl/\Delta ex5\text{-}6}$ mice however notable levels of expression were still detected (grade ++) and only 1 out 12 mutants displayed clear endoglin expression at levels that were comparable to those seen in matched controls (grade +++).

Within group 1 (mice culled 10days following the first tamoxifen injection, days post injection (dpi)) animal BB2 was awarded a higher grade of staining intensity than its mutant counterpart (BB3) due to patches of positive staining that were restricted to one lobe only. Group 2 mutant mice were analysed at 16dpi and showed consistent low levels of endoglin expression throughout the capillary network and major vessels with several intermittent patches of negative staining, which were visible at a higher extent in ZL2 than in DF1. Analysis of group 3 mutant mice one week later revealed greater inconsistency, while DI4 showed negligible endoglin expression DE2 displayed patches of positive staining throughout the capillary network. Similarly whereas AN3 of group 4 displayed extensive positive staining, AO2 showed much lower expression. Of group 5 mutant mice ZE1 showed a high degree of endoglin knock down and ZX2 retained a high degree of endoglin expression that was comparable to matched control mice. Group 6 mutant mice were both negative for endoglin staining.

Analysis of Heart Tissue in Endoglin Knock-Out Mutants

Analysis of endoglin stained heart sections from mutant mice revealed extensive knock down of endoglin expression at all time-points (figure 4.12). Only 3 out of 12 Eng-iKO mutants showed considerable levels of expression following tamoxifen treatment. Both ZL2 (group 2, analysed 16 days post tamoxifen) and AN3 (group 4, analysed 30 days post tamoxifen) exhibited low levels of endoglin positive staining and were awarded grade ++ intensity rating, whereas examination of ZX2 (group 5, analysed 37 days post

tamoxifen) revealed endoglin expression comparable to that seen in $Eng^{fl/\Delta ex5\text{-}6}$ matched controls (+++).

This study failed to demonstrate endothelial replacement following endoglin depletion in a significant number of animals (see table 4.2. for summary of findings). Overall there was a good correlation between the endoglin levels in heart and lung tissues, but there appeared to be more efficient endoglin knockdown in cardiac compared with pulmonary vasculature. Three (ZL2, AN3 and ZX2) out of 12 Eng-iKO mutants demonstrated moderate levels of endoglin protein expression in both heart and lung tissue, suggesting that endoglin knockdown was less efficient in these mice. In fact, ZX2 had expression levels comparable to $Eng^{fl/\Delta ex5\text{-}6}$ controls.

	Group 1		Group 2		Group 3		Group 4		Group 5		Group 6	
	BB2	BB3	DF1	ZL2	DE2	DI4	AN3	AO2	ZE1	ZX2	ZW1	ZW5
X-GAL	+++	+++	+++	+++	+++	++++	++	++++	++++	+++	++++	++++
Eng LUNG	++	+	++	++	++	+	++	+	+	+++	+	+
Eng HEART	+	+	+	++	+	+	++	+	+	+++	+	+
Eng^{bright} (%) BM	0.7	0.875	0.9	0.75	0.925	0.775	0.6	0.825	0.575	0.875	0.625	0.575
Eng^{dim} (%) BM	5.275	5.2	9.225	8.475	10.78	8.225	8.975	10.08	5	6.6	8.675	9
AGE (weeks)	17	17	16.7	25	17	16.6	23.9	23.9	26.9	27.1	28.1	28.1
SEX	f	f	f	m	m	f	f	m	m	f	m	m

Table 4.2. A summary of the effect of systemic endothelial restricted endoglin depletion on endoglin expression in the BM and endothelial replacement in cardiac and pulmonary vasculature. X-Gal staining intensity of lung lobes is consistently high indicating extensive *Cdh5(PAC)-CreER^{T2}* expression in mutant mice (++ = low level or patchy lacZ expression, +++ = majority of vessels exhibiting intense staining, ++++ = maximum staining). Expression of endoglin in lung tissue was notably knocked down in mutants but shows intra and inter animal variability and heart tissue shows extensive knock-down (+ = negligible endoglin expression, ++ = low level or small patches of positive staining, +++ = expression comparable to $Eng^{fl/\Delta ex5\text{-}6}$ controls). Eng^{bright} and Eng^{dim} sub-populations displayed as percentage of total bone marrow. Age of mice at time of first tamoxifen injection and sex also shown (m = male, f = female).

Overall, there was no clear outcome from this study. It is possible that high endoglin expression may be attributable to poor *Cdh5(PAC)-CreER^{T2}* expression and/or induction or it could be due to BM cell-dependent endothelial replacement.

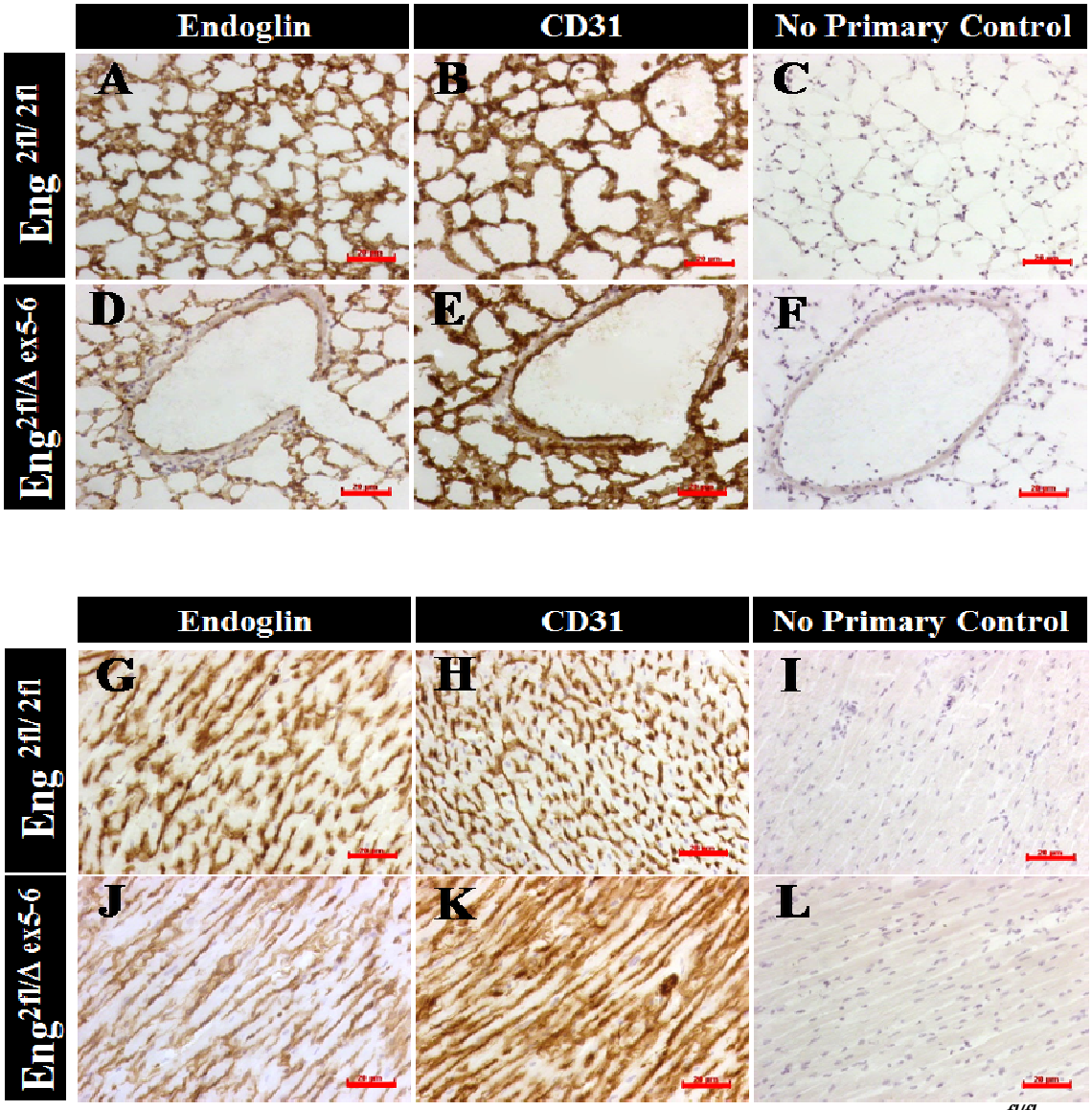

Figure 4.10. Endoglin expression in lung (A-F) and heart (G-L) tissue of *Eng*$^{fl/fl}$ and *Eng*$^{fl/\Delta ex5-6}$ mice. Immunohistochemical staining for endoglin and CD31 (indicated by brown DAB stain) revealed endoglin expression is present throughout the vasculature of heart and lung tissues. Endoglin staining is reduced in *Eng*$^{fl/\Delta ex5-6}$ tissue (D and J) compared with *Eng*$^{fl/fl}$ (A and G). Positive expression of the pan-endothelial cell marker CD31 is shown in both *Eng*$^{fl/fl}$ and *Eng*$^{fl/\Delta ex5-6}$ genotypes for lung (B and E) and heart tissue (H and K). Negative staining is shown in no primary control stained sections (C, F, I and L). All mice were injected with 14mg tamoxifen over 9 days. Scale bars = 20µm.

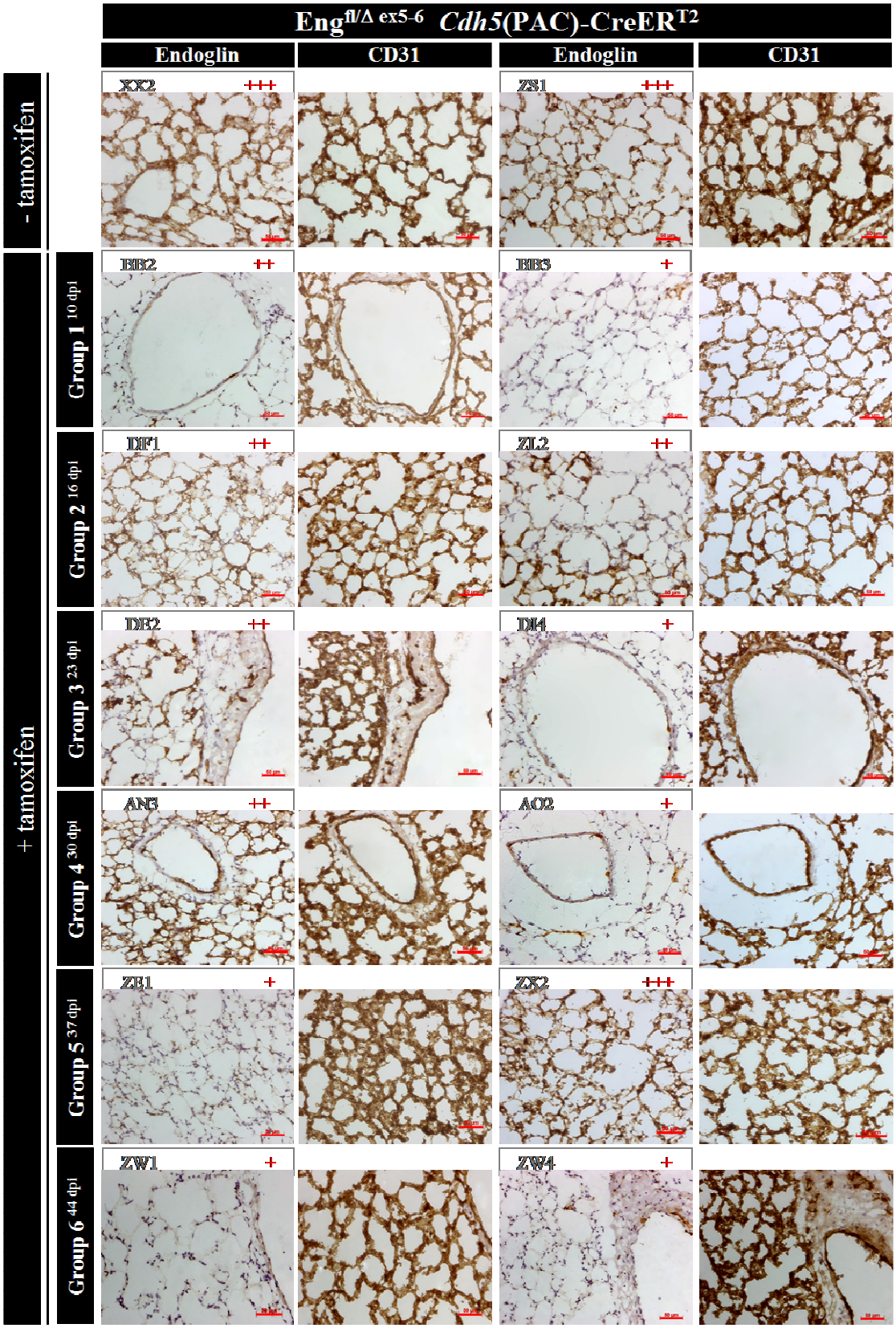

Figure 4.11. Efficient knock-down of endoglin expression in the pulmonary vasculature of Eng-iKO mutant mice. Extensive knock-down of endoglin expression (brown stain) is evident in all tamoxifen recipient groups (second to bottom panels) compared with tamoxifen untreated (top panel) and treated (see figure 4.10) matched controls. Mouse identity and extent of knock-down is graded above each panel; (red, + = negligible endoglin expression, ++ = low level or small patches of positive staining, +++ = expression comparable to $Eng^{fl/\Delta ex5\text{-}6}$ controls). As expected, positive CD31 staining in adjacent sections revealed no difference in mutant mice as compared to matched controls. Scale bars = 50µm.

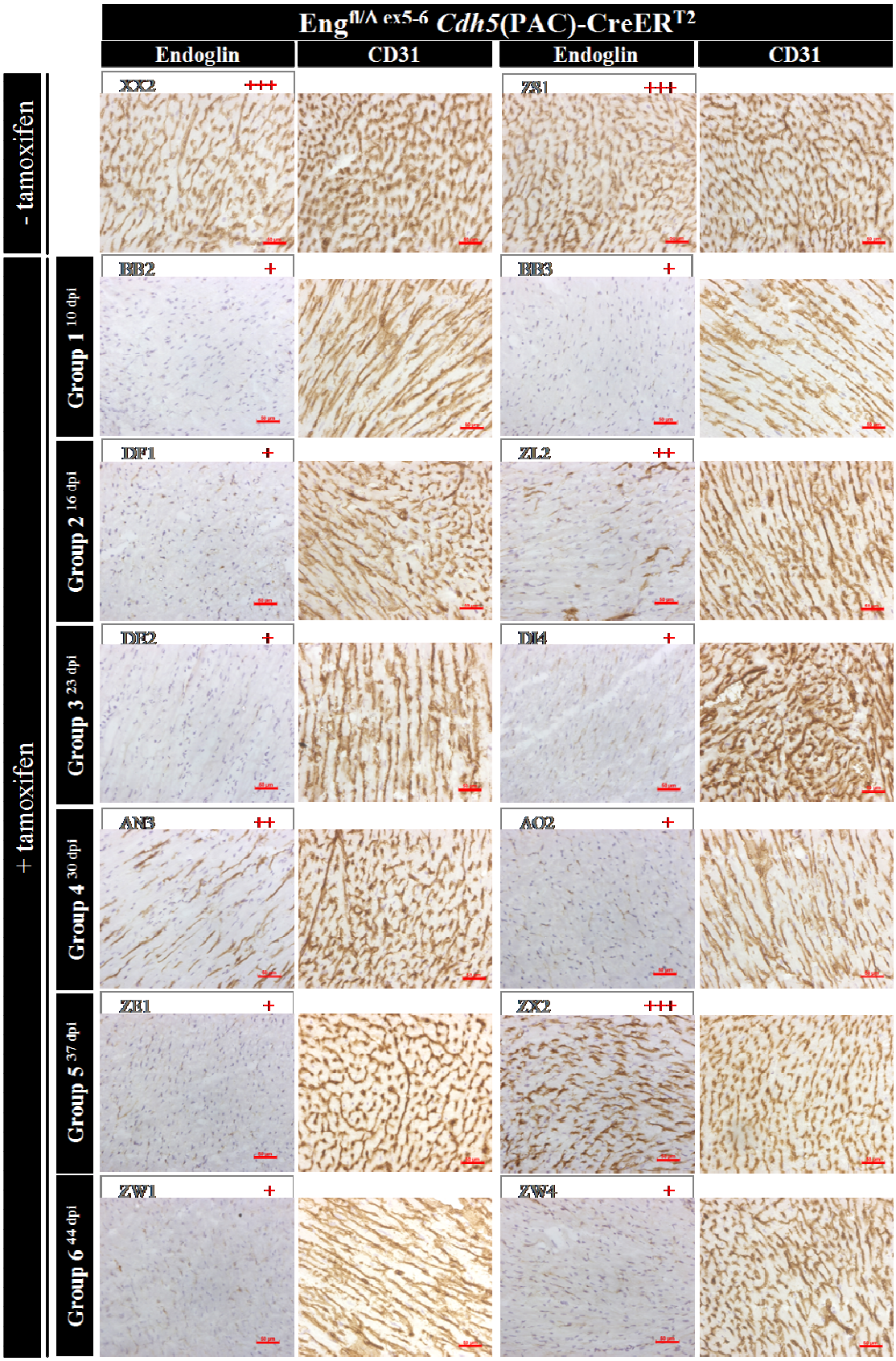

Figure 4.12. Efficient knock-down of endoglin expression in the heart vasculature of Eng-iKO mutant mice. Extensive knock-down of endoglin expression (brown stain) is evident in all tamoxifen recipient groups (second to bottom panels) compared with tamoxifen untreated (top panel) and treated (see figure 4.10) Extent of knock-down is graded adjacent mouse identity; (red, + = negligible endoglin expression, ++ = low level or small patches of positive staining, +++ = expression comparable to *Eng*$^{fl/\Delta ex5\text{-}6}$ controls). Positive CD31 staining revealed no difference in mutant mice as compared to matched controls. Scale bars = 50µm.

4.3. Discussion

The purpose of this pilot study was to test whether endoglin depletion in ECs leads to active endothelial replacement by circulating endoglin positive cells originating from the BM. Considerable endoglin expression in pulmonary vasculature of several mutant mice corroborated the trend of endoglin re-expression initially described by Dr Marwa Mahmoud (unpublished data) however the level of expression was relatively low and extensive endoglin knock-down, with little to no detectable expression of endoglin was evident in a number of additional mutant mice sampled across all time-points (one week to six weeks following tamoxifen induction). The majority of mutants analysed also showed highly efficient endoglin knock-down in the endothelium of the heart. I concluded that the patterns of endoglin expression in lung and heart tissue of mutant mice do not support the hypothesis that circulating EPCs of myeloid origin could replace endoglin negative vascular ECs in adult mice.

4.3.1. Heterogeneity of Endothelial Specific Endoglin Knock-Down in the Pulmonary Vasculature

The mechanism explaining the inter-animal variability of endoglin knock-down observed in the pulmonary vasculature of mutants is unclear however it is highly unlikely to be due to reversal of *Cdh5(PAC)-CreER^{T2}*-mediated genetic excision. Although this reaction is reversible in theory, for kinetic reasons, intermolecular recombination occurs at very low frequency (figure 4.1)[321]. Several possibilities could explain the observed variation including the possible suppression of CreER^{T2} activity in lung endothelium or a dose dependent mechanism which dictates that a higher dose of tamoxifen is necessary to bring about efficient deletion in lung endothelium than is necessary for heart tissue. Indeed a low local concentration of tamoxifen due to blood flow patterns may explain variability of endoglin depletion observed between lung lobes of a single animal. Several additional relevant factors have been associated with CreER^{T2}-mediated recombination efficiency including genetic background, sex, weight and age of mice[325]. Of particular note is the effect of age, Monvoisin *et al* observed that the degree of Cre-mediated genetic recombination correlates inversely with age and identified significant differences between 8 week and 24 week old mice[325]. The reason for this is unknown but the authors postulate that it could be due to alterations in the chromatin status of older cells preventing recombination or the activity of Cre or the

CreER^{T2} fusion protein being suppressed in older animals. It is plausible therefore to expect a greater degree of knockdown with less variation if using young adult, age matched mice. It is of note that the mice with the highest levels of endoglin expression (ZL2 and ZX2) were also amongst the oldest mice in the study, at 25 weeks and 27.1 weeks respectively. This would be consistent with a reduced level of Cre mediated recombination leading to moderate levels of residual endoglin protein expression in these individuals, but it is surprising that this difference was not also observed in the X-Gal stained lung lobes which were also used a readout for Cre activity. It may be that the *Rosa26* (*Thumpd3*) locus is less susceptible to chromatin re-organisation with age than the *endoglin* locus.

4.3.2. *Cdh5*(PAC)-CreER^{T2} Mediated Recombination and Endoglin Expression in BM Cells

The low incidence of recombination in BM cells of mutant mice (0.43%±0.12) is in accordance with a similar VECadherin-CreER^{T2} deleter mouse which describes 0.4%±0.01% recombination (over control) in BM cells[325]. Another mouse line showing constitutive VE-Cadherin-Cre expression shows *lacZ* Cre reporter activity in 50–60% of BM cells. However, this high level is thought to represent the progeny of progenitor cells that expressed VE-Cadherin-Cre during early development[326]. In contrast, the inducible *Cdh5*(PAC)-CreER^{T2} BM lacZ positive cell populations described in this chapter (and in reference[325]), represent adult BM cells in which CreER^{T2} expression driven by the VE-Cadherin promoter is activated only once tamoxifen is administered. The levels of Cre expression shown in figure 4.6 are consistent with the reported expression of VE-Cadherin in healthy adult BM of less than 1 per cent[327]. While many studies report the expression of VE-Cadherin as a property of BM-derived EPCs more detailed analysis has shown that EPCs begin to express VE-Cadherin once they have committed to terminal endothelial differentiation[88] and it is unlikely that more primitive BM-resident cells would strongly express VE-Cadherin.

Following endothelial specific endoglin depletion a small but significant up-regulation of endoglin protein expression was observed in Eng-iKO BM cells compared with matched controls. An increase in an Eng^{bright} subpopulation was detected from as early as week one and an increase in Eng^{dim} cells from week two. The expansion of endoglin

expressing cells in response to systemic endoglin loss would be consistent with a role for circulating BM-derived EPCs in vascular repair in endoglin knock-out mice. However, there was no temporal pattern in endoglin protein expression in lung or heart tissues to indicate such a repair mechanism was occurring.

Interestingly I detected both 'bright' and 'dim' endoglin positive BM cells in this study, whereas analysis of endoglin expression in BM in chapter 3 (figure 3.9) did not reveal such sub-populations. This may be due to different strains of mice being used in these two chapters (chapter 3 analysis represents NIH pure line whereas in chapter 4 I used mice of mixed genetic background). In addition different flow cytometers were used in these two analyses. BM from NIH mice was analysed using a FACS Calibur machine (Becton Dickinson) whereas in the later study I used a LSRII flow cytometer (Becton Dickinson), which may offer better resolution. Although the work described in this chapter has not explored the role of endoglin in the BM, the detection of 'bright' and 'dim' endoglin positive cells could represent heterogeneous sub-populations of cells or mark progenitor cells in the BM at various stages of differentiation. Endoglin is used as a marker for both EPCs and terminally differentiated ECs and onset of expression may represent a transitional phenotype between the primitive EPC and mature EC. A role for endoglin in haemangioblast specification during development has been identified[310] and it has been suggested that an adult equivalent of the embryonic haemangioblast may be the likely source of EPCs in haematopoietic tissues, although this has yet to be proven. It is possible that the expanded endoglin expressing population observed in the current study represents such an adult haemangioblast. Endoglin is also expressed on a sub-population of pro-erythroblasts in healthy adult BM[328] and marks adult long-term repopulating HSCs[257]. It may be beneficial to isolate bright and dim endoglin positive populations and test their capacity to contribute to vessel formation *in vivo,* as well as capacity for differentiation along both the endothelial and haematopoietic lineages.

4.3.3. Is a Secondary Pathological Stimulus Required to Induce EC Replacement?

The lack of evidence for endothelial replacement in Eng-iKO mutant mice may be explained by the stable nature of endothelial cells which have an estimated turnover time of more than 1000 days[322]. A secondary pathological stimulus, such as acute MI,

may be required to fully activate an endothelial repair mechanism. Such a stimulus would increase the turnover rate of the microvascular endothelium and promote active angiogenesis, in which EPCs proliferate, mobilise and home to sites of ischaemia.

Despite the initial enthusiasm surrounding EPC based pro-angiogenic therapies the delivery of mixed populations of poorly defined cells has resulted in only modest benefit in clinical trials[134-136]. While it is likely that the identification and use of a more defined functionally active repair cell will improve the clinical outcomes, the combination of EPCs with MSCs has also been shown to augment neovascularisation *in vivo*[106-107]. Similarly, cardiosphere-derived cells (CDCs), a mesenchymal cell type expanded from cardiac tissue has been shown to promote heart repair following MI[159]. These cells also express endoglin, which may act as a functional marker of cardiac repair cells. This hypothesis was tested *in vitro* and *in vivo* in a murine MI model by depleting endoglin in donor CDC repair cells using inducible knockout technology and is described in chapters 5 and 6 of this thesis.

CHAPTER 5.

The Role of Endoglin in Cardiosphere-derived Cells *in vitro*

5.1. Introduction

The discovery of endogenous cardiac-resident stems cells (CSCs) capable of differentiating into multiple cell lineages has led to intense investigation into their therapeutic potential of (as discussed in section 1.7.4). The isolation of specific cardiac stem cell sub-populations directly from cardiac tissue has also been described[162]. Cells spontaneously migrate from heart biopsy tissue in culture. The resultant population contains distinct cell types expressing stem cell-associated (cKit, Sca1, Abcg2), endothelial (CD31, CD34) and mesenchymal (CD90) markers. The transition of this outgrowth cell population to form cardiospheres reportedly enriches CSCs and increases repair potency[158]. Cell expansion as cardiosphere-derived cells (CDCs) is also possible with cells retaining their multipotent and self-renewal capacity[159, 162, 175]. CDCs have been shown to have therapeutic potential in the treatment of ischaemic heart disease in experimental models and phase I clinical trials (as discussed in section 1.7.4). Of particular interest CDC transplantation into pre-clinical models has been shown to induce an angiogenic response (discussed in section 1.7.3).

Interestingly the majority of human CDCs express endoglin, which is also expressed by ECs, EPCs, HSCs and MSCs (see section 1.9.3.). The role of endoglin has been most extensively studied in ECs and here it acts to regulate the balance of TGFβ signalling through the Alk1 and Alk5 pathways. However, the role of endoglin in CDCs has not yet been determined. This is important to address as endoglin may represent a key surface marker that can be used to define these cardiac repair cells, whilst also facilitating their pro-angiogenic potential by mediating TGFβ family signalling. The study described in this chapter aims to address the role of endoglin in CDCs by testing the effect of endoglin loss on *in vitro* properties related to tissue repair (cellular proliferation and migration) and the activation of Smad1/5/8 and Smad2 TGFβ signalling pathways. Endoglin expression was depleted in the experimental cells *in vitro* using the inducible Cre-recombinase strategy described in section 4.1 (see figures 4.1 and 4.2).

5.2. Results

5.2.1. Derivation and Characterisation of Cardiosphere-derived Cells

5.2.1.1. Optimisation of CDC Culture

CDCs were derived using an adapted version of a protocol described by Smith *et al*[159] (figure 5.1A). Briefly mouse neonatal hearts are enzymatically digested, minced and tissue fragments are plated on fibronectin-coated dishes as explants and cultured (figure 5.1B). After several days a layer of stromal-like cells grows from the adherent explant tissue (figure 5.1B), over which small round 'phase bright cells' migrate (figure 5.1C). Once confluent, all explant derived cells (EDCs, including both stromal-like and phase bright cells) are removed via gentle trypsinisation, plated on low-adherence poly-D-lysine and cultured in a specific growth factor enriched low serum media for several days. Over this time clusters of cells aggregate and proliferate to form spheres, and these cellular structures are termed cardiospheres (figure 5.1D and E). Cardiospheres are loosely adherent and easily removed via gentle trituration, re-plated on a fibronectin matrix and cultured as a monolayer of CDCs in basal medium supplemented with 20% FCS (figure 5.1F and G). Several studies report that EDCs can be harvested repeatedly from the same tissue fragments, however I observed that explants became progressively more rounded with less-defined margins and eventually degraded to a degree which precluded using the same tissue to produce a second generation of EDCs.

Several stages of the culture protocol were adapted in order to obtain optimal cardiosphere and CDC yields. I observed that early adherence of myocardial fragments was essential to ensure sufficient growth of EDCs and that the initial plating of tissue explants in the presence of media was required to prevent heart tissue becoming desiccated. Likewise addition of media at defined intervals during the culture period was also advantageous in preventing explants from drying out. Andersen *et al* have stated that cardiosphere yield is correlated with EDC plating density[174] therefore to enhance cardiosphere number I titrated EDC seeding density on poly-D-lysine coated dishes and assessed the number and size of cardiospheres formed. I found that EDC seeding density positively correlated with increased cardiosphere number and size up to 10^5 cells per well (24 well plate). Therefore, this seeding density was used in all subsequent cultures (figure 5.2A). In addition, I tested the effect of varying the

concentration of growth factors in cardiosphere specific media (CGM). Two different formulations of CGM were compared and they were denoted as high growth factor media (high-GF-CGM; bFGF 80ng/ml, EGF 20ng/ml and thrombin 50ng/ml) and low growth factor (low-GF-CGM; bFGF 20ng/ml, EGF 10ng/ml and thrombin 25ng/ml) supplemented media. Cardiosphere number was compared between these two groups and found to be significantly increased in high-GF-CGM cultures (p=0.008, figure 5.2B). Also, addition of fresh high-GF-CGM at day 4 of cardiosphere culture (6 day total culture period) appeared to have a positive effect on cardiosphere growth (p=0.05, figure 5.2B).

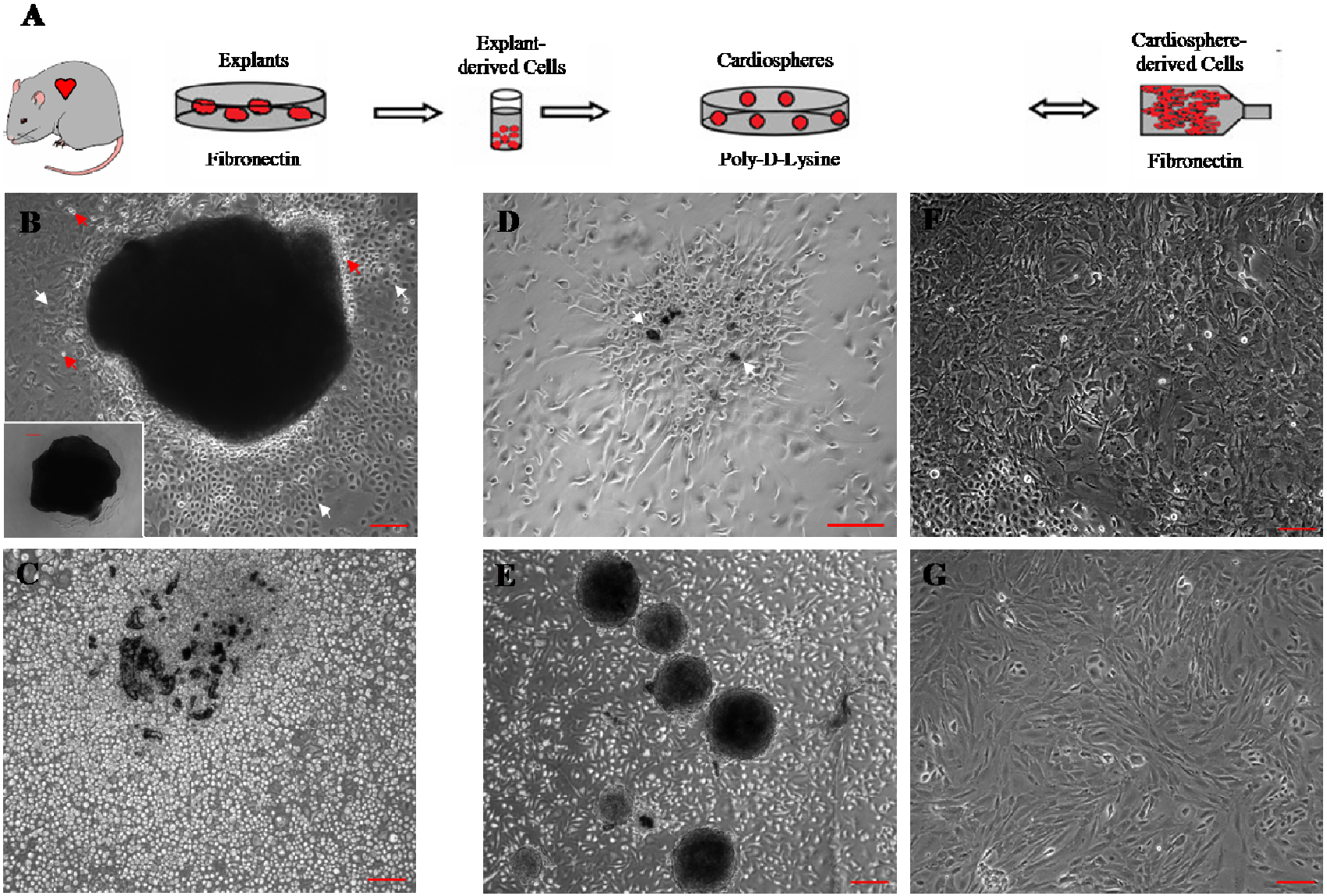
A
Explants
Fibronectin
Explant-
derived Cells
Cardiospheres
Poly-D-Lysine
Cardiosphere-
derived Cells
Fibronectin
B
C
D
E
F
G

Figure 5.1. Cardiosphere and CDC culture. (A) Schematic depicting different stages of CDC culture. (B) Neonatal mouse heart explant at day 4 showing spontaneous outgrowth of EDCs (stromal-like cells (white arrows) and phase bright cells (red arrows) with inset image showing a similar explant just 12 hours after plating). (C) At day 14 EDC outgrowth reaches confluence and is harvested for cardiosphere culture. The myocardial tissue gradually diminishes as the number of outgrowth EDCs increases. (D) EDCs are plated in cardiosphere-culture conditions. At day 2, cells appear to migrate towards each other to form cellular foci. (Note white arrows highlighting small fragments of contaminating myocardial tissue which cardiospheres occasionally form around). (E) Fully formed cardiospheres at day 6. (F) CDCs at passage 2, plated on fibronectin for expansion. (G) CDCs at passage 6. Scale bars = 100μM.

Spontaneous beating of embryonic mouse cardiospheres has previously been described[158], though in the present study while the beating of myocardial explant tissue was often noted, this was only rarely observed in cardiospheres. It has been suggested that beating cardiospheres are due to the presence of 'contaminating' heart tissue fragments[174] therefore I included a sedimentation step following harvest of phase bright cells to ensure that minimal amounts of cardiac tissue were present in subsequent cardiosphere cultures (briefly, following EDC harvest, cells in suspension are left to sit for 1-2min prior to being transferred to a second tube while the myocardial tissue fragments sink to the bottom of the first tube and are discarded). However despite this intervention very small fragments of tissue sometimes did persist in cardiosphere culture and it appeared that EDCs migrated towards these and formed cardiospheres around them (figure 5.1D, white arrows indicate myocardial tissue present in the centre of a cardiosphere in formation). It is possible that these pieces of myocardial tissue enhance cardiosphere formation, although such contamination may be undesirable if this protocol is used to prepare CDCs from human heart tissue biopsies for clinical applications as injecting tissue fragments may increase the risk of micro-thromboli formation, and injecting myocardial tissue that retains intrinsic contractility may interfere with the electrophysiology of the recipient heart. It may be possible to filter out these fragments using an appropriately sized filter mesh, however I opted not to do this in the current study to prevent marked deviation from other published culturing methods[159, 163]. CDCs represent a heterogeneous cell population and so to minimise the 'contamination' of cultures with stromal-like cells, which could become detached during the gentle trituration used to isolate cardiospheres, a second sedimentation step was included during the cardiosphere harvesting stage as suggested by Anderson *et al*[174]. This involves allowing cardiospheres to sink to the bottom of a greiner tube while the supernatant, which contains any contaminating non-cardiosphere cells, is discarded.

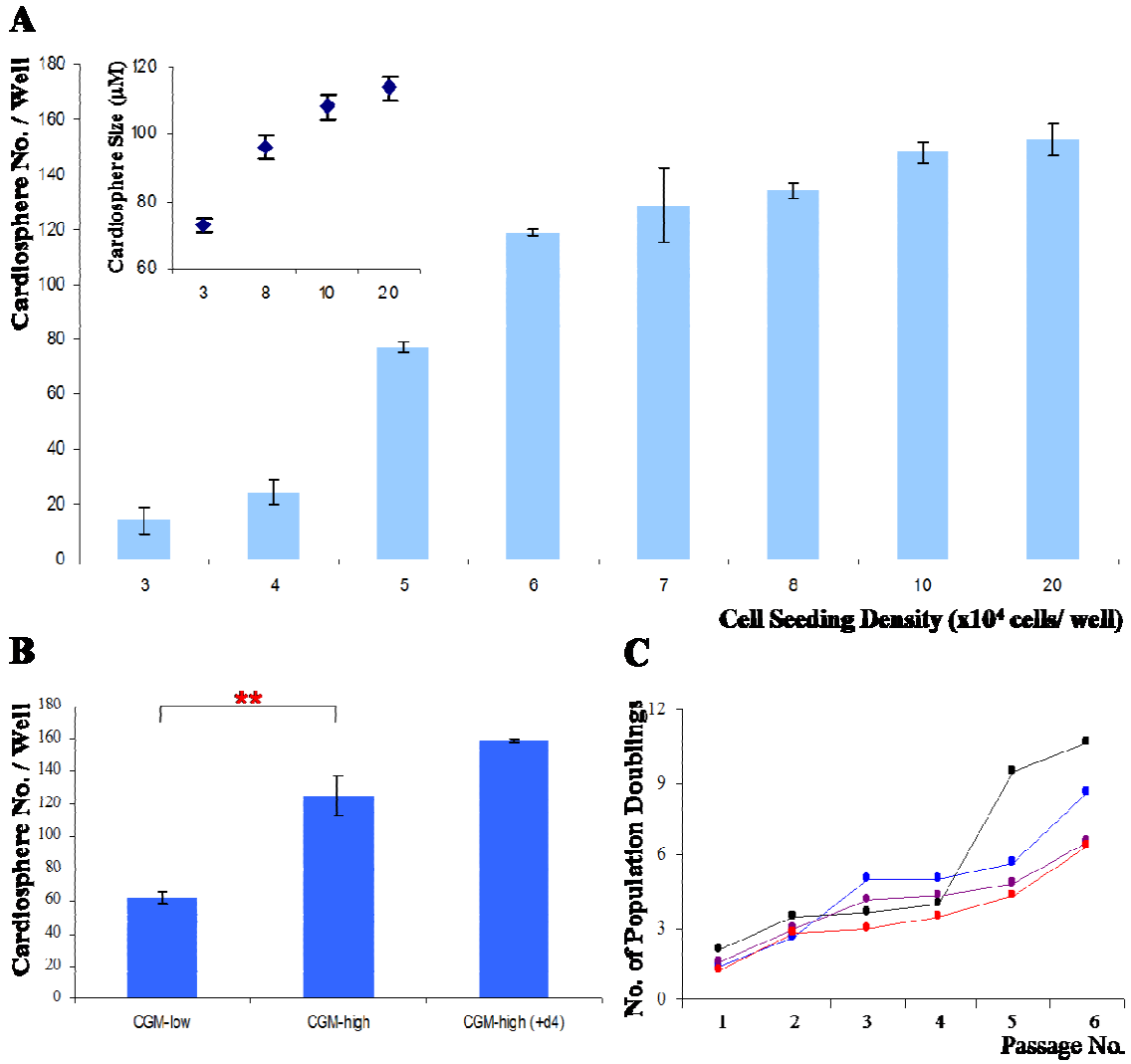

Figure 5.2. Optimising culture conditions to maximise cardiosphere yield and evaluation of CDC expansion. (A) There is a positive correlation between cardiosphere number and EDC seeding density up to 10^5 cells per well. Inset graph, there also appears to be a positive correlation between cardiosphere size and EDC seeding density indicating that cardiospheres may be partially formed by cellular aggregation. (B) A higher concentration of bFGF (80ng/ml versus 20ng/ml), EGF (20ng/ml versus 10ng/ml) and thrombin (50ng/ml versus 25ng/ml) in cardiosphere specific growth media results in a significant increase in cardiosphere number per well (p=0.008), as does replacing CGM-high media with fresh CGM-high media to cardiosphere cultures at day 4 (p=0.05). Experiments were repeated three times and the statistical significance of differences between groups was determined using one-way ANOVA (p=0.001) and unpaired t-tests. (C) Cell growth of 4 separate CDC cultures expressed as number of population doublings between each passage (average time between passaging is 3-5 days). ** denotes $p < 0.01$.

Using an optimised culture protocol, approximately 93%±2 of neonatal cardiac explants adhered to fibronectin coated plates and of these 92%±1 produced an EDC outgrowth which included phase bright cells in 51%±13 of cases. EDCs typically became confluent within 14±2 days and yielded approximately 1.2-2.4x10^6 cells per heart. EDCs were seeded in poly-D-lysine coated 24 well plates at a density of 10^5 cells per

well and started to move together in foci during cardiosphere culture within 24 to 48 hours. By day 6 approximately 159±2.6 complete cardiospheres had formed per well. Cardiospheres were expanded as monolayers of CDCs that required passaging about every 3-5 days. Approximately 2-4x10^6 CDCs at passage 2 were harvested per neonatal mouse heart. All data described above were generated from at least 3 independent experiments.

5.2.1.2. Isolating Progenitor Cells from Different Regions of the Neonatal Mouse Heart

It has been reported that atria of the human heart contain higher numbers of progenitor cells than the ventricles[329-330]. Furthermore, Davis *et al* have shown that human atrial biopsies cultured as explants produce a markedly increased yield of EDCs than cardiac tissue taken from other regions[162]. I investigated whether this was also true for neonatal mouse hearts (aged between 4 to 6 days) by culturing explants of atrial and ventricular tissue separately and monitoring subsequent transition of resultant EDCs to cardiospheres. The aim of this study was to determine conditions that would enable an optimal yield of cardiac resident progenitors to be harvested. End-point measurements were (i) percentage of productive explants (defined as explants producing both stromal-like and phase bright cells), (ii) EDC yield (normalised to total explant number to account for the significantly larger amount of ventricle tissue available), (iii) cardiosphere number and (iv) cardiosphere size. The experiment was repeated three times and differences between atrial and ventricular measurements were statistically analysed using the unpaired *t*-test. Both atrial and ventricular tissue was cultured for the same time period (explant culture period was 14±2 days and cardiosphere culture was 6 days). The average number of explants analysed per experiment was 106±19 atrial fragments versus 231±13 ventricle explants. Cardiospheres were enumerated from 6 wells (10^5 EDCs plated per well of a 24 well plate) per group.

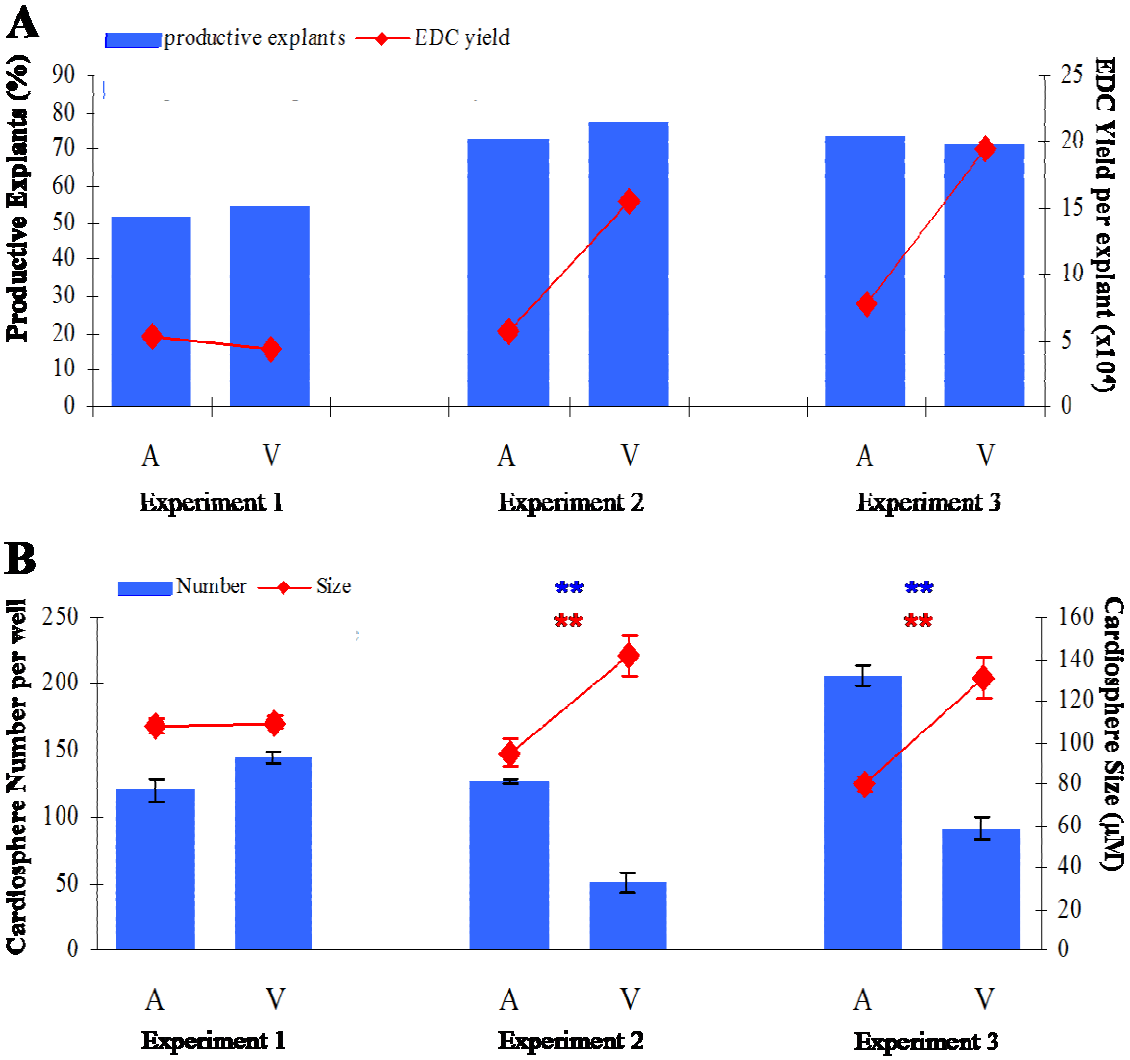

Figure 5.3. Evaluating the potential of atrial versus ventricular tissue to generate cardiospheres. (A) A summary of 3 independent experiments showing percentage of productive explants (blue bars) and EDC yield (red line) derived from atrial (*A*) versus ventricular (*V*) tissue. Percentage of productive explants is comparable between groups, whilst a greater yield of EDC outgrowth is obtained from ventricular explant culture. (B) A summary of 3 independent experiments showing cardiosphere number (blue bars) and size (cardiosphere diameter (µM), red line) derived from atrial (*A*) versus ventricular (*V*) tissue. Whilst cardiosphere yield was higher from atrial tissue cultures, these cell clusters were significantly smaller than their ventricular counterparts (cardiosphere diameter (µM) measured using Axiovision Rel. v4.8 software (Zeiss)). All pups used in this study were between 4 to 6 days old. Data analysed using the unpaired *t*-test. ** denotes $p < 0.01$.

In the first of the three experiments no difference was observed between atrial and ventricular cultures (figure 5.3). However in the second and third experiments significant differences were found between these two groups in all parameters tested with the exception of the percentage of productive explants, which remained comparable in all three experiments (figure 5.3A). EDC yield (normalised to total explant number and expressed as cell number per explant) was significantly increased in

ventricle derived cultures (figure 5.3A), in contrast to findings reported by Davis and colleagues[162]. Furthermore, whilst cardiosphere number was significantly increased in atria-derived cultures these cellular structures were markedly smaller than those derived from ventricular tissue (figure 5.3B). Given the variable outcomes of this experiment, and also that neonatal hearts offer relatively small tissue samples, in all subsequent experiments whole hearts were used to derive CDCs.

5.2.1.3. The Expression of Endothelial, Mesenchymal and Stem cell Markers in Passage 2 Murine CDCs.

Ex vivo expanded CDCs (passage 2) were characterised using immunocytochemistry staining and fluorescent microscopy with specific antibodies against endoglin and CD31. This analysis revealed high endoglin and low CD31 expression levels in CDCs (figure 5.4).

To allow high throughput immunophenotyping of CDCs in passage 2 cells, I used flow cytometry to analyse the expression of endoglin and CD31 as well as the stem cell marker cKit, and the mesenchymal cell marker CD90. Figure 5.5 graphically displays the results of one representative experiment showing the following approximate expression levels: 90.2±1.2% endoglin$^+$, 30.2±0.5% cKit$^+$, 22.1±0.3% CD90$^+$ and 25.8±1.1% CD31$^+$ (figure 5.5). These values are similar to those published in similar studies[159]. The majority of cKit and CD90 positive cells also co-expressed endoglin (approximately 82.5% and 94.6% respectively, figures 5.5C and 5.5D), whilst cKit$^+$ CDCs were largely distinct from the CD90$^+$ subpopulation (figure 5.5B). cKit is expressed by a large proportion of CD31$^+$ cells whereas CD90 expression is largely absent from CD31$^+$ cells (table 5.1).

Table 5.1 summarises the mean percentage values of all cell populations analysed in 6 independent experiments and reveals that there is a degree of inter-culture variation. Endoglin expression ranges from 68% to 92.2%, cKit expression peaked at over 50% in two of the analyses (see experiments B and E in table 5.1) whereas it ranged from 13.9 to 30.2% in the remaining experiments, which is more in keeping with published data[159]. CD90 also peaked at over 50% in one analysis (see experiment D in table 5.1) but remained relatively constant otherwise (11.9% to 22.1%), whilst the expression of CD31 ranged from 19.5% to 37.9% in 5 independent immunophenotyping profiles of passage 2 CDCs. Interestingly CD31 expression appeared to be appreciably lower in

CDCs as measured using immunocytochemistry (figure 5.4, n=1) compared with flow cytometry (n=5). This may be related to the higher sensitivity of FACS analysis which can detect antigen expression even at very low intensities. Furthermore, immunohistochemistry using an anti-CD31 antibody was only performed once and additional staining of independent cultures would be needed to confirm findings. The mice used were all neonates of C57Bl/6 strain and aged between 4 and 6 days (see table 5.1). Furthermore media and culture techniques were consistent between cultures therefore the observed variability in marker expression is presumably due to stochastic events or unknown variables (discussed in greater detail in section 5.3.1.).

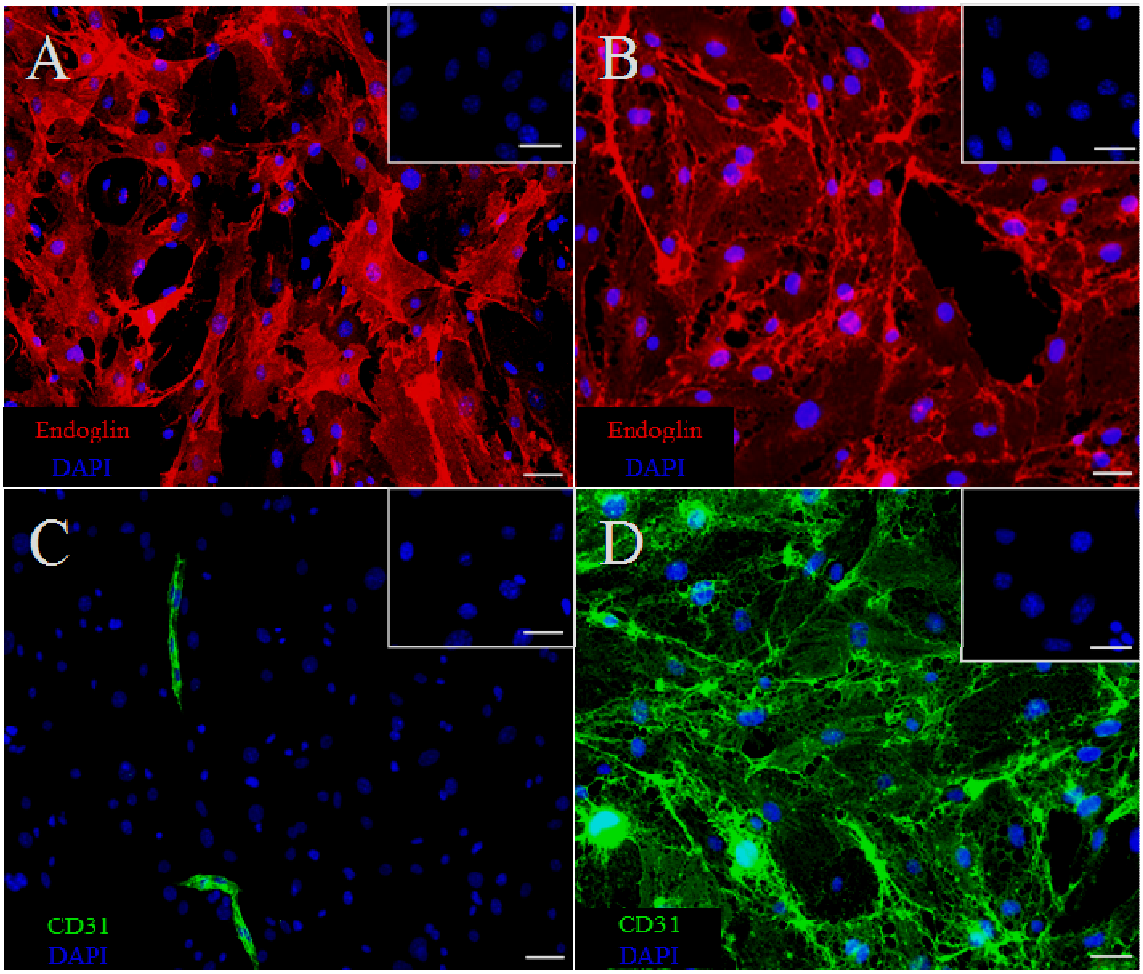

Figure 5.4. Immunofluorescent staining of passage 2 CDCs and primary mouse lung ECs. CDCs stained with anti-endoglin (A) and anti-CD31 (C) specific antibodies. Positive control mouse lung ECs stained with endoglin (B) and CD31 (D). Anti-rat secondary antibodies conjugated to alexa594 (red, A and B) and alexa488 (green, C and D) were used and nuclei stained with DAPI (blue). Inset images representative of no primary controls (A and C) and a negative control NIH-3T3 fibroblast cell line (B and D). N.B. CD31 positive CDCs (C) appear to be forming tubules/linear aggregates, however the presence of coronary vessel fragments cannot be discounted. This staining for CD31 was performed only once and additional replicate experiments would be required to confirm findings. Scale bars = 20μm.

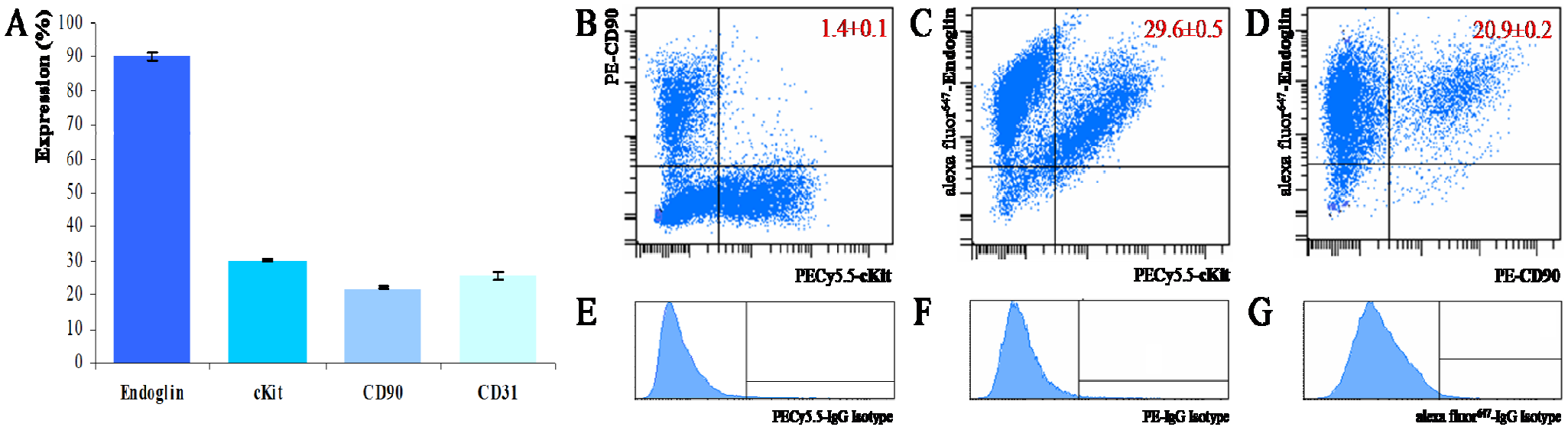

Figure 5.5. Flow cytometric analyses of murine CDCs at passage 2. (A) Summary of the percentage of CDCs expressing endothelial (CD31, endoglin), mesenchymal (CD90, endoglin) and stem cell (cKit) markers from one representative experiment. Dot plots showing populations of CDCs that co-express cKit and CD90 (B), cKit and endoglin (C) and CD90 and endoglin (dual positive cells in upper right quadrant). CDCs expressing cKit are largely distinct from CD90+ cells and the majority of cKit+ or CD90+ cells also co-segregate with endoglin. Histograms E to G show isotype control samples (PECy5.5-IgG, PE-IgG and AF594-IgG respectively). Data is derived from 3 replicate samples and presented as mean percentage ± SEM.

	Age of Pups (Days)	Eng$^+$	cKit$^+$	CD90$^+$	CD31$^+$	cKit$^+$/ CD90$^+$	Eng$^+$/ cKit$^+$	Eng$^+$/ CD90$^+$	CD31$^+$/ cKit$^+$	CD31$^+$/ CD90$^+$
A*	6	90.2±1.2	30.2±0.5	22.1±0.3	25.8±1.1	1.4±0.1	29.6±0.5	20.9±0.2	24.9±0.3	1.6±0.1
B	4	73.1±4.9	53.6±1.0	16.4±0.4	37.9±2.3	1.7±0.2	45.8±1.6	12.4±0.7	36.1±1.4	2.0±0.3
C	5	70.5±0.8	13.9±0.8	15.6±1.7	19.5±0.9	0.7±0.2	13.3±0.9	9.2±0.2	11.7±0.9	5.7±1.5
D	4	68.0±4.2	21.2±1.0	49.1±0.6	20.2±2.1	1.8±0.2	20.4±0.5	32.0±1.4	17.5±1.3	8.0±1.2
E	4	88.5±0.6	56.5±0.6	18.3±0.2	n/a	0.8±0.2	54.4±0.9	16.5±0.2	n/a	n/a
F	5	68.0±0.8	23.7±0.7	11.9±	33.2±1.0	0.68±0.1	23.6±0.3	7.1±0.2	22.4±1.2	3.0±0.1

Table 5.1. Summary of 6 independent FACS analyses performed with murine CDCs at passage 2. * denotes experiment illustrated in figure 5.5. Data is derived from 3 replicate samples and presented as mean percentage ± SEM. (n/a; CD31 stained samples were not included in this experiment).

5.2.1.4. CDCs Do Not Represent a Haematopoietic Cell Population

Flow cytometry demonstrated that passage 2 CDCs were predominantly negative for the haematological marker CD45 (2.1±23%, figure 5.6). This result indicates that haematological-derived cells do not form a major component of *ex vivo* expanded cardiac-derived progenitor cells.

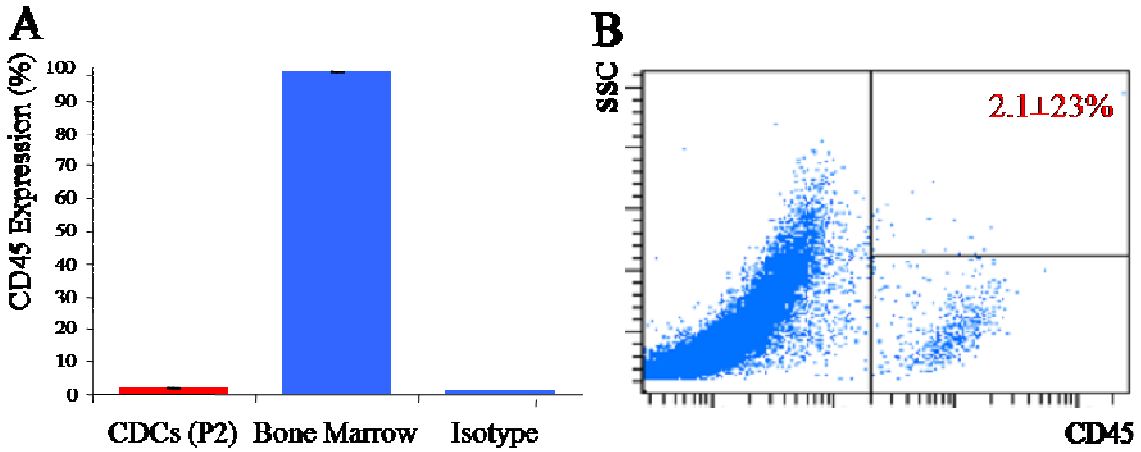

Figure 5.6. CDCs at passage 2 are predominantly negative for CD45. (A) Flow cytometric analysis reveals a very low population of CDCs express the pan-leukocyte marker CD45 (anti-CD45 specific antibody conjugated to FITC), whereas CD45 is expressed by almost all cells isolated from adult bone marrow. (B) A representative dot plot showing the $CD45^{+}$ population against side scatter. Data is derived from 3 replicate samples and presented as mean percentage ± SEM.

5.2.1.5 Dynamic Expression of Endothelial, Mesenchymal and Stem Cell Markers following Extended CDC Expansion

Dramatic differences were observed in the phenotypic profile for endoglin, cKit, CD90 and CD31 following extended *in vitro* CDC expansion. Using flow cytometric based immunophenotyping I analysed the same preparation of CDCs at passages 2, 4 and 6 and compared the marker profiles. This experiment was independently performed 3 times and although results were variable there was a noticeable trend towards a down regulation of cKit, CD31 and endoglin expression, whereas the number of CD90 positive cells increased in higher passage CDCs. Figure 5.7 shows representative FACS plots depicting this trend, while table 5.2 summarises the results of all 3 experiments as a percentage of positive events for all cell populations analysed. Of particular importance cKit levels fell to negligible levels following multiple passages and endoglin expression was also markedly decreased.

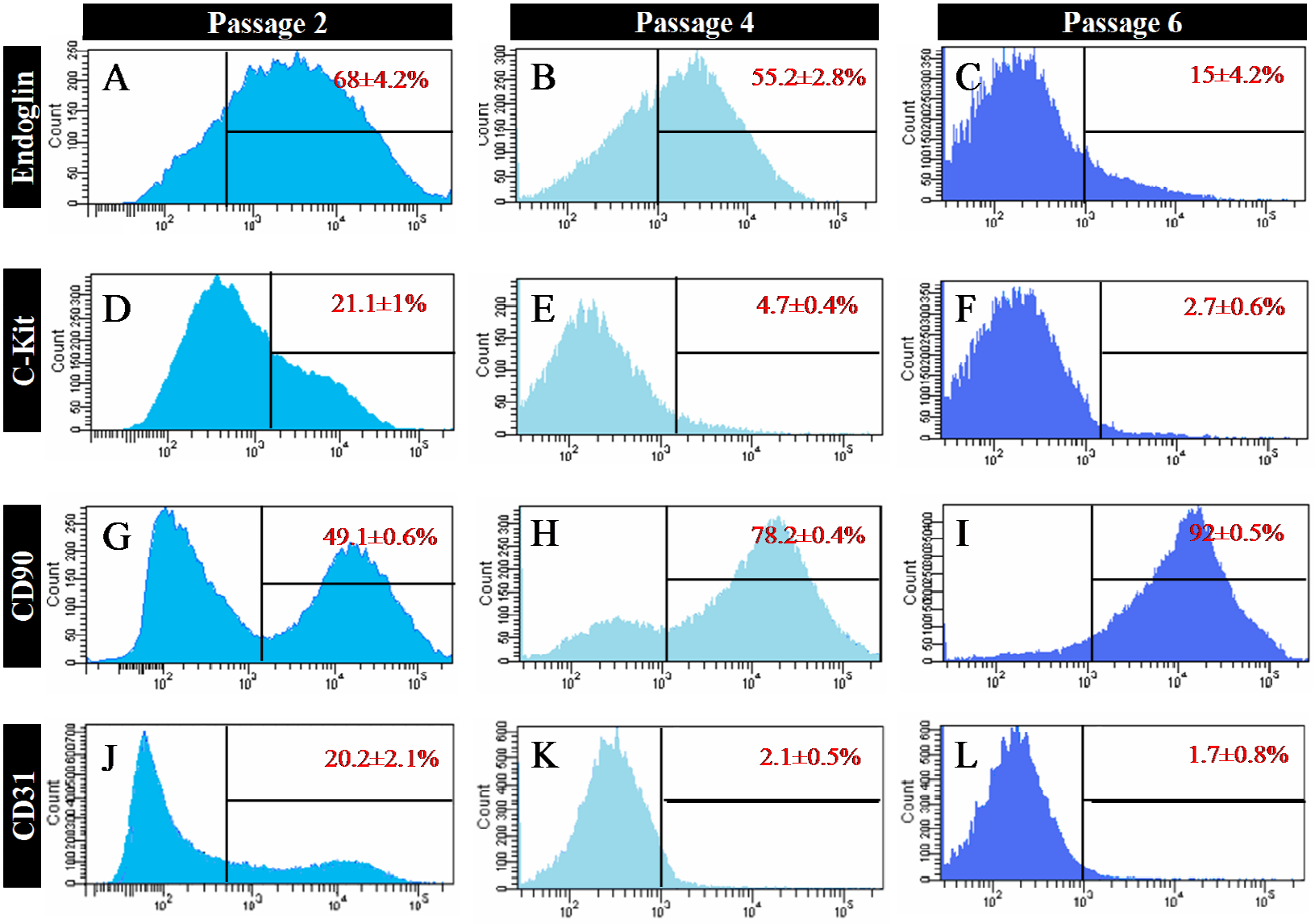
Passage 2
Passage 4
Passage 6
Endoglin
C-Kit
CD90
CD31
A
68±4.2%
B
55.2±2.8%
C
15±4.2%
D
21.1±1%
E
4.7±0.4%
F
2.7±0.6%
G
49.1±0.6%
H
78.2±0.4%
I
92±0.5%
J
20.2±2.1%
K
2.1±0.5%
L
1.7±0.8%
Count

Figure 5.7. Flow cytometric analyses of CDCs showing the down-regulation of endoglin, cKit and CD31 and up-regulation of CD90 following extended culture. CDCs were expanded until passage 6 and cells were sampled and analysed for the expression of endoglin, cKit, CD90 and CD31 at passage 2 (A, D, G and H), passage 4 (B, E, H and K) and passage 6 (C, F, I and L). Histograms D and E show that cKit expression is appreciably decreased from passage 2 to passage 4 (from 21.1% to 4.7%) and decreases further by passage 6 (2.7%). A similar trend was observed for CD31 expression with levels decreasing from 20.2% at passage 2 (J) to 2.1% at passage 4 (K) and falling to 1.7% at passage 6 (L). Endoglin is also markedly decreased following culture (passage 2, 68% (A), passage 4, 55.2% (B), passage 6, 15% (C) while CD90 was upregulated from 49% at passage 2 (G) to 92% at passage 6 (I). Data is derived from 3 replicate samples and presented as mean percentage ± SEM.

		Eng^+ %±SEM	$cKit^+$ %±SEM	$CD90^+$ %±SEM	$CD31^+$ %±SEM
D*	P2	68±4.2	21.2±1	49.1±0.6	20.2±2.1
	P4	55.2±2.8	4.7±0.4	78.2±0.4	2.1±0.5
	P6	15±4.2	2.7±0.6	92±0.5	1.7±0.8
E	P2	88.5±0.6	56.5±0.6	18.3±0.2	n/a
	P4	50±3.7	2.6±0.2	45.9±0.4	n/a
	P6	36.6±1.5	2.3±0.6	47±0.5	n/a
F	P2	68±0.8	23.7±0.7	11.9±0.2	33.2±1
	P4	58.6±3	2.8±0.6	7.7±0.3	3.6±0.5
	P6	49.4±5.6	2.3±0.3	9.1±0.1	0.8±0.2

Table 5.2 Summary of 3 independent FACS analyses performed with murine CDCs at passages 2, 4 and 6. CDC cultures used for passage 2 (P2) FACS analysis in experiments D, E and F (table 5.1.) were further expanded and analysed for marker expression at passage 4 (P4) and 6 (P6). * denotes experiment illustrated in Figure 5.7. Data presented as mean percentage ± SEM, derived from 3 replicate samples.

5.2.2. Endoglin Depletion in *Eng$^{fl/fl}$;Rosa-CreER^{T2}* CDCs

5.2.2.1. Determining an Effective Dose of 4-Hydroxy-Tamoxifen to Achieve Efficient Endoglin Knock-Down in *Eng$^{fl/fl}$;Rosa-CreER^{T2}* CDCs

To achieve efficient knock-down of endoglin in CDCs I prepared cells from *Eng$^{fl/fl}$; Rosa-CreER^{T2}* mice. The *Eng$^{fl/fl}$* mouse model and inducible Cre-recombinase gene knock-out strategy is described in section 4.1. (figures 4.1 and 4.2). To achieve endoglin loss in CDCs a *Rosa-CreER^{T2}* transgene was used, which expresses tamoxifen-activated Cre recombinase under the regulation of the ubiquitously expressed *Rosa26* promoter.

The conversion of tamoxifen to its active metabolite, 4-hydroxy tamoxifen (4OH-tamoxifen), normally occurs in the liver *in vivo* therefore it is necessary to treat cells *in vitro* with 4OH-tamoxifen to activate *Rosa-CreER^{T2}*.

To determine the lowest effective dose and optimal treatment time of 4OH-tamoxifen I performed a series of dose titration experiments and determined the efficiency of endoglin deletion at the protein level using immunofluorescent staining. The percentage of endoglin positive cells within the total cell population is reduced following exposure to hydroxy-tamoxifen (table 5.3.).

4OH-Tamoxifen Dose	Treatment Time	Endoglin Positive Cells (% ± SEM)
Untreated Control	n/a	92.9±3.2
1μM	48h	76.8±7.1
1μM	96h	55.4±8.4
2μM	96h	23.2±5.0
5μM	96h	27.0±5.6

Table 5.3. Endoglin deletion in *Eng$^{fl/fl}$;Rosa-CreER^{T2}* CDCs following treatment with 4OH-tamoxifen; effect of 4OH-tamoxifen dose and incubation time. Endoglin expression was assessed using an anti-endoglin specific antibody and an alexa594 conjugated secondary (see figure 5.8 for representative images of staining). Cells stained positive for endoglin expression were counted in each of 12 fields of view per condition tested and results are presented as a percentage of positive cells per total cell number per field of view±SEM. 2μM 4OH-tamoxifen treatment for 96 hours is the lowest dose required to achieve efficient Cre activation and endoglin gene deletion in *Eng$^{fl/fl}$;Rosa-CreER^{T2}* CDCs**.**

An initial dose of 1μM 4OH-tamoxifen with an exposure time of 48 hours was tested as we had previously shown this to be the most effective regime in the deletion of endoglin in a primary mouse lung EC line. However, I found this method to be insufficient, resulting in only a ~23% reduction in endoglin expression (table 5.3.). An increase in incubation time to 96hours significantly increased efficiency of deletion (approximately 45%) indicating that endoglin protein expression was stable in these cells, however this rate of deletion was still insufficient to create an endoglin null phenotype therefore I performed a 4OH-tamoxifen dose titration experiment (ranging from 1μM to 5μM) with a 96hour exposure time (table 5.3). The lowest effective dose was identified as 2μM

(approximately 77% deletion) which was comparable to higher doses (approximately 73% deletion achieved using 5μM 4OH-tamoxifen). For representative images see figure 5.8 and results are summarised in table 5.3.

In tandem to using immunofluorescence to assay endoglin protein expression and deletion, I also investigated whether Cre enzyme activation was induced following 4OH-tamoxifen treatment using CDCs derived from *Rosa-CreER^{T2};Rosa26R* mice. These cells express the *Rosa26R lacZ* reporter transgene and subsequent X-Gal staining was used to provide a read-out of Cre recombinase activity (see figure 4.4). Cells were treated with 1-5μM 4OH-tamoxifen for 96hours prior to staining (figure 5.9). LacZ expression was inversely proportional to that of endoglin expression and showed maximum Cre activation with 2μM 4OH-tamoxifen treatment, which is in agreement with endoglin protein data. However, not all cells expressed lacZ suggesting that either 4OH-tamoxifen was not taken up by all cells or that the *Rosa26* promoter was not active in all cells and this Cre line could not therefore allow depletion of endoglin in 100% of CDCs at passage 2. Nevertheless this line was the best available for the study and was used to generate knock-down of endoglin in approximately 80% of CDCs.

Verification of endoglin knockdown at the DNA level was also analysed using PCR. I showed that following treatment with 2μM 4OH-tamoxifen exons 5 and 6 of the endoglin gene are successfully deleted in *Eng$^{fl/fl}$;Rosa-CreER^{T2}* CDCs which ultimately leads to the expression of a truncated and non-functional protein (figure 5.10).

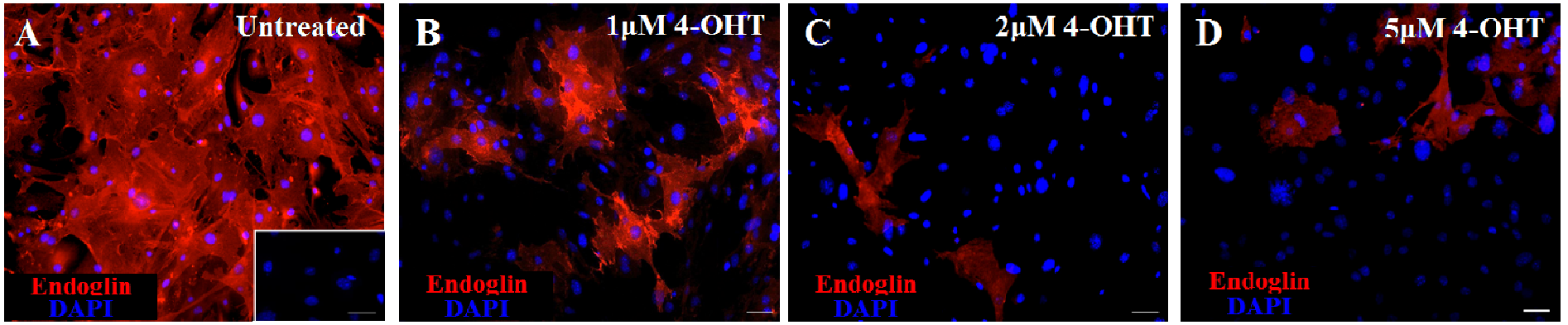

Figure 5.8. Endoglin gene deletion in *Eng$^{fl/fl}$;Rosa-CreER^{T2}* CDCs following treatment with 4OH-tamoxifen. Immunofluorescent anti-endoglin staining of passage 2 *Eng$^{fl/fl}$;Rosa-CreER^{T2}* CDCs; untreated cells (A) versus treatment with 1μM (B), 2μM (C) or 5μM (D) 4OH-tamoxifen for 96hours. An anti-rat secondary antibody conjugated to alexa594 (red) was used and nuclei were stained with DAPI (blue). Inset image in (A) represents a no primary antibody control. 2μM 4OH-tamoxifen treatment is the lowest dose required to achieve maximum Cre activation and efficient endoglin gene deletion. Scale bar = 20μm.

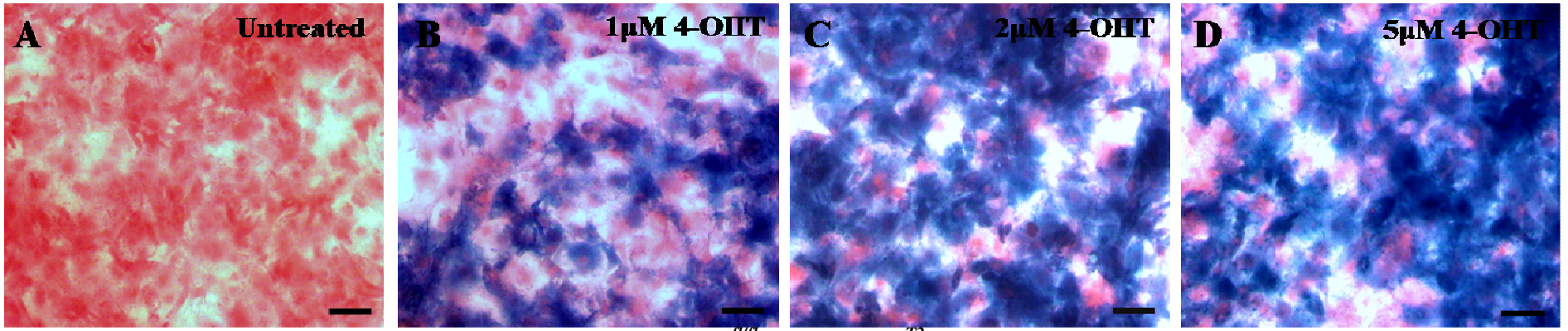

Figure 5.9. Titration of 4OH-tamoxifen and X-Gal staining of *Eng$^{fl/fl}$;Rosa-CreER^{T2}* CDCs carrying the *Rosa26R* reporter gene. X-Gal staining to detect LacZ expression (blue) in passage 2 cells treated with 1μM (B), 2μM (C) or 5μM (D) 4OH-tamoxifen for 96hours. Cells were counterstained with eosin (pink). 2μM 4OH-tamoxifen treatment is revealed as the lowest dose required to achieve maximum Cre activation. Untreated cells (A) show no LacZ expression. Scale bar = 20μm.

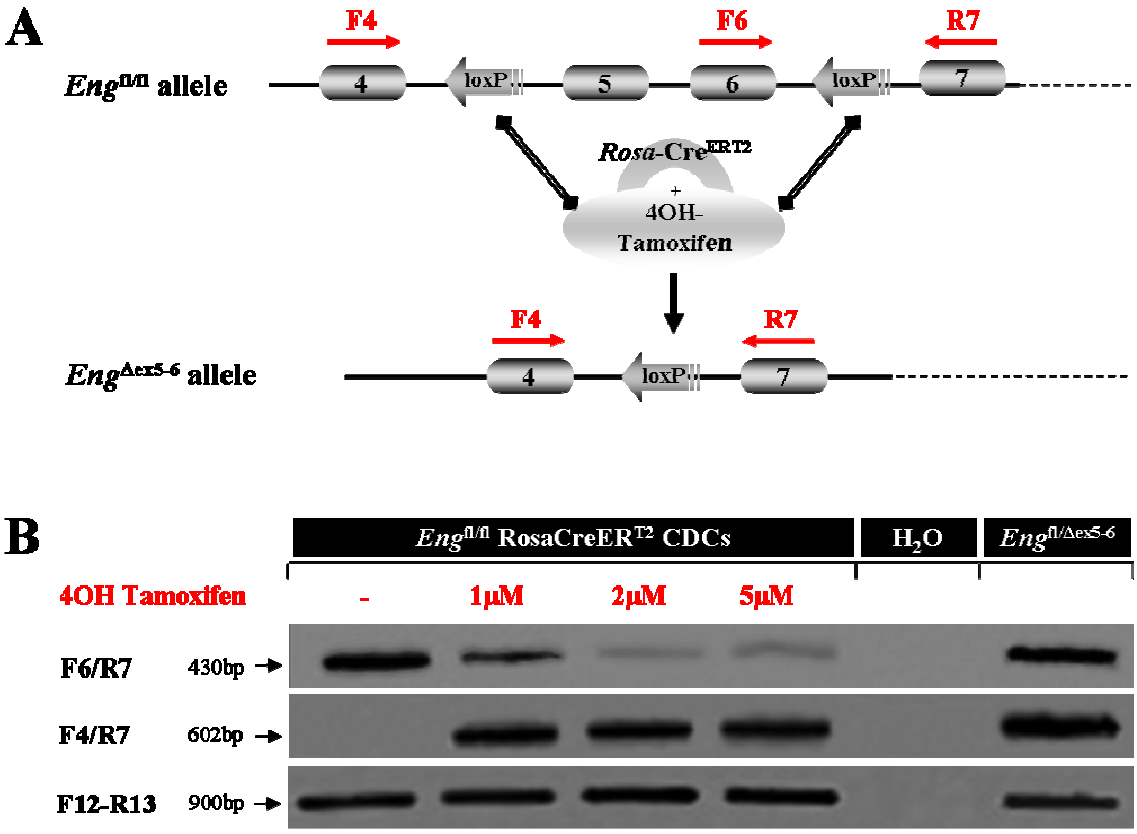

Figure 5.10. Assessing endoglin gene deletion in *Eng$^{fl/fl}$;Rosa-CreER^{T2}* CDCs. (A) Schematic of the *Eng$^{fl/fl}$;Rosa-CreER^{T2}* inducible knock out model showing the position of the primers used to assess endoglin gene deletion at the genomic DNA level. Two PCR reactions using primers F6/R7 and F4/R7 amplify two different regions of the endoglin gene, which can be used to distinguish between endoglin floxed and delete alleles (for further details of primers and PCR programmes see section 2.2.). F6/R7 primers detect the floxed allele and F4/R7 primers detect the delete allele. Primers F12/R13 detect DNA in both endoglin floxed and delete alleles and serve as a positive control. (B) Lanes 1-4 show PCR products from genomic DNA isolated from untreated *Eng$^{fl/fl}$; Rosa-CreER^{T2}* CDCs (lane 1) and from cells treated with 4OH-tamoxifen for 96 hours (lane 2=1μM, lane 3=2μM and lane 4=5μM). A reduction in the amount of F6/R7 PCR product is evident in cells treated with 4OH-tamoxifen and F4/R7 PCR products are only present in treated cells. Lane 5 is a negative control (no DNA template) and lane 6 contains positive control genomic DNA with both floxed and delete endoglin alleles present.

5.2.2.2. The Effect of Endoglin Depletion on CDC Viability/Proliferation

Tamoxifen is known to have toxic effects which may affect subsequent analysis of cellular function therefore I performed a MTT assay to analyse viability/proliferation properties of CDCs following transient (96hour) exposure to 4OH-tamoxifen. Treated cells were re-plated in 96well plates and assayed for metabolic activity as previously described (section 3.2.5.1.). No significant difference was observed between untreated

and treated cells (range of 1µM-5µM 4OH-tamoxifen tested) as confirmed using ANOVA testing (figure 5.11A). These data indicated that 4OH-tamoxifen treatment of CDCs is safe without significant toxicity.

Additionally I have shown that 4OH-tamoxifen treatment and endoglin depletion does not significantly affect cellular viability following serial passaging as cells were analysed using the MTT assay for up to three passages following endoglin deletion and no difference in viability was found (figure 5.11B). Therefore, in all subsequent experiments endoglin depletion was achieved by treating passage 2 CDCs with 2µM 4OH-tamoxifen for 96hours.

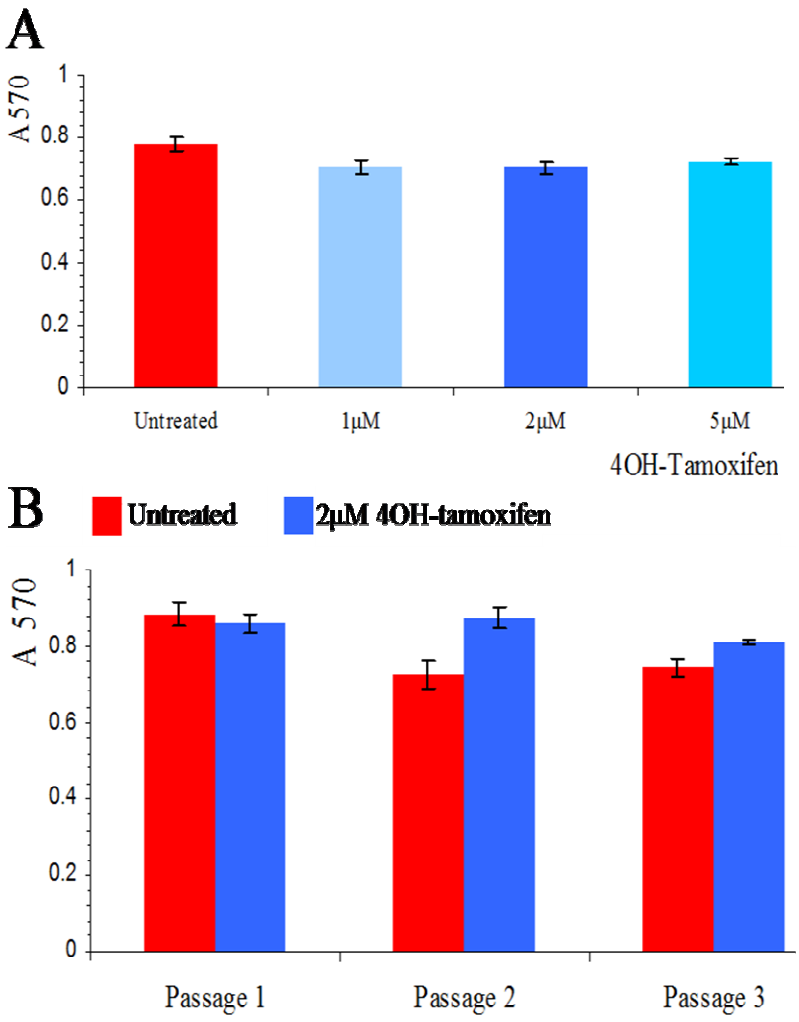

Figure 5.11. Achieving endoglin knockdown in *Eng$^{fl/fl}$;Rosa-CreER^{T2}* CDCs by treating cells with 4OH-tamoxifen treatment has no effect on cell viability. (A) *Eng$^{fl/fl}$; Rosa-CreER^{T2}* CDCs were incubated with or without 4OH-tamoxifen (1µM, 2µM or 5µM) for 96hours. The MTT assay revealed no significant difference in viability/ proliferation properties in untreated versus treated cells. (B) No difference in viability was observed in untreated versus treated (2µM for 96hours) CDCs following subsequent passaging.

5.2.3. Endoglin Depletion has a Modest Adverse Effect on CDC Proliferation and Migration

Effective tissue repair is a complex process that involves a series of coordinated events including cell proliferation and migration. These properties were tested in WT versus Eng-iKO passage 2 (P2) CDCs *in vitro* to determine whether endoglin is important for proliferation or migration of CDCs. Passage 1 *Eng$^{fl/fl}$; Rosa-CreER^{T2}* CDCs were treated with (Eng-iKO) or without (WT) 2μm 4OH-tamoxifen for 96hours, prior to passaging cells again (P2) and performing the analyses. Obtaining Eng-iKO and WT cells from the same starting culture allowed me to control for cell heterogeneity (see table 5.1) and tamoxifen was carefully washed away prior to passaging cells (P2) to remove any residual non-specific effects.

To analyse cellular proliferation CDCs were seeded into multiwell plates and the growth curves of WT versus Eng-iKO cells were created using mean cell counts calculated from 3 wells per group (and from 4 fields of view per well) at 6 hourly intervals over a 72 hour period (using the method described in section 2.5.1). Endoglin depletion was associated with a declining cell growth rate (figure 5.12A), and at the 60 hour time point this difference became statistically significant (p=0.046). At 72 hours I observed the maximum significant difference in mean cell count between WT and Eng-iKO cells (p=0.009). Cell cultures were approaching confluence at this stage which precluded analysis at later time-points. The average cell doubling time was revealed to be markedly higher in Eng-iKO CDCs compared to WT controls (27.6±0.8 hours versus 33.4±4 (p=0.07), figure 5.12B).

The migration assay is described in section 2.5.3. This involved creating scratch 'wounds' in sub-confluent monolayers of endoglin WT and Eng-iKO passage 2 CDCs using a sterile pipette tip. Cell migration was measured by calculating the extent of 'wound' closure over 33 hours. Digital microscopy was used to record images at 3 hourly intervals (3 fields of view per well per time point, 3 wells per group) and 'wound' closure was determined at each time point by calculating migrated distance/total 'wound' distance using Axiovision Rel. v4.8 software (Zeiss) (for representative images see figure 5.13). Eng-iKO cells exhibited a slower rate of migration compared to control WT cells (figure 5.14A). At the end of the 33hour period

endoglin depleted CDCs had migrated a significantly shorter distance, covering 10% less of the wound area than WT control cells (74.2±1.8% versus 84.7±2% (p=0.001), figure 5.14B).

These results suggest that endoglin loss has a significant, yet modest effect on CDC proliferation and migration.

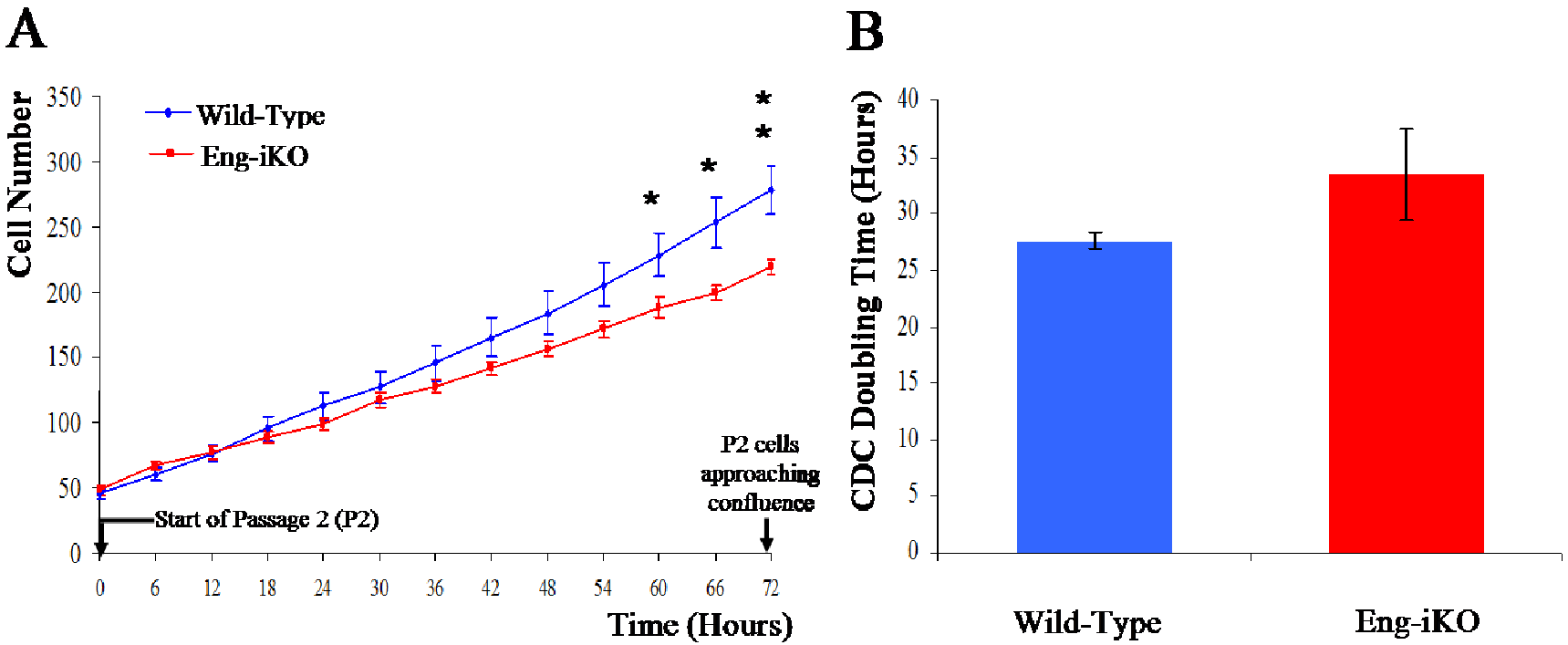

Figure 5.12. Inhibitory effect of endoglin depletion on CDC proliferation. (A) CDCs (Wild-Type, blue) or (Eng-iKO, red) were seeded at 30-40% confluence in multiwell plates and phase contrast microscopy was used to record images at 6hourly intervals for 72hours. Cell number was counted at each time point (each data point represents the mean value derived from a minimum of 9 fields of view). Analysis revealed a significant reduction in Eng-iKO CDC count from 60h onwards with maximum reduction observed at 72h. (B) The mean doubling time of cells was calculated and found to be markedly higher in Eng-iKO cells (27.6±0.8 hours versus 33.4±4 hours, p=0.07). Experiments were independently performed three times to confirm results and statistical significance was determined using the unpaired t-test. Error bars = SEM. (* $p<0.05$, ** $p<0.01$).

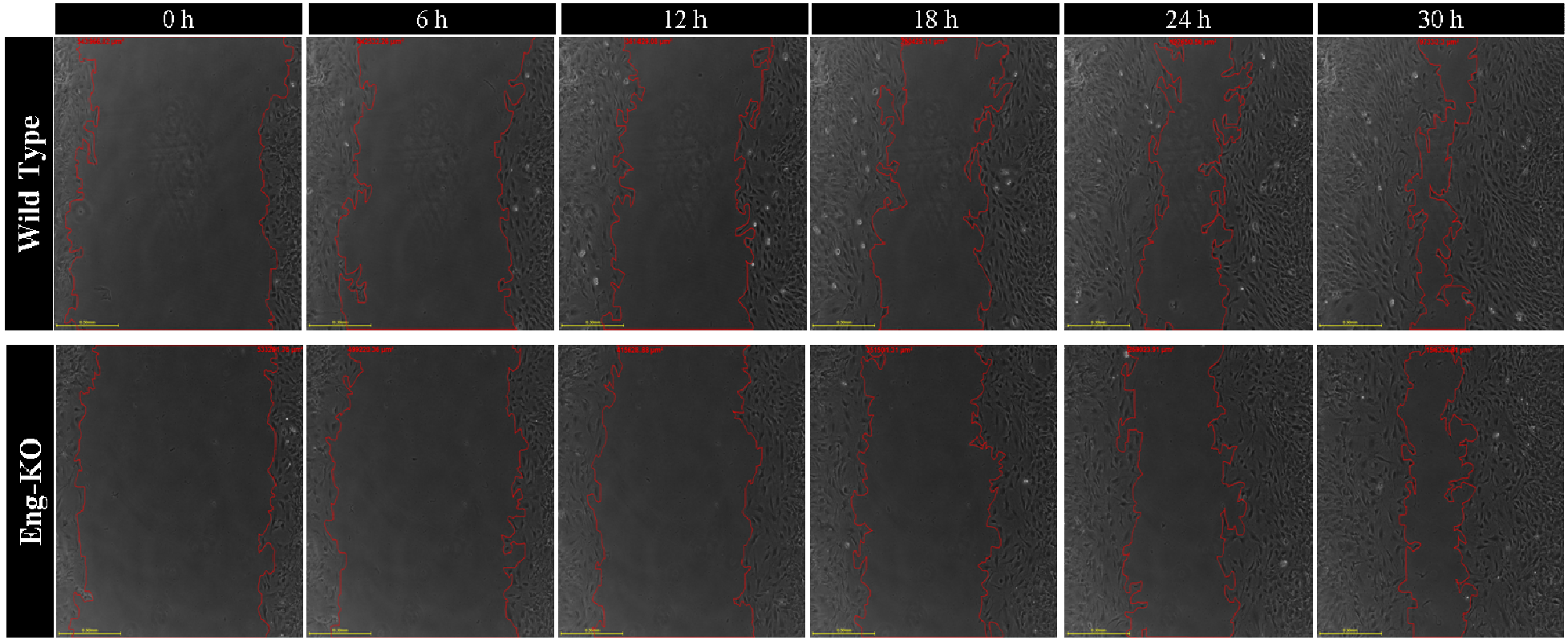

<u>Figure 5.13</u> Representative images of CDC scratch-'wound healing' assay comparing control and Eng-iKO CDCs. Control (top panel) and Eng-iKO (bottom panel) CDCs were grown to 80-90% confluence, wounded with a scratch and maintained in full CDC medium to facilitate cell migration. The migration and proliferation of cells into the 'wounded area' resulted in gradual sealing of the scratch. Cell migration into the 'wounded' area was recorded by phase contrast microscopy over a 33 hour time course at 3 hourly intervals (6 hourly interval representative images shown). Scale bar=0.5mm.

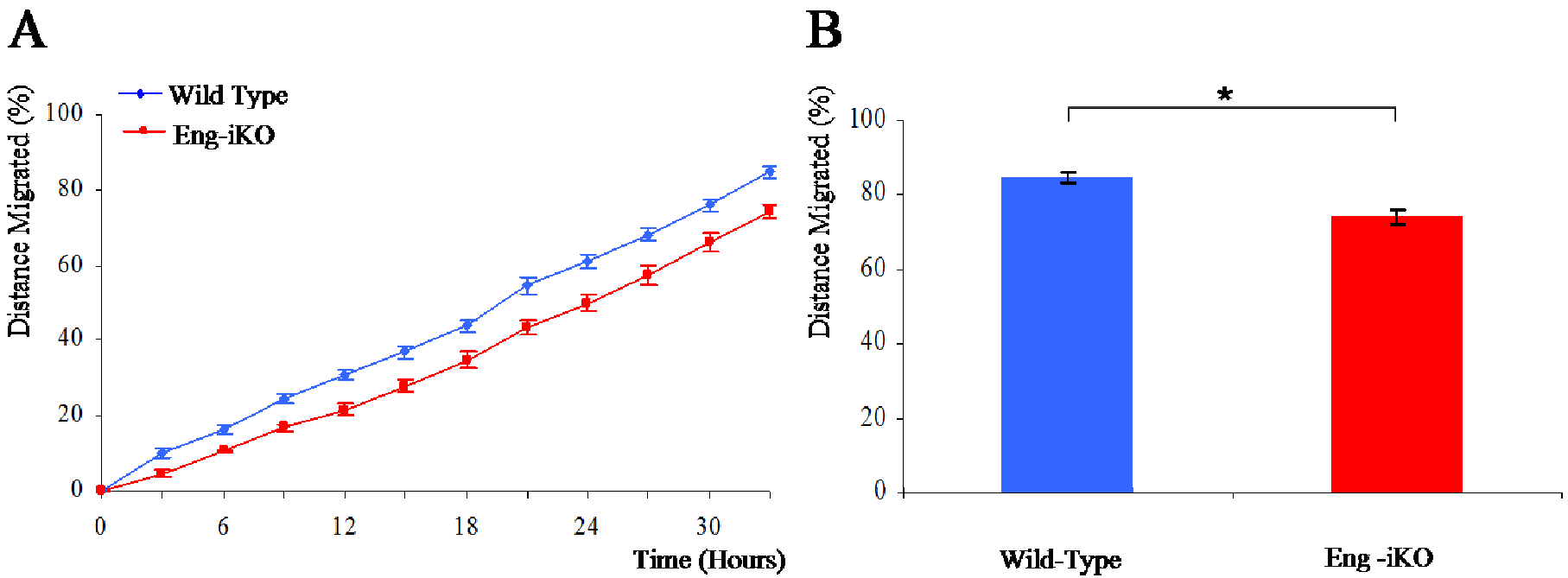

Figure 5.14. Inhibitory effect of endoglin depletion on CDC migration. (A) Representative scratch-migration assay displaying significant reduction in migration rate (p=0.001) in Endoglin depleted CDCs over a 33h time course. 'Wound' closure was determined at 3 hourly intervals by calculating migrated distance/total original 'wound' distance using Axiovision Rel. v4.8 software (Zeiss). Each data point represents the mean value calculated from a minimum of 9 fields of view. (B) Graphical display of decreased 'wound' closure by endoglin knock down CDCs at 33 hours (p=0.001). Data are presented as percentage of original wound area ± SEM. Experiments were repeated independently three times to confirm results and statistical significance was determined using the unpaired t-test. * denotes $p < 0.05$.

5.2.4. The Effect of Endoglin Depletion on TGFβ Signalling

5.2.4.1. The Effect of Endoglin Depletion on TGFβ Receptor Expression in CDCs

The expression of TGFβ pathway receptors in CDCs were assessed at the RNA level using semi-quantitative RT-PCR and results were compared between WT and Eng-iKO CDCs. I detected the expression of all the receptors analysed (*Tgfbr2*, *Bmpr2*, *Alk1*, *Alk5* and *endoglin*) in both WT and endoglin depleted cells (figure 5.15). I observed a moderate increase in *Tgfbr2* and a slight decrease in *Alk1* transcript levels, as well as confirmed a marked reduction in *endoglin* expression in Eng-iKO samples. Unfortunately due to time restraints the analysis was only performed once precluding statistical testing. rtPCR using the house-keeping gene *β-actin* was used as a loading control, while 'no RNA' template reactions and mouse lung endothelial cells were included as negative and positive controls, respectively.

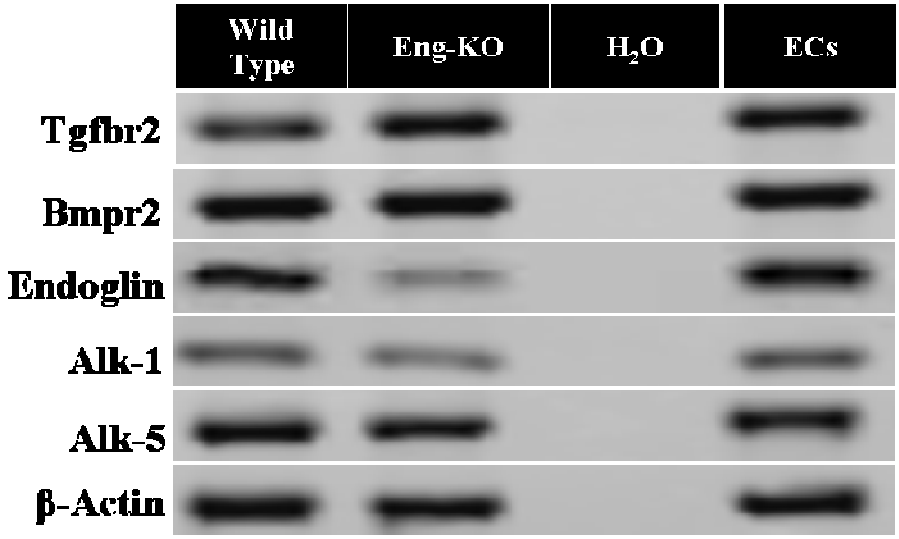

Figure 5.15. RT-PCR analysis of TGFβ receptor expression in CDCs with and without endoglin depletion. Representative images of TGFβ receptor expression in WT (lane 1) and Eng-iKO (lane 2) passage 2 CDCs. Lane 3 is a negative control (no RNA template) and lane 6 contains positive control RNA derived from primary mouse lung ECs. The intensity of *Tgfbr2* expression, following 4OH-tamoxifen treatment expression appears marginally increased whereas endoglin expression is significantly reduced.

5.2.4.2. Analysis of Downstream Smad Activation in Wild-Type versus Endoglin Depleted CDCs

To determine how loss of endoglin affects TGFβ signalling in CDCs, I examined the phosphorylation of Smad2 and Smad1/5 (downstream targets of TGFβ/Alk5 and TGFβ/Alk1 signalling respectively) in WT versus Eng-iKO cells using western blotting and antibodies that specifically recognise the phosphorylated forms of these Smad proteins. Both WT and Eng-iKO cells were treated with or without TGFβ1 (5ng/ml) or BMP9 (1ng/ml) ligands for 30, 60 or 120 minutes and cell lysates (containing total protein extracts) were subjected to western blotting (see section 2.8 for further methodological details). In WT cells TGFβ1 ligand stimulated an appreciable increase in Smad2 phosphorylation in a time-dependent manner (figure 5.16B) whilst phospho-Smad1/5/8 expression was elevated to a lesser extent and transiently peaked at 60minutes (figure 5.16A). The reciprocal pattern was observed in BMP9 treated cell samples which showed a time-dependent increase in Smad1/5 phosphorylation (figure 5.16A) and a transient peak of phospho-Smad2 levels at 60 minutes, which was greatly diminished in cell samples stimulated with BMP9 for 120 minutes (figure 5.16B).

To determine the effect of endoglin knock down on downstream TGFβ signalling pathways, phospho-Smad responses in response to TGFβ or BMP9 ligands were compared in WT and endoglin depleted CDCs. Whilst phospho-Smad1/5 levels appeared to be relatively unchanged in Eng-iKO CDCs (figure 5.16A), phospho-Smad2 levels were dramatically increased in all endoglin depleted samples (figure 5.16B). Western blots were stripped and re-probed (see section 2.8 for details) with antibodies against total Smad1 and Smad2 proteins and α-tubulin, which acted as loading controls. Endoglin protein levels were extremely low in Eng-iKO cell samples confirming efficient knockdown (figure 5.16).

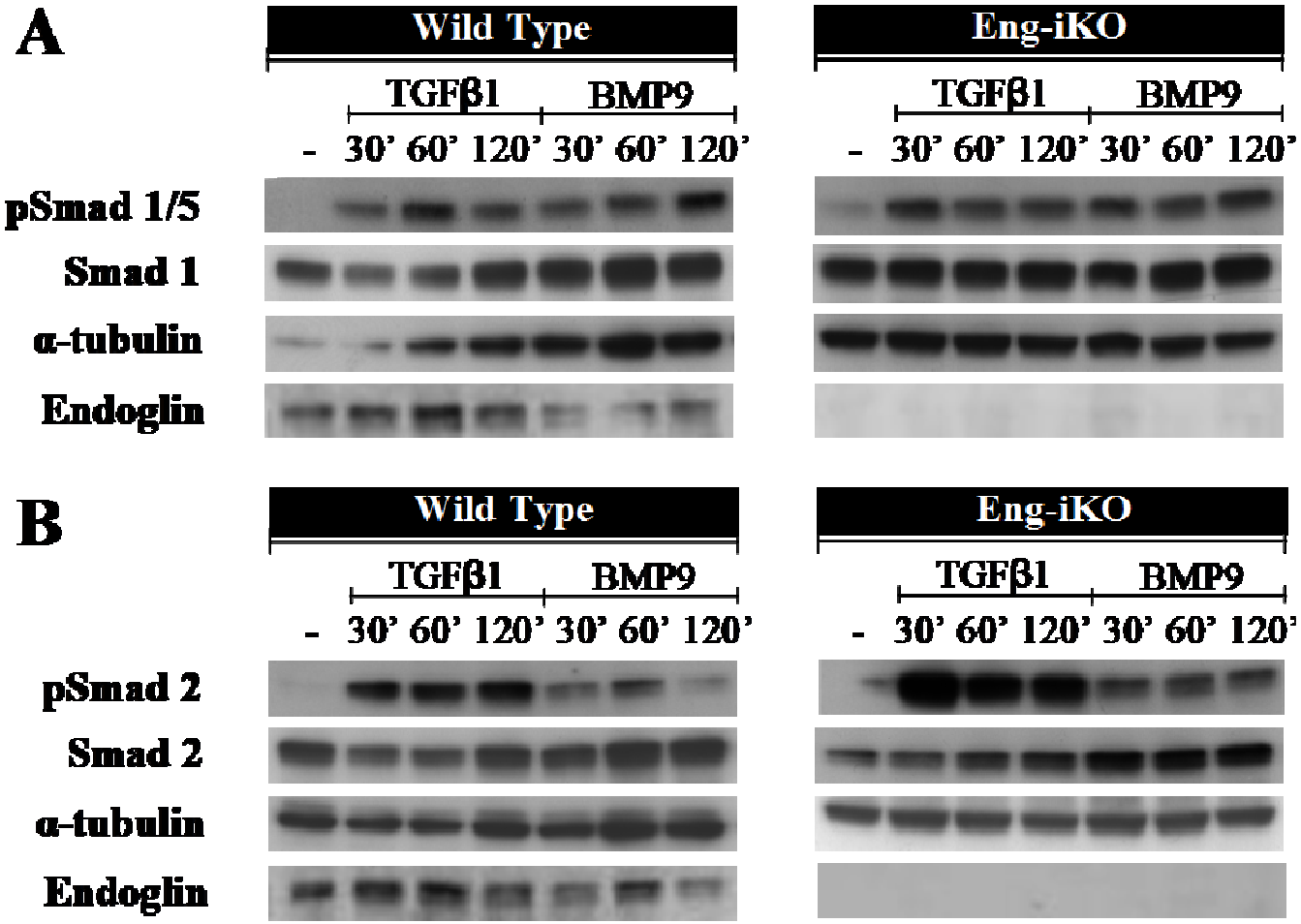

Figure 5.16. Endoglin loss in CDCs leads to increased Smad2 phosphorylation in response to TGFβ1 and BMP9 stimulation. Whole cell protein extracts from wild type and endoglin knock-out CDCs were subjected to western blotting to establish levels of phosphorylated smad1/5 (A) and phosphorylated Smad2 (B). Cells were stimulated with TGFβ1 (5ng/ml) or BMP9 (1ng/ml) ligands (prior to preparing lysates) where indicated for times specified (30, 60 or 120 minutes). Endoglin loss leads to an increase in TGFβ/Alk5 signalling (Smad2 phosphorylation) in response to TGFβ1 and BMP9 ligand treatment. Phosphorylation of Smad1/5 is not notably different. Blots were stripped and re-probed with specific antibodies against Smad2 or Smad1/5 and α-tubulin was included as a loading control. Blots were also probed using an anti-endoglin antibody to confirm that endoglin is depleted in Eng-iKO CDCs.

5.3. Discussion

5.3.1. Heterogeneity of Murine CDCs; Significance and Practical Implications

FACS based immunophenotyping of CDCs revealed marked inter-culture variation in endothelial (CD31, endoglin), mesenchymal (CD90, endoglin) and stem cell-related (cKit) marker expression in cells expanded to passage 2. The functional significance of this observation was not tested but it is prudent to consider that variations in the specific composition of this heterogeneous population could have important effects on the functional capacity of these cells. For example, do high cKit expressing cultures possess increased repair potential?, and if the CD90 sub-population is indeed responsible for providing physical or paracrine support to the cKit sub-population (as proposed by Smith *et al*[159]) is there a threshold level of expression for efficient function? These proposals remain to be explored, however we are currently investigating methods to increase CDC expression of cKit and Sca-1 expression (including preconditioning cells in hypoxic conditions) prior to testing their ability to contribute to repair (specifically their pro-angiogenic potential) following heart injury, as well as performing lineage tracing experiments using *Col1a2-CreER*^{T2} mice to deduce what proportion of CDCs are derived from the collagen producing cells of the heart (the fibroblast lineage)[331].

The post-cardiosphere CDC expansion step aims to generate a clinically feasible number of cells for transplantation from small amounts of tissue[159]. However, the stark difference in CDC antigenic profile or 'phenotypic drift' following extended *ex vivo* expansion (up to 6 passages) suggests that CDCs may have a limited useful lifespan. For example the loss of cKit expression in later passages indicates the stem cell component of the population may be diluted by less useful cell types and late passage CDCs may have a reduced potential for heart repair. Further investigation would be required to test this hypothesis. However, careful profiling of the heterogeneous CDC population along with functional testing may aid in the identification of an optimal mixture of *ex vivo* expanded cardiac-derived progenitor cells and may also help to elucidate key mechanisms of tissue repair.

As there is intrinsic variability between cultures of CDCs, I have continuously endeavoured to reduce inter-culture variation by following a strict culture protocol (see section 2.3.1.2). Davis *et al*[175] claim that even subtle variations in technique can markedly alter CDC phenotype, for example this group claim that the inclusion of an EDC filtration step (suggested by Andersen *et al*[174] to remove contaminating myocardial tissue from subsequent culture steps) can result in the enrichment of fibroblasts. Another possible point of variation is the sex of donor pups used to derive CDCs. Differences in stem cell mechanics and repair efficiency have been attributed to gender, with female muscle-derived stem cells[332] and BM-MSCs[333] displaying increased tissue regeneration capacity in comparison to male-derived cells. This would suggest that stem cell gender could in principle affect CDC phenotype. Conversely, Drowley *et al*[334] have found that sex of donor muscle-derived stem cells had no significant effect on cell engraftment, angiogenesis or cardiac function following experimental MI. Due to the difficulty of sexing young pups I did not record the gender of pups used in this study (although this could be done by PCR) therefore it is possible that this may have played a role in CDC variability. However, given the conflicting published findings this issue remains open to debate. In addition, the age of the neonatal mice used may have influenced phenotypic variability between independent CDC cultures. In this thesis, mice aged between 3 and 6 days were used to derive CDCs in a bid to maintain consistency. However notable differences in the expression of stem, endothelial and mesenchymal markers were observed in cultures derived from mice of the same age (see table 5.1) indicating that variability in outcomes may be due to stochastic events or unknown variables. Finally differences in FCS (which was not batch-tested) contained within the culture media may have influenced cell phenotype and inter-culture variation.

5.3.2. Suitability of using Murine Neonatal Cardiac Tissue to Derive and Study Progenitor Cells

There is a recognised inverse relationship between increasing stem cell age and decreased functional capacity. Therefore it has been suggested that stem cells derived from younger patients may be better adapted in times of stress, such as during/post ischaemia, and thus offer superior repair potential. Indeed, Madhur *et al*[335] found that BM-MSCs from younger adult donors displayed significantly improved functional benefit following transplantation into rats following MI. Given the effect of increasing

age on adult stem cells it is likely that significant differences will also exist between neonatal stem cells and their adult counterparts. Markel and colleagues[336] found that neonatal BM-MSCs exhibited functional and key cell signalling differences compared to their adult derived counterparts. Of particular importance, whilst a noted decrease in neonatal IL6 (compared to adult) suggested that neonatal stem cells may assist in decreasing adverse local inflammatory responses following MI, a decrease in neonatal VEGF production (compared to adult) inferred that these cells may be stunted in their ability to stimulate angiogenesis and stem cell survival. Markel *et al*[337] later reported that neonatal and adult BM-MSCs are distinctly different with respect to the level of tissue protection and repair potential following experimental MI. Adult stem cell transplantation resulted in a significantly greater improvement in myocardial function than was achieved using neonatal cells. The authors suggest that a critical age may mark when stem cells become fully primed for repair. It remains unclear whether neonatal cells have distinct roles or differing efficacy in cardiovascular repair compared to their adult counterparts or indeed whether or not any such differences would be cell type or source tissue dependent. However it is known that whilst some human neonatal tissue (umbilical cord, foetal membrane and placenta) represent plausible sources of clinically relevant stem cells, derivation of human neonatal cardiac resident stem cells is not clinically feasible or ethical. Despite this, the practical consideration of ease of culture of neonatal CDCs compared with adult CDCs allows an opportunity to try and define the mechanisms that improve stem cell treatment efficacy, irrespective of age, to better inform work using more clinically relevant cell populations.

5.3.3. The Effect of Endoglin Depletion on CDC Function and TGFβ Signalling *in vitro*

One of the major aims of this chapter was to investigate the effect of endoglin depletion on properties of CDCs that relate to tissue repair and TGFβ signalling.

Interestingly I found that whilst endoglin depletion had no effect on passage 2 CDC viability/proliferation using the MTT viability assay there was a modest, yet significant, negative effect on CDC proliferation detected using a simple cell counting method. The reasons for these disparate results are likely the time differences involved in the assays as well as the manner of assessment. Whereas the MTT assay only measured metabolic

activity and therefore indirectly cell proliferation for up to 24 hours, simple cell counting, which represents a more direct method of assessment, did not detect a significant difference in cell number until 60hours had elapsed. This together with the reduced migratory potential of passage 2 Eng-iKO CDCs as assessed using the scratch assay (which measures a combination of proliferation and migration) agrees with my original hypothesis stating that endoglin is a positive mediator of cardiac resident stem cells and suggests that endoglin depletion may impair the repair potential of these cells.

Unexpectedly, despite endoglin's reported role in promoting activation of the Alk1 pathway[237] I found that endoglin knockdown in unstimulated CDCs had little effect on Smad1 phosphorylation. Furthermore, although endoglin depletion has been shown to reduce TGFβ1 and BMP9 induced Smad1 responses in many cell types[237, 338-339], little difference was observed in phopsho-Smad1 levels in CDCs treated with either ligand following endoglin depletion while the Smad2 response was markedly increased in response to TGFβ1 and moderately increased following BMP9 stimulation of Eng-iKO cells. These results are in contrast to those of Santibanez *et al*[340] who have reported that endoglin enhances Smad2 activation by stabilising Smad2 protein levels and potentiating TGFβ signalling in ECs. However my findings do agree with those of Finnson and colleagues[339] who found that endoglin inhibits TGFβ-induced Smad2 phosphorylation in human chondrocytes. These studies illustrate the cell type-specific and context dependent roles of endoglin. In CDCs it appears that endoglin represses Alk5/Smad2 signalling whereas endoglin loss has little effect on the Smad1 response. This may be due to an adaptive response which sees an increase in Alk1/Smad1 signalling in response to reduced endoglin levels. This proposed model is in contrast with the adaptive process suggested by Lebrin *et al*[204] who show reduced Alk5 expression in endoglin depleted cells. However no difference in Alk5 expression was observed in Eng-iKO CDCs, whereas a slight decrease in Alk1 expression was found using semi-quantitative RT-PCR (figure 5.15).

In endoglin knockout embryos, activation of Smad2 is abolished within the endothelium but treatment with TGFβ1 results in phosphorylated Smad2 levels that exceed those observed in WT mice[341]. My results also show an increase in Smad2 phosphorylation in Eng-iKO TGFβ1 treated CDCs suggesting that following endoglin depletion Tgfbr2/Alk5 complexes on the surface of CDCs can be activated by exogenous TGFβ1

treatment. However unstimulated mutant cells also showed equivalent or modestly increased levels of phosphorylated Smad2 compared to WT CDC samples. This may be related to the reported activation of Smad2 in the endocardium of hearts from endoglin mutant embryos[341], proposedly due to Alk4 or Alk7 compensatory signalling pathways which have also been implicated in the activation of Smad2 in Alk5 mutants[342]. It would therefore be interesting to assess whether increased levels of Alk4 are present in Eng-iKO CDCs.

Technical issues may also be of importance in the analysis of TGFβ signalling responses. Variable endoglin expression in CDC cultures (approximately 70-90%, table 5.1) may at least partly explain my findings and greater differences in Smad1 phosphorylation may be observed in cultures pre-selected for endoglin expression using FACS sorting. Similarly high levels of stimulating ligand may be present in the culture media (supplemented with 20% FCS) thus generating a high basal Smad phosphorylation response (as is evident in figure 5.16) which could theoretically mask the effect of exogenous ligand application or endoglin loss. To remove this possibility one option would be to titrate the FCS contained within the media, however this may adversely affect cell growth/function therefore another viable option would be to pre-treat cells with an Alk5 kinase inhibitor or Noggin to lower basal Smad2 and Smad1/5 responses respectively prior to western blotting.

As discussed previously the role of endoglin within TGFβ signalling and angiogenesis remains incompletely understood, however it is accepted that this role is likely to be cell type specific and context dependent. The significance of my findings require further investigation, including a more detailed study of the effect of ligand time/dose concentration on Smad1/5 and Smad2 phosphorylation, and the expression of a panel of downstream genes such as *Id1* and *Pai1* that are upregulated specifically by Alk1/TGFβ and Alk5/TGFβ, respectively. In addition as both BMP9-induced Smad1 and Smad2 phosphorylation have been identified to be mediated via Alk1/Bmpr2 and/or Alk1/Actr2 signalling[240] it would also be important assess what proportion of CDCs express Alk1 using FACS. Finally, as previously mentioned, it would be advantageous to sort the endoglin positive CDCs using flow cytometry to provide a pure population for investigating the effect of endoglin knock-down on cell signalling and function.

Paracrine mechanisms are thought to be responsible for a large proportion of CDC mediated cardiac repair[187]. This may in part be due to a pro-angiogenic mechanism. Therefore in addition to testing the effect of endoglin depletion on cellular responses associated with angiogenesis, such as proliferation and migration, it will also be important to evaluate the effect of endoglin loss on pro-angiogenic cytokine production. Endoglin heterozygote ECs display increased collagen production and decreased NO synthase expression and VEGF secretion, which results in reduced angiogenic responses[343]. It is possible that endoglin loss could impair CDC-mediated therapeutic angiogenesis in a similar manner. Although time restraints excluded this analysis from the present study it would be of major interest to investigate the effect of endoglin loss on pro-angiogenic cytokine production in CDCs.

Endoglin loss in CDCs results in perturbed cellular proliferation, migration and there was also a notable effect on TGFβ and BMP signalling through Smad2. Although the effects were modest they may nevertheless be important during heart repair and may also affect pro-angiogenic signals that would require further investigation. In order to determine whether this would be a fruitful avenue to pursue, I first performed a functional test in a pilot group of animals to examine whether endoglin depletion had any effect on the ability of CDCs to promote heart repair, either directly on donor cell retention and differentiation, or indirectly via pro-angiogenic effects. To this end, I developed a murine model of MI and performed intramyocardial CDC transplantations to compare the extent of any heart repair mediated by WT versus and Eng-iKO cells. This study is discussed in chapter 6.

CHAPTER 6.

Investigating the Role of Endoglin in CDC-Mediated Heart Repair *in vivo*

6.1. Introduction

Therapeutic angiogenesis following cardiac ischaemic injury aims to re-establish an adequate blood supply to the affected myocardium to minimise further damage caused by cardiac cell death. Transplanted cardiospheres and/or CDCs exert their cardio-protective effects, in part, by augmenting neovascularisation via either direct vascular differentiation or paracrine enhancement of angiogenesis[159, 187]. As discussed in section 1.9, TGFβ family signalling is pivotal to blood vessel formation and homeostasis and endoglin has a critical role in the regulation of both vascular remodelling and angiogenesis[344]. Previous work has shown that reduced endoglin levels in circulating mononuclear cells (*Eng*$^{+/-}$ cells derived from HHT1 patients) affects their homing ability and subsequently leads to impaired neovascularisation and accentuated deterioration of cardiac function following MI[275-276]. In chapter 5 I demonstrated that endoglin depletion results in impaired CDC proliferation and migration *in vitro* as well as perturbed canonical TGFβ signalling. I propose that the high level of endoglin expressed by CDCs is critical to their pro-angiogenic activity. Establishing an important functional role for endoglin in a cardiac derived stem cell population will enable the exploitation of the pro-angiogenic properties of this receptor in the development of stem cell therapies and will aid our understanding of the mechanisms underlying cell-mediated heart repair.

To confirm the ability of murine WT-CDCs to promote neovascularisation and improve cardiac function *in vivo* I first established a surgical mouse model of permanent coronary artery occlusion combined with direct intramyocardial CDC transfer. To investigate the subsequent effect of endoglin loss on donor cell mediated cardiac repair process following MI, transplanted CDCs were derived from *Eng*$^{fl/fl}$*;Rosa-CreER*^{T2} mice which enabled endoglin to be knocked out *in vitro* (Eng-iKO CDCs) using Cre/*loxP* recombination (as described in section 4.1.).

Pre-clinical models of MI have been described in several animal species with the pig ameroid model thought to most closely resemble human physiology and the clinical phenotype[345]. However the expense and practical demands of large animal surgery significantly limits the use of such studies to test novel therapeutic approaches. Cardiac surgery in mice is extremely technically challenging due to their small size and fast heart rate, however they are of particular interest because of the increasing availability

of useful transgenic and knock-out mouse strains. A rodent MI model was first developed over 3 decades ago[346] and later a murine model of ischaemia/reperfusion was described[347]. Distinct pathohistological differences have been observed between the reperfused and permanent coronary artery occlusion models of MI[348-349]. Briefly, less myocardial damage is observed in reperfused hearts compared to their non-reperfused counterparts due in part to a higher inflammatory cell influx and enhanced angiogenic response following the restoration of blood flow[348]. Reperfusion is currently the preferred clinical therapy for MI patients therefore the ischaemia/reperfusion technique provides a more clinically relevant model of heart injury. However the permanent occlusion model is still useful for some basic science studies. For example, the greater and accelerated inflammatory response associated with reperfusion may directly interfere with delivered cells (e.g. the greater number of macrophages may increase phagocytosis and removal of donor cells) and would have important implications regarding the timing of experimental intervention. Moreover, following reperfusion the healing response is made more complex due to the effect of 'reperfusion injury', whereas the response of permanent occlusion is mainly dependent on the effect of ischaemia on the heart. Therefore the permanent occlusion model is arguably more suited to 'proof of principle' studies that aim to identify important genes or proteins that may aid the development of novel therapies such as proposed in this study.

As described in chapter 1 (section 1.2), the cardiac healing response following MI results in significant structural and functional changes. This frequently results in detrimental ventricular remodelling, which ultimately leads to deterioration of cardiac function. Global left ventricular (LV) function is often used as a measure of LV remodelling in many pre-clinical studies assessing the repair potential of novel therapies. In the current study, cine cardiac MRI was used by my colleague Dr Ben Davison to assess cardiac functional parameters of my mouse models. The 1 and 4 week time points following infarction were chosen because the maximum angiogenic response has been observed 1 week following infarct[275] and at 4 weeks LV remodelling and fibrosis is essentially resolved in mice[12].

Following the initial healing process, the surviving myocardium can be divided into tissue bordering the infarct and remote myocardium. The infarct border zone corresponds to the tissue adjacent to the area of ischaemia and fibrosis, in which

myocytes are initially in a state of reversible injury. Due to a reduction in border zone capillary density this region constitutes an area at risk even after the completion of the healing process[350]. Therapeutic strategies aim to salvage this jeopardised tissue and decrease the level of myocardial necrosis and infarct extension. In this study CDCs were injected directly into the infarct border zone immediately following coronary artery occlusion. After 4 weeks, the effect of CDC transfer (with and without endoglin expression) on neovascularisation was assessed by quantifying vessel density in the ischaemic border zone using immunofluorescent staining.

6.2. Results

6.2.1. Establishing the Mouse Surgical Myocardial Infarction Model

I established a mouse model of acute MI at Newcastle University using a protocol described by van Laake *et al*[351] (see section 2.12 for detailed protocol). Briefly adult (12 to 14 weeks old) mice from a C57Bl/6 genetic background were intubated and mechanically ventilated with 2% isoflurane/98% oxygen. The left anterior descending (LAD) coronary artery was exposed following left side thoracotomy in the fourth intercostal space and was occluded using a 7-0 prolene ligature just below the inferior border of the left atria. Successful infarction was characterised by immediate blanching of the LV free wall, which forms a clear border between ischaemic and non-affected myocardium (figure 6.1), as well as reduced motility of the infarcted area. Sham-operated control mice were also subjected to left-side thoracotomy without coronary artery occlusion.

Four weeks following experimental MI mice were humanely killed and the hearts were removed and processed to prepare paraffin sections for Masson trichrome staining (see section 2.9.2.2.). This stain illustrates the structural changes associated with ventricular remodelling including LV chamber dilatation with thinning of the free wall, extensive collagen deposition and established fibrosis with mature scar formation (figure 6.2).

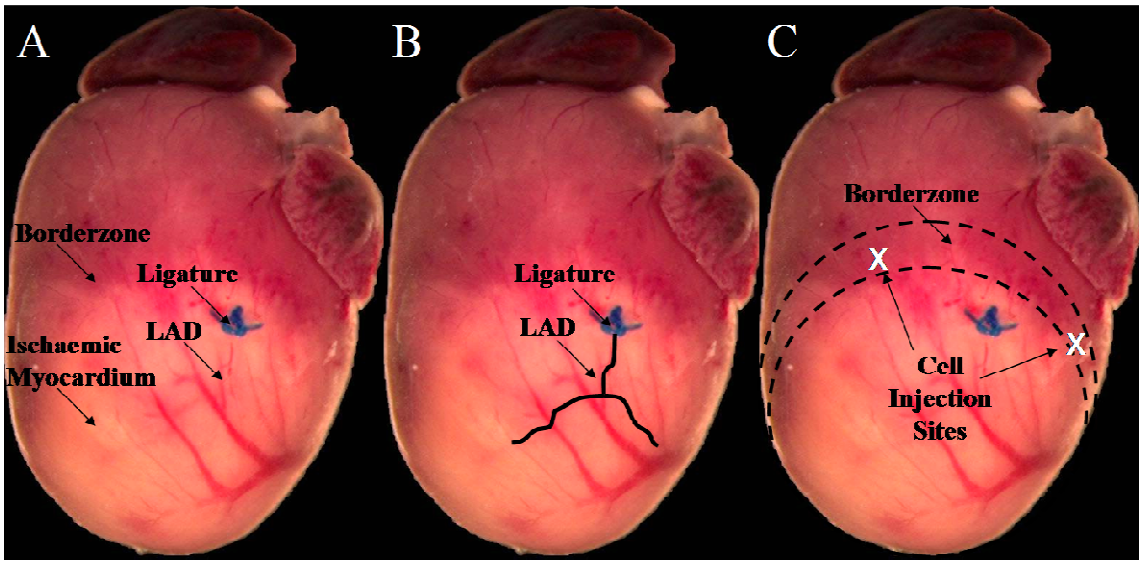

Figure 6.1. Image of a murine heart 24 hours following the occlusion of the LAD coronary artery. (A) MI was achieved by placing a 7-0 prolene ligature (blue) around the LAD coronary artery below the inferior border of the left atria. (B) The position of the LAD coronary artery has been digitally enhanced (black) to aid visualisation. (C) The ischaemic myocardium (pale zone) represents the area at risk and extends over the interventricular septum to the basal-posterior region. The inner and outer boundaries of the ischaemic border zone are delineated by dashed black lines and white X's mark the CDC injection sites (see section 6.2.2.1.).

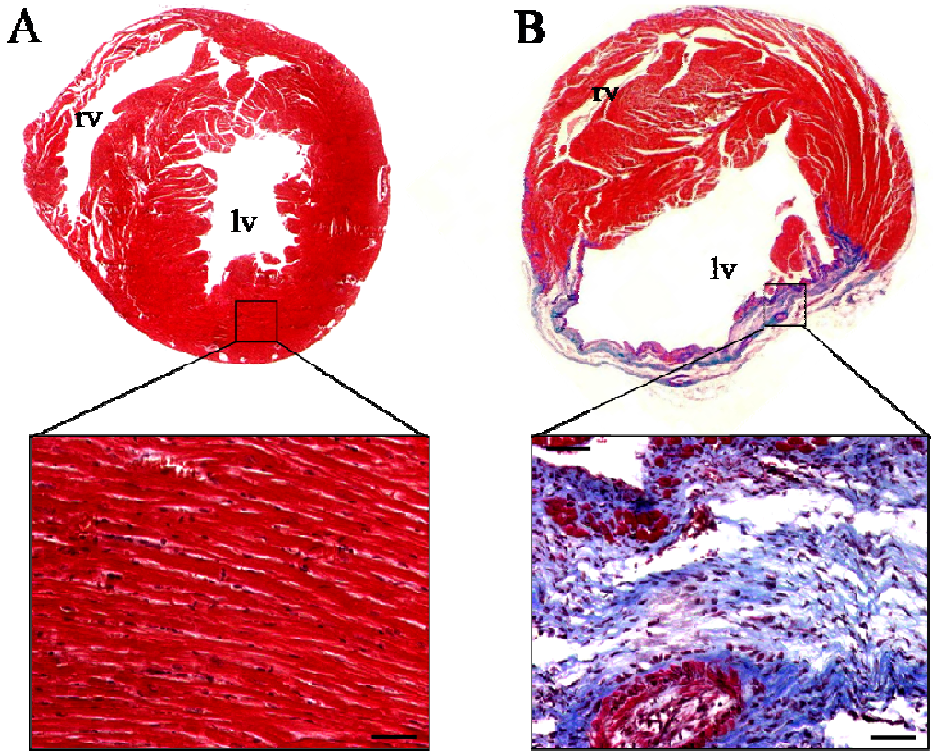

Figure 6.2. Remodelling and fibrosis of infarcted mouse heart. (A) Masson trichrome staining of sham-operated control heart showing normal morphology. (B) Mouse heart 4 weeks post-MI; note the extensive remodelling and thinning of the left ventricular free wall and extensive collagen deposition/fibrotic regions (blue staining) plus small islands of viable myocardium within the scar tissue (red)).Abbreviations: rv, right ventricle; lv, left ventricle. Scale bar = 10μM.

To demonstrate that we were able to identify and quantify changes in LV function using cardiac cine MRI we measured LV functional parameters in small cohorts of infarcted (n=10) and sham-operated (n=8) mice 4 weeks following surgery.

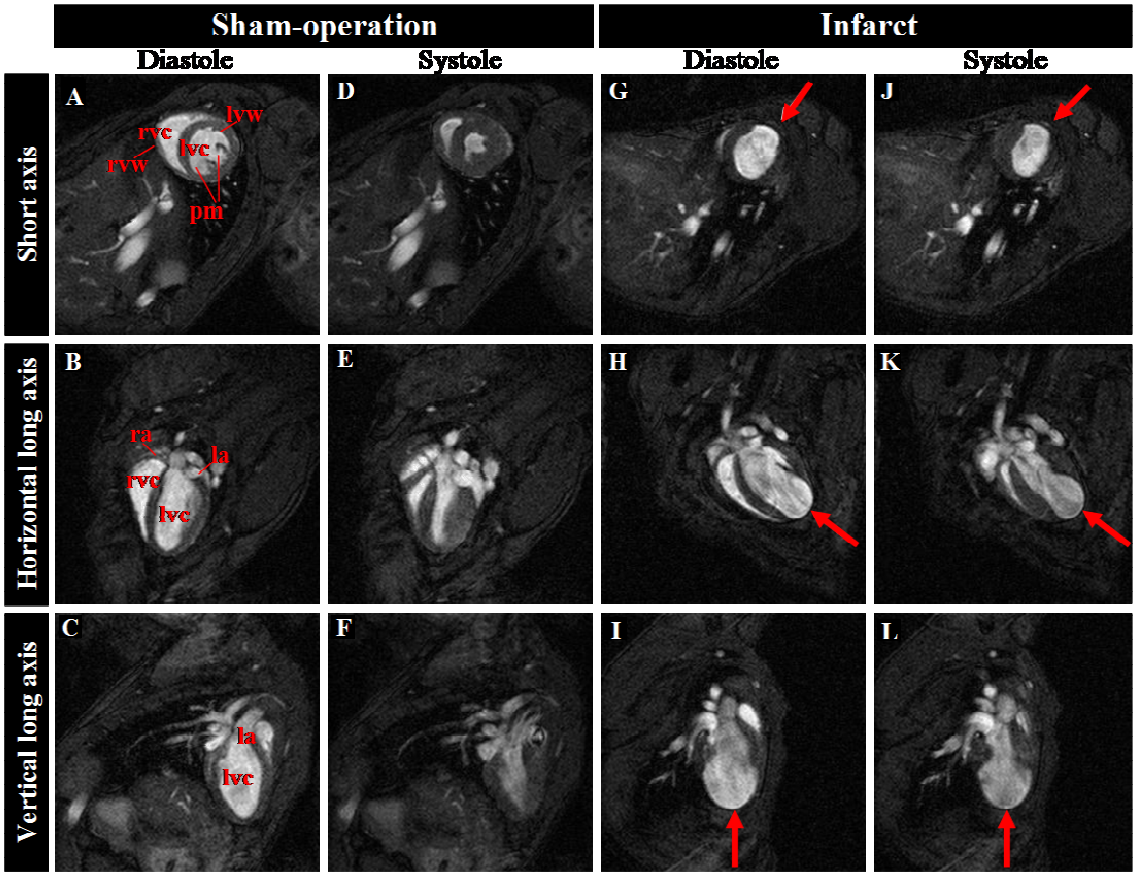

Figure 6.3. Cine MR images of a sham operated mouse heart (A to C, diastole; D to F, systole) and 4 weeks following coronary artery occlusion (G to I, diastole; J to L, systole). Images of the sham-operated heart show normal wall thickness and motion whereas following MI increased left ventricular volume as well as wall thinning and akinesis in the anterolateral and apical regions is evident (red arrows). Abbreviations: lvc, left ventricular cavity; rvc, right ventricular cavity; lvw, left ventricular wall; rvw, right ventricular wall; la, left atrium; ra, right atrium; pm, pulmonary muscle. Images courtesy of Dr Ben Davison.

Representative MRI images (figure 6.3) clearly show the increased dilatation of the LV 4 weeks following LAD coronary artery occlusion, with marked myocardial wall thinning in comparison to sham controls (figure 6.3G-L, red arrows indicate regions of myocardial akinesis in the anterolateral and LV apical walls). MRI-assessed LV functional parameter measurements for both sham control and infarcted mice (4 weeks post-MI) are shown in table 6.1. Mean myocardial mass and LV volume indices were significantly greater in the MI group (myocardial mass index, 4.9±0.1 versus 3.9±0.2

(p<0.001); end diastolic volume index (EDVI), 5±0.5µl/g versus 2.3±0.1µl/g (p<0.001); end systolic volume index (ESVI), 3.8±0.5µl/g versus 0.76±0.05µl/g (p<0.001)), whereas stroke volume index (SVI), ejection fraction (EF) and cardiac output index (CI) were all significantly reduced compared to sham operated mice (SVI, 1.2±0.04µl/g versus 1.6±0.1µl/g (p=0.008); EF, 26.6±2.8% versus 67.1±0.9% (p<0.001); CI, 0.5±0.02ml/min/g versus 0.64±0.05ml/min/g (p=0.05). N.B. to account for the significant difference in pre-operative body weight (p=0.02) between sham and MI mice, which is due to dissimilar proportions of male and female mice included in each group, indices measurements (data normalised to pre- operative body weight) were calculated for all parameters. Cardiac MRI was able to identify changes related to LV remodelling following MI and thus was used to assess the effect of cell transplantation in this disease model.

	SHAM n=8	**INFARCT n=10**	***t-test p Value***
Sex	5M 3F	3M 7F	n/a
Age at Infarct (weeks)	12.4±0.5	12±0.4	n/s
Pre-operation Weight (g)	29±1.3	25.2±0.9	0.020
Mean HR(bpm)	409±9.5	416±12.1	n/s
CO(ml/min)	18.2±0.8	12.6±0.7	<0.001
CI (ml/min/g)	0.64±0.05	0.5±0.02	0.050
Mean myocardial mass (mg)	111.9±1.7	122.3.7±2.9	0.011
Mean mass index (mg/g)	3.9±0.2	4.9±0.1	<0.001
EDV (µl)	66.4±1.6	116.7±11.5	0.001
EDVI (µl/g)	2.3±0.1	5±0.5	<0.001
ESV (µl)	21.8±0.9	85.1±12.5	<0.001
ESVI (µl/g)	0.76±0.05	3.8±0.5	<0.001
SV (µl)	44.6±1.5	30.4±1.3	<0.001
SVI (µl/g)	1.6±0.1	1.2±0.04	0.008
EF (%)	67.1±0.9	26.6±2.8	<0.001
Infarct Size (% LV)	n/a	36.2±1.8	n/a

Table 6.1. Functional analysis of global left ventricular function in sham-operated mice (n=8) and 4 weeks following LAD coronary artery occlusion (n=10). Data is presented as mean ± SEM. Statistical differences between sham and infarct groups were calculated using the Student's *t* test for all parameters, *p*-values < 0.05 are considered statistically significant and are highlighted in red. Abbreviations: HR, heart rate; CO, cardiac output; CI, cardiac index; EDV, end diastolic volume; EDVI, end diastolic volume index; ESV, end systolic volume; ESVI, end systolic volume index; SV, stroke volume; SVI, stroke volume index; EF, ejection fraction; LV, left ventricle. n/a = not applicable, n/s = not significant (p > 0.05). MRI data analysis performed by Dr Ben Davison.

Post-surgical survival rates were deduced from a cohort of 28 infarcted mice that were sacrificed 4 weeks following surgery. In this experimental group, my peri-operative (within 24 hours) survival rate was 100%, while 4 week survival was 86% (figure 6.4), which is superior to survival rates reported in similar studies (approximately 50-63%)[352]. Additionally, I observed a 100% survival rate in a smaller cohort of mice (n=6) that were permitted to live for 12 weeks following MI demonstrating that this model is compatible with high survival rates over extended periods.

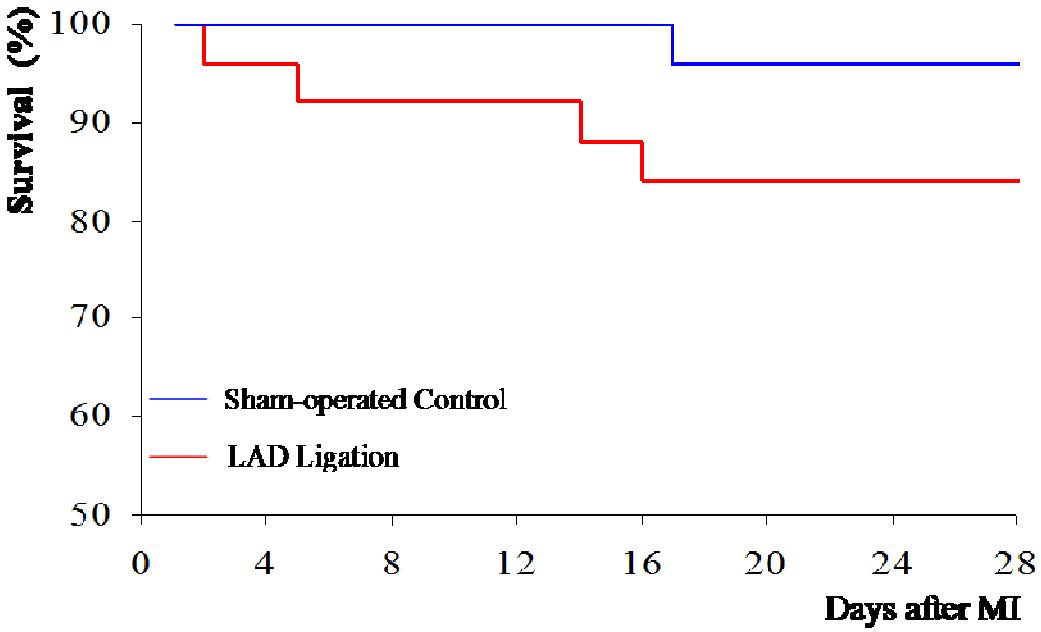

Figure 6.4. Survival of mice at 4 weeks following MI. Survival data shows high survival rates (86%) reflecting good surgical technique. Sham operated control survival was 92%. (MI, n = 28; Sham, n = 12).

In summary I established a reliable model of experimental MI to test the ability of CDCs to contribute to heart repair *in vivo* and using an inducible endoglin knock-out mouse model I subsequently tested the effect of endoglin loss on the repair potential of these cells.

6.2.2. Investigating the Role of Endoglin in CDC Mediated Cardiac Repair

6.2.2.1. Wild-Type CDC Mediated Heart Repair following MI

To test the ability of CDCs to contribute to heart rescue following ischaemic injury, cells (at passage 2) were injected directly into the ischaemic border zone immediately following surgical MI. In order to allow donor cell tracking in cardiac rescue experiments CDCs were genetically tagged with enhanced green fluorescent protein (eGFP) using the CAG-farnesylated-eGFP line (unpublished line kindly given by Professor Alexander Medvinsky, Edinburgh University). In this line eGFP expression is driven by the ubiquitous CAG promoter which is a combination of the chicken β-actin and the CMV promoters, whilst the farnesyl group anchors eGFP to the cell membrane. The majority of passage 2 CDCs derived from *Eng$^{fl/fl}$;Rosa-CreER^{T2};CAG-farnesyl-eGFP* mice express eGFP (92.5±1.7%), which was readily detected by FACS analysis (Figure 6.5A, B). However, endogenous eGFP expression was difficult to detect using fluorescent microscopy (Figure 6.5C). Therefore staining was performed using anti-GFP antibody conjugated to alexa488 (Figure 6.5D). This antibody was also required to detect endogenous eGFP in cryosections of heart tissue from *Eng$^{fl/fl}$;Rosa-CreER^{T2};CAG-farnesyl-eGFP* mice.

It was important for the work described in this chapter to specifically identify which cardiac cell lineages express eGFP to enable the identification of cell types that are derived from donor cells following the transplantation of *CAG-farnesyl-eGFP* CDCs. Therefore colocalisation experiments were performed on cryosections of the CAG-farnesyl-eGFP mouse heart to examine the co-expression of eGFP with CD31 (a specific marker of endothelial cells), α-actinin (a marker of cardiomyocytes) and α-SMA (a marker of vascular smooth muscle or myofibroblasts). I found that only a small proportion of ECs in the heart express eGFP (figure 6.6 C and D), whilst expression in cardiomyocytes is strong and uniform (figure 6.6G). Interestingly, I observed perivascular eGFP expression (figure 6.6H) although only some vascular smooth muscle cells expressed eGFP (figure 6.6E and F). These findings suggested that using this line, only a subpopulation of eGFP positive cells would be detected following transplantation and differentiation into ECs or SMCs, although the majority of CDCs

that had differentiated to cardiomyocytes would be detectable. Further details on tracking and identification of transplanted CDCs *in vivo* are described in section 6.2.4.

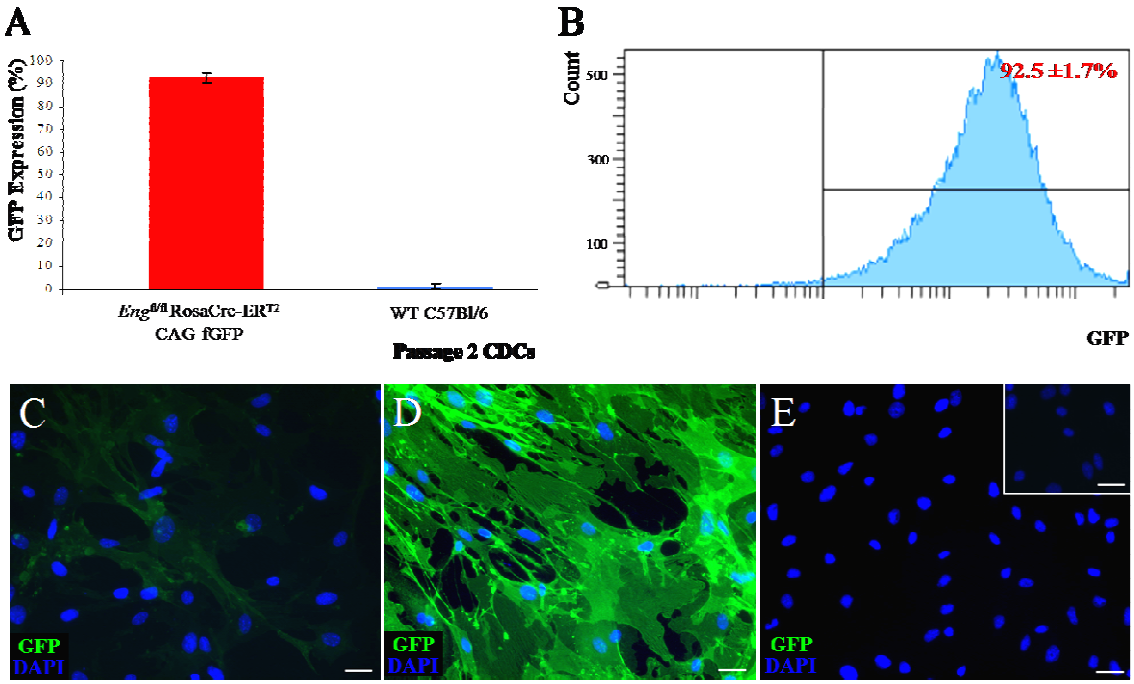

Figure 6.5. Expression of eGFP in passage 2 CDCs derived from *CAG-farnesyl-eGFP* mice. (A) Flow cytometric analysis reveals that the majority of passage 2 CDCs from *Eng$^{fl/fl}$;Rosa-CreER^{T2};CAG-farnesyl-eGFP* mice express eGFP (92.5±1.7%), whereas negligible GFP expression is detected in CDCs derived from C57Bl/6 mice (1.6±1%). (B) A representative histogram showing the CDC eGFP positive population. Data was derived from 4 replicate samples and is presented as mean percentage ± SEM. (C-E) Representative fluorescent microscopy images of passage 2 CDCs from *Eng$^{fl/fl}$;RosaCreER^{T2};CAG-farnesyl-eGFP* mice showing endogenous eGFP expression (C), following immunostaining with a specific anti-GFP antibody conjugated to alexa 488 (D) and sEND-1 an endothelial cell line that served as a negative control (E, inset image, no primary control). The negligible endogenous eGFP expression in (C) demonstrates the need to use an anti-GFP antibody to track transplanted CDCs *in vivo*. Scale bar = 20μm.

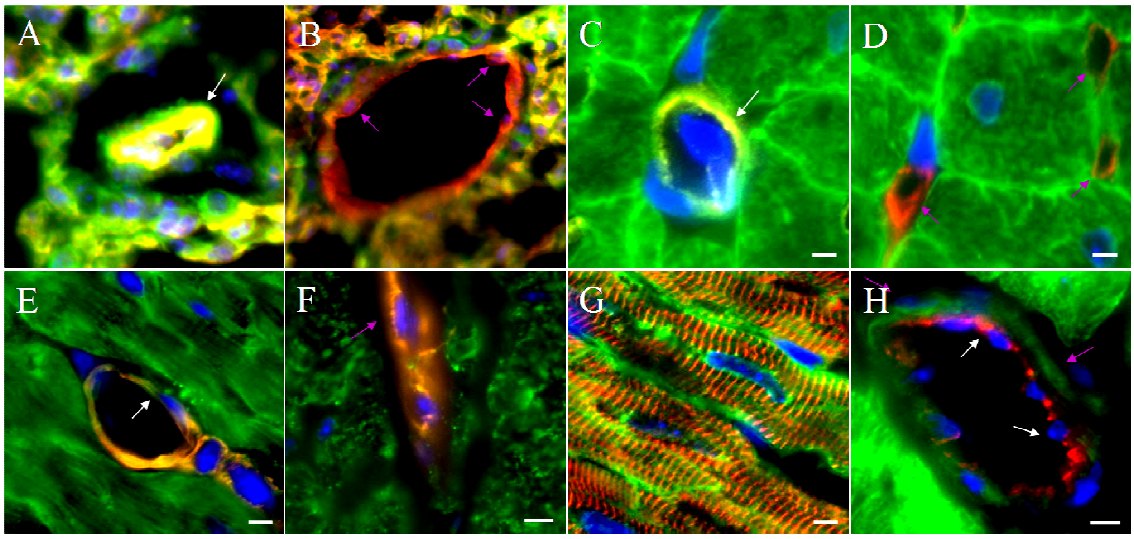

Figure 6.6. Expression of eGFP in cardiac and vascular cell types in pulmonary and cardiac tissue harvested from the *CAG-farnesyl-eGFP* mice. (A and B) pulmonary tissue co-stained with alexa 488 conjugated-GFP antibody (green) and alexa 594 conjugated-CD31 (red). Representative images show endothelial GFP expression in some large blood vessels (A, co-expression appears yellow and is highlighted with a white arrow) but not in others (B, endothelial cells not expressing GFP highlighted with purple arrows). (C and D) Co-expression of eGFP and CD31 in the myocardium. A small proportion of capillary-associated ECs in the heart co-express CD31 and eGFP (C, highlighted with white arrow) although the majority of vessels failed to demonstrate co-expression (D, GFP negative capillaries highlighted with purple arrows). (E and F) Co-expression of eGFP (alexa 488, green) and SMA (Cy5.5, orange) in the myocardium. GFP co-expresses with a small proportion of SMA positive cells (E, dual positive cell highlighted with white arrow) whilst other SMA cells were GFP negative (F, SMA positive/GFP negative cell highlighted with purple arrow). (G) Co-staining of myocardium with alexa 488 conjugated-anti GFP (green) and alexa-594 conjugated-anti α-actinin (red) antibodies show that cardiomyocytes strongly express GFP. (H) Myocardium co-stained with alexa 488 conjugated-anti GFP (green) and alexa-594 conjugated-anti CD31 (red) antibodies. Representative image shows perivascular expression of GFP (endothelial cells highlighted with white arrows, GFP positive cells in close association with vascular ECs highlighted with purple arrows). Scale bar = 2μM.

In CDC transfer experiments a total of 10^6 cells were transplanted into each animal. CDCs were re-suspended in 5μl of PBS and delivered via intramyocardial injection into two sites bordering the ischaemic zone of the LV wall. Successful injection was evident by the absence of cell backwash and the appearance of a white area in the myocardium. To ensure that CDC viability was not adversely affected by injection using a 25μl Hamilton Microliter™ syringe and 33 gauge needle I performed an MTT viability assay on CDCs that had been passed through the syringe needle. This needle has an internal diameter of 110μm whilst the average diameter of a murine CDC at P2 is 15.4±1.5μm. CDCs were harvested and re-plated onto a 96 well plate either directly or following

passage through the syringe/needle either once or else 5 times. Following a 24hour culture period cell viability was assessed using a previously described protocol (see section 3.2.5.1). Passing cells through the needle once had no effect, whereas repeated trituration (x5) significantly reduced cell viability (figure 6.7). Additionally, as the MTT assay measures the effect of trituration on viability only after a period of *in vitro* culture (24 hours), I also used the ViCell automated cell viability analyser (which uses a standard trypan blue assay) to measure viability directly following passage through the Hamilton syringe. The ViCell analyser indicated there was no immediate difference between the viability of cells that passed through the syringe once and those that were not (92.8%versus 94.2%). The concern raised from low cell viability in the MTT assay following repeated (5X) trituration is two-fold; (i) low cell viability would impair our ability to test the repair capacity of these cells and (ii) lysed cells are known to release potassium, therefore injecting a sufficiently large number of lysed/damaged cells could lead to hyperkalaemia resulting in cardiac arrest. Therefore care was taken to ensure that cells were passed only once through the needle prior to injection.

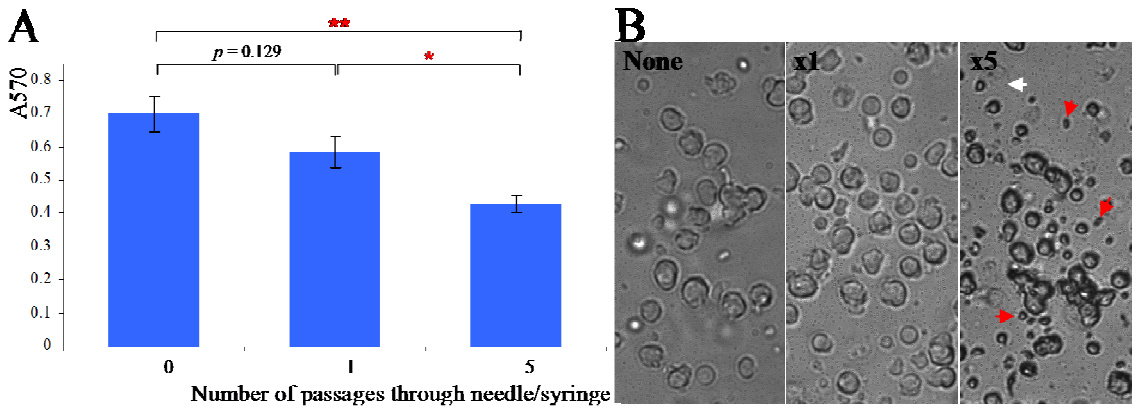

Figure 6.7. Evaluating CDC viability using the MTT assay following cell passage through a syringe. CDC viability is not significantly affected by passing cells through a 25µl Hamilton syringe/33G needle once (p=0.129). However, repeated trituration (x5) significantly reduces cell viability. Student's t-test used to assess statistical significance, *p<0.05 **p<0.01. (B) Representative bright field images of cells following no, 1 or 5 passes through the syringe/needle. Note that following only 1 pass the cells look healthy with intact membranes whereas there is evidence of increased cell debris following repeated trituration (highlighted with red arrows) with some cell lysis present (white arrow, difficult to detect in phase bright image).

To further reduce the risk of increased mortality associated with intramyocardial cell injections I ensured that the injection volume was small and constant (a total of 5µl split between 2 sites), the injection was superficial preventing perforation of the LV wall and

also that the injection sites were distal to the septum and right ventricle to minimise contact with the conduction system. Additionally I injected the cells into akinetic myocardium close to the ischaemic border zone, which also reduced cell backwash following injection. Despite these efforts I saw a considerable increase in mortality with mice experiencing cardiac arrhythmias immediately following cell injection (approximately 33% of mice (12/36) went into ventricular fibrillation and died immediately following intra-myocardial cell injection). In addition to this cell injection related mortality I also experienced severe problems associated with mechanical ventilation and anaesthesia. For several months prior to beginning this study I observed that whilst under isoflurane induced anaesthesia mice experienced spontaneous respiration that was not synchronised with mechanical ventilation although this did not adversely affect mortality rates (100% peri-operative survival, 86% survival at 4 weeks (see figure 6.4)). This issue did however become progressively worse and eventually led to increased mortality at a time that coincided with the MI surgeries and cell transfers described in this study reducing the numbers of mice per group (see section 6.3 for a fuller discussion of this problem).

6.2.2.2. Left Ventricular Functional Analysis Post MI Reveals that WT-CDCs have a Cardioprotective Effect

Directly following LAD coronary artery occlusion a small group of mice received WT CDCs via intramyocardial injection into the infarct border zone (n=6), whilst a second group of infarcted mice received vehicle (PBS) only (n=3). An additional control group consisted of sham-operated mice (n=4). Discounting perioperative mortality including the first 24hours following surgery, the 4 week survival rates of each group were comparable (sham operated, 100%; MI+ PBS 100%; MI plus WT CDC transplantation 87%).

LV function was assessed in these mice by MRI analysis at 1 week and 4 weeks following surgically induced MI. Figure 6.8 shows representative cine cardiac MR images 4 weeks following sham-operation (figure 6.8A-F), MI with PBS injection (figure 6.8G-L) and MI with WT-CDC infusion (figure 6.8M-R), whilst figure 6.9 graphically displays measurements of selected parameters of cardiac function and remodelling for these groups. Data was normally distributed and differences between

treatment groups were initially assessed using one-way ANOVA. Where this analysis suggested significant differences existed, the students unpaired *t*-test was used to calculate precise differences between pairs of groups. Data for all parameters are presented in table 6.2 along with relevant statistical information.

Cine MR images reveal striking LV dilatation and wall thinning in the MI with PBS group 4 weeks following surgery (figure 6.8G-L) compared to sham-operated control hearts (figure 6.8A-F). Furthermore, comparison of LV functional parameters between these two groups revealed markedly increased end diastolic and end systolic LV volumes in the MI group as well as significantly reduced EF both at 1 week and at 4 weeks following surgery (table 6.2). At 1 week, none of the parameters analysed were significantly different between PBS and WT-CDC recipient infarcted mice, however at 4 weeks the reduction in LV volume indices in the WT-CDC recipient group reached statistical significance compared to PBS controls (EDVI, 8.4±1.1µl/g versus 5.2±0.6µl/g (p=0.032) and ESVI, 6.8±0.9µl/g versus 3.9±0.7µl/g (p=0.048)). Representative cine MRI images also demonstrate attenuated LV remodelling by showing reduced cavity dilatation of the LV in WT-CDC compared to PBS recipient mice. The primary endpoint in many cell transplantation studies is an increase in left ventricular EF, which is a common parameter used to indicate the level of effect a therapeutic intervention has on cardiac function. The EF in CDC recipient mice was found to be appreciably increased relative to PBS controls, but this difference failed to reach statistical significance (18.6±0.8% versus 32±6.3% at 1 week (p=0.19) and 18.4±1.7% versus 30.8±6.1% at 4 weeks post MI (p=0.21)) which may have been due to small sample sizes. Similarly a small reduction in infarct size in WT-CDC recipient mice compared to PBS controls did not reach statistical significance at 1 or 4 weeks following surgery (40.1±3.7% of LV versus 50.2±4.7% at 1 week and 42.1±4.7 versus 51.8±1.9 at 4 weeks, figure 6.13).

Changes in cardiac function over time (between week 1 and week 4 following surgery) were also analysed and WT-CDC infusion following MI resulted in significantly attenuated increases in myocardial mass index and ventricular volume indices compared to the PBS injected group (figure 6.10, table 6.3). These data suggest that CDC transplantation results in reduced adverse left ventricular remodelling following MI.

Overall, the MRI-assessment employed in this study confirms that WT-CDC transplantation augments cardiac function in injured hearts.

6.2.2.3. Wild-Type CDC Transplantation following MI results in Increased Neovessel Formation

To establish the contribution of neovascularisation to CDC-mediated cardiac rescue following MI, I quantified blood vessel density in the infarct border zone at 4 weeks following surgery. Multiple sagittal cryosections (n=8 to 10 sections per mouse) were taken from the mid-point of the infarcted heart (or equivalent region in sham-operated controls) and stained with anti-CD31 antibody. The percentage area stained positively with CD31 was calculated per section using ImageJ software (NIH) and normalised to total area to derive mean percentage CD31 expression per mm^2 (26±6 images were analysed per heart). Data was normally distributed and differences in vascular density between groups were initially assessed using one-way ANOVA (p=0.001) and subsequently significant differences between pairs of groups were verified using the students unpaired t-test.

Comparisons between groups revealed that vascularity at the infarct border zone was significantly reduced in MI mice with PBS injection compared to sham-operated controls (0.073±0.002 versus 0.135±0.007% CD31 expression/mm^2 (p<0.001)) (figure 6.11). Whereas CDC transplantation following MI resulted in a significant increase in capillary density than was observed in PBS treated infarcted mice (0.088±0.003 versus 0.073±0.002 CD31 expression/mm^2 (p<0.001)) (figure 6.11).

These results demonstrate that injection of WT-CDCs into the infarct border zone results in functional cardiac improvement by MRI analysis and immunofluorescent analysis of vascularity indicates that this is likely, in part, due to an enhanced angiogenic response.

6.2.2.4. Endoglin Depleted CDCs Improve Cardiac Function without an Enhanced Angiogenic Response

To determine the effect of endoglin loss on CDC-mediated heart repair, CDCs were prepared from *Eng$^{fl/fl}$;Rosa-CreER^{T2};CAG-farnesyl-eGFP* mice and treated with 2μM 4OH-tamoxifen for 96hours *in vitro* to achieve gene deletion via Cre/*loxP* recombination (as described in section 5.2.2.1). The aim of this part of the study was to compare the effects of transplanting Eng-iKO CDCs into the infarct border zone with the effects of transplanting untreated control CDCs (WT-CDCs).

Figure 6.12 shows images of a sample of donor *Eng$^{fl/fl}$;Rosa-CreER^{T2};CAG-farnesyl-eGFP* CDCs cultured for *in vivo* cell transfer and demonstrate a clear knock-down of endoglin expression in 4OH-tamoxifen treated cultures. As previously discussed in chapter 5 (see tables 5.1 and 5.3), I have observed that 70-90% of CDCs express endoglin and I am able to achieve approximately 80% endoglin knock down following treatment with 4OH-tamoxifen. These findings have also been replicated by an independent researcher using my protocols (personal communication, Muhammad Amirrasouli). Although it would have been desirable to verify the precise endoglin levels in all WT and Eng-iKO cells used for *in vivo* transfer, due to time constraints this was not possible. However it is likely that expression levels fall within the boundaries quoted above.

The 4 week survival data for the MI with Eng-iKO CDC transfer mice (80% discounting perioperative mortality, final group size n=4) was similar to survival rates described for the other experimental groups (see section 6.2.2.2). MRI analysis 4 weeks after surgery revealed there was a significant increase in EF (35.1±10. 6% versus 18.4±1.7% (p=0.024)) in mice that received Eng-iKO CDCs compared to PBS recipient controls. In parallel there was a non significant trend of reduced myocardial mass index (5.7±0.8mg/g versus 6.6±0.9mg/g (p>0.05)) and decreased left ventricular volume indices (EDVI; 5.7±1.6μl/g versus 8.4±1.1μl/g (p=0.271) and ESVI; 4.3±1.8μl/g versus 6.8±0.9μl/g, (p=0.313)) (see figure 6.9. figure 6.8. for representative cine MR images and table 6.2. for full data set). Although these differences did not reach statistical significance they do indicate that Eng-iKO CDCs retain a capacity to contribute to repair following heart injury. Furthermore, comparisons between WT-CDC and Eng-iKO CDC infused hearts revealed no significant difference in cardiac function by MRI assessment (see figure 6.9). In fact myocardial mass and LV volume indices were similar between these two groups at 4 weeks post surgery (myocardial mass index,

4.9±0.2mg/g versus 5.7±0.8mg/g (p>0.05); EDVI, 5.2±0.6µl/g versus 5.7±1.6µl/g (p=767); ESVI, 3.9±0.7µl/g versus 4.3±1.8µl/g (p=0.804)) as well as CI, SVI, EF and infarct size (CI, 0.65±0.06ml/min/g versus 0.62±0.07ml/min/g (p>0.05); SVI, 1.4±0.1µl/g versus 1.4±0.2µl/g (p>0.05); EF, 30.8±6.1% versus 35.1±10.6% (p=0.711); infarct size, 42.1±4.7% of LV versus 38.3±6.8%).

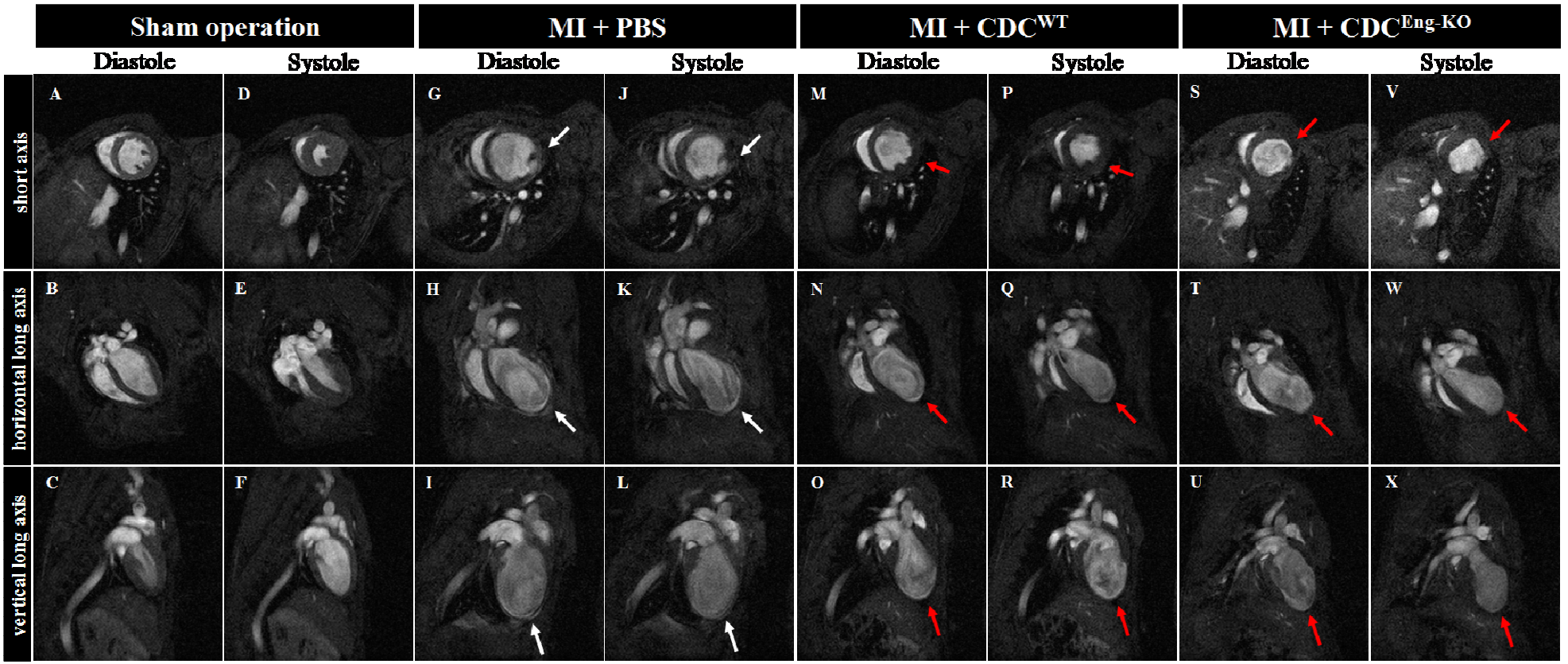

Figure 6.8. Representative cine MR images of post infarct murine hearts following intramyocardial CDC transplantation. Images of a sham-operated heart show normal wall thickness and motion (diastole A-C, systole D-F), whereas images of an infarcted heart (diastole G-I, systole J-L) show increased LV dilatation as well as wall thinning and akinesis in the anterolateral and apical regions (see white arrows). Transplantation of WT-CDCs (diastole M-O, systole P-R) and Eng-iKO cells (diastole S-U, systole V-X) immediately following LAD coronary artery occlusion leads to attenuated adverse remodelling, note the reduced LV wall thinning and cavity dilatation (see red arrows) compared with MI controls at 4 weeks following surgery.

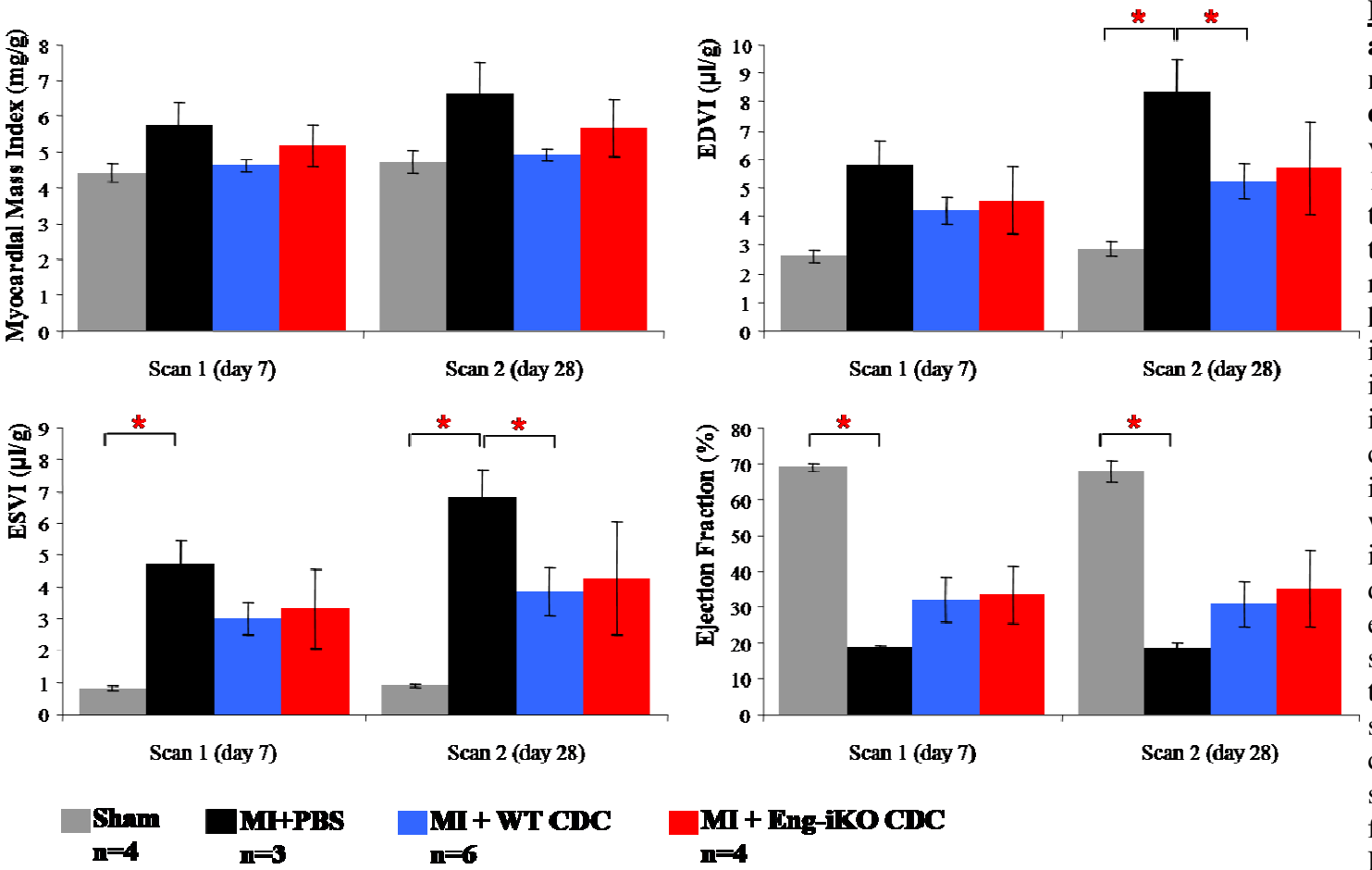

Figure 6.9. MRI-assessed analysis of cardiac function reveals a cardioprotective effect for CDCs. Left ventricular functional analysis at 1 and 4 weeks post infarct shows that both WT and Eng-iKO CDC transfer protects against adverse remodelling and dilatation of the heart. Reduced myocardial mass index and ventricular volume indices are observed at 4 weeks in both cell recipient groups compared to the MI with PBS injection control group. One-way ANOVA was used to assess if statistically significant differences were present for each parameter, then the students unpaired t-test was used to calculate *p*-values between specific pairs of groups, $p<0.05$ considered statistically significant (please see table 6.2 for detailed statistical analyses). Error bars represent SEM and * denotes $p<0.05$.

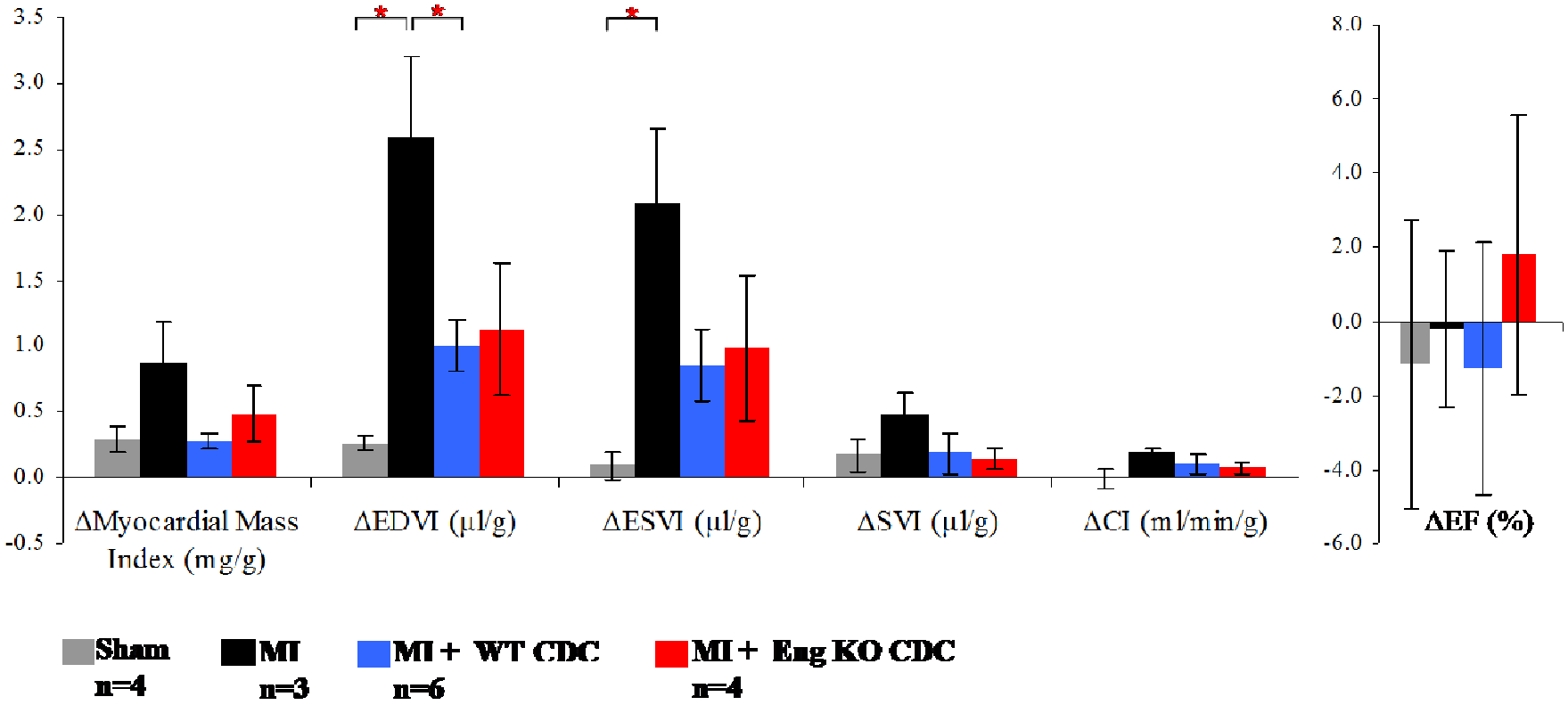

Figure 6.10. Changes in cardiac function between 1 and 4 weeks following MI and cell transplantation. The data demonstrates attenuated increases in myocardial mass index and ventricular volume indices in both WT and Eng-iKO CDC injected groups compared to PBS-only recipient mice. There was no significant difference in the change in EF between 1 and 4 weeks following surgery. These results suggest reduced adverse LV remodelling in CDC recipients. One-way ANOVA was used to assess if statistically different changes were present between groups for each parameter, then the students unpaired *t*-test was used to calculate *p*-values between specific pairs of groups, (please see table 6.3 for detailed statistical analyses). Error bars represent SEM and * denotes $p<0.05$.

	SHAM n=4	MI + PBS n=3	MI + CDC^{WT} n=6	MI + CDC^{EngKO} n=4	*p* Values				
					ANOVA	Sham vs MI+PBS	MI+PBS vs MI+CDC^{WT}	MI+PBS *vs* MI+CDC^{EngKO}	MI+CDC^{WT} *vs* MI+CDC^{EngKO}
Age at Infarct (weeks)	12.9±0.1	12.7±0.3	12.8±0.2	12.7±0.2	0.921	n/a	n/a	n/a	n/a
Pre-operative Weight (g)	25.7±1.6	25.3±1.04	29.6±1.2	29.2±3.2	0.303	n/a	n/a	n/a	n/a
Day 7 SCAN									
Mean HR (bpm)	423.5±15	429±27.9	447.7±24	432.3±9.1	0.842	n/a	n/a	n/a	n/a
CO(ml/min)	19.4±1.3	11.7±2.2	16.1±1.4	16.1±2.6	0.114	n/a	n/a	n/a	n/a
CI (ml/min/g)	0.76±0.03	0.46±0.08	0.54±0.09	0.54±0.04	0.003	0.01	0.305	0.346	0.976
Mean myocardial mass (mg)	113±6.1	146±18	136±4.3	146.6±7.5	0.049	0.105	0.477	0.976	0.218
Mean mass index (mg/g)	4.4±0.2	5.8±0.6	4.6±0.2	5.2±0.6	0.147	n/a	n/a	n/a	n/a
EDV (µl)	66.26±3.6	146.3±24.6	125.8±14.8	124.9±20.8	0.038	0.013	0.473	0.534	0.972
EDVI (µl/g)	2.6±0.2	5.8±0.9	4.2±0.5	4.6±1.2	0.081	n/a	n/a	n/a	n/a
ESV (µl)	20.5±1.5	119.4±20.7	87.7±15.4	87.4±25.6	0.019	0.002	0.267	0.400	0.992
ESVI (µl/g)	0.8±0.08	4.7±0.7	3±0.5	3.3±1.3	0.032	0.001	0.099	0.419	0.804
SV (µl)	45.72±2.31	26.9±4	36.7±4.2	37.5±6.6	0.137	n/a	n/a	n/a	n/a
SVI (µl/g)	1.79±0.1	1.06±0.1	1.2±0.1	1.3±0.1	0.011	0.01	0.394	0.282	0.898
EF (%)	69.1±1	18.6±0.8	32±6.3	33.4±7.9	0.001	<0.001	0.190	0.176	0.899
Infarct size (% of LV)	n/a	50.2±4.7	40.1±3.7	38.2±6.5	0.304	n/a	n/a	n/a	n/a
Weight (g)	23.78±2.27	23.2±1.5	25.5±0.9	25.5±2.3	0.750	n/a	n/a	n/a	n/a
Day 28 SCAN									
Mean HR(bpm)	425±11.2	420.7±7.9	456.2±15.2	440±15.1	0.305	n/a	n/a	n/a	n/a
CO(ml/min)	21.2±2.2	16.5±3.3	19.2±1.9	18.3±3.2	0.693	n/a	n/a	n/a	n/a
CI (ml/min/g)	0.84±0.1	0.65±0.1	0.65±0.06	0.62±0.07	0.320	n/a	n/a	n/a	n/a
Mean myocardial mass (mg)	120.9±8.7	167.7±21.9	144.5±4.7	159.5±9.3	0.040	0.076	0.187	0.715	0.151
Mean mass index (mg/g)	4.7±0.3	6.6±0.9	4.9±0.2	5.7±0.8	0.097	n/a	n/a	n/a	n/a
EDV (µl)	72.9±4.1	210.5±27.3	153.1±17.2	153.9±30.1	0.008	0.002	0.106	0.238	0.982
EDVI (µl/g)	2.9±0.2	8.4±1.1	5.2±0.6	5.7±1.6	0.025	0.003	0.032	0.271	0.767
ESV (µl)	23.3±2.2	171.3±20.4	110.6±20.7	111.7±37.7	0.013	<0.001	0.109	0.267	0.980
ESVI (µl/g)	0.9±0.04	6.8±0.9	3.9±0.7	4.3±1.8	0.023	0.001	0.048	0.313	0.804
SV (µl)	44.7±6.1	39.2±7.6	41.2±4.9	42.2±8	0.956	n/a	n/a	n/a	n/a
SVI (µl/g)	2±0.2	1.6±0.3	1.4±0.1	1.4±0.2	0.187	n/a	n/a	n/a	n/a
EF (%)	67.9±3	18.4±1.7	30.8±6.1	35.1±10.6	0.002	<0.001	0.212	0.240	0.711
Infarct size (% of LV)	n/a	51.8±1.9	42.1±4.7	38.3±6.8	0.310	n/a	n/a	n/a	n/a
Weight (g)	26.3±2.4	25.5±2	28.3±1	28.9±2.8	0.630	n/a	n/a	n/a	n/a

Table 6.2. Summary of MRI assessed LV functional analyses at 1 and 4 weeks following sham-operation (thoracotomy) and MI with or without CDC transfer (with or without endoglin depletion). All parameters are expressed as mean ± SEM. Table illustrates the results of one-way ANOVA and the significant results of unpaired *t*-tests between specific pairs of groups. Significant values ($p<0.05$) are highlighted in red. Abbreviations: HR, heart rate; CO, cardiac output; CI, cardiac index; EDV, end diastolic volume; EDVI, end diastolic volume index; ESV, end systolic volume; ESVI, end systolic volume index; SV, stroke volume; SVI, stroke volume index; EF, ejection fraction; LV, left ventricle. n/a = not applicable. MRI data analysis performed by Dr Ben Davison.

					p Values				
	SHAM	**MI + PBS**	**MI + CDC^{WT}**	**MI + CDC^{EngKO}**	***ANOVA***	**Sham vs MI+PBS**	**MI+PBS vs MI+CDC^{WT}**	**MI+PBS vs MI+CDC^{EngKO}**	**MI+CDC^{WT} *vs* MI+ CDC^{EngKO}**
ΔMean HR (bpm)	1.5±24.6	-8.3±31.8	8.5±19.7	7.8±13.7	0.956	n/a	n/a	n/a	n/a
ΔCO (ml/min)	1.8±2.2	4.9±1.1	3.1±2.4	2.3±1.1	0.284	n/a	n/a	n/a	n/a
ΔCI (ml/min/g)	0.004±0.07	0.2±0.04	0.11±0.08	0.08±0.04	0.309	n/a	n/a	n/a	n/a
ΔMean myocardial mass (mg)	7.9±2.7	21.7±7	8.5±1.7	12.8±4.5	0.096	n/a	n/a	n/a	n/a
ΔMean mass index (mg/g)	0.3±0.1	0.9±0.3	0.3±0.1	0.5±0.2	0.092	n/a	n/a	n/a	n/a
ΔEDV (μl)	6.7±1.1	64.2±12.8	27.3±5.4	29±11.2	0.004	0.003	0.015	0.094	0.885
ΔEDVI (μl/g)	0.3±0.1	2.6±0.6	1±0.2	1.1±0.5	0.007	0.007	0.015	0.127	0.781
ΔESV (μl)	2.7±2.7	51.9±12	23±7.6	24.3±12.8	0.035	0.006	0.071	0.189	0.926
ΔESVI (μl/g)	0.1±0.1	2.1±0.6	0.9±0.3	1±0.6	0.038	0.009	0.057	0.228	0.821
ΔSV (μl)	-1±6.8	12.4±3.9	4.5±4.8	4.7±2.1	0.442	n/a	n/a	n/a	n/a
ΔSVI (μl/g)	0.2±0.1	0.5±0.16	0.19±0.16	0.15±0.08	0.440	n/a	n/a	n/a	n/a
ΔEF (%)	-1.2±3.9	-0.2±2.1	-1.3±3.4	1.78±3.8	0.926	n/a	n/a	n/a	n/a
ΔInfarct size (%)	n/a	1.6±3.5	2.1±1.7	0.1±0.9	0.755	n/a	n/a	n/a	n/a

Table 6.3. Summary of changes in cardiac function between 1 and 4 weeks following MI and cell transplantation. All parameters are expressed as mean ± SEM. Table illustrates the results of one-way ANOVA and unpaired t-tests between specific pairs of groups, Significant values ($p<0.05$) are highlighted in red. Abbreviations: Δ, difference between week 1 and 4 measurement; HR, heart rate; CO, cardiac output; CI, cardiac index; EDV, end diastolic volume; EDVI, end diastolic volume index; ESV, end systolic volume; ESVI, end systolic volume index; SV, stroke volume; SVI, stroke volume index; EF, ejection fraction; LV, left ventricle; n/a = not applicable. MRI data analysis performed by Dr Ben Davison.

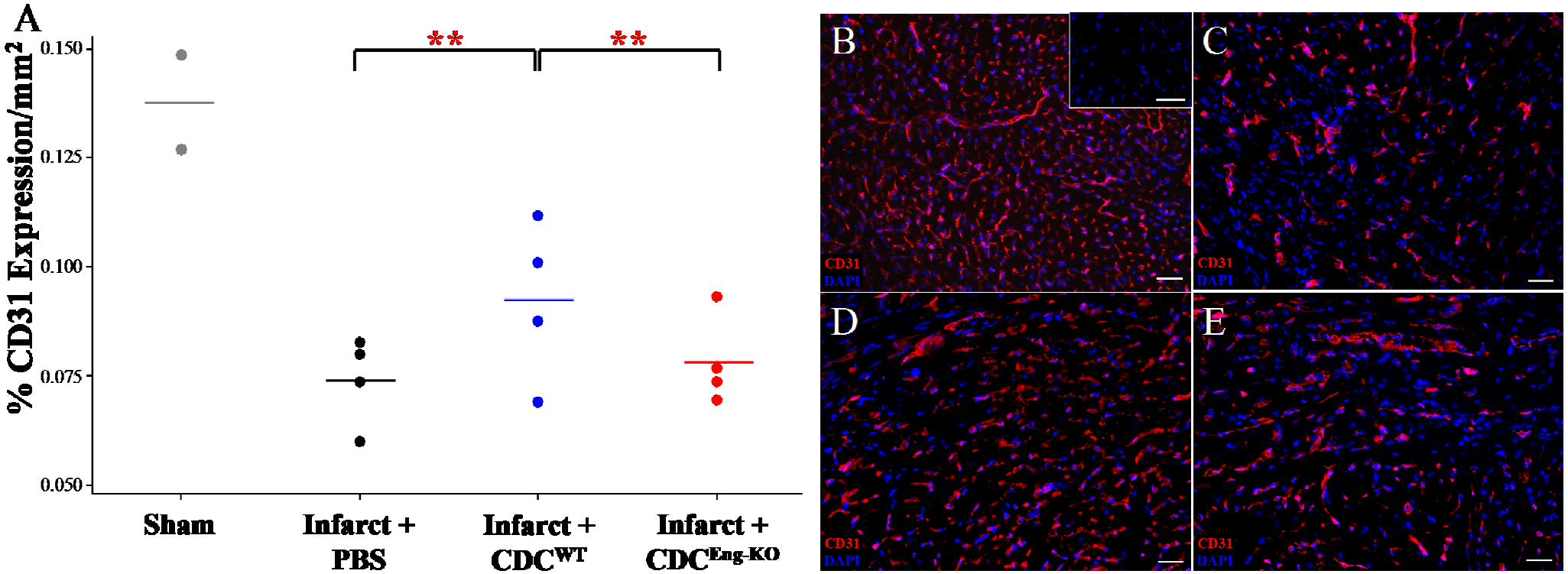

Figure 6.11. WT-CDC transplantation, but not Eng-iKO CDC infusion, results in an increased angiogenic response in the infarct border zone. Angiogenesis in the border zone of the infarcted heart was quantified using multiple CD31 immunostained sections (examples are shown in (B-E)) of hearts harvested 4 weeks post injury. Images were analysed using image J software and vessel density is represented as percentage CD31 expression per mm^2. WT-CDC injection into the border zone at the time of infarct led to an increased angiogenic response, which was significantly reduced when endoglin was genetically removed from the CDCs (A). Data was analysed using one-way ANOVA (p=0.001) and individual students t-test were performed to identify significant differences between pairs of groups. Representative images of the infarct border zone (or equivalent) in hearts of sham-operated mice (B, n=2), infarct with PBS injection (C, n=4), infarct with WT-CDC injection (D, n=4) and infarct with Eng-iKO CDC injection (E, n=4). Inset image (A) representative of no primary antibody control. ** denotes $p < 0.01$.

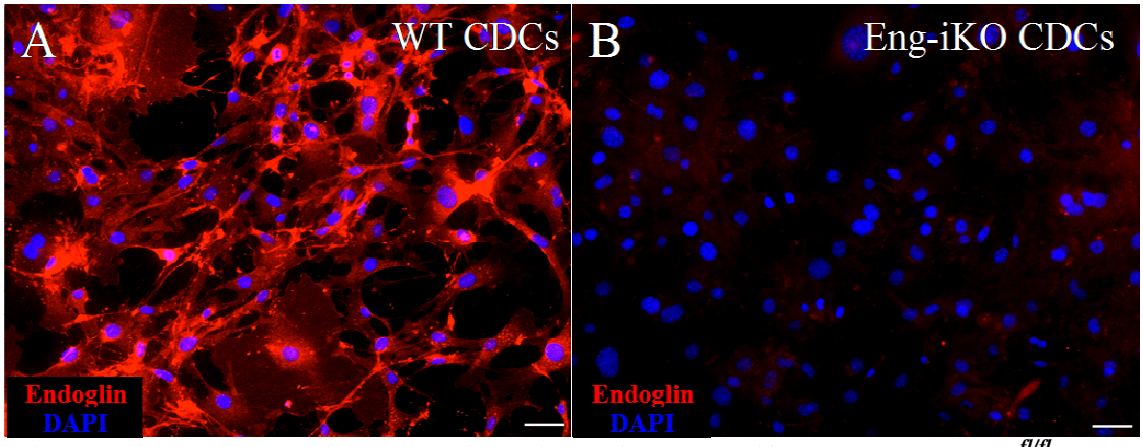

Figure 6.12. Endoglin depletion in 4OH-tamoxifen treated *Eng$^{fl/fl}$;Rosa-CreER^{T2};CAG-farnesyl-eGFP* CDC cultures. CDCs were immunostained with anti-endoglin (primary) and alexa-594 conjugated (secondary) antibodies (red). High endoglin expression is observed in WT-CDC cultures (A), whereas there is a marked reduction in expression in CDC cultures treated with 2μM 4OH-tamoxifen (B). Scale bar, 20μm. N.B. these cells were treated in the same way as those used for recipient expeimental mice and serve as an indicator of gene deletion efficiency.

Additionally, changes in cardiac function between 1 and 4 weeks following MI demonstrated significantly attenuated increases in myocardial mass index and LV volume indices in the Eng-iKO CDC injected group in comparison to PBS injected controls (figure 6.10). These differences are similar to those observed in the WT-CDC infused group (table 6.3) and suggest that both WT and Eng-iKO CDCs are able to reduce adverse LV remodelling following infarction. This data suggests that endoglin expression in CDCs is not necessary to improve cardiac function following LAD coronary occlusion and direct intramyocardial cell transplantation. Larger sample sizes would be required to verify this conclusion.

Interestingly analysis of vascularity (using anti-CD31 staining) revealed that intramyocardial injection of Eng-iKO CDCs led to significantly reduced angiogenesis in the border zone at 4 weeks following MI compared with WT CDCs (0.075±0.001 versus 0.088±0.003% CD31 expression/mm^2 (p<0.001) (figure 6.11). In fact levels of CD31 in Eng-iKO CDC treated mice were comparable to infarcted controls receiving only PBS (0.073±0.002% CD31 expression/mm^2 (p=0.545)) suggesting that endoglin expression is necessary to stimulate an enhanced angiogenic response in CDC mediated heart repair.

To follow up these results, I analysed the relationship between infarct border zone vessel density (measured as % CD31 expression/mm2) and infarct size as well as EF (as a readout of cardiac function) for each individual mouse using the pearson correlation method (figure 6.13). Interestingly no correlation was detected between CD31 expression and infarct size (r= 0.036, p= 0.915) or between CD31 expression and EF (r= -0.006 , p= 0.987), suggesting that in this study vessel density does not significantly correlate with either infarct size or global LV function (Figure 6.13). As expected infarct size displayed inverse correlation with EF (r= -0.977, p= 0.00; Figure 6.13E).

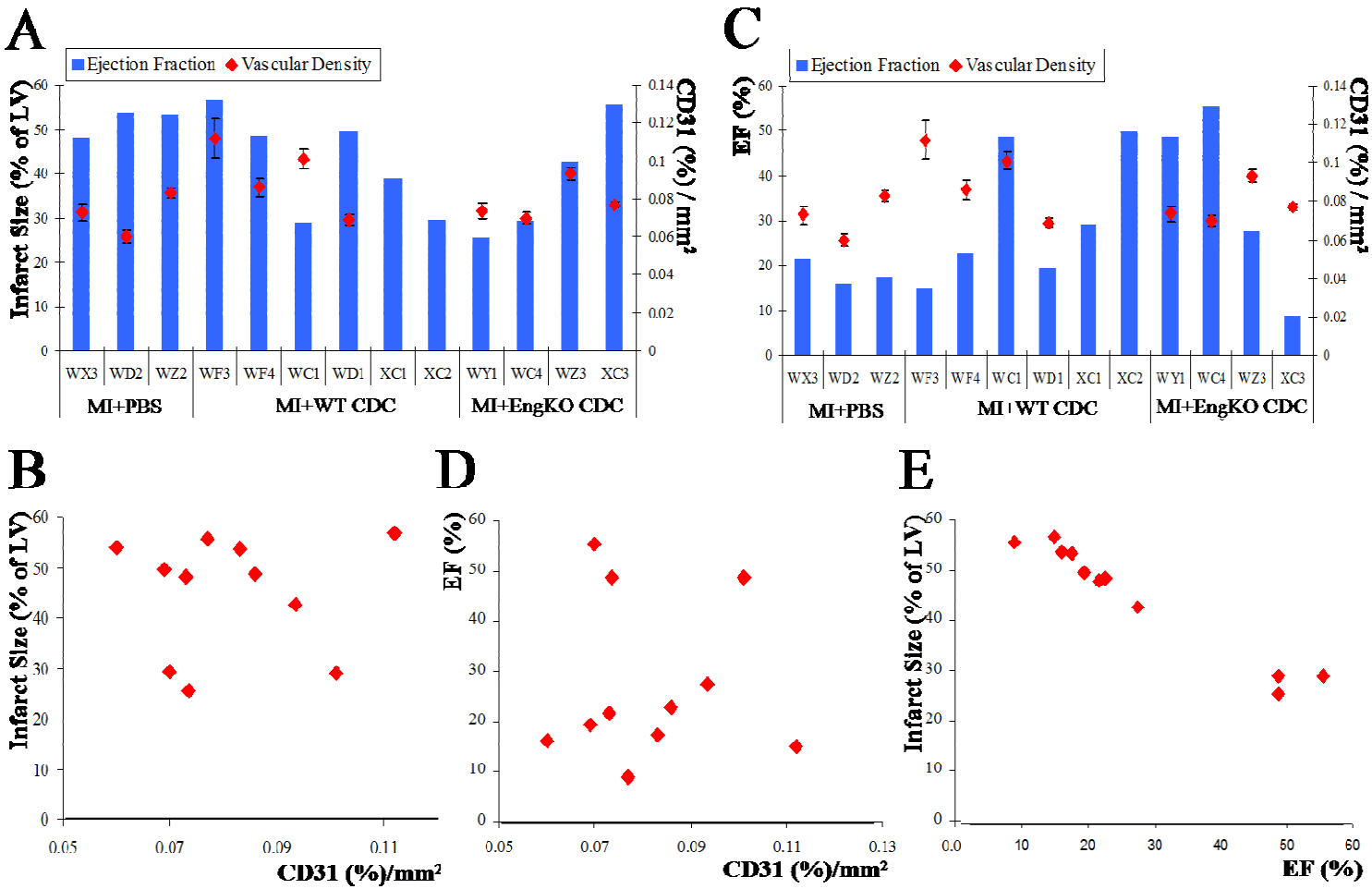

Figure 6.13. Relationship between ischaemic border zone vessel density and infarct size or EF. Charts displaying the vessel density of the infarct border zone per mm^2 (red) and either infarct size (% of LV; A, blue) or EF (%; C, blue) for each individual infarcted mouse included in this study. N.B. There is no correlation between blood vessel density in the infarct border zone and infarct size (r = 0.036, p = 0.915; B) or cardiac function as measured by EF (r = -0.006, p = 0.987; D). As expected infarct size displayed inverse correlation with EF (r = -0.977, p = 0.00; E).

6.2.2.5. Tracking GFP Positive CDCs 4 Weeks following Intramyocardial Transplantation into Infarcted Hearts

Transplanted CDCs were genetically tagged with eGFP (see section 6.2.2.1.) to allow *in vivo* tracking following intramyocardial cell injection 4 weeks following surgery. Multiple cryosections (approximately 6 to 8 per heart) from both WT-CDC (n=4) and Eng-iKO CDC (n=4) recipient hearts were stained with an anti-GFP antibody (directly conjugated to alexa 488). No eGFP expression was detected in sham-operated mice (n=2) or infarcted animals that received PBS only (n=4) (figure 6.14B). Of the cell injected groups, in 2 of 4 WT-CDC and 1 of 4 Eng-iKO-CDC recipient hearts analysed, I observed small clusters eGFP positive cells within the infarcted scar region, proximal to the border zone (figure 6.14A). This initially suggested survival of eGFP positive CDCs 4 weeks following intramyocardial injection.

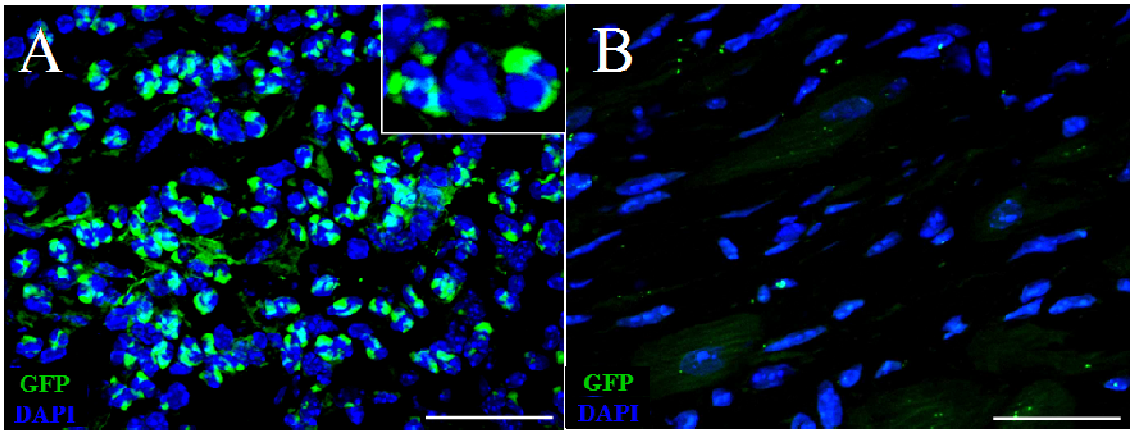

Figure 6.14. Identification of GFP positive cells within infarcted hearts 4 weeks following intramyocardial injection of eGFP tagged CDCs. Cryosections from CDC (A) and PBS (B) recipient hearts were stained with anti-GFP antibody (directly conjugated to alexa 488) and imaged using fluorescent microscopy. No GFP positive cells were identified in PBS treated heart tissue, whereas in 2/4 WT-CDC and 1/4 Eng-iKO-CDC recipient hearts included in this study I observed small clusters of small, round GFP positive cells in the scar tissue. Inset image (A) is a digital zoom magnification of representative GFP positive cells. Scale bars = 20μm.

Morphologically the vast majority of these GFP positive cells were small and round, resembling a primitive, stem-like cell rather than a terminally differentiated cell type. To assess whether transplanted CDCs differentiated into cardiomyocyte or vascular cells I co-stained heart cryosections with specific lineage markers (CD31, endoglin, α-actinin or α-SMA) and anti-GFP. Careful analysis revealed that none of the small GFP positive cells colocalised with any of these cell type specific markers (for representative

images see figure 6.15). This indicates that the pro-angiogenic effect generated by CDC infusion is most likely attributable to a paracrine mechanism. However, due to selective non-expression of eGFP in CAG-farnesyl-eGFP endothelial and aSMA cells (see section 6.2.2.1.) it is not possible to definitely determine lineage expression in this study. Additionally, within one WT-CDC recipient heart I was able to identify a very small number of eGFP positive cells (approximately 8-10, representing less than 2% of total visible eGFP positive cell population) that were larger and morphologically distinct to those previously described (figure 6.16.). Imaging of these cells required lower exposure times suggesting enhanced eGFP expression and approximately 3-4 cells co-stained with eGFP and either α-actinin, CD31 or endoglin. I used only double immunofluorescent staining (GFP and α-actinin, endoglin or CD31) so was unable to determine whether these GFP positive cells displayed antigenic plasticity and expressed multiple lineage markers (figure 6.16.).

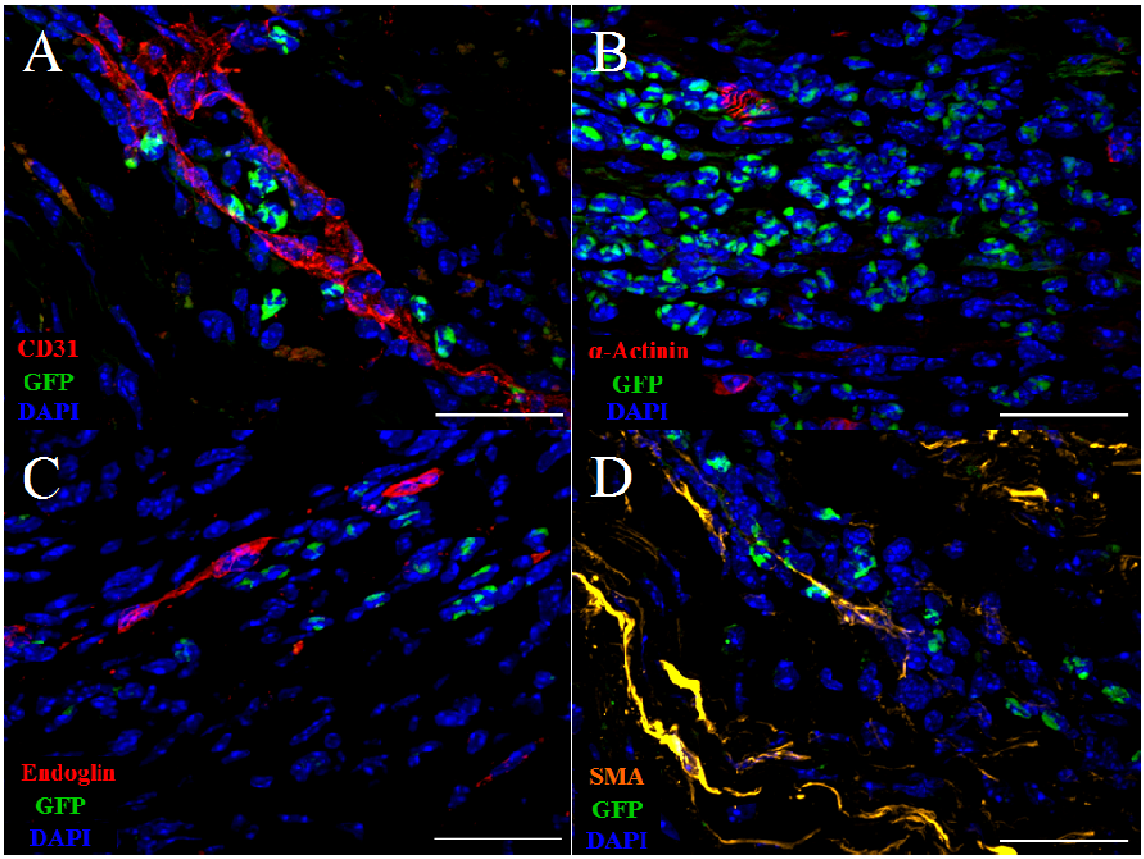

Figure 6.15. The majority of GFP positive cells do not express cardiac or vascular markers. Cryosections prepared from heart tissues 4 weeks after MI and cell transplantation were co-stained with anti-GFP antibody (conjugated to alexa 488, green) and either (A) anti-α-actinin, (B) anti-CD31 (C) anti-endoglin, (visualised using alexa 594 conjugated secondary antibodies, red) or (D) anti-SMA (conjugated to Cy5, orange). The images clearly show that GFP expression does not co-localise with any of the terminally differentiated cell type specific markers included in this analysis. This suggests that the cardioprotective effects associated with CDC transplantation are achieved by paracrine mechanisms. Inset images representative of no antibody (A) and no primary antibody (B) controls. Scale bars = 20μm.

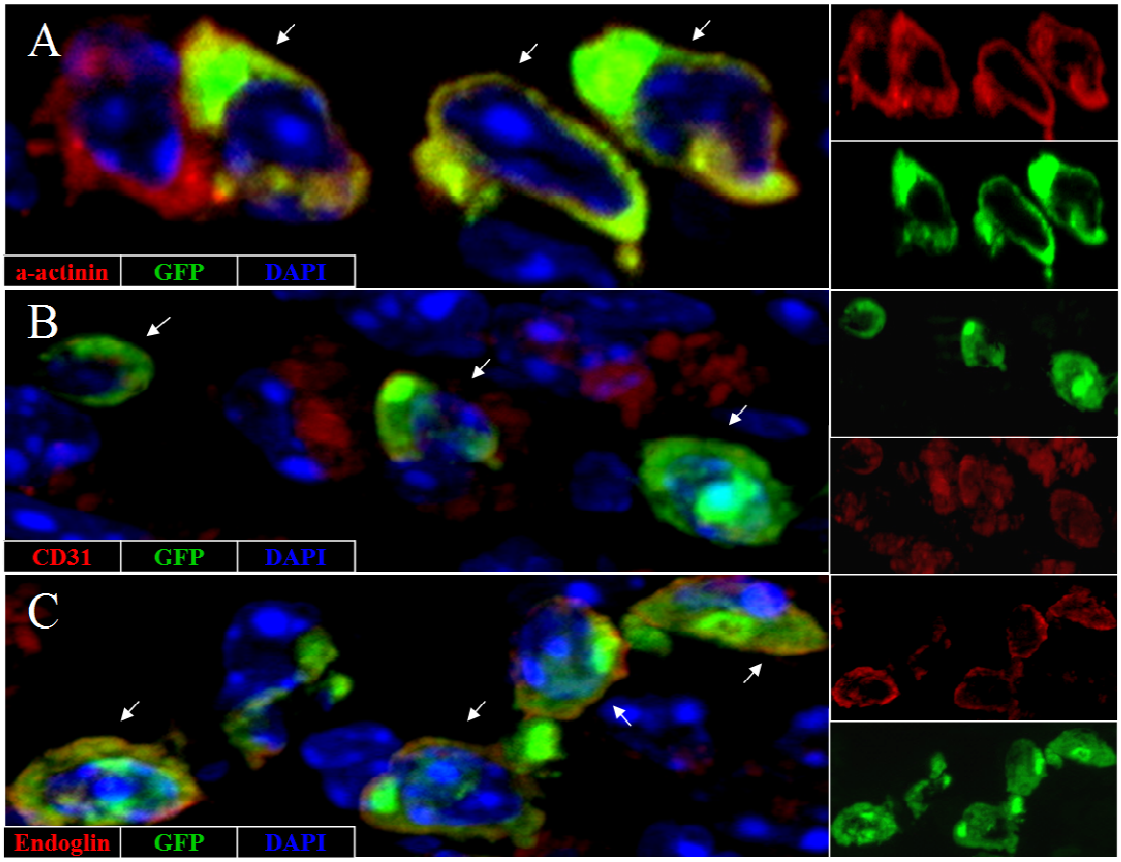

Figure 6.16. Co-expression of eGFP with cardiac and vascular markers in a WT-CDC recipient heart. Heart cryosections were co-stained with eGFP antibody conjugated to alexa 488 and either (A) α-actinin, (B) CD31 or (C) endoglin specific antibodies (visualised using alexa 594 conjugated secondary antibodies). A small number of eGFP positive cells co-expressed cell type specific markers in putative WT-CDCs (dual positive cells highlighted with white arrows).

Further analysis of stained heart sections revealed evidence of small, round eGFP positive cells (similar to those shown in figure 6.15) within the lumen of a blood vessel (figure 6.17) suggesting that these cells may represent an endogenous inflammatory infiltrate with the capacity to ingest transplanted eGFP positive CDCs or GFP-positive cell debris. To further characterise and identity these cells as either a donor cell population or resident inflammatory cells I co-stained heart sections with antibodies to GFP and either cKit or CD11b (a marker expressed predominantly by macrophages and monocytes but also by other immune response cell types including natural killer and granulocytes). I was unable to detect cKit expression although it is possible that the immunostaining method may require further optimisation. However, the majority of eGFP-positive cells were positive for CD11b (figure 6.18). The scale of CD11b positive cells strongly suggests that the eGFP expression observed in CDC recipient hearts

represents endogenous macrophages that have ingested donor GFP positive cells or cellular debris.

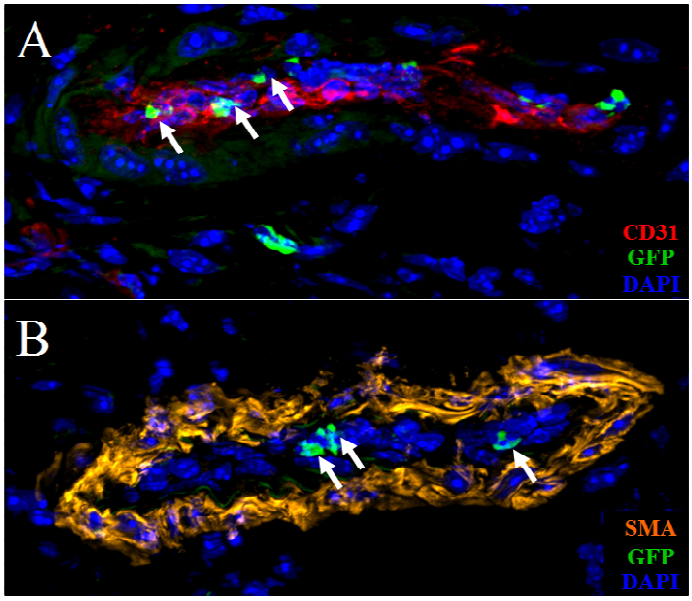

Figure 6.17. GFP positive cells within a blood vessel lumen. Serial heart cryosections from a WT-CDC recipient mouse were co-stained for GFP (green) and either CD31 (A, red) or SMA (B, orange) markers. Both images show GFP positive cells that appear to reside within the blood vessel lumen (see white arrows) consistent with a circulating cell population with the capacity to ingest GFP positive cells.

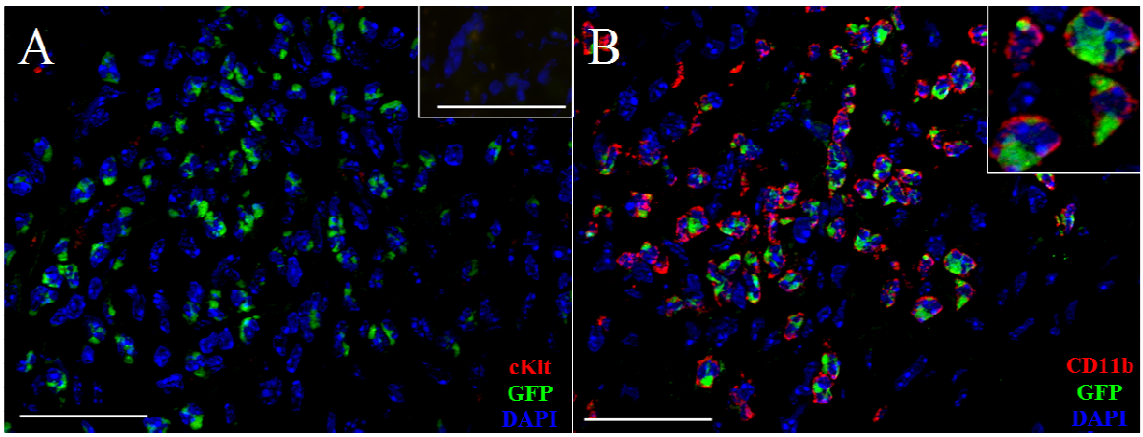

Figure 6.18. GFP positive cells within CDC recipient infarcted hearts express the macrophage marker CD11b but not cKit. Serial heart cryosections from a CDC recipient mouse were co-stained for GFP (green) and either cKit (A, red) or CD11b (B, red). These representative images clearly show that whilst eGFP positive cells do not express cKit, they do express the macrophage marker CD11b. These results suggest that the majority of observed GFP expression in CDC recipient hearts does not represent true transplanted donor cells but rather the remnants of these cells following inflammatory cell ingestion. Inset images representative of a no primary antibody control (A) and a digital zoom magnification of GFP/CD11b dual positive cells (B). Scale bars = 20μm.

6.3. Discussion

The aims of this study were to (i) confirm that mouse CDC transplantation rescues heart function following acute MI and (ii) to investigate if endoglin is essential in this process. Specifically, I tested whether or not increased endoglin expression results in an enhanced pro-angiogenic response in the infarct border zone.

Using a surgical MI mouse model I have successfully shown that intramyocardial injection of WT-CDCs into the infarct border zone leads to significantly attenuated adverse LV remodelling. At 4 weeks post MI, I observed an approximate 12% increase in EF as well as significantly reduced left ventricular volumes in those mice receiving WT-CDCs compared to PBS recipient controls. This improvement in cardiac function is comparable to other published studies[159, 161, 163, 169, 187] (see table 1.1 for study details) therefore I have independently confirmed the beneficial effect of CDC delivery following acute MI. Furthermore, this functional improvement was associated with increased neovessel formation in the ischaemic border zone. Deriving CDCs from *Eng$^{fl/fl}$;Rosa-CreER^{T2}* mice enabled me to test the effect of endoglin depletion *in vivo* following *in vitro* gene deletion. Surprisingly, I observed no significant difference between WT- and Eng-iKO-CDCs in their ability to rescue global LV function post infarct with both groups showing a similar increase in EF and decreased LV volumes compared to PBS recipient controls. However, in agreement with my original hypothesis intramyocardial injection of Eng-iKO CDCs did lead to significantly reduced angiogenesis in the infarct border zone 4 weeks following MI compared to WT-CDCs. In the following section I will discuss this discrepancy and suggest some alternative hypotheses to help explain these results.

The reduced secretion of VEGF[343], decreased NO synthase expression[353-354] as well as defective proliferation and migration[237, 264] observed in *Eng$^{+/-}$* endothelium helped lead to the hypothesis that endoglin depletion in cardiac repair cells would significantly impair post infarct neovascularisation resulting in deterioration of cardiac function. However the attenuation of adverse LV remodelling observed in Eng-iKO cell recipient mice has led me to revise this hypothesis. An alternative scenario that explains the improved cardiac function without concurrent increased neovascularisation, is that both WT and Eng-iKO CDCs are able to stimulate an enhanced angiogenic response in the

acute phase of infarct healing (within 7 days) via pleiotropic means. However, due to the important role of endoglin in vascular stabilisation and homeostasis, the neovessels formed following Eng-iKO CDC transplantation do not persist at later stages of remodelling (i.e. 4 weeks) when the analysis of angiogenesis was performed (Figure 6.11). As discussed in section 1.2 following MI a complex healing response consisting of cytokine release, inflammatory cell infiltration, EC proliferation and myofibroblast activity is necessary to create a mature scar[9]. At an early stage of the initial inflammatory response, neovessels form to support this healing process and during the maturation phase (approximately 7 days post-MI in mice) the neovessels regress from the infarct to prevent excessive fibrosis[9]. In this process exposed, uncoated neovessels regress, whilst other vessels acquire a mural coat, mature and stabilise. It has previously been shown that during mouse development, ECs lacking endoglin entirely are defective in their ability to process and secrete active TGFβ protein, which in turn affects their ability to differentiate and attract mural cells to the vessel wall[341]. Therefore defective processing of TGFβ or other cytokines associated with mural cell recruitment (e.g. PDGF-BB) by CDCs could play a role in the stability of neovessels. In this scenario endoglin loss may not affect CDC-mediated neovessel formation during the acute phase of infarct remodelling resulting in improved cardiac function, however due to an impaired ability to process and secrete important paracrine factors there is a failure to stabilise neovessels in the border zone through pericyte maturation and recruitment leading to their regression at a later stage. This would result in a lower vessel density at the border zone with decreased perfusion of viable myocardium which could increase the risk of heart failure at a later stage. To test this hypothesis it would be useful to compare CD31 and vascular smooth muscle staining of vessels at the infarct border zone at 1 week (which marks the peak phase of angiogenic activity[275]) and at 4 weeks post MI to compare vessel number as well as vessel maturation. It would also be interesting to perform a protein array analysis of CDC conditioned media with or without endoglin expression and assess the relative amounts of relevant cytokines and growth factors important in this process (e.g. TGFβ or PDGF-BB etc).

Infarct healing and repair actually encompasses a highly coordinated, complex process involving multiple networks of molecular mediators with pleiotropic effects, dictated by multiple cell types as well as spatial and temporal variables. As demonstrated by studies addressing the post infarct inflammatory response, pathways within this system often

display redundancy as well as pleiotropic, synergistic and antagonistic effects on each other[9]. In this respect it is plausible that therapeutic interventions aimed at enhancing cardiac repair may have both cardioprotective and injurious effects or indeed that an approach may have a beneficial effect on the mechanical and functional properties of the infarcted heart irrespective of deleterious changes elsewhere. With respect to the present study it is therefore possible that endoglin expression does mediate neovessel formation in the border zone but additional endoglin-independent CDC mediated effects attenuate adverse LV remodelling by other unknown mechanisms. For example, in addition to promoting angiogenesis the paracrine effects of CDCs may also attenuate mass cardiomyocyte loss which is the basic cause of heart failure following MI. Although this theory would have to be investigated (for example by looking at Akt and caspase protein levels or TUNEL staining), such an effect could be endoglin independent and hence help to explain the lack of significant differences in LV function between recipient groups following transplantation of WT and Eng-iKO CDCs. Further studies are required to investigate these mechanisms.

Regardless of the above suppositions regarding the role of endoglin in CDC-mediated repair, it is imperative that longer term studies are performed. Critically, it has been shown that although transplantation of human ESC derived cardiomyocytes into an experimental model of MI improves cardiac function at 4 weeks, this cardio-protective effect disappeared at 3 months[355]. This not only exemplifies the need for longer term studies to determine the efficacy of novel treatments but more specifically related to the current study, analysis of cardiac function and angiogenesis in CDC recipient mice at 3 months would also allow me to investigate whether or not the increased number of vessels observed in WT-CDC recipient hearts persist and similarly whether the decreased vessel density associated with Eng-iKO CDCs leads to deteriorated cardiac function or heart failure. Additional modifications to a second larger study would also include perfusion studies (e.g. with FITC lectin) to gauge whether neovessels associated with cell treatment are functional and ideally the inclusion of a cardiac fibroblast control group to exclude non-specific effects of CDC transplantation.

An important limitation of this study is the small group sizes, which occurred as a result of peri-operative mortality which was high in all groups: sham operated mice, 43% (n=7); MI mice with PBS 60% (n=10); and MI with CDC transfer 50% (n=36). This

was due to problems with anaesthesia and ventilation that induced a condition diagnosed as 'exaggerated breathing reflex' (Paul Flecknell personal communication). The original power calculations used to determine group numbers assumed a 17% difference in LVEF[159] and indicated that groups of 8 animals would provide 80% power at alpha 0.05. I therefore intended to begin with groups of 10 animals to allow for 20% mortality however the final sample sizes were between 3 and 6 mice per group. This gave insufficient power to provide reliable answers to the questions under investigation. Therefore although this study provides important preliminary data, larger animal numbers are required to reliably interpret results.

Follow up investigation of this problem revealed that peri-operative mortality was also observed in intubated/ventilated mice that did not undergo thoracotomy. Mice were adequately anaesthetised with depth assessed by testing the loss of primitive reflexes (e.g. pedal reflex) as more sophisticated measures of depth were not available (e.g. MAC – minimum alveolar concentration). Inspiratory and expiratory ventilatory pressures were determined using pre-set parameters provided by the ventilator manufacturer (standardised to mouse weight). I routinely used a mouse pulse oximeter to measure oxygen saturation and found it to be consistently >90% and body temperature was maintained at 37^{o}C. Additionally it would have been informative to measure CO_2 levels, but unfortunately our rodent capnograph did not provide reliable results. Several precautions were taken to minimise the impact of this anaesthesia/mechanical ventilation related problem, including optimisation of ventilator parameters (stroke volume and rate) to oppose any possible retention of CO_2 and also the administration of a pre-anaesthetic sedative (0.2ml/kg hypnorm administered via I.P injection prior to inducing surgical depth of anaesthesia with isoflurane). Following the completion of this study we discovered that our Harvard minivent was delivering a stroke volume that was approximately 20% lower than that which was set. We have since invested in a Harvard 687 volume controlled rodent ventilator which allows increased control over stroke volume and rate but also offers the ability to introduce positive end expiratory pressure and change the inspiration: expiration ratio. This new ventilator will allow a larger more refined study to be performed to give adequate group sizes.

The reduced power of the study is further confounded by an increase in infarct variability which occurred as a result of the problems associated with sub-optimal anaesthesia and mechanical ventilation protocols. The extent of adverse LV remodelling following MI is directly proportional to infarct size[9] and similarly decreasing capillary density in the infarct border zone is observed with increasing infarct size[350]. Therefore, the generation of infarcts of comparable size between experimental groups is critically important when testing interventions aimed at influencing LV remodelling and angiogenesis. The murine LAD coronary artery occlusion model is known to produce a wide range of infarct sizes (10-70% of the LV)[356], most likely due to differences in rodent coronary artery branching patterns which are apparent even between littermates[357]. However with careful attention to surgical technique it is possible to reduce variability in infarct size by placing ligations proximal to the site where the artery emerges from under the left atria, immediately before the bifurcation of the major left coronary artery and also by eliminating mice that clearly show evidence of exceptionally small or large infarcts as indicated by the degree of myocardial blanching seen directly following coronary artery occlusion (see figure 6.1). Serial contrast-enhanced studies have indicated that infarct size in mice reaches 95% of its final size within 1 hour in a reperfusion model of experimental MI[12]. This indicates that it would be advantageous to measure infarct size using a non-invasive technique such as MRI[358] at an early time point i.e. within 24-48 hours following infarct (allowing some time for the animal to recuperate) to give baseline data. However for my infarcted mice this was not possible due to cardiac surgery and MR imaging being performed at different sites (approximately one mile apart) and strict regulations regarding animal transportation. Therefore the earliest time point that infarct size could be measured was 1 week following MI. To give an indication of the variation in infarct size that I initially observed after establishing the MI model, MRI was used in a pilot group of mice (n=10) 4 weeks following coronary artery occlusion (table 6.1.). Infarcted tissue was characterized as the area of akinesis and the infarct size measurement is calculated as a percentage of the LV wall using mid-ventricular end-diastolic cine MRI slices and the following dimensions; length of infarcted epicardial and endocardial circumference and length of total epicardial and endocardial circumference. Infarct size ranged from 27.6-45% of the LV wall with a mean size of 36.2±1.8% indicating good reproducibility which is essential to detect changes in cardiac structural and functional parameters (table 6.1.). However, in the current study (with its increased mortality) although infarct

size measurements recorded at both 1 week and 4 weeks following coronary artery occlusion showed no significant differences between groups, marked variation within groups was noted (table 6.2). This could be directly due to cell treatment or, if associated with variation in surgical technique, an important confounding factor in conjunction with small sample sizes. Interestingly, no correlation between border zone vascularity and either infarct size or EF was observed as would have been expected. This is potentially due to compensatory endogenous repair mechanisms as discussed above but may also reflect the reduced power of the study (i.e. small sample sizes and increased variation in surgical technique) and further illustrates the need for larger group sizes.

At week 4, I analysed eGFP expression in heart cryosections and observed what I believed to be putative donor CDCs. However further analysis revealed that these cells were negative for both endoglin and cKit (both markers of CDC subsets), but were CD11b positive. Therefore they most likely represent host response inflammatory cells. The implications of this are unknown but it is worthy of note that such a strong immune response is still present at 4 weeks following infarct and it would be interesting to study this in greater detail to ascertain whether the endogenous immune response plays an important role in CDC mediated repair. Although an excessive or extended inflammatory response can be deleterious and extend cardiac injury[9], substantial evidence has shown that the immune response in the post-infarct heart can promote repair by enhancing phagocytosis and paracrine secretion of growth factors and cytokines related to scar formation and angiogenesis[9]. Additionally it would be desirable to investigate whether endoglin loss differentially affects this process (e.g. by attracting different subsets of circulating immune cells to the healing infarct). A very small number of GFP cells co-stained with terminally differentiated cell markers however they appeared primitive in morphology rather than mature, functioning vascular or cardiac cells. Therefore this data suggests that the cardioprotective effects of CDC transplantation result from paracrine mechanisms rather than direct cellular differentiation. Secreted angiogenic factors (such as VEGF, bFGF or EGF) could be analysed using a protein array to help us to begin to define the precise mechanisms that have led to this CDC-dependent repair. It would also be useful to track GFP expression at earlier time points to assess how long these cells remain within the myocardium and

possibly to introduce strategies aimed at propagating their effect *in vivo* (such as sealing the injection site with fibrin glue[194] or employing magnetic targeting[161].

Van Laake *et al*[275] have also tested the ability of endoglin deficient cells to rescue heart function following experimental MI in mice. Importantly whereas both of our studies show reduced neoangiogenesis in the infarct border zone following injection of endoglin deficient cells versus WT controls, van Laake and colleagues further demonstrate that $Eng^{+/-}$ cells are impaired in their ability to rescue heart function. However there are several important differences between this study and my own. Primarily, in the van Laake study human circulating MNCs (derived from healthy volunteers or HHT1 patients) were systemically delivered to the mouse via tail vein injection 1 to 3 hours following surgery whereas I delivered murine CDCs (with or without genetic deletion of endoglin) via intramyocardial injection. This is an important distinction because by delivering the cells into the peripheral circulation the authors were in effect also measuring the ability of these cells to home to the ischaemic heart rather than directly assessing their contribution to heart repair and angiogenesis. Indeed $Eng^{+/-}$ MNCs were found to reach the heart at a significantly lower rate than WT cells[275] and a subsequent study has gone on to show that these cells have a defective SDF1/CXCR4 homing axis[276]. Thus it is not known whether the delivery of a similar number of WT and $Eng^{+/-}$ MNCs directly into the heart would have rescued cardiac function to a similar degree. Furthermore van Laake *et al*[275] only delivered cells to infarcted $Eng^{+/-}$ mice which show a defective angiogenic response and a greater deterioration in cardiac function relative to WT animals following MI. Therefore this study informs on the ability of transplanted cells to restore cardiac function in patients with defective TGFβ signalling (e.g. HHT patients) and suggests that BM cell-mediated endogenous repair is impaired in these individuals and that they would benefit less from autologous BM infusion into the heart. It would be of interest to know whether the same outcomes would occur following MI and cell transplantation in WT mice. A further obvious difference between the two studies is cell type. It is possible that CDCs have a greater ability to attenuate adverse LV remodelling than MNCs independent of angiogenic response. In addition the mice used in the van Laake study were immunosuppressed and it is possible that this may have affected WT and $Eng^{+/-}$ cells differently.

The work described in this chapter confirms that CDC transfer can produce benefit over 4 weeks post MI with an associated increase in neoangiogenesis. The mechanism underlying this repair is likely a paracrine one however the exact role of endoglin in this process remains uncertain and will require further study.

CHAPTER 7.

Final Discussion and Future Directions

TGFβ signalling mediates a range of cellular responses in a variety of cell types and the canonical TGFβ/Smad signalling pathway is known to regulate endothelial activation and is essential for angiogenesis. Many studies support the TGFβ/Alk1 versus TGFβ/Alk5 angiogenic switch hypothesis in which the former pathway is pro-angiogenic while the latter is important for the resolution phase of angiogenesis[204]. In this model endoglin is able to mediate the angiogenic response and is thought to be a positive regulator of TGFβ/Alk1 and angiogenic activation while antagonistically regulating the TGFβ/Alk5 pathway[237]. However conflicting reports have arisen and it is now accepted that endoglin's role is likely to be context dependent[306].

I hypothesised that the endothelial TGFβ signalling axis plays an important role in cardiac repair cell biology; specifically by mediating cellular proliferation, differentiation and pro-angiogenic properties.

In chapter 3 I have shown that the inhibition of Alk5 kinase activity leads to an increased yield of WT BM-derived STC-EPCs. This suggests that manipulating the TGFβ/Alk5 pathway in EPCs could have clinical applications and may be used to expand endothelial progenitors *ex vivo*. However the effect of Alk5 inhibition on the ability of cells to contribute to angiogenesis *in vivo* would also have to be investigated. While my data indicated that Alk5 inhibition resulted in increased cellular proliferation it is also possible that inhibiting TGFβ/Alk5 signalling facilitates endothelial differentiation by blocking the acquisition of a mesenchymal phenotype. This hypothesis is in agreement with the findings of Diez *et al*[299] as they have reported that the process of EndMT is abrogated in EPCs treated with an Alk5 inhibitor. I also found that endoglin deficient BM-MNC cultures (derived from $Eng^{+/-}$ mice) yielded a reduced number of STC-EPCs in comparison to WT cultures indicating that endoglin expression is important in EPC proliferation and/or endothelial differentiation. Interestingly, I did not detect a difference in proliferation/viability between WT and $Eng^{+/-}$ cells as may have been expected. Therefore my data suggests that endoglin may play a more prominent role in the differentiation, rather than the proliferation, of endothelial progenitors. This is in contrast to studies suggesting that endothelial differentiation is unaffected by endoglin loss during development[232-234]. However, I did find that treatment of $Eng^{+/-}$ BM-MNC cultures with the Alk5 inhibitor rescued the associated reduction in STC-EPC number with levels increasing to those observed with WT cells.

This shows that endoglin is important in modulating vascular progenitor cell fate and it is possible that endoglin may also have an important role in EndMT. This would help to explain how Alk5 inhibition is able to counteract the effects of endoglin deficiency. Indeed endoglin has an identified role in the mediation of the related process of epithelial-to-mesenchymal transition (EMT) during development[359] and there is growing interest to elucidate whether endoglin is also involved in EMT or EndMT leading to cardiac fibrosis. Additional work is required to elucidate the exact mechanisms of action underlying the observations made in this study. Nethertheless my findings do suggest that TGFβ and endoglin play regulatory roles in endothelial progenitors and manipulation of these signalling pathways may prove to be of therapeutic benefit.

In chapter 4 I tested whether endothelial-specific endoglin depletion would result in EC replacement by BM-derived progenitor cells. My subsequent analysis of cardiac and pulmonary vasculature did not support this hypothesis. However I did observe an increase in endoglin expression within the BM of Eng-iKO mutant animals suggesting that endoglin positive cells expand in response to vascular assault. However, Eng-iKO adult mice appear phenotypically normal and no evidence of vascular malformations have been detected in the lung vasculature following endoglin depletion (personal communication, Dr Marwa Mahmoud). This is likely due to the fact that the role of endoglin in mediating TGFβ signalling in the endothelium is largely restricted to areas of active angiogenesis whereas the adult pulmonary vasculature is likely to remain relatively quiescent. Therefore it may be that a second pathological and/or angiogenic stimulus, such as inflammation or ischaemia, is required for EPC mobilisation from the BM and subsequent repair/replacement of the endoglin deficient endothelium. Indeed in HHT1 patients vascular lesions appear at distinct sites in certain organs and Bernabeu *et al*[306] hypothesise that this is because an external trigger (e.g. infection) is required that synergises with endoglin deficiency to generate a lesion localised to the area of the trigger. Mahmoud *et al*[270] support this model of 'second hit' by showing that in a conditional Eng-iKO model AVMs form only when endoglin loss is combined with an angiogenic stimulus. Therefore, in a similar way an additional angiogenic stimulus may be required to mobilise the expanded BM-resident endothelial progenitors.

In chapters 5 and 6 I analysed the effect of endoglin loss on CDCs both *in vitro* and *in vivo*. *In vitro* data revealed that endoglin depletion results in a small but significant

reduction in cellular proliferation and migration which concurs with a positive role for endoglin in endothelial cell proliferation and angiogenesis as reported by several published *in vitro* studies (refer to section 1.9.3). Unexpectedly, endoglin loss in CDCs did not affect TGFβ/Alk1 responses (as indicated by western blotting for phospho-Smad1). This was in contrast to reported effects of endoglin depletion on pSmad1 signalling in ECs[237] and any effects may have been masked by the high basal levels of signalling caused by the serum rich media used for this work. The increased levels of phospho-Smad2 that I detected in Eng-iKO CDCs, indicating that the TGFβ/Alk5 pathway is upregulated in the absence of endoglin, was in agreement with the previously reported role of endoglin in the canonical TGFβ signalling pathway in ECs. I then proceeded to test whether endoglin loss affected CDC-mediated angiogenic responses and functional rescue *in vivo* using a murine MI model. Following LAD coronary artery ligation the transplantation of WT cells resulted in a significant improvement in cardiac function as evidenced by an increase in EF and an attenuation of adverse LV remodelling. This was associated with a significant increase in ischaemic border zone vessel density at 4 weeks as compared with PBS injected controls. Intramyocardial injection of Eng-iKO cells led to significantly reduced angiogenesis relative to WT-CDC recipient mice though intriguingly cardiac function in these two groups was comparable. This suggests that while endoglin is likely to be important in mediating the pro-angiogenic effects of CDCs *in vivo*, endoglin-independent mechanisms may be responsible for improving cardiac function by other means, for example by preserving cardiomyocyte viability. I also observed that very few donor cells differentiated to vascular or cardiac cell phenotypes indicating that CDCs generated a pro-angiogenic effect and improved cardiac function via a paracrine mechanism. In addition only a small number of CDCs were detected in recipient hearts at 4 weeks suggesting that the pro-repair effects of transplanted cells occur at an early stage following infarct. Given the length of time taken to culture CDCs (approximately 4-6 weeks from human tissue[159]) this will be an important consideration in the clinical transition of CDC therapy. This is further made evident by meta-analysis data indicating that cardiac function is improved to a significantly greater degree when BM cells are transplanted within 7 days of MI[135] and the knowledge that early cell-based intervention following MI is likely to promote vascular regeneration to a greater extent than treatment at later stages. Therefore alternative options such as a readily available tissue

typed cell bank or the use of universal donor cells that possess immune privilege may be required for the optimisation of future cell-based therapies.
The general aims of future studies will be to investigate the mechanisms underlying the role of endoglin in CDC-mediated repair as well as optimising efficient neovessel formation following ischaemic heart injury.

I have shown that endoglin depletion impairs the ability of CDCs to stimulate an increased angiogenic response in the ischaemic border zone of mice following MI. The mechanisms underlying this defect remain unclear therefore it will be important to further investigate the precise role that endoglin plays in CDC-mediated pro-angiogenic repair. Given that my findings suggest that transplanted cells act via paracrine means it would be advantageous to assess which proteins are synthesised by CDCs (with and without endoglin depletion) using a protein array focusing on angiogenesis and mural cell recruitment. To help inform on prospective targets I could take advantage of a custom Q-PCR array developed in my host laboratory for analysis of gene expression downstream of endoglin in primary ECs to reveal pathways and specific components required to promote CDC-mediated angiogenesis. In addition given that very few donor cells were detected in recipient hearts at 4 weeks post MI my data also indicates that CDCs may exert their effects at an earlier stage of remodelling therefore it may prove more informative to analyse tissue at 1 week as this represents the stage of maximal angiogenic response. At this earlier time point an in depth assessment of vessel size and density would be performed as well as tracking genetically tagged donor cells. In addition it will be essential to assess the effect of endoglin loss in CDCs on heart repair and angiogenesis over a longer time course (minimum of 12 weeks) to assess whether the effects observed at 4 weeks persist. Vascular perfusion studies could also be performed by injecting FITC-lectin into tail veins prior to harvest to inform on whether the neovessels are functional.

It will also be important to progress to utilising more clinically relevant models such as a MI reperfusion mouse model (see section 6.1). Furthermore, in this thesis the CDCs used in all experiments described in chapters 5 and 6 were derived from neonatal tissue primarily due to the reduced time required for culture compared with adult hearts (approximately 5 weeks versus over 8 weeks using adult mouse heart tissue). The use of adult–derived cells in future studies would provide a more clinically relevant scenario.

However, the use of human CDCs derived from atrial tissue obtained from surgical waste is achievable and represents the gold standard of cell-type for pre-clinical studies. In addition to investigating the role of endoglin in CDC-mediated heart repair another major focus of future studies will be to develop strategies to optimise efficient neovessel formation *in vivo*. On going work in my host laboratory is the investigation into whether pre-acclimatising CDCs to sub-physiological oxygen levels (3%) prior to injecting into a heart repair model will improve donor cell survival and promote a greater angiogenic response. Furthermore, the Bischoff laboratory have shown that a combination of endothelial progenitor and mesenchymal cells are able to generate neovessels with a higher efficiency than either cell type alone using an *in vivo* subdermal Matrigel mouse model[107]. Therefore we would like to investigate if supplementing CDCs (which express mesenchymal markers such as CD90 and endoglin) with an endothelial cell source (for example human circulating EPCs or human cells derived from induced pluripotent fibroblast cells that are differentiated to an endothelial lineage) would enhance CDC-mediated angiogenesis and improve cardiac function to a greater extent than CDCs alone.

The results of recent clinic trials assessing the safety and efficacy of BM and cardiac stem cell therapy for MI patients have revealed this to be a promising avenue to pursue however cell types tend to be poorly defined and only modest positive effects have been observed. Therefore to improve patient outcomes functionally active cells need to be better characterised and it would be advantageous to actively prime these cells for repair, for example by exposing cells to sub-physiological oxygen levels as described above. Future work on endoglin and TGFβ could potentially influence further improvements for example the enrichment of endoglin expressing cells may lead to enhanced pro-angiogenic repair. Additionally, it is known that there are dynamic changes in TGFβ ligand expression following MI such that levels of TGFβ1 are elevated from 3 days post infarction for up to 8 weeks in rodents. While it is believed that TGFβ1 plays a beneficial role in infarct healing at a very early stage (24-72 hours following infarct) by suppressing a deleterious immune response and promoting fibrosis, thereafter this ligand is thought to cause harm by inhibiting efficient scar tissue formation[360]. However little is known about the effect of TGFβ1 on vessel formation in the infarcted heart therefore it would be interesting to investigate the effect of inhibiting this ligand in both early and late preclinical models of MI and focussing both on

vascular regeneration as well as inflammatory cell recruitment. Indeed an improved understanding of the panel of TGFβ family cytokine (including BMP9, a circulating angiogenic quiescence factor) expression following infarct may facilitate in optimising pro-angiogenic therapy. Expanding this point in more general terms evidence suggests that indirect (paracrine) effects may be more relevant to cell-mediated repair than direct cellular differentiation and regeneration. Although further research is required to validate this theory and evaluate the relative contribution of paracrine factors, it may transpire that delivery of an optimised array of paracrine factors via slow release nanobeads may be a more useful treatment than cell transplantation. Further work is awaited.

The results reported in this thesis serve to highlight the important regulatory and pro-angiogenic roles that TGFβ signalling and endoglin are likely to play in cell-mediated cardiac repair. Additional pre-clinical studies such as those outlined above will be required to verify these conclusions and may provide direction to enable the translation of this knowledge to the development of more effective future therapies.

REFERENCES

1. Carmeliet P. Mechanisms of angiogenesis and arteriogenesis. Nature Medicine 2000;6:389-95.
2. Carmeliet P. Angiogenesis in life, disease and medicine. Nature 2005;438:932-6.
3. Adams RH, Alitalo K. Molecular regulation of angiogenesis and lymphangiogenesis. Nat Rev Mol Cell Biol 2007;8:464-78.
4. Kamei M, Brian Saunders W, Bayless KJ, Dye L, Davis GE, Weinstein BM. Endothelial tubes assemble from intracellular vacuoles in vivo. Nature 2006;442:453-6.
5. Betsholtz C, Lindblom P, Gerhardt H. Role of pericytes in vascular morphogenesis Mechanisms of Angiogenesis. In: Clauss M, Breier G, eds.: Birkhäuser Basel; 2005:115-25.
6. Goumans MJ, Lebrin F, Valdimarsdottir G. Controlling the angiogenic switch: A balance between two distinct TGF-β receptor signaling pathways. Trends in Cardiovascular Medicine 2003;13:301-7.
7. ten Dijke P, Arthur HM. Extracellular control of TGF[beta] signalling in vascular development and disease. Nat Rev Mol Cell Biol 2007;8:857-69.
8. Tonnesen MG, Feng X, Clark RAF. Angiogenesis in Wound Healing. J Investig Dermatol Symp Proc 2000;5:40-6.
9. Frangogiannis NG. The immune system and cardiac repair. Pharmacological Research 2008;58:88-111.
10. Jopling C, Sleep E, Raya M, Marti M, Raya A, Izpisua Belmonte J. Zebrafish heart regeneration occurs by cardiomyocyte dedifferentiation and proliferation. Circ Res 2010;107:570-2.
11. Porrello ER, Mahmoud AI, Simpson E, et al. Transient Regenerative Potential of the Neonatal Mouse Heart. Science 2011;331:1078-80.
12. French BA, Kramer CM. Mechanisms of postinfarct left ventricular remodeling. Drug Discovery Today: Disease Mechanisms 2007;4:185-96.
13. Sutton MGSJ, Sharpe N. Left Ventricular Remodeling After Myocardial Infarction : Pathophysiology and Therapy. Circulation 2000;101:2981-8.
14. Ren G, Michael LH, Entman ML, Frangogiannis NG. Morphological Characteristics of the Microvasculature in Healing Myocardial Infarcts. Journal of Histochemistry & Cytochemistry 2002;50:71-9.
15. Lee SH, Wolf PL, Escudero R, Deutsch R, Jamieson SW, Thistlethwaite PA. Early Expression of Angiogenesis Factors in Acute Myocardial Ischemia and Infarction. New England Journal of Medicine 2000;342:626-33.
16. Virag JI, Murry CE. Myofibroblast and Endothelial Cell Proliferation during Murine Myocardial Infarct Repair. The American Journal of Pathology 2003;163:2433-40.
17. Helisch A, Schaper W. Arteriogenesis The Development and Growth of Collateral Arteries. Microcirculation 2003;10:83-97.
18. Sabia PJ, Powers ER, Ragosta M, Sarembock IJ, Burwell LR, Kaul S. An Association between Collateral Blood Flow and Myocardial Viability in Patients with Recent Myocardial Infarction. New England Journal of Medicine 1992;327:1825-31.
19. Losordo DW, Dimmeler S. Therapeutic angiogenesis and vasculogenesis for ischemic disease. Part I: angiogenic cytokines. Circulation 2004;109:2487-91.
20. Dor Y, Djonov V, Abramovitch R, et al. Conditional switching of VEGF provides new insights into adult neovascularization and pro-angiogenic therapy. EMBO J 2002;21:1939-47.

21. Zachary I, Morgan RD. Therapeutic angiogenesis for cardiovascular disease: biological context, challenges, prospects. Heart 2011;97:181-9.
22. Malliaras K, Marbán E. Cardiac cell therapy: where we've been, where we are, and where we should be headed. British Medical Bulletin 2011;98:161-85.
23. Davis DR, Stewart DJ. Autologous cell therapy for cardiac repair. Expert Opinion on Biological Therapy 2011;11:489-508.
24. Asahara T, Murohara T, Sullivan A, et al. Isolation of Putative Progenitor Endothelial Cells for Angiogenesis. Science 1997;275:964-6.
25. Timmermans F, Plum J, Yöder MC, Ingram DA, Vandekerckhove B, Case J. Endothelial progenitor cells: identity defined? Journal of Cellular and Molecular Medicine 2009;13:87-102.
26. Prater DN, Case J, Ingram DA, Yoder MC. Working hypothesis to redefine endothelial progenitor cells. Leukemia 2007;21:1141-9.
27. Peichev M, Naiyer AJ, Pereira D, et al. Expression of VEGFR-2 and AC133 by circulating human CD34+ cells identifies a population of functional endothelial precursors. Blood 2000;95:952-8.
28. Reyes M, Dudek A, Jahagirdar B, Koodie L, Marker PH, Verfaillie CM. Origin of endothelial progenitors in human postnatal bone marrow. The Journal of Clinical Investigation 2002;109:337-46.
29. Shi Q, Rafii S, Wu MH-D, et al. Evidence for Circulating Bone Marrow-Derived Endothelial Cells. Blood 1998;92:362-7.
30. Cheng J, Baumhueter S, Cacalano G, et al. Hematopoietic defects in mice lacking the sialomucin CD34. Blood 1996;87:479-90.
31. Fina L, Molgaard H, Robertson D, et al. Expression of the CD34 gene in vascular endothelial cells. Blood 1990;75:2417-26.
32. Shalaby F, Rossant J, Yamaguchi TP, et al. Failure of blood-island formation and vasculogenesis in Flk-1-deficient mice. Nature 1995;376:62-6.
33. Shalaby F, Ho J, Stanford WL, et al. A Requirement for Flk1 in Primitive and Definitive Hematopoiesis and Vasculogenesis. Cell 1997;89:981-90.
34. Yin AH, Miraglia S, Zanjani ED, et al. AC133, a Novel Marker for Human Hematopoietic Stem and Progenitor Cells. Blood 1997;90:5002-12.
35. Gehling UM, Ergün S, Schumacher U, et al. In vitro differentiation of endothelial cells from AC133-positive progenitor cells. Blood 2000;95:3106-12.
36. Quirici N, Soligo D, Caneva L, Servida F, Bossolasco P, Deliliers GL. Differentiation and expansion of endothelial cells from human bone marrow CD133+ cells. British Journal of Haematology 2001;115:186-94.
37. Garlanda C, Dejana E. Heterogeneity of Endothelial Cells : Specific Markers. Arterioscler Thromb Vasc Biol 1997;17:1193-202.
38. Case J, Mead LE, Bessler WK, et al. Human CD34+AC133+VEGFR-2+ cells are not endothelial progenitor cells but distinct, primitive hematopoietic progenitors. Experimental Hematology 2007;35:1109-18.
39. Timmermans F, Van Hauwermeiren F, De Smedt M, et al. Endothelial Outgrowth Cells Are Not Derived From CD133+ Cells or CD45+ Hematopoietic Precursors. Arterioscler Thromb Vasc Biol 2007;27:1572-9.
40. Elsheikh E, Uzunel M, He Z, Holgersson J, Nowak G, Sumitran-Holgersson S. Only a specific subset of human peripheral-blood monocytes has endothelial-like functional capacity. Blood 2005;106:2347-55.

41. Sharpe EE, III, Teleron AA, Li B, et al. The Origin and in Vivo Significance of Murine and Human Culture-Expanded Endothelial Progenitor Cells. Am J Pathol 2006;168:1710-21.
42. Kalka C, Masuda H, Takahashi T, et al. Transplantation of ex vivo expanded endothelial progenitor cells for therapeutic neovascularization. Proceedings of the National Academy of Sciences of the United States of America 2000;97:3422-7.
43. Griese DP, Ehsan A, Melo LG, et al. Isolation and Transplantation of Autologous Circulating Endothelial Cells Into Denuded Vessels and Prosthetic Grafts. Circulation 2003;108:2710-5.
44. Werner N, Kosiol S, Schiegl T, et al. Circulating Endothelial Progenitor Cells and Cardiovascular Outcomes. New England Journal of Medicine 2005;353:999-1007.
45. Hill JM, Zalos G, Halcox JPJ, et al. Circulating Endothelial Progenitor Cells, Vascular Function, and Cardiovascular Risk. New England Journal of Medicine 2003;348:593-600.
46. Ingram DA, Mead LE, Tanaka H, et al. Identification of a novel hierarchy of endothelial progenitor cells using human peripheral and umbilical cord blood. Blood 2004;104:2752-60.
47. Güven H, Shepherd RM, Bach RG, Capoccia BJ, Link DC. The Number of Endothelial Progenitor Cell Colonies in the Blood Is Increased in Patients With Angiographically Significant Coronary Artery Disease. Journal of the American College of Cardiology 2006;48:1579-87.
48. Loomans CJM, de Koning EJP, Staal FJT, et al. Endothelial Progenitor Cell Dysfunction. Diabetes 2004;53:195-9.
49. Tepper OM, Galiano RD, Capla JM, et al. Human Endothelial Progenitor Cells From Type II Diabetics Exhibit Impaired Proliferation, Adhesion, and Incorporation Into Vascular Structures. Circulation 2002;106:2781-6.
50. Min TQ, Zhu CJ, Xiang WX, Hui ZJ, Peng SY. Improvement in Endothelial Progenitor Cells from Peripheral Blood by Ramipril Therapy in Patients with Stable Coronary Artery Disease. Cardiovascular Drugs and Therapy 2004;18:203-9.
51. Chen JZ, Zhang FR, Tao QM, Wang XX, Zhu JH, Zhu JH. Number and activity of endothelial progenitor cells from peripheral blood in patients with hypercholesterolaemia. Clin Sci 2004;107:273-80.
52. Pistrosch F, Herbrig K, Oelschlaegel U, et al. PPARγ-agonist rosiglitazone increases number and migratory activity of cultured endothelial progenitor cells. Atherosclerosis 2005;183:163-7.
53. Rohde E, Bartmann C, Schallmoser K, et al. Immune Cells Mimic the Morphology of Endothelial Progenitor Colonies In Vitro. STEM CELLS 2007;25:1746-52.
54. Yoder MC, Mead LE, Prater D, et al. Redefining endothelial progenitor cells via clonal analysis and hematopoietic stem/progenitor cell principals. Blood 2007;109:1801-9.
55. de Groot K, Hermann Bahlmann F, Sowa J, et al. Uremia causes endothelial progenitor cell deficiency. Kidney Int 2004;66:641-6.
56. Rehman J, Li J, Orschell CM, March KL. Peripheral Blood "Endothelial Progenitor Cells" Are Derived From Monocyte/Macrophages and Secrete Angiogenic Growth Factors. Circulation 2003;107:1164-9.

57. Vasa M, Fichtlscherer S, Aicher A, et al. Number and Migratory Activity of Circulating Endothelial Progenitor Cells Inversely Correlate With Risk Factors for Coronary Artery Disease. Circulation Research 2001;89:e1-e7.
58. Lambiase PD, Edwards RJ, Anthopoulos P, et al. Circulating Humoral Factors and Endothelial Progenitor Cells in Patients With Differing Coronary Collateral Support. Circulation 2004;109:2986-92.
59. Lin Y, Weisdorf DJ, Solovey A, Hebbel RP. Origins of circulating endothelial cells and endothelial outgrowth from blood. Journal of Clinical Investigation 2000;105:71-7.
60. Sieveking DP, Buckle A, Celermajer DS, Ng MKC. Strikingly Different Angiogenic Properties of Endothelial Progenitor Cell Subpopulations: Insights From a Novel Human Angiogenesis Assay. J Am Coll Cardiol 2008;51:660-8.
61. Fernandez-L A, Sanz-Rodriguez F, Zarrabeitia R, et al. Blood outgrowth endothelial cells from Hereditary Haemorrhagic Telangiectasia patients reveal abnormalities compatible with vascular lesions. Cardiovascular Research 2005;68:235-48.
62. Urbich C, Heeschen C, Aicher A, Dernbach E, Zeiher AM, Dimmeler S. Relevance of Monocytic Features for Neovascularization Capacity of Circulating Endothelial Progenitor Cells. Circulation 2003;108:2511-6.
63. Gulati R, Jevremovic D, Peterson TE, et al. Diverse Origin and Function of Cells with Endothelial Phenotype Obtained from Adult Human Blood. Circulation Research 2003;93:1023-5.
64. Harraz M, Jiao C, Hanlon HD, Hartley RS, Schatteman GC. CD34– Blood-Derived Human Endothelial Cell Progenitors. STEM CELLS 2001;19:304-12.
65. Kawamoto A, Gwon H-C, Iwaguro H, et al. Therapeutic Potential of Ex Vivo Expanded Endothelial Progenitor Cells for Myocardial Ischemia. Circulation 2001;103:634-7.
66. Schmeisser A, Garlichs CD, Zhang H, et al. Monocytes coexpress endothelial and macrophagocytic lineage markers and form cord-like structures in Matrigel® under angiogenic conditions. Cardiovascular Research 2001;49:671-80.
67. Barber CL, Iruela-Arispe ML. The Ever-Elusive Endothelial Progenitor Cell: Identities, Functions and Clinical Implications. Pediatr Res 2006;59:26R-32R.
68. Kaushal S, Amiel GE, Guleserian KJ, et al. Functional small-diameter neovessels created using endothelial progenitor cells expanded ex vivo. Nat Med 2001;7:1035-40.
69. Walter DH, Rittig K, Bahlmann FH, et al. Statin Therapy Accelerates Reendothelialization. Circulation 2002;105:3017-24.
70. Werner N, Junk S, Laufs U, et al. Intravenous Transfusion of Endothelial Progenitor Cells Reduces Neointima Formation After Vascular Injury. Circulation Research 2003;93:e17-e24.
71. Takahashi T, Kalka C, Masuda H, et al. Ischemia- and cytokine-induced mobilization of bone marrow-derived endothelial progenitor cells for neovascularization. Nat Med 1999;5:434-8.
72. Schatteman GC, Hanlon HD, Jiao C, Dodds SG, Christy BA. Blood-derived angioblasts accelerate blood-flow restoration in diabetic mice. J Clin Invest 2000;106:571-8.
73. Kalka C, Masuda H, Takahashi T, et al. Vascular Endothelial Growth Factor165 Gene Transfer Augments Circulating Endothelial Progenitor Cells in Human Subjects. Circulation Research 2000;86:1198-202.

74. Murohara T, Ikeda H, Duan J, et al. Transplanted cord blood–derived endothelial precursor cells augment postnatal neovascularization. J Clin Invest 2000;105:1527-36.
75. Asahara T, Masuda H, Takahashi T, et al. Bone Marrow Origin of Endothelial Progenitor Cells Responsible for Postnatal Vasculogenesis in Physiological and Pathological Neovascularization. Circulation Research 1999;85:221-8.
76. Asahara T, Takahashi T, Masuda H, et al. VEGF contributes to postnatal neovascularization by mobilizing bone marrow-derived endothelial progenitor cells. EMBO J 1999;18:3964-72.
77. Crosby JR, Kaminski WE, Schatteman G, et al. Endothelial Cells of Hematopoietic Origin Make a Significant Contribution to Adult Blood Vessel Formation. Circulation Research 2000;87:728-30.
78. Sata M, Saiura A, Kunisato A, et al. Hematopoietic stem cells differentiate into vascular cells that participate in the pathogenesis of atherosclerosis. Nat Med 2002;8:403-9.
79. Luttun A, Tjwa M, Moons L, et al. Revascularization of ischemic tissues by PlGF treatment, and inhibition of tumor angiogenesis, arthritis and atherosclerosis by anti-Flt1. Nat Med 2002;8:831-40.
80. Lyden D, Hattori K, Dias S, et al. Impaired recruitment of bone-marrow-derived endothelial and hematopoietic precursor cells blocks tumor angiogenesis and growth. Nat Med 2001;7:1194-201.
81. Orlic D, Kajstura J, Chimenti S, et al. Mobilized bone marrow cells repair the infarcted heart, improving function and survival. Proceedings of the National Academy of Sciences 2001;98:10344-9.
82. Orlic D, Kajstura JAN, Chimenti S, Bodine DM, Leri A, Anversa P. Transplanted Adult Bone Marrow Cells Repair Myocardial Infarcts in Mice. Annals of the New York Academy of Sciences 2001;938:221-30.
83. Kocher AA, Schuster MD, Szabolcs MJ, et al. Neovascularization of ischemic myocardium by human bone-marrow-derived angioblasts prevents cardiomyocyte apoptosis, reduces remodeling and improves cardiac function. Nat Med 2001;7:430-6.
84. Kawamoto A, Tkebuchava T, Yamaguchi J-I, et al. Intramyocardial Transplantation of Autologous Endothelial Progenitor Cells for Therapeutic Neovascularization of Myocardial Ischemia. Circulation 2003;107:461-8.
85. Schuster MD, Kocher AA, Seki T, et al. Myocardial neovascularization by bone marrow angioblasts results in cardiomyocyte regeneration. American Journal of Physiology - Heart and Circulatory Physiology 2004;287:H525-H32.
86. Ott I, Keller U, Knoedler M, et al. Endothelial-like cells expanded from CD34+ blood cells improve left ventricular function after experimental myocardial infarction. The FASEB Journal 2005;19:992-4.
87. Iwasaki H, Kawamoto A, Ishikawa M, et al. Dose-Dependent Contribution of CD34-Positive Cell Transplantation to Concurrent Vasculogenesis and Cardiomyogenesis for Functional Regenerative Recovery After Myocardial Infarction. Circulation 2006;113:1311-25.
88. Hur J, Yoon CH, Kim HS, et al. Characterization of Two Types of Endothelial Progenitor Cells and Their Different Contributions to Neovasculogenesis. Arteriosclerosis, Thrombosis, and Vascular Biology 2004;24:288-93.
89. Richardson MR, Yoder MC. Endothelial progenitor cells: Quo Vadis? Journal of Molecular and Cellular Cardiology 2011;50:266-72.

90. Ziegelhoeffer T, Fernandez B, Kostin S, et al. Bone Marrow-Derived Cells Do Not Incorporate Into the Adult Growing Vasculature. Circulation Research 2004;94:230-8.
91. Rajantie I, Ilmonen M, Alminaite A, Ozerdem U, Alitalo K, Salven P. Adult bone marrow-derived cells recruited during angiogenesis comprise precursors for periendothelial vascular mural cells. Blood 2004;104:2084-6.
92. Udani VM, Santarelli JG, Yung YC, et al. Hematopoietic Stem Cells Give Rise to Perivascular Endothelial-like Cells During Brain Tumor Angiogenesis. Stem Cells and Development 2005;14:478-86.
93. He T, Smith LA, Harrington S, Nath KA, Caplice NM, Katusic ZS. Transplantation of Circulating Endothelial Progenitor Cells Restores Endothelial Function of Denuded Rabbit Carotid Arteries. Stroke 2004;35:2378-84.
94. Urbich C, Dimmeler S. Endothelial Progenitor Cells. Circulation Research 2004;95:343-53.
95. Kamihata H, Matsubara H, Nishiue T, et al. Implantation of Bone Marrow Mononuclear Cells Into Ischemic Myocardium Enhances Collateral Perfusion and Regional Function via Side Supply of Angioblasts, Angiogenic Ligands, and Cytokines. Circulation 2001;104:1046-52.
96. Heil M, Ziegelhoeffer T, Mees B, Schaper W. A Different Outlook on the Role of Bone Marrow Stem Cells in Vascular Growth. Circulation Research 2004;94:573-4.
97. Salven P, Mustjoki S, Alitalo R, Alitalo K, Rafii S. VEGFR-3 and CD133 identify a population of CD34+ lymphatic/vascular endothelial precursor cells. Blood 2003;101:168-72.
98. Polverini PJ, Cotran RS, Gimbrone MA, Unanue ER. Activated macrophages induce vascular proliferation. Nature 1977;269:804-6.
99. Berse B, Brown LF, Van de Water L, Dvorak HF, Senger DR. Vascular permeability factor (vascular endothelial growth factor) gene is expressed differentially in normal tissues, macrophages, and tumors. Molecular Biology of the Cell 1992;3:211-20.
100. Yoon C-H, Hur J, Park K-W, et al. Synergistic Neovascularization by Mixed Transplantation of Early Endothelial Progenitor Cells and Late Outgrowth Endothelial Cells: The Role of Angiogenic Cytokines and Matrix Metalloproteinases. Circulation 2005;112:1618-27.
101. Bergers G, Song S. The role of pericytes in blood-vessel formation and maintenance. Neuro-Oncology 2005;7:452-64.
102. Koike N, Fukumura D, Gralla O, Au P, Schechner JS, Jain RK. Tissue engineering: Creation of long-lasting blood vessels. Nature 2004;428:138-9.
103. Fruttiger M. Development of the retinal vasculature. Angiogenesis 2007;10:77-88.
104. Melero-Martin JM, Khan ZA, Picard A, Wu X, Paruchuri S, Bischoff J. In vivo vasculogenic potential of human blood-derived endothelial progenitor cells. Blood 2007;109:4761-8.
105. Au P, Daheron LM, Duda DG, et al. Differential in vivo potential of endothelial progenitor cells from human umbilical cord blood and adult peripheral blood to form functional long-lasting vessels. Blood 2008;111:1302-5.

106. Au P, Tam J, Fukumura D, Jain RK. Bone marrow–derived mesenchymal stem cells facilitate engineering of long-lasting functional vasculature. Blood 2008;111:4551-8.
107. Melero-Martin JM, De Obaldia ME, Kang S-Y, et al. Engineering Robust and Functional Vascular Networks In Vivo With Human Adult and Cord Blood–Derived Progenitor Cells. Circulation Research 2008;103:194-202.
108. Papayannopoulou T. Current mechanistic scenarios in hematopoietic stem/progenitor cell mobilization. Blood 2004;103:1580-5.
109. Heissig B, Hattori K, Dias S, et al. Recruitment of Stem and Progenitor Cells from the Bone Marrow Niche Requires MMP-9 Mediated Release of Kit-Ligand. Cell 2002;109:625-37.
110. Gill M, Dias S, Hattori K, et al. Vascular Trauma Induces Rapid but Transient Mobilization of VEGFR2+AC133+ Endothelial Precursor Cells. Circulation Research 2001;88:167-74.
111. Shintani S, Murohara T, Ikeda H, et al. Mobilization of Endothelial Progenitor Cells in Patients With Acute Myocardial Infarction. Circulation 2001;103:2776-9.
112. Pillarisetti K, Gupta S. Cloning and Relative Expression Analysis of Rat Stromal Cell Derived Factor-1 (SDF-1): SDF-1 α mRNA Is Selectively Induced in Rat Model of Myocardial Infarction. Inflammation 2001;25:293-300.
113. Ceradini DJ, Kulkarni AR, Callaghan MJ, et al. Progenitor cell trafficking is regulated by hypoxic gradients through HIF-1 induction of SDF-1. Nat Med 2004;10:858-64.
114. Cottler-Fox MH, Lapidot T, Petit I, et al. Stem Cell Mobilization. Hematology 2003;2003:419-37.
115. Moore MAS, Hattori K, Heissig B, et al. Mobilization of Endothelial and Hematopoietic Stem and Progenitor Cells by Adenovector-Mediated Elevation of Serum Levels of SDF-1, VEGF, and Angiopoietin-1. Annals of the New York Academy of Sciences 2001;938:36-47.
116. Irhimeh MR, Fitton JH, Lowenthal RM. Fucoidan ingestion increases the expression of CXCR4 on human CD34+ cells. Experimental Hematology 2007;35:989-94.
117. Hattori K, Dias S, Heissig B, et al. Vascular Endothelial Growth Factor and Angiopoietin-1 Stimulate Postnatal Hematopoiesis by Recruitment of Vasculogenic and Hematopoietic Stem Cells. The Journal of Experimental Medicine 2001;193:1005-14.
118. Kalka C, Tehrani H, Laudenberg B, et al. VEGF gene transfer mobilizes endothelial progenitor cells in patients with inoperable coronary disease. Ann Thorac Surg 2000;70:829-34.
119. Kryczek I, Lange A, Mottram P, et al. CXCL12 and Vascular Endothelial Growth Factor Synergistically Induce Neoangiogenesis in Human Ovarian Cancers. Cancer Research 2005;65:465-72.
120. Heeschen C, Aicher A, Lehmann R, et al. Erythropoietin is a potent physiological stimulus for endothelial progenitor cell mobilization. Blood 2003.
121. Laterveer L, Lindley I, Hamilton M, Willemze R, Fibbe W. Interleukin-8 induces rapid mobilization of hematopoietic stem cells with radioprotective capacity and long-term myelolymphoid repopulating ability. Blood 1995;85:2269-75.

122. Kocher AA, Schuster MD, Bonaros N, et al. Myocardial homing and neovascularization by human bone marrow angioblasts is regulated by IL-8/Gro CXC chemokines. Journal of Molecular and Cellular Cardiology 2006;40:455-64.
123. Adams V, Lenk K, Linke A, et al. Increase of Circulating Endothelial Progenitor Cells in Patients with Coronary Artery Disease After Exercise-Induced Ischemia. Arteriosclerosis, Thrombosis, and Vascular Biology 2004;24:684-90.
124. Llevadot J, Murasawa S, Kureishi Y, et al. HMG-CoA reductase inhibitor mobilizes bone marrow–derived endothelial progenitor cells. The Journal of Clinical Investigation 2001;108:399-405.
125. Dimmeler S, Aicher A, Vasa M, et al. HMG-CoA reductase inhibitors (statins) increase endothelial progenitor cells via the PI 3-kinase/Akt pathway. The Journal of Clinical Investigation 2001;108:391-7.
126. Wang C-H, Verma S, Hsieh IC, et al. Enalapril increases ischemia-induced endothelial progenitor cell mobilization through manipulation of the CD26 system. Journal of Molecular and Cellular Cardiology 2006;41:34-43.
127. Bahlmann FH, de Groot K, Mueller O, Hertel B, Haller H, Fliser D. Stimulation of Endothelial Progenitor Cells. Hypertension 2005;45:526-9.
128. Assmus B, Urbich C, Aicher A, et al. HMG-CoA Reductase Inhibitors Reduce Senescence and Increase Proliferation of Endothelial Progenitor Cells via Regulation of Cell Cycle Regulatory Genes. Circulation Research 2003;92:1049-55.
129. George J, Goldstein E, Abashidze A, et al. Erythropoietin promotes endothelial progenitor cell proliferative and adhesive properties in a PI 3-kinase-dependent manner. Cardiovascular Research 2005;68:299-306.
130. Aicher A, Heeschen C, Mildner-Rihm C, et al. Essential role of endothelial nitric oxide synthase for mobilization of stem and progenitor cells. Nat Med 2003;9:1370-6.
131. Laufs U, Werner N, Link A, et al. Physical Training Increases Endothelial Progenitor Cells, Inhibits Neointima Formation, and Enhances Angiogenesis. Circulation 2004;109:220-6.
132. Iwakura A, Luedemann C, Shastry S, et al. Estrogen-Mediated, Endothelial Nitric Oxide Synthase–Dependent Mobilization of Bone Marrow–Derived Endothelial Progenitor Cells Contributes to Reendothelialization After Arterial Injury. Circulation 2003;108:3115-21.
133. Landmesser U, Engberding N, Bahlmann FH, et al. Statin-Induced Improvement of Endothelial Progenitor Cell Mobilization, Myocardial Neovascularization, Left Ventricular Function, and Survival After Experimental Myocardial Infarction Requires Endothelial Nitric Oxide Synthase. Circulation 2004;110:1933-9.
134. Abdel-Latif A, Bolli R, Tleyjeh IM, et al. Adult Bone Marrow-Derived Cells for Cardiac Repair: A Systematic Review and Meta-analysis. Arch Intern Med 2007;167:989-97.
135. Martin-Rendon E, Brunskill SJ, Hyde CJ, Stanworth SJ, Mathur A, Watt SM. Autologous bone marrow stem cells to treat acute myocardial infarction: a systematic review. European Heart Journal 2008;29:1807-18.
136. Jiang M, He B, Zhang Q, et al. Randomized controlled trials on the therapeutic effects of adult progenitor cells for myocardial infarction: meta-analysis. Expert Opinion on Biological Therapy 2010;10:667-80.

137. Schächinger V, Erbs S, Elsässer A, et al. Intracoronary Bone Marrow–Derived Progenitor Cells in Acute Myocardial Infarction. New England Journal of Medicine 2006;355:1210-21.
138. Schächinger V, Erbs S, Elsässer A, et al. Improved clinical outcome after intracoronary administration of bone-marrow-derived progenitor cells in acute myocardial infarction: final 1-year results of the REPAIR-AMI trial. European Heart Journal 2006;27:2775-83.
139. Wollert KC, Meyer GP, Lotz J, et al. Intracoronary autologous bone-marrow cell transfer after myocardial infarction: the BOOST randomised controlled clinical trial. The Lancet 2004;364:141-8.
140. Meyer GP, Wollert KC, Lotz J, et al. Intracoronary Bone Marrow Cell Transfer After Myocardial Infarction: Eighteen Months' Follow-Up Data From the Randomized, Controlled BOOST (BOne marrOw transfer to enhance ST-elevation infarct regeneration) Trial. Circulation 2006;113:1287-94.
141. Lunde K, Solheim S, Aakhus S, et al. Intracoronary Injection of Mononuclear Bone Marrow Cells in Acute Myocardial Infarction. New England Journal of Medicine 2006;355:1199-209.
142. Janssens S, Dubois C, Bogaert J, et al. Autologous bone marrow-derived stem-cell transfer in patients with ST-segment elevation myocardial infarction: double-blind, randomised controlled trial. The Lancet 2006;367:113-21.
143. Tendera M, Wojakowski W, Rużyłło W, et al. Intracoronary infusion of bone marrow-derived selected CD34+CXCR4+ cells and non-selected mononuclear cells in patients with acute STEMI and reduced left ventricular ejection fraction: results of randomized, multicentre Myocardial Regeneration by Intracoronary Infusion of Selected Population of Stem Cells in Acute Myocardial Infarction (REGENT) Trial. European Heart Journal 2009;30:1313-21.
144. Losordo DW, Schatz RA, White CJ, et al. Intramyocardial Transplantation of Autologous CD34+ Stem Cells for Intractable Angina: A Phase I/IIa Double-Blind, Randomized Controlled Trial. Circulation 2007;115:3165-72.
145. Hossein Ahmadi HB, Saeed Kazemi Ashtiani, Massoud Soleimani, Hakimeh Sadeghian, Jalil Madjd Ardekani, Narges Zare Mehrjerdi, Azam Kouhkan, Mehrnaz Namiri, Manouchehr Madani-Civi, Fatemeh Fattahi, Abdolhossein Shahverdi, Ahmad Vosough Digaji Safety Analysis and Improved Cardiac Function Following Local Autologous Transplantation of CD133+ Enriched Bone Marrow Cells After Myocardial Infarction Current Neurovascular Research 2007;4:153-60.
146. Stamm C, Westphal B, Kleine H-D, et al. Autologous bone-marrow stem-cell transplantation for myocardial regeneration. The Lancet 2003;361:45-6.
147. Stamm C, Kleine HD, Westphal B, et al. CABG and Bone Marrow Stem Cell Transplantation after Myocardial Infarction. Thorac cardiovasc Surg 2004;52:152,8.
148. Manginas A, Goussetis E, Koutelou M, et al. Pilot study to evaluate the safety and feasibility of intracoronary CD133+ and CD133− CD34+ cell therapy in patients with nonviable anterior myocardial infarction. Catheterization and Cardiovascular Interventions 2007;69:773-81.
149. Bartunek J, Vanderheyden M, Vandekerckhove B, et al. Intracoronary Injection of CD133-Positive Enriched Bone Marrow Progenitor Cells Promotes Cardiac Recovery After Recent Myocardial Infarction: Feasibility and Safety. Circulation 2005;112:I-178-83.

150. Assmus B, Schachinger V, Teupe C, et al. Transplantation of Progenitor Cells and Regeneration Enhancement in Acute Myocardial Infarction (TOPCARE-AMI). Circulation 2002;106:3009-17.
151. Assmus B, Honold J, Schächinger V, et al. Transcoronary Transplantation of Progenitor Cells after Myocardial Infarction. New England Journal of Medicine 2006;355:1222-32.
152. Hu Y, Davison F, Zhang Z, Xu Q. Endothelial Replacement and Angiogenesis in Arteriosclerotic Lesions of Allografts Are Contributed by Circulating Progenitor Cells. Circulation 2003;108:3122-7.
153. Rafii S, Lyden D, Benezra R, Hattori K, Heissig B. Vascular and haematopoietic stem cells: novel targets for anti-angiogenesis therapy? Nat Rev Cancer 2002;2:826-35.
154. Bartunek J, Dimmeler S, Drexler H, et al. The consensus of the task force of the European Society of Cardiology concerning the clinical investigation of the use of autologous adult stem cells for repair of the heart. European Heart Journal 2006;27:1338-40.
155. Tongers J, Losordo DW, Landmesser U. Stem and progenitor cell-based therapy in ischaemic heart disease: promise, uncertainties, and challenges. European Heart Journal 2011;32:1197–206.
156. Barile L, Messina E, Giacomello A, Marbán E. Endogenous Cardiac Stem Cells. Progress in Cardiovascular Diseases 2007;50:31-48.
157. Mouquet F, Pfister O, Jain M, et al. Restoration of Cardiac Progenitor Cells After Myocardial Infarction by Self-Proliferation and Selective Homing of Bone Marrow–Derived Stem Cells. Circulation Research 2005;97:1090-2.
158. Messina E, De Angelis L, Frati G, et al. Isolation and Expansion of Adult Cardiac Stem Cells From Human and Murine Heart. Circulation Research 2004;95:911-21.
159. Smith RR, Barile L, Cho HC, et al. Regenerative Potential of Cardiosphere-Derived Cells Expanded From Percutaneous Endomyocardial Biopsy Specimens. Circulation 2007;115:896-908.
160. Li T-S, Cheng K, Lee S-T, et al. Cardiospheres Recapitulate a Niche-Like Microenvironment Rich in Stemness and Cell-Matrix Interactions, Rationalizing Their Enhanced Functional Potency for Myocardial Repair. STEM CELLS 2010;28:2088-98.
161. Cheng K, Li T-S, Malliaras K, Davis DR, Zhang Y, Marbán E. Magnetic Targeting Enhances Engraftment and Functional Benefit of Iron-Labeled Cardiosphere-Derived Cells in Myocardial Infarction. Circulation Research 2010;106:1570-81.
162. Davis DR, Kizana E, Terrovitis J, et al. Isolation and expansion of functionally-competent cardiac progenitor cells directly from heart biopsies. Journal of Molecular and Cellular Cardiology 2010;49:312-21.
163. Carr CA, Stuckey DJ, Tan JJ, et al. Cardiosphere-Derived Cells Improve Function in the Infarcted Rat Heart for at Least 16 Weeks – an MRI Study. PLoS ONE 2011;6:e25669.
164. Bartosh TJ, Wang Z, Rosales AA, Dimitrijevich SD, Roque RS. 3D-model of adult cardiac stem cells promotes cardiac differentiation and resistance to oxidative stress. Journal of Cellular Biochemistry 2008;105:612-23.
165. Aghila Rani KG, Kartha CC. Effects of epidermal growth factor on proliferation and migration of cardiosphere-derived cells expanded from adult human heart. Growth Factors 2010;28:157-65.

166. Tang YL, Zhu W, Cheng M, et al. Hypoxic Preconditioning Enhances the Benefit of Cardiac Progenitor Cell Therapy for Treatment of Myocardial Infarction by Inducing CXCR4 Expression. Circulation Research 2009;104:1209-16.
167. Koninckx R, Daniëls A, Windmolders S, et al. Mesenchymal stem cells or cardiac progenitors for cardiac repair? A comparative study. Cellular and Molecular Life Sciences 2011;68:2141-56.
168. Hodgkiss-Geere HM, Argyle DJ, Corcoran BM, et al. Characterisation and cardiac directed differentiation of canine adult cardiac stem cells. The Veterinary Journal 2012;191:176-82.
169. Lee S-T, White AJ, Matsushita S, et al. Intramyocardial Injection of Autologous Cardiospheres or Cardiosphere-Derived Cells Preserves Function and Minimizes Adverse Ventricular Remodeling in Pigs With Heart Failure Post-Myocardial Infarction. Journal of the American College of Cardiology 2011;57:455-65.
170. Johnston PV, Sasano T, Mills K, et al. Engraftment, Differentiation, and Functional Benefits of Autologous Cardiosphere-Derived Cells in Porcine Ischemic Cardiomyopathy. Circulation 2009;120:1075-83.
171. Takehara N, Tsutsumi Y, Tateishi K, et al. Controlled Delivery of Basic Fibroblast Growth Factor Promotes Human Cardiosphere-Derived Cell Engraftment to Enhance Cardiac Repair for Chronic Myocardial Infarction. J Am Coll Cardiol 2008;52:1858-65.
172. Mishra R, Vijayan K, Colletti EJ, et al. Characterization and Functionality of Cardiac Progenitor Cells in Congenital Heart Patients / Clinical Perspective. Circulation 2011;123:364-73.
173. Shenje LT, Field LJ, Pritchard CA, et al. Lineage Tracing of Cardiac Explant Derived Cells. PLoS ONE 2008;3:e1929.
174. Andersen DC, Andersen P, Schneider M, Jensen HB, Sheikh SP. Murine "Cardiospheres" Are Not a Source of Stem Cells with Cardiomyogenic Potential. STEM CELLS 2009;27:1571-81.
175. Davis DR, Zhang Y, Smith RR, et al. Validation of the Cardiosphere Method to Culture Cardiac Progenitor Cells from Myocardial Tissue. PLoS ONE 2009;4:e7195.
176. Davis DR, Ruckdeschel Smith R, Marbán E. Human Cardiospheres Are a Source of Stem Cells with Cardiomyogenic Potential. STEM CELLS 2010;28:903-4.
177. Passier R, van Laake LW, Mummery CL. Stem-cell-based therapy and lessons from the heart. Nature 2008;453:322-9.
178. Massberg S, Schaerli P, Knezevic-Maramica I, et al. Immunosurveillance by Hematopoietic Progenitor Cells Trafficking through Blood, Lymph, and Peripheral Tissues. Cell 2007;131:994-1008.
179. Quaini F, Urbanek K, Beltrami AP, et al. Chimerism of the Transplanted Heart. New England Journal of Medicine 2002;346:5-15.
180. Thiele J, Varus E, Wickenhauser C, et al. Mixed Chimerism of Cardiomyocytes and Vessels After Allogeneic Bone Marrow and Stem-Cell Transplantation in Comparison With Cardiac Allografts. Transplantation 2004;77:1902-5.
181. Eberhard D, Jockusch H. Patterns of myocardial histogenesis as revealed by mouse chimeras. Developmental Biology 2005;278:336-46.

182. White AJ, Smith RR, Matsushita S, et al. Intrinsic cardiac origin of human cardiosphere-derived cells. European Heart Journal 2011.
183. Ye J, Boyle A, Shih H, et al. Sca-1⁺ Cardiosphere-Derived Cells Are Enriched for Isl1-Expressing Cardiac Precursors and Improve Cardiac Function after Myocardial Injury. PLoS ONE 2012;7:e30329.
184. Anversa P, Kajstura J, Leri A. If I Can Stop One Heart From Breaking. Circulation 2007;115:829-32.
185. Urbanek K, Cesselli D, Rota M, et al. Stem cell niches in the adult mouse heart. Proceedings of the National Academy of Sciences 2006;103:9226-31.
186. Zakharova L, Mastroeni D, Mutlu N, et al. Transplantation of cardiac progenitor cell sheet onto infarcted heart promotes cardiogenesis and improves function. Cardiovascular Research 2010.
187. Chimenti I, Smith RR, Li T-S, et al. Relative Roles of Direct Regeneration Versus Paracrine Effects of Human Cardiosphere-Derived Cells Transplanted Into Infarcted Mice. Circulation Research 2010;106:971-80.
188. Vulliet PR, Greeley M, Halloran SM, MacDonald KA, Kittleson MD. Intra-coronary arterial injection of mesenchymal stromal cells and microinfarction in dogs. The Lancet 2004;363:783-4.
189. Li Z, Lee A, Huang M, et al. Imaging Survival and Function of Transplanted Cardiac Resident Stem Cells. Journal of the American College of Cardiology 2009;53:1229-40.
190. Ellison GM, Torella D, Dellegrottaglie S, et al. Endogenous Cardiac Stem Cell Activation by Insulin-Like Growth Factor-1/Hepatocyte Growth Factor Intracoronary Injection Fosters Survival and Regeneration of the Infarcted Pig Heart. Journal of the American College of Cardiology 2011;58:977-86.
191. Robey TE, Saiget MK, Reinecke H, Murry CE. Systems approaches to preventing transplanted cell death in cardiac repair. Journal of Molecular and Cellular Cardiology 2008;45:567-81.
192. Teng CJ, Luo J, Chiu RCJ, Shum-Tim D. Massive mechanical loss of microspheres with direct intramyocardial injection in the beating heart: Implications for cellular cardiomyoplasty. The Journal of Thoracic and Cardiovascular Surgery 2006;132:628-32.
193. Li T-S, Cheng K, Malliaras K, et al. Expansion of human cardiac stem cells in physiological oxygen improves cell production efficiency and potency for myocardial repair. Cardiovascular Research 2011;89:157-65.
194. Terrovitis J, Lautamäki R, Bonios M, et al. Noninvasive Quantification and Optimization of Acute Cell Retention by In Vivo Positron Emission Tomography After Intramyocardial Cardiac-Derived Stem Cell Delivery. Journal of the American College of Cardiology 2009;54:1619-26.
195. Tomanek RJ. Formation of the coronary vasculature during development. Angiogenesis 2005;8:273-84.
196. Wu SM, Chien KR, Mummery C. Origins and Fates of Cardiovascular Progenitor Cells. Cell 2008;132:537-43.
197. The CADUCEUS (CArdiosphere-Derived aUtologous stem Cells to reverse ventricular dysfunction) Trial. . American Heart Association, 2011. (Accessed at http://my.americanheart.org/idc/groups/ahamah-public/@wcm/@sop/@scon/documents/downloadable/ucm_433695.pdf.)
198. Makkar RR, Smith RR, Cheng K, et al. Intracoronary cardiosphere-derived cells for heart regeneration after myocardial infarction (CADUCEUS): a prospective, randomised phase 1 trial. The Lancet 2012.

199. The CADUCEUS Trial: Commentary. American Heart Association, 2011. (Accessed January 2012, at http://my.americanheart.org/idc/groups/ahamah-public/@wcm/@sop/@scon/documents/downloadable/ucm_433696.pdf.)
200. Bolli R, Chugh AR, D'Amario D, et al. Cardiac stem cells in patients with ischaemic cardiomyopathy (SCIPIO): initial results of a randomised phase 1 trial. The Lancet 2011;378:1847-57.
201. Pardali E, Goumans M-J, ten Dijke P. Signaling by members of the TGF-β family in vascular morphogenesis and disease. Trends in Cell Biology 2010;20:556-67.
202. Chang H, Brown CW, Matzuk MM. Genetic Analysis of the Mammalian Transforming Growth Factor-β Superfamily. Endocrine Reviews 2002;23:787-823.
203. Reddi H. Interplay between bone morphogenetic proteins and cognate binding proteins in bone and cartilage development: noggin, chordin and DAN. Arthritis Res 2001;3:1 - 5.
204. Lebrin F, Deckers M, Bertolino P, ten Dijke P. TGF-β receptor function in the endothelium. Cardiovascular Research 2005;65:599-608.
205. Wieser R, Wrana JL, Massague J. GS domain mutations that constitutively activate TβR-I, the downstream signaling component in the TGF-β receptor complex. EMBO Journal 1995;14:2199-208.
206. Derynck R, Zhang YE. Smad-dependent and Smad-independent pathways in TGF-β family signalling. Nature 2003;425:577-84.
207. Ten Dijke P, Hill CS. New insights into TGF-β-Smad signalling. Trends in Biochemical Sciences 2004;29:265-73.
208. Nakao A, Imamura T, Souchelnytskyi S, et al. TGF-β receptor-mediated signalling through Smad2, Smad3 and Smad4. EMBO Journal 1997;16:5353-62.
209. Lagna G, Hata A, Hemmati-Brivanlou A, Massague J. Partnership between DPC4 and SMAD proteins in TGF-β signalling pathways. Nature 1996;383:832-6.
210. Imamura T, Takase M, Nishihara A, et al. Smad6 inhibits signalling by the TGF-β superfamily. Nature 1997;389:622-6.
211. Nakao A, Afrakhte M, Morn A, et al. Identification of Smad7, a TGF[beta]-inducible antagonist of TGF-[beta] signalling. Nature 1997;389:631-5.
212. Kavsak P, Rasmussen RK, Causing CG, et al. Smad7 binds to Smurf2 to form an E3 ubiquitin ligase that targets the TGFβ receptor for degradation. Molecular cell 2000;6:1365-75.
213. Suzuki C, Murakami G, Fukuchi M, et al. Smurf1 regulates the inhibitory activity of Smad7 by targeting Smad7 to the plasma membrane. Journal of Biological Chemistry 2002;277:39919-25.
214. Shi W, Sun C, He B, et al. GADD34-PP1c recruited by Smad7 dephosphorylates TGFβ type I receptor. Journal of Cell Biology 2004;164:291-300.
215. Pepper MS. Transforming growth factor-beta: Vasculogenesis, angiogenesis, and vessel wall integrity. Cytokine and Growth Factor Reviews 1997;8:21-43.
216. David L, Feige J-J, Bailly S. Emerging role of bone morphogenetic proteins in angiogenesis. Cytokine & Growth Factor Reviews 2009;20:203-12.
217. Dickson MC, Martin JS, Cousins FM, Kulkarni AB, Karlsson S, Akhurst RJ. Defective haematopoiesis and vasculogenesis in transforming growth factor-β1 knock out mice. Development 1995;121:1845-54.

218. Oshima M, Oshima H, Taketo MM. TGF-β receptor type II deficiency results in defects of yolk sac hematopoiesis and vasculogenesis. Developmental Biology 1996;179:297-302.
219. Goumans M-J, Valdimarsdottir G, Itoh S, Rosendahl A, Sideras P, ten Dijke P. Balancing the activation state of the endothelium via two distinct TGF-[beta] type I receptors. EMBO J 2002;21:1743-53.
220. Ota T, Fujii M, Sugizaki T, et al. Targets of transcriptional regulation by two distinct type I receptors for transforming growth factor-β in human umbilical vein endothelial cells. Journal of Cellular Physiology 2002;193:299-318.
221. Goumans MJ, Valdimarsdottir G, Itoh S, et al. Activin receptor-like kinase (ALK)1 is an antagonistic mediator of lateral TGFβ/ALK5 signaling. Molecular cell 2003;12:817-28.
222. Beppu H, Kawabata M, Hamamoto T, et al. BMP Type II Receptor Is Required for Gastrulation and Early Development of Mouse Embryos. Developmental Biology 2000;221:249-58.
223. Beppu H, Ichinose F, Kawai N, et al. BMPR-II heterozygous mice have mild pulmonary hypertension and an impaired pulmonary vascular remodeling response to prolonged hypoxia. American Journal of Physiology - Lung Cellular and Molecular Physiology 2004;287:L1241-L7.
224. Liu D, Wang J, Kinzel B, et al. Dosage-dependent requirement of BMP type II receptor for maintenance of vascular integrity. Blood 2007;110:1502-10.
225. Larsson J, Goumans MJ, Sjöstrand LJ, et al. Abnormal angiogenesis but intact hematopoietic potential in TGF-β type I receptor-deficient mice. EMBO Journal 2001;20:1663-73.
226. Oh SP, Seki T, Goss KA, et al. Activin receptor-like kinase 1 modulates transforming growth factor-β1 signaling in the regulation of angiogenesis. Proceedings of the National Academy of Sciences of the United States of America 2000;97:2626-31.
227. Urness LD, Sorensen LK, Li DY. Arteriovenous malformations in mice lacking activin receptor-like kinase-1. Nature Genetics 2000;26:328-31.
228. Chang H, Huylebroeck D, Verschueren K, Guo Q, Matzuk MM, Zwijsen A. Smad5 knockout mice die at mid-gestation due to multiple embryonic and extraembryonic defects. Development 1999;126:1631-42.
229. Yang X, Castilla LH, Xu X, et al. Angiogenesis defects and mesenchymal apoptosis in mice lacking SMAD5. Development 1999;126:1571-80.
230. Lechleider RJ, Ryan JL, Garrett L, et al. Targeted mutagenesis of Smad1 reveals an essential role in chorioallantoic fusion. Developmental Biology 2001;240:157-67.
231. Tremblay KD, Dunn NR, Robertson EJ. Mouse embryos lacking Smad1 signals display defects in extra-embryonic tissues and germ cell formation. Development 2001;128:3609-21.
232. Arthur HM, Ure J, Smith AJH, et al. Endoglin, an Ancillary TGF[beta] Receptor, Is Required for Extraembryonic Angiogenesis and Plays a Key Role in Heart Development. Developmental Biology 2000;217:42-53.
233. Bourdeau A, Dumont DJ, Letarte M. A murine model of hereditary hemorrhagic telangiectasia. The Journal of Clinical Investigation 1999;104:1343-51.
234. Li DY, Sorensen LK, Brooke BS, et al. Defective Angiogenesis in Mice Lacking Endoglin. Science 1999;284:1534-7.

235. Stenvers KL, Tursky ML, Harder KW, et al. Heart and liver defects and reduced transforming growth factor β2 sensitivity in transforming growth factor β type III receptor-deficient embryos. Molecular and Cellular Biology 2003;23:4371-85.
236. Lamouille S, Mallet C, Feige J-J, Bailly S. Activin receptor–like kinase 1 is implicated in the maturation phase of angiogenesis. Blood 2002;100:4495-501.
237. Lebrin F, Goumans M-J, Jonker L, et al. Endoglin promotes endothelial cell proliferation and TGF-[beta]/ALK1 signal transduction. EMBO J 2004;23:4018-28.
238. David L, Mallet C, Mazerbourg S, Feige J-J, Bailly S. Identification of BMP9 and BMP10 as functional activators of the orphan activin receptor-like kinase 1 (ALK1) in endothelial cells. Blood 2007;109:1953-61.
239. Scharpfenecker M, van Dinther M, Liu Z, et al. BMP-9 signals via ALK1 and inhibits bFGF-induced endothelial cell proliferation and VEGF-stimulated angiogenesis. Journal of Cell Science 2007;120:964-72.
240. Upton PD, Davies RJ, Trembath RC, Morrell NW. Bone Morphogenetic Protein (BMP) and Activin Type II Receptors Balance BMP9 Signals Mediated by Activin Receptor-like Kinase-1 in Human Pulmonary Artery Endothelial Cells. Journal of Biological Chemistry 2009;284:15794-804.
241. David L, Mallet C, Keramidas M, et al. Bone Morphogenetic Protein-9 Is a Circulating Vascular Quiescence Factor. Circulation Research 2008;102:914-22.
242. Shao ES, Lin L, Yao Y, Bostrom KI. Expression of vascular endothelial growth factor is coordinately regulated by the activin-like kinase receptors 1 and 5 in endothelial cells. Blood 2009.
243. Mitchell D, Pobre EG, Mulivor AW, et al. ALK1-Fc Inhibits Multiple Mediators of Angiogenesis and Suppresses Tumor Growth. Molecular Cancer Therapeutics 2010;9:379-88.
244. Suzuki Y, Ohga N, Morishita Y, Hida K, Miyazono K, Watabe T. BMP-9 induces proliferation of multiple types of endothelial cells in vitro and in vivo. Journal of Cell Science 2010;123:1684-92.
245. Cunha SI, Pardali E, Thorikay M, et al. Genetic and pharmacological targeting of activin receptor-like kinase 1 impairs tumor growth and angiogenesis. The Journal of Experimental Medicine 2010;207:85-100.
246. ten Dijke P, Goumans M-J, Pardali E. Endoglin in angiogenesis and vascular diseases. Angiogenesis 2008;11:79-89.
247. Barbara NP, Wrana JL, Letarte M. Endoglin Is an Accessory Protein That Interacts with the Signaling Receptor Complex of Multiple Members of the Transforming Growth Factor-β Superfamily. Journal of Biological Chemistry 1999;274:584-94.
248. Letamendía A, Lastres P, Botella LM, et al. Role of endoglin in cellular responses to transforming growth factor- β: A comparative study with betaglycan. Journal of Biological Chemistry 1998;273:33011-9.
249. Castonguay R, Werner ED, Matthews RG, et al. Soluble Endoglin Specifically Binds Bone Morphogenetic Proteins 9 and 10 via Its Orphan Domain, Inhibits Blood Vessel Formation, and Suppresses Tumor Growth THE JOURNAL OF BIOLOGICAL CHEMISTRY 2011;286:30034–46.
250. Mummery MJGaC. Functional analysis of the TGFbeta receptor/Smad pathway through gene ablation in mice. Int J Dev Biol 2000;44:253-65.

251. Lastres P, Bellon T, Cabañas C, et al. Regulated expression on human macrophages of endoglin, an Arg-Gly-Asp-containing surface antigen. European Journal of Immunology 1992;22:393-7.
252. Conley BA, Smith JD, Guerrero-Esteo M, Bernabeu C, Vary CPH. Endoglin, a TGF-beta receptor-associated protein, is expressed by smooth muscle cells in human atherosclerotic plaques. Atherosclerosis 2000;153:323-35.
253. Chen K, Mehta J, Li D. TGF-b receptor endoglin is expressed in cardiac fibroblasts and modulates profibrogenic actions of angiotensin II. Circ Res 2004;95:1167-73.
254. Barry F, Boynton R, Haynesworth S, Murphy J, Zaia J. The monoclonal antibody SH-2, raised against human mesenchymal stem cells, recognizes an epitope on endoglin (CD105). Biochem Biophys Res Commun 1999;265:134-9.
255. Mancini ML, Verdi JM, Conley BA, et al. Endoglin is required for myogenic differentiation potential of neural crest stem cells. Developmental Biology 2007;308:520-33.
256. St-Jacques S, Forte M, Lye SJ, Letarte M. Localization of endoglin, a transforming growth factor-beta binding protein, and of CD44 and integrins in placenta during the first trimester of pregnancy. Biology of Reproduction 1994;51:405-13.
257. Chen C-Z, Li M, de Graaf D, et al. Identification of endoglin as a functional marker that defines long-term repopulating hematopoietic stem cells. Proceedings of the National Academy of Sciences of the United States of America 2002;99:15468-73.
258. Chen C-Z, Li L, Li M, Lodish HF. The EndoglinPositive Sca-1Positive RhodamineLow Phenotype Defines a Near-Homogeneous Population of Long-Term Repopulating Hematopoietic Stem Cells. Immunity 2003;19:525-33.
259. Johnson DW, Berg JN, Baldwin MA, et al. Mutations in the activin receptor-like kinase 1 gene in hereditary haemorrhagic telangiectasia type 2. Nat Genet 1996;13:189-95.
260. McAllister KA, Grogg KM, Johnson DW, et al. Endoglin, a TGF-[beta] binding protein of endothelial cells, is the gene for hereditary haemorrhagic telangiectasia type 1. Nat Genet 1994;8:345-51.
261. McAllister KA, Baldwin MA, Thukkani AK, et al. Six novel mutations in the endoglin gene in hereditary hemorrhagic telangiectasia type 1 suggest a dominant-negative effect of receptor function. Human Molecular Genetics 1995;4:1983-5.
262. Torsney E, Charlton R, Diamond AG, Burn J, Soames JV, Arthur HM. Mouse Model for Hereditary Hemorrhagic Telangiectasia Has a Generalized Vascular Abnormality. Circulation 2003;107:1653-7.
263. Bourdeau A, Faughnan ME, McDonald M-L, Paterson AD, Wanless IR, Letarte M. Potential Role of Modifier Genes Influencing Transforming Growth Factor-[beta]1 Levels in the Development of Vascular Defects in Endoglin Heterozygous Mice with Hereditary Hemorrhagic Telangiectasia. The American Journal of Pathology 2001;158:2011-20.
264. LI C, HAMPSON IN, HAMPSON L, KUMAR P, BERNABEU C, KUMAR S. CD105 antagonizes the inhibitory signaling of transforming growth factor ß1 on human vascular endothelial cells. The FASEB Journal 2000;14:55-64.
265. Lastres P, Letamendía A, Zhang H, et al. Endoglin modulates cellular responses to TGF-beta 1. The Journal of Cell Biology 1996;133:1109-21.

266. Obreo J, Díez-Marques L, Lamas S, et al. Endoglin expression regulates basal and TGF-β1-induced extracellular matrix synthesis in cultured L6E9 myoblasts. Cellular Physiology and Biochemistry 2004;14:301-10.
267. She X, Matsuno F, Harada N, Tsai H, Seon BK. Synergy between anti-endoglin (CD105) monoclonal antibodies and TGF-β in suppression of growth of human endothelial cells. International Journal of Cancer 2004;108:251-7.
268. GUO B, SLEVIN M, LI C, et al. CD105 Inhibits Transforming Growth Factor-ß-Smad3 Signalling. Anticancer Research 2004;24:1337-46.
269. Pece-Barbara N, Vera S, Kathirkamathamby K, et al. Endoglin Null Endothelial Cells Proliferate Faster and Are More Responsive to Transforming Growth Factor β1 with Higher Affinity Receptors and an Activated Alk1 Pathway. Journal of Biological Chemistry 2005;280:27800-8.
270. Mahmoud M, Allinson KR, Zhai Z, et al. Pathogenesis of Arteriovenous Malformations in the Absence of Endoglin. Circ Res 2010;106:1425-33.
271. Bagley RG, Walter-Yohrling J, Cao X, et al. Endothelial Precursor Cells As a Model of Tumor Endothelium. Cancer Research 2003;63:5866-73.
272. Henrich D, Hahn P, Wahl M, et al. Serum Derived from Multiple Trauma Patients Promotes the Differentiation of Endothelial Progenitor Cells In Vitro: Possible Role of Transforming Growth Factor-[beta]1 and Vascular Endothelial Growth Factor165. Shock 2004;21:13-6.
273. Zhu C, Ying D, Zhou D, et al. Expression of TGF-beta1 in Smooth Muscle Cells Regulates Endothelial Progenitor Cells Migration and Differentiation1. Journal of Surgical Research 2005;125:151-6.
274. Sales VL, Engelmayr GC, Mettler BA, Johnson JA, Sacks MS, Mayer JE. Transforming Growth Factor-β1 Modulates Extracellular Matrix Production, Proliferation, and Apoptosis of Endothelial Progenitor Cells in Tissue-Engineering Scaffolds. Circulation 2006;114:I-193-I-9.
275. van Laake LW, van den Driesche S, Post S, et al. Endoglin Has a Crucial Role in Blood Cell–Mediated Vascular Repair. Circulation 2006;114:2288-97.
276. Post S, Smits AM, van den Broek AJ, et al. Impaired recruitment of HHT-1 mononuclear cells to the ischaemic heart is due to an altered CXCR4/CD26 balance. Cardiovascular Research 2010;85:494-502.
277. Gaebel R, Furlani D, Sorg H, et al. Cell Origin of Human Mesenchymal Stem Cells Determines a Different Healing Performance in Cardiac Regeneration. PLoS ONE 2011;6:e15652.
278. Allinson KR, Carvalho RLC, Van Den Brink S, Mummery CL, Arthur HM. Generation of a floxed allele of the mouse endoglin gene. Genesis 2007;45:391-5.
279. Soriano P. Generalized lacZ expression with the ROSA26 Cre reporter strain. Nat Genet 1999;21:70-1.
280. Mosmann T. Rapid colorimetric assay for cellular growth and survival: Application to proliferation and cytotoxicity assays. Journal of Immunological Methods 1983;65:55-63.
281. Rozen S, Skaletsky H. Primer3 on the WWW for general users and for biologist programmers. In: Krawetz S, Misener S (eds) Bioinformatics Methods and Protocols: Methods in Molecular Biology 2000;Humana Press, Totowa, NJ 365-86
282. Roelen BAJ, Lin HY, Knežević V, Freund E, Mummery CL. Expression of TGF-βs and Their Receptors during Implantation and Organogenesis of the Mouse Embryo. Developmental Biology 1994;166:716-28.

283. St-Jacques S, Cymerman U, Pece N, Letarte M. Molecular characterization and in situ localization of murine endoglin reveal that it is a transforming growth factor-beta binding protein of endothelial and stromal cells. Endocrinology 1994;134:2645-57.
284. Oxburgh L, Chu GC, Michael SK, Robertson EJ. TGFβ superfamily signals are required for morphogenesis of the kidney mesenchyme progenitor population. Development 2004;131:4593-605.
285. Guerrero-Esteo M, Sánchez-Elsner T, Letamendia A, Bernabéu C. Extracellular and Cytoplasmic Domains of Endoglin Interact with the Transforming Growth Factor-β Receptors I and II. Journal of Biological Chemistry 2002;277:29197-209.
286. Inman GJ, Nicolás FJ, Callahan JF, et al. SB-431542 Is a Potent and Specific Inhibitor of Transforming Growth Factor-β Superfamily Type I Activin Receptor-Like Kinase (ALK) Receptors ALK4, ALK5, and ALK7. Molecular Pharmacology 2002;62:65-74.
287. Alroy J, Goyal V, Skutelsky E. Lectin histochemistry of mammalian endothelium. Histochemistry and Cell Biology 1987;86:603-7.
288. Voyta JC, Via DP, Butterfield CE, Zetter BR. Identification and isolation of endothelial cells based on their increased uptake of acetylated-low density lipoprotein. The Journal of Cell Biology 1984;99:2034-40.
289. Strasser ASaRH. Phenotypic Overlap Between Hematopoietic Cells with Suggested Angioblastic Potential and Vascular Endothelial Cells. Journal of Hematotherapy & Stem Cell Research 2002;11:69-79.
290. Somani A, Nguyen J, Milbauer LC, Solovey A, Sajja S, Hebbel RP. The establishment of murine blood outgrowth endothelial cells and observations relevant to gene therapy. Translational research : the journal of laboratory and clinical medicine 2007;150:30-9.
291. Zen K, Okigaki M, Hosokawa Y, et al. Myocardium-targeted delivery of endothelial progenitor cells by ultrasound-mediated microbubble destruction improves cardiac function via an angiogenic response. Journal of Molecular and Cellular Cardiology 2006;40:799-809.
292. Yang Z, Wang JM, Chen L, Luo CF, Tang AL, Tao J. Acute exercise-induced nitric oxide production contributes to upregulation of circulating endothelial progenitor cells in healthy subjects. J Hum Hypertens 2007;21:452-60.
293. Prokoph S, Chavakis E, Levental KR, et al. Sustained delivery of SDF-1α from heparin-based hydrogels to attract circulating pro-angiogenic cells. Biomaterials 2012;33:4792-800.
294. Freundlich B, Avdalovic N. Use of gelatin/plasma coated flasks for isolating human peripheral blood monocytes. Journal of immunological methods 1983;62:31-7.
295. Schniedermann J, Rennecke M, Buttler K, et al. Mouse lung contains endothelial progenitors with high capacity to form blood and lymphatic vessels. BMC Cell Biology 2010;11:50.
296. Lidington EA, Rao RM, Marelli-Berg FM, Jat PS, Haskard DO, Mason JC. Conditional immortalization of growth factor-responsive cardiac endothelial cells from H-2Kb-tsA58 mice. American Journal of Physiology - Cell Physiology 2002;282:C67-C74.
297. Watabe T, Nishihara A, Mishima K, et al. TGF-β receptor kinase inhibitor enhances growth and integrity of embryonic stem cell–derived endothelial cells. The Journal of Cell Biology 2003;163:1303-11.

298. James D, Nam H-s, Seandel M, et al. Expansion and maintenance of human embryonic stem cell-derived endothelial cells by TGF[beta] inhibition is Id1 dependent. Nat Biotech 2010;28:161-6.
299. Díez M, Musri MM, Ferrer E, Barberà JA, Peinado VI. Endothelial progenitor cells undergo an endothelial-to-mesenchymal transition-like process mediated by TGFβRI. Cardiovascular Research 2010;88:502-11.
300. Liu Z, Kobayashi K, van Dinther M, et al. VEGF and inhibitors of TGFβ type-I receptor kinase synergistically promote blood-vessel formation by inducing α5-integrin expression. Journal of Cell Science 2009;122:3294-302.
301. Xu J, Lamouille S, Derynck R. TGF-[beta]-induced epithelial to mesenchymal transition. Cell Res 2009;19:156-72.
302. Zeisberg EM, Tarnavski O, Zeisberg M, et al. Endothelial-to-mesenchymal transition contributes to cardiac fibrosis. Nat Med 2007;13:952-61.
303. Moonen J-RAJ, Krenning G, Brinker MGL, Koerts JA, van Luyn MJA, Harmsen MC. Endothelial progenitor cells give rise to pro-angiogenic smooth muscle-like progeny. Cardiovascular Research 2010;86:506-15.
304. Díez M, Barberà JA, Ferrer E, et al. Plasticity of CD133+ cells: Role in pulmonary vascular remodeling. Cardiovascular Research 2007;76:517-27.
305. Jankovic V, Ciarrocchi A, Boccuni P, DeBlasio T, Benezra R, Nimer SD. Id1 restrains myeloid commitment, maintaining the self-renewal capacity of hematopoietic stem cells. Proceedings of the National Academy of Sciences 2007;104:1260-5.
306. López-Novoa JM, Bernabeu C. The physiological role of endoglin in the cardiovascular system. American Journal of Physiology - Heart and Circulatory Physiology 2010;299:H959-H74.
307. Pierelli L, Scambia G, Bonanno G, et al. CD34+/CD105+ cells are enriched in primitive circulating progenitors residing in the G0 phase of the cell cycle and contain all bone marrow and cord blood CD34+/CD38low/− precursors. British Journal of Haematology 2000;108:610-20.
308. Cho SK, Bourdeau A, Letarte M, Zúñiga-Pflücker JC. Expression and function of CD105 during the onset of hematopoiesis from Flk1+ precursors. Blood 2001;98:3635-42.
309. Rokhlin O, Cohen M, Kubagawa H, Letarte M, Cooper M. Differential expression of endoglin on fetal and adult hematopoietic cells in human bone marrow. The Journal of Immunology 1995;154:4456-65.
310. Perlingeiro RCR. Endoglin is required for hemangioblast and early hematopoietic development. Development 2007;134:3041-8.
311. Cogle CR, Wainman DA, Jorgensen ML, Guthrie SM, Mames RN, Scott EW. Adult human hematopoietic cells provide functional hemangioblast activity. Blood 2004;103:133-5.
312. Grant MB, May WS, Caballero S, et al. Adult hematopoietic stem cells provide functional hemangioblast activity during retinal neovascularization. Nat Med 2002;8:607-12.
313. Bailey AS, Jiang S, Afentoulis M, et al. Transplanted adult hematopoietic stems cells differentiate into functional endothelial cells. Blood 2004;103:13-9.
314. Xu B, Wu YQ, Huey M, et al. Vascular Endothelial Growth Factor Induces Abnormal Microvasculature in the Endoglin Heterozygous Mouse Brain. J Cereb Blood Flow Metab 2004;24:237-44.

315. Sauer B. Inducible Gene Targeting in Mice Using the Cre/loxSystem. Methods 1998;14:381-92.
316. Hoess RH, Abremski K. Interaction of the bacteriophage P1 recombinase Cre with the recombining site loxP. Proceedings of the National Academy of Sciences of the United States of America 1984;81:1026-9.
317. Feil R, Wagner J, Metzger D, Chambon P. Regulation of Cre Recombinase Activity by Mutated Estrogen Receptor Ligand-Binding Domains. Biochemical and Biophysical Research Communications 1997;237:752-7.
318. Indra AK, Warot X, Brocard J, et al. Temporally-controlled site-specific mutagenesis in the basal layer of the epidermis: Comparison of the recombinase activity of the tamoxifen-inducible Cre-ER(T) and Cre-ER(T2) recombinases. Nucleic Acids Research 1999;27:4324-7.
319. Dejana E. Endothelial cell-cell junctions: happy together. Nat Rev Mol Cell Biol 2004;5:261-70.
320. Wang Y, Nakayama M, Pitulescu ME, et al. Ephrin-B2 controls VEGF-induced angiogenesis and lymphangiogenesis. Nature 2010;465:483-6.
321. Metzger D, Feil R. Engineering the mouse genome by site-specific recombination. Current Opinion in Biotechnology 1999;10:470-6.
322. Hobson B, Denekamp J. Endothelial proliferation in tumours and normal tissues: Continuous labelling studies. British Journal of Cancer 1984;49:405-13.
323. Rotman B, Zderic JA, Edelstein M. Fluorogenic substrates for beta-D-galactosidases and phosphatases derived from flurescein (3,6-dihydroxyfluoran) and its monomethylether. Proceedings of the National Academy of Sciences of the United States of America 1963;50:1-6.
324. Plovins A, Alvarez AM, Ibanez M, Molina M, Nombela C. Use of fluorescein-di-β-D-galactopyranoside (FDG) and C12-FDG as substrates for β-galactosidase detection by flow cytometry in animal, bacterial, and yeast cells. Applied and Environmental Microbiology 1994;60:4638-41.
325. Monvoisin A, Alva JA, Hofmann JJ, Zovein AC, Lane TF, Iruela-Arispe ML. VE-cadherin-CreERT2 transgenic mouse: A model for inducible recombination in the endothelium. Developmental Dynamics 2006;235:3413-22.
326. Alva JA, Zovein AC, Monvoisin A, et al. VE-Cadherin-Cre-recombinase transgenic mouse: A tool for lineage analysis and gene deletion in endothelial cells. Developmental Dynamics 2006;235:759-67.
327. Kim I, Yilmaz OH, Morrison SJ. CD144 (VE-cadherin) is transiently expressed by fetal liver hematopoietic stem cells. Blood 2005;106:903-5.
328. Buhring HJ, Muller CA, Letarte M, et al. Endoglin is expressed on a subpopulation of immature erythroid cells of normal human bone marrow. Leukemia 1991;5:841-7.
329. Leri A, Kajstura J, Anversa P. Cardiac Stem Cells and Mechanisms of Myocardial Regeneration. Physiological Reviews 2005;85:1373-416.
330. Laugwitz K-L, Moretti A, Lam J, et al. Postnatal isl1+ cardioblasts enter fully differentiated cardiomyocyte lineages. Nature 2005;433:647-53.
331. Ponticos M, Abraham D, Alexakis C, et al. Col1a2 enhancer regulates collagen activity during development and in adult tissue repair. Matrix Biology 2004;22:619-28.

332. Deasy BM, Lu A, Tebbets JC, et al. A role for cell sex in stem cell–mediated skeletal muscle regeneration: female cells have higher muscle regeneration efficiency. The Journal of Cell Biology 2007;177:73-86.
333. Crisostomo PR, Markel TA, Wang M, Lahm T, Lillemoe KD, Meldrum DR. In the adult mesenchymal stem cell population, source gender is a biologically relevant aspect of protective power. Surgery 2007;142:215-21.
334. Drowley L, Okada M, Payne TR, et al. Sex of Muscle Stem Cells Does Not Influence Potency for Cardiac Cell Therapy. Cell Transplantation 2009;18:1137-46.
335. Madhur NAP, Guangyong Chen, Ray C. J. Chiu, Satya Prakash, and Dominique Shum-Tim. Superior Therapeutic Potential of Young Bone Marrow Mesenchymal Stem Cells by Direct Intramyocardial Delivery in Aged Recipients with Acute Myocardial Infarction: In Vitro and In Vivo Investigation. Journal of Tissue Engineering 2011;2011.
336. Markel TA, Wang M, Crisostomo PR, Manukyan MC, Poynter JA, Meldrum DR. Neonatal stem cells exhibit specific characteristics in function, proliferation, and cellular signaling that distinguish them from their adult counterparts. American Journal of Physiology - Regulatory, Integrative and Comparative Physiology 2008;294:R1491-R7.
337. Markel TA, Crisostomo PR, Manukyan MC, et al. Are Neonatal Stem Cells as Effective as Adult Stem Cells in Providing Ischemic Protection? The Journal of surgical research 2009;152:325-30.
338. Lee NY, Ray B, How T, Blobe GC. Endoglin Promotes Transforming Growth Factor β-mediated Smad 1/5/8 Signaling and Inhibits Endothelial Cell Migration through Its Association with GIPC. Journal of Biological Chemistry 2008;283:32527-33.
339. Finnson KW, Parker WL, Chi Y, et al. Endoglin differentially regulates TGF-β-induced Smad2/3 and Smad1/5 signalling and its expression correlates with extracellular matrix production and cellular differentiation state in human chondrocytes. Osteoarthritis and cartilage / OARS, Osteoarthritis Research Society 2010;18:1518-27.
340. Santibanez JF, Letamendia A, Perez-Barriocanal F, et al. Endoglin increases eNOS expression by modulating Smad2 protein levels and Smad2-dependent TGF-β signaling. Journal of Cellular Physiology 2007;210:456-68.
341. Carvalho RLC, Jonker L, Goumans MJ, et al. Defective paracrine signalling by TGFβ in yolk sac vasculature of endoglin mutant mice: A paradigm for hereditary haemorrhagic telangiectasia. Development 2004;131:6237-47.
342. Carvalho RLC, Itoh F, Goumans M-J, et al. Compensatory signalling induced in the yolk sac vasculature by deletion of TGFβ receptors in mice. Journal of Cell Science 2007;120:4269-77.
343. Jerkic M, Rodríguez-Barbero A, Prieto M, et al. Reduced angiogenic responses in adult endoglin heterozygous mice. Cardiovascular Research 2006;69:845-54.
344. Lebrin F, Mummery CL. Endoglin-Mediated Vascular Remodeling: Mechanisms Underlying Hereditary Hemorrhagic Telangiectasia. Trends in Cardiovascular Medicine 2008;18:25-32.
345. Degabriele NM, Griesenbach U, Sato K, et al. Critical appraisal of the mouse model of myocardial infarction. Experimental Physiology 2004;89:497-505.
346. Zolotareva AG, Kogan ME. Production of experimental occlusive myocardial infarction in mice. Cor et Vasa 1978;20:308-14.

347. Michael LH, Entman ML, Hartley CJ, et al. Myocardial ischemia and reperfusion: A murine model. American Journal of Physiology - Heart and Circulatory Physiology 1995;269:H2147-H54.
348. Vandervelde S, Van Amerongen MJ, Tio RA, Petersen AH, Van Luyn MJA, Harmsen MC. Increased inflammatory response and neovascularization in reperfused vs. nonreperfused murine myocardial infarction. Cardiovascular Pathology 2006;15:83-90.
349. Michael LH, Ballantyne CM, Zachariah JP, et al. Myocardial infarction and remodeling in mice: Effect of reperfusion. American Journal of Physiology - Heart and Circulatory Physiology 1999;277:H660-H8.
350. Olivetti G, Ricci R, Beghi C. Response of the border zone to myocardial infarction in rats. American Journal of Pathology 1986;125:476-83.
351. van Laake LW, Passier R, Monshouwer-Kloots J, et al. Monitoring of cell therapy and assessment of cardiac function using magnetic resonance imaging in a mouse model of myocardial infarction. Nature protocols 2007;2:2551-67.
352. Klocke R, Tian W, Kuhlmann MT, Nikol S. Surgical animal models of heart failure related to coronary heart disease. Cardiovascular Research 2007;74:29-38.
353. Jerkic M, Rivas-Elena JV, Prieto M, et al. Endoglin regulates nitric oxide-dependent vasodilatation. The FASEB journal : official publication of the Federation of American Societies for Experimental Biology 2004;18:609-11.
354. Jerkic M, Rivas-Elena JV, Santibanez JF, et al. Endoglin regulates cyclooxygenase-2 expression and activity. Circulation Research 2006;99:248-56.
355. van Laake LW, Passier R, Monshouwer-Kloots J, et al. Human embryonic stem cell-derived cardiomyocytes survive and mature in the mouse heart and transiently improve function after myocardial infarction. Stem Cell Research 2007;1:9-24.
356. Lygate C. Letter to the editor: Infarct size measurements are critically important when comparing interventions affecting ventricular remodeling [1]. American Journal of Physiology - Heart and Circulatory Physiology 2007;293.
357. Ahn D, Cheng L, Moon C, Spurgeon H, Lakatta EG, Talan MI. Induction of myocardial infarcts of a predictable size and location by branch pattern probability-assisted coronary ligation in C57BL/6 mice. American Journal of Physiology - Heart and Circulatory Physiology 2004;286:H1201-H7.
358. Schneider J, Wiesmann F, Lygate C, Neubauer S. How to perform an accurate assessment of cardiac function in mice using high-resolution magnetic resonance imaging. Journal of Cardiovascular Magnetic Resonance 2006;8:693-701.
359. Mercado-Pimentel ME, Hubbard AD, Runyan RB. Endoglin and Alk5 regulate epithelial–mesenchymal transformation during cardiac valve formation. Developmental Biology 2007;304:420-32.
360. Okada H, Takemura G, Kosai K-i, et al. Postinfarction Gene Therapy Against Transforming Growth Factor-β Signal Modulates Infarct Tissue Dynamics and Attenuates Left Ventricular Remodeling and Heart Failure. Circulation 2005;111:2430-7.